Control strategies for permanent magnet synchronous machines without mechanical sensors by sliding modes

Carlos Enrique Alvaro Mendoza

THESE DE DOCTORAT DE

L'ÉCOLE CENTRALE DE NANTES
Et UNIVERSIDAD AUTÓNOMA DE NUEVO LEÓN

ECOLE DOCTORALE N° 601
Mathématiques et Sciences et Technologies
de l'Information et de la Communication
Spécialité : Automatique, productique et robotique

Par

Carlos Enrique ALVARO MENDOZA

Control strategies for permanent magnet synchronous machines without mechanical sensors by sliding modes

Thèse présentée et soutenue à l'École Centrale de Nantes le 29 novembre 2022
Unité de recherche : UMR 6004, Laboratoire des Sciences du Numérique de Nantes (LS2N)

Rapporteurs avant soutenance :

Fabrice LOCMENT Professeur des universités, Université de technologie de Compiègne
Michael DEFOORT Professeur des universités, Université Polytechnique Hauts-de-France

Composition du Jury :

Président :	Mohamed Fouad BENKHORIS	Professeur des universités, Nantes Université
Examinateurs :	Philippe MARTIN	Maître de recherche, MINES ParisTECH
	Sandrine MOREAU	Maître de conférences, Université de Poitiers
Dir. de thèse	Malek GHANES	Professeur des universités, École Centrale de Nantes
Dir. de thèse :	Jesús DE LEÓN MORALES	Full professor, Universidad Autónoma de Nuevo León, Mexique
Co-encadrant :	Mohamed Assaad HAMIDA	Maître de conférences, École Centrale de Nantes

Acknowledgement

I want to thank my family for all the support they have given me during my studies, in the same way I want to thank Claudia Luna in a very special way, who has been with me unconditionally throughout my doctoral study process.

I respectfully thank Professor Jesús de León Morales for providing me with the necessary guidance, training, and support during my master's and doctoral studies.

Also, I want to thank Professor Mohamed Hamida and Professor Malek Ghanes for thesis supervision and support during my stay in France.

I also want to thank Professor Fouad BENKHORIS for having agreed to be the president of the jury in the defense of my thesis. To the reviewers Professor Fabrice LOCMENT and Professor Michael DEFOORT for their comments and the time spent reviewing my thesis. To Professor Philippe MARTIN and Professor Sandrine MOREAU for agreeing to be part of the jury.

And last and most importantly, I want to thank CONACYT in México for the financial support, which facilitated my doctoral studies as well as the stay in France during my thesis.

Table of Contents

List of Figures

List of Tables

NOMENCLATURE

Abbreviations

AC Alternative Current

AHOSMO Adaptive High-Order Sliding Mode Observer

ASTWC Adaptive Super-Twisting Control

DC Direct Current

EKF Extended Kalman Filter

EMF Electromotive Force

HF High Frequency

IGBT Insulates Gate Bipolar Transistor

IPMSM Interior Permanent Magnet Synchronous Motor

kW Kilowatt

LTI Linear Time Invariant

PMSM Permanent Magnet Synchronous Motor

PWM Pulse width modulated

Transformation matrices

$\mathbb{Q}^T$ Matrix for simplified Concordia transformation

$\mathbb{T}^T$ Matrix for Park transformation

$\begin{bmatrix} x_a & x_b & x_c \end{bmatrix}^T$ Vector: x represents voltages, currents or fluxs

$\begin{bmatrix} x_\alpha & x_\beta & x_0 \end{bmatrix}^T$ Vector: x represents voltages, currents or fluxs

$\begin{bmatrix} x_d & x_q \end{bmatrix}^T$ Vector: x represents voltages, currents or fluxs

$\mathbb{Q}_o^T$ Matrix for Concordia transformation

Notation for electric motor

$\hat{\alpha}$	Estimated acceleration
$\hat{\Omega}$	Estimated mechanical speed
$\hat{\omega}$	Estimated electrical speed
$\hat{\theta}$	Estimated angular position
Ω	Mechanical speed
$\omega = p\Omega$	Electrical speed
Ω^*	Speed reference
ψ_{abc}	$abc-$axes stator fluxes
ψ_r	Permanent-magnet flux linkage
θ	Mechanical angular position
$\theta_e = p\theta$	Electrical angular position
e_{θ_e}	Angular position estimation error
f_v	Viscous friction coefficient
$i_{\alpha\beta}$	$\alpha\beta-$axes stator currents
i_{abc}	$abc-$axes stator currents
i_{dq}	$dq-$axes stator currents
i_d^*	Current$-i_d$ reference
J	Inertia
L_d, L_q	$dq-$axes winding inductance
L_{so}, L_{sv}	Own inductances
M_{so}	Mutual inductances
p	Number of pole pairs
R_s	Stator resistance
T_e	Electromagnetic torque

T_l Load Torque

$v_{\alpha\beta}$ $\alpha\beta-$axes stator voltages

v_{abc} $abc-$axes stator voltages

v_{dq} $dq-$axes stator voltages

Observer parameters

k_{o_2}, γ_{o_2} Constant parameters

k_o, γ_o Constant parameters

L_{o_2} Constant parameter

$L_{o_2}(t)$ Adaptive parameter

L_o Constant parameter

$L_o(t)$ Adaptive parameter

Control parameters

$\vartheta_{1i}; i = 1, 2, 3.$ Constant parameter

$\vartheta_{2i}; i = 1, 2, 3.$ Constant parameter

$k_{c_\Omega}, \gamma_{c_\Omega}$ Constant parameter

$k_{c_{\Omega_2}}, \gamma_{c_{\Omega_2}}$ Constant parameter

$k_{c_{i_d}}, \gamma_{c_{i_d}}$ Constant parameter

$k_{c_{i_{d_2}}}, \gamma_{c_{i_{d_2}}}$ Constant parameter

L_{c_2} Constant parameter

$L_{c_2}(t), L_{c_{\Omega_2}}(t), L_{c_{i_{d_2}}}(t)$ Adaptive parameters

L_c Constant parameter

$L_c(t), L_{c_\Omega}(t), L_{c_{i_d}}$ Adaptive parameters

INTRODUCTION

State of the art

Electrical machines are designed to transform electrical energy into mechanical energy, mechanical energy into electrical energy or modify the level of the same electrical energy according to the required use, so that electrical machines can be classified into three groups: Generators, transformers and motors. Generators transform mechanical energy into electrical energy. Transformers use electrical energy and have the ability to change the dimension of this energy and motors are used to transform electrical energy into mechanical energy, in such a way that, since the electrical machine was invented, they have been used in domestic products, industrial process, electricity production, robotics, electric vehicles, etc.

Regarding to the motors, these can be mainly classified into two groups: Direct Current (DC) motors and Alternating Current (AC) motors. DC motors have been traditionally used for decades in different applications. However, their commutators, brushes, and required maintenance are the main disadvantages of these devices. On the other hand, AC motors can be classified into two groups: Asynchronous or induction motors and synchronous motors. The main difference between these machines is that the rotor speed of the synchronous motor has the same frequency as the magnetic field, unlike induction motors, where the rotor speed is slower than the magnetic field generated in the stator, i.e., the speed is asynchronous. The predominant motor technology for many years has been cage induction motors. Their superior dynamic behavior coupled with their brushless nature, which allows operation without the presence of commutators or slip rings, makes them suitable for high performance controlled operation in electric drive applications. Advances in the area of power electronics and automatic control technologies have contributed significantly to their establishment as standard motors in electric drives. However, induction motor technology also has numerous disadvantages, both in construction and in operation. For example, its relatively small air gap length and its inferiority to synchronous motors in terms of overall efficiency and power factor are the main drawbacks. Also, induction motors have windings on the rotor, which increases the temperature of

the machine. Nevertheless, a clear indication towards the possible limitation in the use of induction motors and their eventual replacement has not yet been established.[1].

Consequently, permanent magnet synchronous motors (PMSM) have attracted increasing interest within the scientific community, especially for high power density applications, highlighting the need for their investigation. The most important advantages of permanent magnent synchronous motor lie in the fact that permanent magnets constitute a strong and independent excitation system, i.e., field current needed for induction machine is not necessary, and secondary copper loss does not occur, therefore high efficiency can be achieved [2]. This feature allows substantial overloading of the motor while providing higher torque density values. The fact that no electromagnetic drive system is employed further improves its transient behaviour, while small size and maintenance are also two significant benefit factors. The above advantages have led PMSM to be considered a viable and attractive solution for control drives [3], [4].

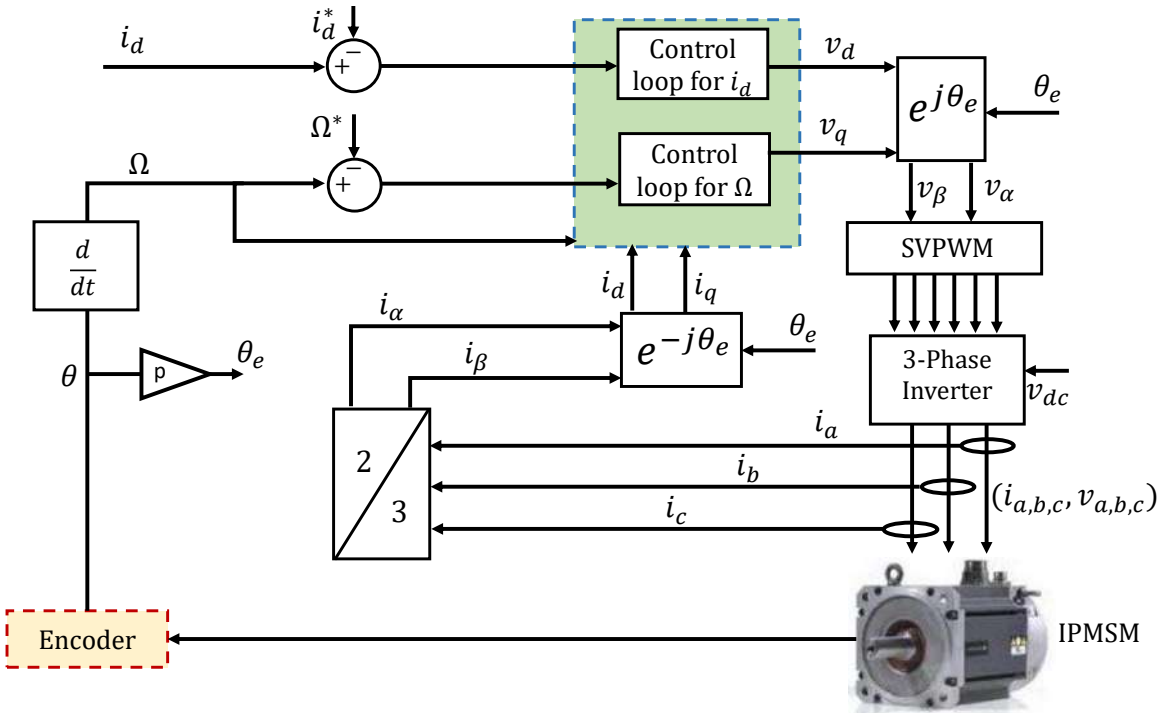

Figure 1 – Control of an electric motor by using encoder

Interior permanent magnet synchronous motor (IPMSM) is the most popular in the fields of electric drive application due to torque capability, power density, simple structure, efficiency and can operate in high speeds [5]. In variable speed motor drives, speed controllers are applied by using encoders [6]. This devices can measure angular position

and with this information, the speed can be extracted [7]–[10], as can be seen in Figure 1. However, implementing encoders to control the electric motor requires additional electronics, preventative maintenance, and additional wiring. For these reasons, this technique has become less attractive due to high cost and lower reliability, encouraging researchers to avoid its implementation and study the sensorless strategy. Nowadays, sensorless strategy is an indirect technique under development to estimate angular position from measurable currents and voltages of the IPMSM, increasing robustness and reliability, eliminating wiring, and reducing signal noise [11]–[13]. In Figure 2, a general structure for sensorless case is shown. In the literature, various approaches to the sensorless technique have been

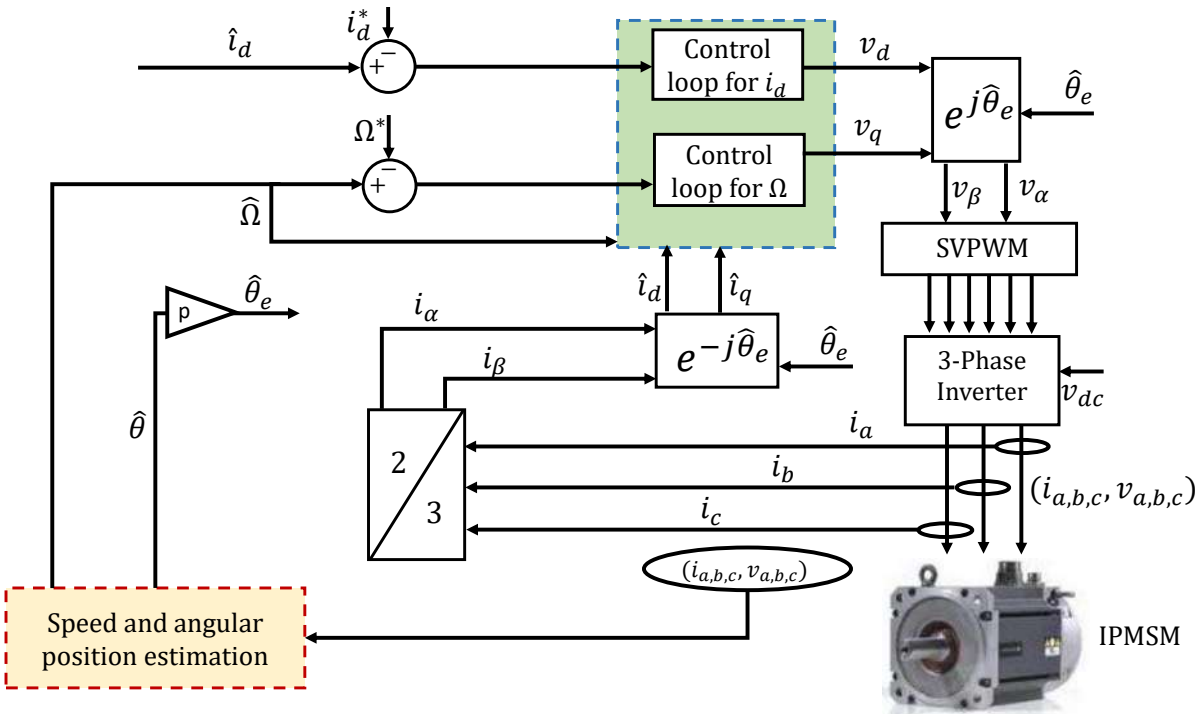

Figure 2 – Control of an electric motor without the use of an encoder (sensorless case)

addressed. Among sensorless control methods, model-based method and saliency-based method are the most popular.

Model-based method for sensorless control

According to model-based method, this method is applied in high and medium speed regions; and rotor position is acquired from the stator voltages and currents without requiring additional high frequency signal injection. Back-electromotive force (EMF)-based

technique [14]–[17] is commonly applied in this method. Considering that back-EMF induced in motor is directly proportional to rotor speed, with this information is possible effectively estimate the rotor position [18]. Several observers based on the dynamical model of the electrical motor have been used for estimating angular position, for example, Luenberger observer [19], [20], extended Kalman filter (EKF)[21], [22] and sliding mode observer [23], [24]. However, being that the model-based approach has a direct dependency on the dynamical model, parametric uncertainties can lead to performance degradation of control systems. It is known that parameters vary depending on operation conditions, e.g., mechanical parameters, viscous coefficient and inertia, could vary according to the applied load torque, weight, road type and tires quality in automotive applications; and electrical parameters, inductance and resistance, could vary depending on the temperature variations or magnetic circuit saturation.

An alternative to overcome this challenge is the development of algorithms for online or offline parameter identification. Among offline algorithms for parameter estimation can be found the DC Current Decay Test [25], [26] and the AC standstill method [27], [28] to measure inductances. However, there are disadvantages with these strategies due to the fact that it requires additional equipment and the measurement errors are caused by the estimation at a single operating point. Now, among online parameter estimation techniques, recursive least square is a technique that uses known variables as currents and voltages to estimate unknown parameters, for instance, in [29] has been proposed a strategy to identify stator resistance, machine torque and inductances. Similarly, EKF is an optimal recursive estimator that considers the effects of the measurement noise, for instance, in [30] has been proposed a permanent magnet flux identification technique of the IPMSM. Other methods for online parameter estimation are given in [31]–[33] in order to constantly update the machine parameters. However, a highly efficient microprocessor is required to handle the relatively complex procedure.

Another alternative to overcome the challenge of parametric uncertainties is the use of robust techniques. A technique that has been widely studied in recent decades is sliding modes proposed by [34]. Its main advantage is its robustness against disturbances and parametric uncertainties. This technique has found wide application in different areas such as fault reconstruction, condition monitoring and fault detection [35]. Classical sliding mode technique has been adopted in electrical machines for the angular position estimation, for instance [36]. However, the main drawback of this strategy is the chattering caused by the switching (discontinuity) of the signum function, generating high-frequency

oscillation components in the estimated signal of the sliding mode observer (SMO). Then, low-pass filters are often used, causing phase delay, such that classical sliding mode is not a good alternative. One option to reduce the chattering phenomenon is to replaced the signum function by a sigmoid function [37], [38], showing relatively a good performance. Similarly, the popular super twisting [39] and high-order sliding mode techniques [40] have achieved a clear improvement in the chattering reduction as well as good performance and finite-time convergence in presence of disturbances and uncertainties. In [41], a high order terminal SMO is proposed in order to achieve finite time convergence of the estimated states and chattering suppression. In [42], a third order super-twisting extended state observer is designed to improve the estimation of angular position, speed and disturbance of IPMSM; achieving a fast convergence. On the other side, in [14], a super-twisting sliding-mode observer with online stator resistance, position and speed estimation for sensorless control is proposed. However, during observer tuning, choosing constant gains in the observer sometimes results in an overestimation of gains that causes chattering, increasing the error in the estimates. Adaptive observers have been proposed in order to avoid this overestimation and reduce the chattering. For instance, in [43] is addressed an adaptive super twisting for online tuning according to the perturbation value, such that, angular position error is reduced in a wide-speed range. In [44], an adaptive super-twisting sliding mode observer with time-varying gains is introduced, to minimize the chattering and estimate back-EMF that is required for the angular position estimation. Another strategies are addressed in [45], [46]. However, these approaches need to choose several parameters to tune the system, increasing the tuning time.

In summary, the main drawback of the model-based methods is the loss of observability at low speeds due to the fact that there is a direct dependency of the back-EMF with speed rotor, i.e., the magnitude of the back-EMF decreases proportionally with the speed.

Saliency-based method for sensorless control

As previously mentioned, model-based angular position estimation is possible at high and medium speed. However, it can fail at low and zero speed. Therefore, saliency-based methods are an alternative to achieve this challenge. In saliency-based methods a sufficient excitation, either by high frequency (HF) voltage or current signal injection or by using pulsewidth-modulated (PWM) inverter switching, is mandatory in order to maintain a persistent excitation in the system to extract angular position information and estimate

the angular position at low and zero speed [47]–[50].

Voltage injection techniques can be classified according to the shape of the test signal: sine or square wave injection techniques. In addition, one can distinguish between rotating and pulsing test signal injection. For the HF rotary signal injection scheme, a balanced voltage signal is injected into the stationary reference frame to form a rotary excitation that is superimposed on the fundamental excitation. Then, by applying a synchronous reference frame filter, the negative sequence carrier current containing the position information can be derived and used to estimate the rotor position. For pulsed signal injection methods, a pulsed HF carrier signal is injected on the d-axis or q-axis in the estimated synchronous reference frame, such that, the angular position can be estimated by minimizing the amplitude modulated carrier current response that is measured along the axis orthogonal to the injection axis [51]–[55]. However, the performance of sensorless control with the conventional HF pulsed or rotating sinusoidal signal is still insufficient for some applications, as the filtering process limits the dynamic bandwidths.

To overcome the limitations of sensorless control with conventional sinusoidal signal injection, square wave injection in the stationary reference frame or in the estimated rotor reference frame has been developed. The injection frequency can be increased to the PWM switching frequency, and thus the filtering process can be eliminated and the dynamic performance can be improved [56]–[61].

Nevertheless, in saliency-based methods, additional losses and audible noise are negative effects caused by injected signal reducing the system performance. Reducing the amplitude of the signal could be an option to remove the disadvantages. However, this would cause a degradation in the estimation of the angular position. In order to overcome these disadvantages, a new alternative has been presented in [62] to improve the performance. Nevertheless, the use of saliency-based methods is still limited.

Control techniques for speed regulation

Now, regarding speed controls used in electrical machines, several nonlinear control methods have been applied to enhance the control performance in presence of uncertainties and disturbances, for instance, in [45], [63] were proposed robust backstepping controllers with integral and sliding mode actions to achieve speed regulation despite uncertainties and disturbances. A robust control has been proposed in [64], and sliding mode controls in [65]–[67].

As previously mentioned, sliding mode technique is one of the most studied techniques in recent years due to robustness against disturbances and uncertainties. Nevertheless, just like observers, controllers based on sliding mode have chattering problems and overestimation of gains. Therefore, adaptive laws for sliding mode controllers of the motor have been proposed to remove these drawbacks [68]–[70]. Some adaptive laws have also been proposed in a general way for the sliding mode control. For instance in [71], an adaptive super-twisting control is proposed, removing the requirement to know the upper bounds of external disturbance and reducing the chattering phenomenon without affecting the control performance. In [72], the chattering problem and its relation with the high activity of control action have been studied. In this way, an adaptive law is developed to get a minimum possible value of control. Another proposal was introduced in [73], offering continuous control signal, adaptation for dealing with unknown uncertainty/perturbations, non-overestimation of control gains, and reduced chattering. In [74], adaptive gains have been proposed for a super-twisting control in order to adapt in such a way that the gains are as small as possible, and yet large enough to sustain a sliding motion. Nonetheless, due to large number of control gain parameters, tuning these strategies could be complex.

Contributions in this work

In this work, the main contributions are the following:

— An extraction of the angular error $(\theta - \hat{\theta})$ is made, and based on a virtual system without parameters of the IPMSM, two Adaptive High-Order Sliding Mode Observers (AHOSMOs) are designed to estimate angular position, speed and acceleration over a wide speed range. The robustness is improved, overcoming the disadvantages of other methods (model-based and saliency-based methods) that require knowledge of the machine parameters, use of filters as well as high-frequency signal injection to estimate angular position.

— Two Adaptive Super-Twisting Controllers (ASTWCs) are designed in order to track a desired speed reference and a desired d-axis current reference. These controller are interconnected with the AHOSMO achieving a sensorless control strategy.

— The gains for both, controllers and observers, are reparameterized in terms of a single parameter. The main advantage of this strategy is that adaptive laws are easy to implement, which avoids overestimation of gains that increases chattering, reduces time to adjust gains, and reduces damage to actuators.

— Closed-loop stability analysis under the action of the observer is improved thanks to it is simpler to analyse and the separation principle holds.

Thesis organization

This manuscript is organized as follows:

Chapter 1

In the chapter 1, an introduction to the PMSM is given. The different configurations for PMSM according to permanent magnet position is addressed. After that, the Park an Concordia transformation are introduced. From these transformation, the electrical equations of the PMSM can be used to compute the dynamical model of the IPMSM in a $\alpha\beta$ stationary reference frame and in a dq synchronous reference frame. Moreover, the thesis problem statement and benchmark for the observers and the controllers are presented, the benchmark will be used in simulation and experimentation. In addition, a specific benchmark is presented and will be used to show the performance of the observer in different operation point.

Chapter 2

In the chapter 2, a method for the extraction of the angular position estimation error in PMSM is presented. This information can be extracted by using α, β currents, i.e., the dynamical model of the electrical machine is not used. Then, considering the extraction of the angular error and a virtual system without machine parameters, the design of two Adaptive High Order Sliding Mode Observers are addressed to estimate angular position, speed and acceleration. The gains of the observers have been reparameterized in terms of a single parameter facilitating the design of an adaptive law for each observer. Simulation tests of the proposed observers and a comparative study are carried out.

Chapter 3

In the chapter 3, the design of two Adaptive Super-Twisting Controllers is introduced. These controllers have been designed considering reparameterized gains in terms of a single parameter. It has allowed to design an adaptive law for each control, which reduces time to adjust gains and avoids overestimation of gains that can increase chattering. Moreover, a stability analysis based on Lyapunov approach is given. After that, the proposed controllers are evaluated under simulation tests. In addition, a comparative study is carried out considering constant gains and adaptive gains.

Chapter 4

From the angular position estimation error extraction, the proposed observers in chapter 2 are able to estimate the angular position and speed. These estimates will be interconnected with the proposed controllers presented in chapter 3. Therefore, in chapter 4 is presented the sensorless control scheme. The stability analysis in closed-loop under the estimates of the observer is introduced. Finally, simulation and experimental tests are carried out in order to show the performance and effectiveness of the proposed schemes.

Chapter 5

Finally, a general conclusion about the proposed work is addressed. Moreover, some perspectives for this work are introduced.

Publications

In this thesis, different publications have been accepted or submitted in indexed journals and scientific conferences.

Journal papers

— E. Alvaro-Mendoza, J. De-Leon Morales, M. A. Hamida, M. Ghanes. (2022). Angular position estimation error extraction for speed and angular position estimation of IPMSM using a parameter-free adaptive observer. Journal of The Franklin Institute, 359(13), 7140-7164.

— E. Alvaro-Mendoza, J. De León-Morales, O. Salas-Peña. (2021). State and parameter estimation for a class of nonlinear systems based on sliding mode approach. ISA transactions, 112, 99-107.

— E. Alvaro-Mendoza, O. Salas-Peña, J. De León-Morales. (2022). Sensorless control scheme based on sliding modes for interior permanent magnet synchronous motor. Proceedings of the Institution of Mechanical Engineers, Part I: Journal of Systems and Control Engineering, 236(2), 227-243.

— E. Alvaro-Mendoza, J. De-Leon Morales, M. A. Hamida, M. Ghanes, Adaptive sensorless control for interior permanent magnet synchronous machine based on sliding mode approach, ISA Transactions. (Under review: 2nd review)

Conference papers

— E. Alvaro-Mendoza, J. De León-Morales, M. A. Hamida and M. Ghanes. (2021, October). A novel approach to extract the angular position estimation error for position and speed estimation of Interior Permanent Magnet Synchronous Machine. In IECON 2021–47th Annual Conference of the IEEE Industrial Electronics Society (pp. 1-6). IEEE.

— E. Alvaro-Mendoza, J. De León-Morales, M. A. Hamida and M. Ghanes. (2022, August). Sensorless control of an interior permanent magnet synchronous motor based on an adaptive sliding mode observer using position error extraction method. In 2022 IEEE Conference on Control Technology and Applications (CCTA) (pp. 956-961). IEEE.

— E. Alvaro-Mendoza, M. A. Hamida J. De León-Morales and M. Ghanes. (2022, September). Application of a sensorless control based on sliding mode in permanent magnet synchronous machine using an angular error extraction. In 2022 16th International Workshop on Variable Structure Systems (VSS) (pp. 141-146). IEEE.

Chapter 1

Dynamical model of Interior Permanent Magnet Synchronous Motor

In this chapter, a summary of the PMSM is addressed. Second, the Concordia and Park transformations are recalled. From these transformations, the dynamical model of the IPMSM in a $\alpha\beta$ stationary reference frame and a dq synchronous reference frame can be calculated. Subsequently, the problem statement of this thesis is introduced and, finally, the benchmark used for simulation and experimental tests is addressed.

1.1 Permanent magnet synchronous motor

The PMSM control system has attracted much attention in the field of AC adjustable speed drives with the rapid development of automatic control technology, power electronics, high-speed microprocessors, sensors, special converters, and permanent magnetic materials. Until recently, the widespread use of PMSM was in some cases restrained by relatively high prices for magnetic materials with high specific magnetic energy values. However, in recent years, prices for such materials have significantly decreased. This may imply future growth of PMSM drive systems in the industry and technology. The reason are their indisputable advantages, such as a high efficiency factor, low noise emissions, simple construction, easy maintenance and low rotor inertia. Then, they are widely used in household appliances, transportation, aviation and robotics [12], [13], [75].

Now, according to the operation and configuration of the PMSM, it has a speed of rotation directly proportional to the frequency of the alternating current network that feeds it. The stator has a three-phase wound, represented by the axes a, b, c, with 120° degree phase difference between them. The rotor produces a magnetic field with the permanent magnets, this removes the need of a DC source to generate it. Then, according

to the configuration of the permanent magnets in the rotor, there exists a classification of PMSM and this is given as follows.

a) Surface permanent magnet synchronous motor

In this type of motors the magnets are placed on the surface of the rotor, as shown in Figure 1.1. The inductances of this type of motor do not depend on the position of the rotor. This type of motor has $d-$axis inductance equal to $q-$axis inductance, such that the reluctance torque generated by the motor is zero. In this motor, the magnets are on the surface and are exposed to a demagnetizing field. Furthermore, the relative permeability of permanent magnets is similar to that of air, which leads to a low inductance of the machine, since the effective length of the air gap is large. The air gap reluctance is theoretically constant for the different positions of the rotor, then, the starting torque of the surface permanent magnet machine is low. In addition, the magnets are subject to centrifugal forces, which can cause the magnets in the rotor to detach.

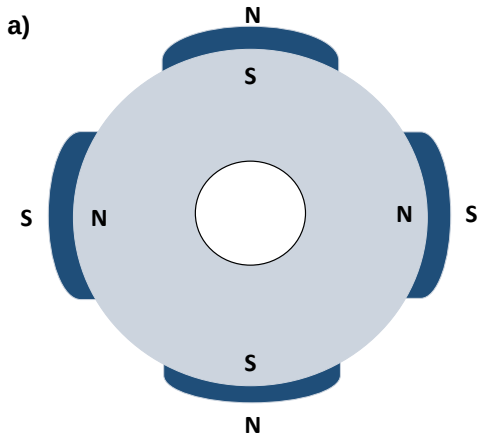

Figure 1.1 – PMSM rotor permanent magnets layout: a) Surface permanent magnets.

b) Inset permanent-magnet synchronous motor

In this type of motor, the magnets are inserted on the surface of the rotor as shown in Figure 1.2, and d-axis inductance is slightly different from q-axis inductance. The iron parts between the permanent magnets have interpolar spaces that add saliency. The value of this salience depends on the height of the magnets relative to the iron and the aperture of the magnets.

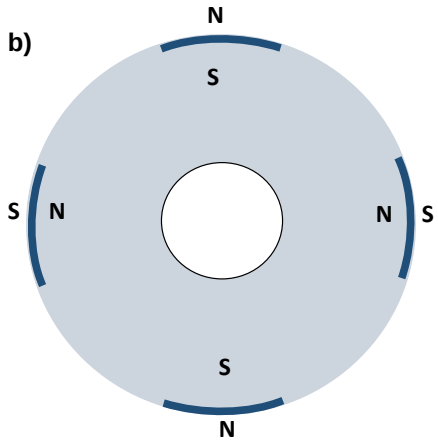

Figure 1.2 – PMSM rotor permanent magnets layout: b) Inset permanent magnets.

c) Permanent magnet synchronous motor with flux concentration

In this type of motor, the magnets are located inside the rotor as can be seen in Figure 1.3. The magnets are placed radially into the rotor and buried deep inside the rotor. In this configuration, the magnets are in the directions of the circumference. The magnetic poles are then formed at the level of the ferromagnetic parts of the rotor by concentrating the flux coming from the permanent magnets. One of the main advantages of this type of PMSM is the concentration of the flux generated by the magnets and a higher inductance is obtained. Just like interior magnet machines, in this machine, the magnets are also well protected against demagnetization and mechanical stress. The synchronous reactance on the q axis is greater than on the d axis.

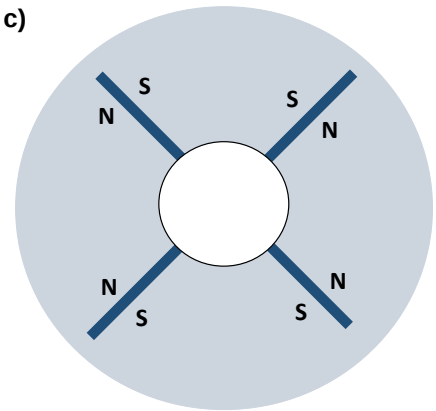

Figure 1.3 – PMSM rotor permanent magnets layout: c) Flux concentrating.

d) Interior permanent-magnet synchronous motor

The IPMSM has the magnets integrated inside the rotor as can be seen in Figure 1.4, to protect the permanent magnets in deflux mode or in case of short circuit and improve the mechanical resistance. With interior magnets, the active air gap space is less than that of the equivalente machine with surface magnets. The d-axis and q-axis inductances of the IPMSM are different, $L_d < L_q$. Therefore, there is the reluctance torque, and the torque density can be higher than the equivalent surface permanent magnet machine. Due to that the magnets are internal and effectively shielded from the armature reaction field, the interior magnet machine is suitable for applications with constant power over a wide speed range. Moreover, the IPMSM inductances values change according to the rotor position and create a geometric saliency which is an important feature for low speed control.

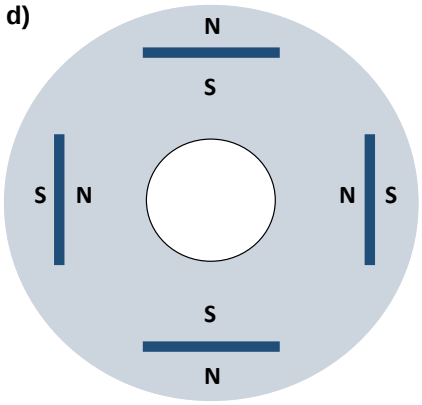

Figure 1.4 – PMSM rotor permanent magnets layout: d) Interior permanent magnets.

The work carried out in this document addresses the case of the IPMSM, since its configuration is recommended due to its torque capacity, power density, simple structure, efficiency and can operate at high speeds. Moreover, considering that the values of the inductances change according to the position of the rotor and create geometric saliency, this is an important feature for low speed operation.

1.2 Concordia and Park transformations

Concordia and Park transformations are coordinate changes used to change a balanced three-phase system to an equivalent system with two orthogonal axes. It can be used to

simplify the study of electric motors.

Concordia transformation

The Concordia transformation is employed to simplify the analysis of three-phase system (a, b, c) in a coordinates system (α, β) as follows.

$$\begin{bmatrix} x_\alpha \\ x_\beta \\ x_o \end{bmatrix} = \mathbb{Q}_o^T \begin{bmatrix} x_a \\ x_b \\ x_c \end{bmatrix} \tag{1.1}$$

where $\mathbb{Q}_o$ is given by

$$\mathbb{Q}_o = \sqrt{\frac{2}{3}} \begin{bmatrix} 1 & 0 & \frac{1}{\sqrt{2}} \\ -\frac{1}{2} & \frac{\sqrt{3}}{2} & \frac{1}{\sqrt{2}} \\ -\frac{1}{2} & -\frac{\sqrt{3}}{2} & \frac{1}{\sqrt{2}} \end{bmatrix} \tag{1.2}$$

Moreover, this transformation has direct and inverse transform symmetry and can preserve the active and reactive powers. Since in a balanced system $x_a + x_b + x_c = 0$ and thus $x_o = 0$, then one can also consider the simplified transformation

$$\begin{bmatrix} x_\alpha \\ x_\beta \end{bmatrix} = \mathbb{Q}^T \begin{bmatrix} x_a \\ x_b \\ x_c \end{bmatrix} \tag{1.3}$$

which is simply the original Concordia transformation with the 3rd equation excluded, where $\mathbb{Q}$ is expressed as follows

$$\mathbb{Q} = \sqrt{\frac{2}{3}} \begin{bmatrix} 1 & 0 \\ -\frac{1}{2} & \frac{\sqrt{3}}{2} \\ -\frac{1}{2} & -\frac{\sqrt{3}}{2} \end{bmatrix} \tag{1.4}$$

In Figure 1.5, the representation of the concordia transformation is illustrated, where θ_e represents the angular position and the x_α and x_β components represent the coordinates of the rotating space vector x_R in a fixed reference frame whose $\alpha-$axis is aligned with phase x_a axis.

Park transformation

The Park transformation transforms the components$-\alpha\beta$ to reference system$-dq$, the objective of this transformation is to convert the variables sinusoidally in time to constant values dq, in permanent regime.

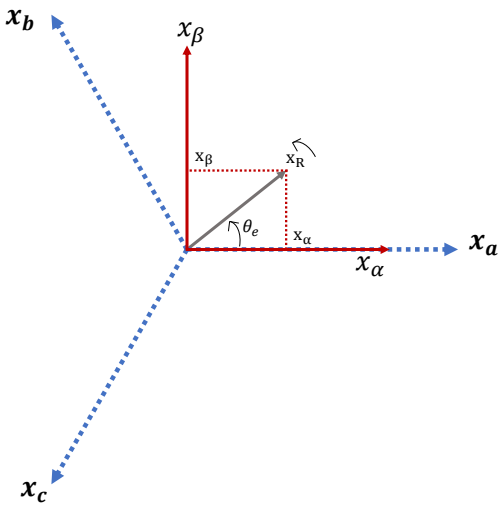

Figure 1.5 – Concordia transformation

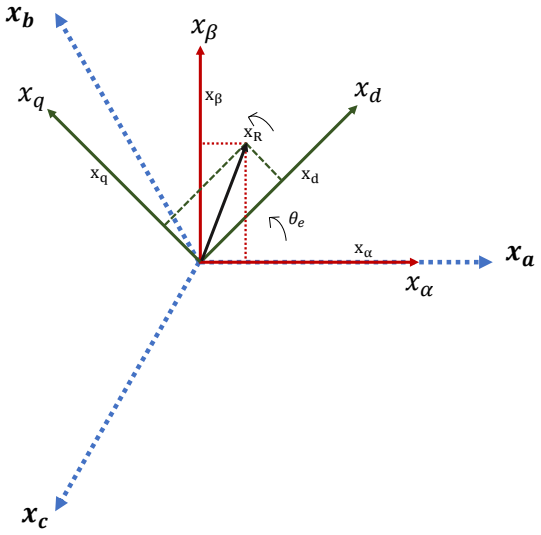

Figure 1.6 – Park transformation

$$\begin{bmatrix} x_d \\ x_q \end{bmatrix} = \mathbb{T}^T \begin{bmatrix} x_\alpha \\ x_\beta \end{bmatrix} \tag{1.5}$$

where $\mathbb{T}$ is given by

$$\mathbb{T} = \begin{bmatrix} cos(\theta_e) & -sin(\theta_e) \\ sin(\theta_e) & cos(\theta_e) \end{bmatrix} = e^{j\theta_e} \tag{1.6}$$

In Figure 1.6, the representation of the Park transformation is illustrated.

1.3 Electrical equations of the Permanent Magnet Synchronous Motor

The three-phase stator voltage equations, represented in the three-phase stationary frame ($abc - axes$), can be expressed as follows

$$v_{abc} = R_s i_{abc} + \frac{d\psi_{abc}}{dt} \tag{1.7}$$

where $v_{abc} = \begin{bmatrix} v_a & v_b & v_c \end{bmatrix}^T$ represents stator voltages, R_s is stator resistance, $i_{abc} = \begin{bmatrix} i_a & i_b & i_c \end{bmatrix}^T$ represents stator currents and $\psi_{abc} = \begin{bmatrix} \psi_a & \psi_b & \psi_c \end{bmatrix}^T$ represents stator fluxes. Moreover, ψ_{abc} is defined as follows

$$\psi_{abc} = \mathbb{L}_{ss} \begin{bmatrix} i_a \\ i_b \\ i_c \end{bmatrix} + \begin{bmatrix} \psi_{af} \\ \psi_{bf} \\ \psi_{cf} \end{bmatrix} \tag{1.8}$$

where

$$\begin{bmatrix} \psi_{af} \\ \psi_{bf} \\ \psi_{cf} \end{bmatrix} = \psi_r \begin{bmatrix} cos\,(p\theta) \\ cos\left(p\theta - \frac{2\pi}{3}\right) \\ cos\left(p\theta + \frac{2\pi}{3}\right) \end{bmatrix} \tag{1.9}$$

and p represents the number of poles, θ the mechanical angular position, ψ_r is the permanent-magnet flux linkage and $\mathbb{L}_{ss}$ is expressed as follows

$$\mathbb{L}_{ss} = \mathbb{L}_{so} + \mathbb{L}_{sv} \tag{1.10}$$

where

$$\mathbb{L}_{so} = \begin{bmatrix} L_{so} & M_{so} & M_{so} \\ M_{so} & L_{so} & M_{so} \\ M_{so} & M_{so} & L_{so} \end{bmatrix} \tag{1.11}$$

and

$$\mathbb{L}_{sv} = L_{sv} \begin{bmatrix} cos\,(2p\theta) & cos\left(2p\theta - \frac{2\pi}{3}\right) & cos\left(2p\theta + \frac{2\pi}{3}\right) \\ cos\left(2p\theta - \frac{2\pi}{3}\right) & cos\left(2p\theta + \frac{2\pi}{3}\right) & cos\,(2p\theta) \\ cos\left(2p\theta + \frac{2\pi}{3}\right) & cos\,(2p\theta) & cos\left(2p\theta - \frac{2\pi}{3}\right) \end{bmatrix} \tag{1.12}$$

defining M_{so}, L_{so} and L_{sv} as the mutual and own inductances, respectively; for $M_{so} = -\frac{1}{2}L_{so}$. Moreover, L_{so} and L_{sv} are positive parameters depending on the machine.

Now, the system (1.7) can be written as follow

$$\begin{bmatrix} v_a \\ v_b \\ v_c \end{bmatrix} = R_s \begin{bmatrix} i_a \\ i_b \\ i_c \end{bmatrix} + \frac{d}{dt} \left\{ [\mathbb{L}_{ss}] \begin{bmatrix} i_a \\ i_b \\ i_c \end{bmatrix} + \begin{bmatrix} \psi_{af} \\ \psi_{bf} \\ \psi_{cf} \end{bmatrix} \right\} \tag{1.13}$$

and considering the Concordia transformation (1.3), the system (1.7) expressed in $\alpha\beta$ stationary reference frame is the following

$$\begin{bmatrix} v_\alpha \\ v_\beta \end{bmatrix} = R_s \begin{bmatrix} i_\alpha \\ i_\beta \end{bmatrix} + \frac{d}{dt} \begin{bmatrix} \psi_\alpha \\ \psi_\beta \end{bmatrix} \tag{1.14}$$

1.3.1 Dynamical model of the Interior Permanent Magnet Synchronous Motor in dq synchronous reference frame

In this section, the dynamical model of the IPMSM is introduced. Then, from the three-phase stator voltage equations in a three-phase stationary frame ($abc - axes$) given by

$$v_{abc} = R_s \quad i_{abc} + \frac{d}{dt} \{\mathbb{L}_{ss} \quad i_{abc} + \psi_{afbfcf}\} \tag{1.15}$$

the following equation can be written

$$v_{abc} = R_s i_{abc} + \frac{d}{dt} \{\mathbb{L}_{ss} i_{abc}\} + \frac{d}{dt} \{\psi_{afbfcf}\} \tag{1.16}$$

where

$$\frac{d}{dt}\left\{\psi_{afbfcf}\right\} = \frac{d}{dt}\begin{bmatrix}\psi_{af}\\ \psi_{bf}\\ \psi_{cf}\end{bmatrix} = -\psi_r p\Omega \begin{bmatrix} sin\left(p\theta\right)\\ sin\left(p\theta - \frac{2\pi}{3}\right)\\ sin\left(p\theta + \frac{2\pi}{3}\right)\end{bmatrix} \tag{1.17}$$

and Ω represents the mechanical speed. Then, replacing (1.17) in (1.16), the following equation is obtained

$$\begin{bmatrix}v_a\\ v_b\\ v_c\end{bmatrix} = R_s\begin{bmatrix}i_a\\ i_b\\ i_c\end{bmatrix} + \frac{d}{dt}\left\{\mathbb{L}_{ss}\begin{bmatrix}i_a\\ i_b\\ i_c\end{bmatrix}\right\} - \psi_r p\Omega \begin{bmatrix} sin\left(p\theta\right)\\ sin\left(p\theta - \frac{2\pi}{3}\right)\\ sin\left(p\theta + \frac{2\pi}{3}\right)\end{bmatrix} \tag{1.18}$$

Now, taking into account the following transformation

$$\begin{bmatrix}x_d\\ x_q\end{bmatrix} = \mathbb{T}^T\mathbb{Q}^T\begin{bmatrix}x_a\\ x_b\\ x_c\end{bmatrix} \tag{1.19}$$

where x represents a variable (voltage, current or flux). Then, combining (1.19) with (1.18) and multiplying the left side of (1.19) by $\mathbb{QT}$, the following system is obtained

$$\begin{aligned}\mathbb{QTT}^T\mathbb{Q}^T\begin{bmatrix}v_a\\ v_b\\ v_c\end{bmatrix} =& R_s\mathbb{QTT}^T\mathbb{Q}^T\begin{bmatrix}i_a\\ i_b\\ i_c\end{bmatrix} + \frac{d}{dt}\left\{\mathbb{L}_{ss}\mathbb{QTT}^T\mathbb{Q}^T\begin{bmatrix}i_a\\ i_b\\ i_c\end{bmatrix}\right\}\\ &- \psi_r p\Omega\mathbb{QTT}^T\mathbb{Q}^T\begin{bmatrix} sin\left(p\theta\right)\\ sin\left(p\theta - \frac{2\pi}{3}\right)\\ sin\left(p\theta + \frac{2\pi}{3}\right)\end{bmatrix}\end{aligned} \tag{1.20}$$

such that

$$\mathbb{QT}\begin{bmatrix}v_d\\ v_q\end{bmatrix} = R_s\mathbb{QT}\begin{bmatrix}i_d\\ i_q\end{bmatrix} + \frac{d}{dt}\left\{\mathbb{L}_{ss}\mathbb{QT}\begin{bmatrix}i_d\\ i_q\end{bmatrix}\right\} + \mathbb{QT}\begin{bmatrix}0\\ \psi_r p\Omega\end{bmatrix} \tag{1.21}$$

Consider that $\mathbb{Q}^T\mathbb{Q} = I_{2\times 2}$ and $\mathbb{T}^T\mathbb{T} = I_{2\times 2}$, where $I_{2\times 2}$ is a identity. Then, multiplying the left side of above equation by $\mathbb{T}^T\mathbb{Q}^T$, it follows that

$$\begin{bmatrix}v_d\\ v_q\end{bmatrix} = R_s\begin{bmatrix}i_d\\ i_q\end{bmatrix} + \mathbb{T}^T\mathbb{Q}^T\frac{d}{dt}\left\{\mathbb{L}_{ss}\mathbb{QT}\begin{bmatrix}i_d\\ i_q\end{bmatrix}\right\} + \begin{bmatrix}0\\ \psi_r p\Omega\end{bmatrix} \tag{1.22}$$

and can be rewritten as follows

$$\begin{bmatrix} v_d \\ v_q \end{bmatrix} = R_s \begin{bmatrix} i_d \\ i_q \end{bmatrix} + \mathbb{T}^T \frac{d}{dt} \{\Gamma_{ss} \mathbb{T}\} \begin{bmatrix} i_d \\ i_q \end{bmatrix} + \mathbb{T}^T \Gamma_{ss} \mathbb{T} \frac{d}{dt} \begin{bmatrix} i_d \\ i_q \end{bmatrix} + \begin{bmatrix} 0 \\ \psi_r p\Omega \end{bmatrix} \tag{1.23}$$

where

$$\Gamma_{ss} = \mathbb{Q}\mathbb{L}_{ss}\mathbb{Q} = \frac{3}{2} L_{sv} \begin{bmatrix} cos\,(2p\theta) & sin\,(2p\theta) \\ sin\,(2p\theta) & -cos\,(2p\theta) \end{bmatrix} + \frac{3}{2} L_{so} \begin{bmatrix} 1 & 0 \\ 0 & 1 \end{bmatrix} \tag{1.24}$$

Now, L_{so} and L_{sv} are defined as follows

$$L_{so} = \frac{L_d + L_q}{3} \qquad L_{sv} = \frac{L_d - L_q}{3} \tag{1.25}$$

where L_d and L_q are the $dq-$axes winding inductance. Therefore, Γ_{ss} given by (1.24) can be expressed by

$$\Gamma_{ss} = \frac{L_d - L_q}{2} \begin{bmatrix} cos\,(2p\theta) & sin\,(2p\theta) \\ sin\,(2p\theta) & -cos\,(2p\theta) \end{bmatrix} + \frac{L_d + L_q}{2} \begin{bmatrix} 1 & 0 \\ 0 & 1 \end{bmatrix} = \begin{bmatrix} L_\alpha & L_{\alpha\beta} \\ L_{\alpha\beta} & L_\beta \end{bmatrix} \tag{1.26}$$

Then, the solution for $\mathbb{T}\frac{d}{dt}\{\Gamma_{ss}\mathbb{T}\}$ in (1.23) is given by

$$\mathbb{T}\frac{d}{dt}\{\Gamma_{ss}\mathbb{T}\} = p\Omega \begin{bmatrix} 0 & -L_q \\ L_d & 0 \end{bmatrix} \tag{1.27}$$

and the solution for $\mathbb{T}^T\Gamma_{ss}\mathbb{T}$ is given by

$$\mathbb{T}^T\Gamma_{ss}\mathbb{T} = \begin{bmatrix} L_d & 0 \\ 0 & L_q \end{bmatrix} \tag{1.28}$$

Therefore, the system (1.23) expressed in a dq reference frame is given by

$$\begin{bmatrix} v_d \\ v_q \end{bmatrix} = R_s \begin{bmatrix} i_d \\ i_q \end{bmatrix} + p\Omega \begin{bmatrix} 0 & -L_q \\ L_d & 0 \end{bmatrix} \begin{bmatrix} i_d \\ i_q \end{bmatrix} + \begin{bmatrix} L_d & 0 \\ 0 & L_q \end{bmatrix} \frac{d}{dt} \begin{bmatrix} i_d \\ i_q \end{bmatrix} + \begin{bmatrix} 0 \\ \psi_r p\Omega \end{bmatrix} \tag{1.29}$$

Mechanical equations

The equation for the mechanical model is given by

$$\frac{d\theta}{dt} = \Omega \tag{1.30}$$

where θ is mechanical angular position and Ω mechanical speed. Moreover, the following equality is defined as follows

$$J\frac{d\Omega}{dt} + fv\Omega = T_e - T_l \tag{1.31}$$

where J represents the inertia, f_v the viscous friction coefficient, T_l the load torque and T_e the electromagnetic torque. The electromagnetic torque T_e is defined as follows

$$T_e = p(\psi_\alpha i_\beta - \psi_\beta i_\alpha) = p(\psi_d i_q - \psi_q i_d) \tag{1.32}$$

where the terms ψ_d and ψ_q are defined by

$$\psi_d = L_d i_d + \psi_r, \qquad \psi_q = L_q i_q \tag{1.33}$$

Then, the electromagnetic torque can be expressed as follows

$$T_e = p(L_d - L_q) i_d i_q + p\psi_r i_q \tag{1.34}$$

Therefore, the mechanical system for the IPMSM is given by

$$\begin{aligned} \frac{d\theta}{dt} &= \Omega \\ \frac{d\Omega}{dt} &= \frac{p}{J}(L_d - L_q) i_d i_q + \frac{p}{J}\psi_r i_q - \frac{T_l}{J} - \frac{fv\Omega}{J} \end{aligned} \tag{1.35}$$

Dynamic model of the Interior Permanent Magnet Synchronous Motor: Electrical and mechanical equations

The dynamical model of the IPMSM with electrical and mechanical equations is the following

$$\Sigma_{elec} : \begin{cases} \frac{di_d}{dt} &= -\frac{R_s}{L_d} i_d + p\Omega \frac{L_q}{L_d} i_q + \frac{v_d}{L_d} \\ \frac{di_q}{dt} &= -\frac{R_s}{L_q} i_q - p\Omega \frac{L_d}{L_q} i_d + \frac{v_q}{L_q} - p\Omega \frac{\psi_r}{L_q} \end{cases} \tag{1.36}$$

$$\Sigma_{mech} : \begin{cases} \frac{d\theta}{dt} &= \Omega \\ \frac{d\Omega}{dt} &= \frac{p}{J}\left(L_d - L_q\right) i_d i_q + \frac{p}{J}\psi_r i_q - \frac{f_v}{J}\Omega - \frac{1}{J}T_l \end{cases} \tag{1.37}$$

1.3.2 Dynamical model of the Interior Permanent Magnet Synchronous Motor in $\alpha\beta$ stationary reference frame

In this section the dynamical model of the IPMSM in a $\alpha\beta$ stationary reference frame is addressed. Then, transforming (1.29) into $\alpha\beta$ stationary reference frame, the following system is obtained

$$\begin{bmatrix} v_\alpha \\ v_\beta \end{bmatrix} = \begin{bmatrix} R + \frac{d}{dt}L_\alpha & \frac{d}{dt}L_{\alpha\beta} \\ \frac{d}{dt}L_{\alpha\beta} & R + \frac{d}{dt}L_\beta \end{bmatrix} \begin{bmatrix} i_\alpha \\ i_\beta \end{bmatrix} + p\Omega \begin{bmatrix} -sin(\theta_e) \\ cos(\theta_e) \end{bmatrix} \tag{1.38}$$

where $\theta_e = p\theta$ is the electrical angular position and $L_\alpha = L_o + L_1 cos(2\theta_e)$, $L_\beta = L_o - L_1 cos(2\theta_e)$, $L_{\alpha,\beta} = L_1 sin(2\theta_e)$, $L_o = \dfrac{(L_d + L_q)}{2}$ and $L_1 = \dfrac{(L_d - L_q)}{2}$. The system (1.38) can be written in a compact form as follows

$$v_{\alpha\beta} = A_{\alpha\beta} + B_{\alpha\beta} + C_{\alpha\beta} + D_{\alpha\beta} \tag{1.39}$$

where $v_{\alpha\beta} = \begin{bmatrix} v_\alpha & v_\beta \end{bmatrix}^T$, $A_{\alpha\beta} = R_s \begin{bmatrix} i_\alpha & i_\beta \end{bmatrix}^T$

$$B_{\alpha\beta} = \frac{d}{dt}\left\{ L_o \begin{bmatrix} i_\alpha \\ i_\beta \end{bmatrix} \right\}, C_{\alpha\beta} = p\Omega\psi_r \begin{bmatrix} -sin(\theta_e) \\ cos(\theta_e) \end{bmatrix}, D_{\alpha\beta} = \frac{d}{dt}\left\{ L_1 \begin{bmatrix} cos(2\theta_e) & sin(2\theta_e) \\ sin(2\theta_e) & -cos(2\theta_e) \end{bmatrix} \begin{bmatrix} i_\alpha \\ i_\beta \end{bmatrix} \right\}$$

The system structure (1.39) is not easy for mathematical processing, having functions of rotor position θ_e, which makes the equation difficult to solve. An easy way to solve this issue is to use the estimated position $\hat{\theta}_e$ instead of θ_e. This is possible if the amplitude of $D_{\alpha\beta}$ is smaller enough than $C_{\alpha\beta}$, i.e., $|L_1 i_{\alpha,\beta}| << \psi_r$. In fact, the approximation made in (1.38) and (1.39) is based on the assumption that this condition is valid. Then, it is true for motors with relatively small reluctance torque. However, if the motor reluctance torque cannot be neglected, such as the permanent magnet torque, the sensorless estimation could be unstable. On the other side, in (1.39), the system contains the terms $2\theta_e$. The reason why term $2\theta_e$ appears in (1.39) is due to that impedance matrix is asymmetric. Therefore, if the impedance matrix is rewritten symmetrically as

$$\begin{bmatrix} v_d \\ v_q \end{bmatrix} = \begin{bmatrix} R_s + pL_d & -p\Omega L_q \\ p\Omega L_q & R + pL_d \end{bmatrix} \begin{bmatrix} i_d \\ i_q \end{bmatrix} + \begin{bmatrix} 0 \\ (L_d - L_q)(p\Omega i_d - \dot{i}_q) + p\Omega\psi_r \end{bmatrix} \tag{1.40}$$

then, the $\alpha\beta$ stationary reference frame can be written as follows

$$\begin{bmatrix} v_\alpha \\ v_\beta \end{bmatrix} = \begin{bmatrix} R_s + pL_d & p\Omega(L_d - L_q) \\ -p\Omega(L_d - L_q) & R + pL_d \end{bmatrix} \begin{bmatrix} i_\alpha \\ i_\beta \end{bmatrix} + [(L_d - L_q)(p\Omega i_d - \dot{i}_q) + p\Omega\psi_r] \begin{bmatrix} -sin(\theta_e) \\ cos(\theta_e) \end{bmatrix} \tag{1.41}$$

The system (1.41) is a transformation of (1.38) without any approximation. It is a general form of the mathematical model of IPMSM. Moreover, if $L_d = L_q$, the model of the surface permanent magnet synchronous motor is obtained and if $\psi = 0$, it is possible to obtain the synchronous reluctance motor.

1.4 Problem statement

In industrial applications, the control of IPMSM requires the knowledge of the angular position and speed, which usually are not available by measurement. Then, one solution is to estimate angular position and speed by using observers based on model. Frequently, the mathematical model used for control and observer design is given in dq synchronous reference frame (1.36)-(1.37) [45], [76] or in a $\alpha\beta$ stationary reference frame (1.41) [77], [78]. However, parametric uncertainties and external disturbances affect the estimation and they must be considered. Then, one solution to overcome this drawback is to design a robust observer to estimate the angular position and speed of the IPMSM.

In this work, in order to estimate the angular position and overcome the issues caused by the parametric uncertainties present in the model of the IPMSM, an observer based on an angular position estimation error (e_{θ_e}) extraction is considered, using a parameter-free virtual system. Then, a different strategy has been proposed by considering only the measurable signals of the IPMSM, i.e., the currents i_α and i_β, which can be obtained from the *abc* triphasic components of the IPMSM and can be used for extracting the electrical angular position estimation error e_{θ_e}.

Notice that, to overcome the use of the mathematical model of the IPMSM depending on parameters; mechanical angular position and mechanical speed will be estimated by the following parameter free virtual system

$$\frac{d\theta_e}{dt} = \omega, \qquad \frac{d\omega}{dt} = \alpha, \qquad \frac{d\alpha}{dt} = \rho(t) \tag{1.42}$$

where $\theta_e = p\theta$ is the electrical angular position, $\omega = p\Omega$ is the electrical speed, p the number of pole pairs and α is the acceleration, where the time derivative of the acceleration

is equal $\rho(t)$, which is an unknown and bounded function depending on the angular position, speed, currents and parameters. Therefore, from the information of θ_e and ω, it is possible to compute the mechanical angular position $\left(\theta = \frac{\theta_e}{p}\right)$ and the mechanical speed $\left(\Omega = \frac{\omega}{p}\right)$.

It is clear that the mechanical sub-system (1.37) of the IPMSM does not depend on the acceleration, however, to estimate the position and the speed, the mechanical sub-system has been extended including the acceleration in order to improve the estimation of those variables. In other words, the first two equations of (1.42) are enough to have a good estimation with low transient modes. However, with fast dynamics, speed estimation errors could increase due to that its derivative is supposed to be equal to zero. To overcome this problem, the machine acceleration$-\alpha$ is also estimated to achieve a more precise estimation in transient mode. Therefore, the virtual system (1.42) will be used to estimate angular position, speed and acceleration by using an extraction of the angular position estimation error e_{θ_e}.

The main objectives in this work are:

Observation objective: By extracting the electrical angular position estimation error given by

$$e_{\theta_e} = \theta_e - \hat{\theta}_e \tag{1.43}$$

and based on a virtual system, design an adaptive observer to estimate the angular position, speed and acceleration.

Control objective: Design an adaptive control to track a desired speed reference Ω^* and a reference current i_d^*, despite the presence of disturbances.

The sliding mode approach is the strategy that will be used in the observer and control design due to its robustness and finite time convergence. Moreover, in order to reduce the tuning time in the observer and control, the gains will be reparameterized in terms of a single parameter. In addition, adaptive laws will be designed for the observer and control to avoid overestimations of gains that can cause the increase of chattering and damage the system.

1.5 Benchmark

In this section, the benchmark for the IPMSM is introduced. Simulation and experimental tests are going to be evaluated in order to show the performance of the proposed strategies. The parameters of the IPMSM are presented in the Table 1.1.

Table 1.1 – IPMSM nominal parameters

Symbol	Parameter	Value	Unit
R_s	Stator resistance	1.4	ohms
J	Moment of inertia	$7.3e^{-3}$	kg.m^2
p	Number of pole pairs	5	
T_l	Torque	4	N-m
ψ_r	Permanent-magnet flux linkage	0.18	Wb
L_d	d-axis winding inductance	0.0057	H
L_q	q-axis winding inductance	0.0099	H
f_v	Viscous friction coefficient	0.0034	kg-m^2/s

The simulation and experimentation are carried out by using different profiles of load torque and speed, as shown in Figure 1.7.

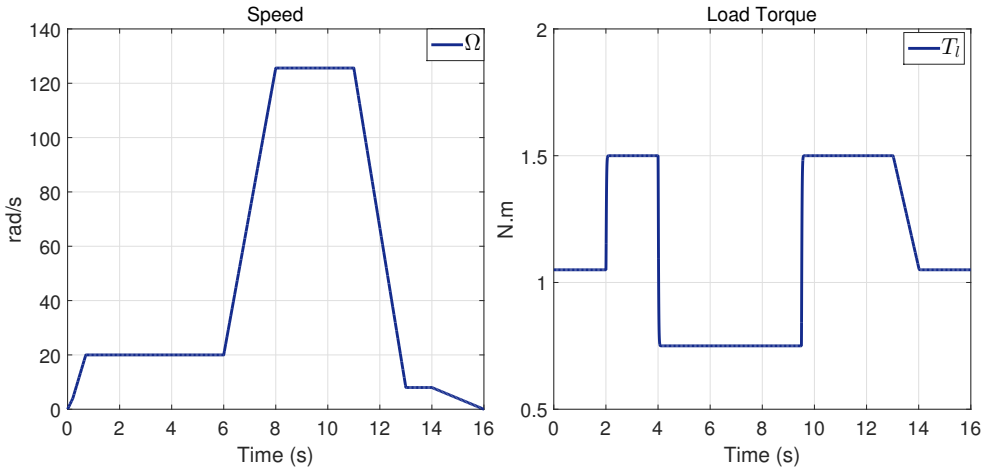

Figure 1.7 – Load torque and speed profiles used during experimental and simulation tests

As mentioned in the introduction, electrical parameters could vary during the operation of the motor due to magnetic saturation or temperature variations; mechanical parameters could vary depending on the load torque, weight, road type and so on. However, since it is not possible to have access to motor parameters experimentally, the experimen-

tal tests are carried out over a large time interval to see the effect of the parameters on the estimation based on a virtual system without parameters. In addition, a simulation test is carried out under resistance, inertia and inductance variations, as shown in Figure 1.8 in order to show the robustness of the proposed strategy. On the other hand, from

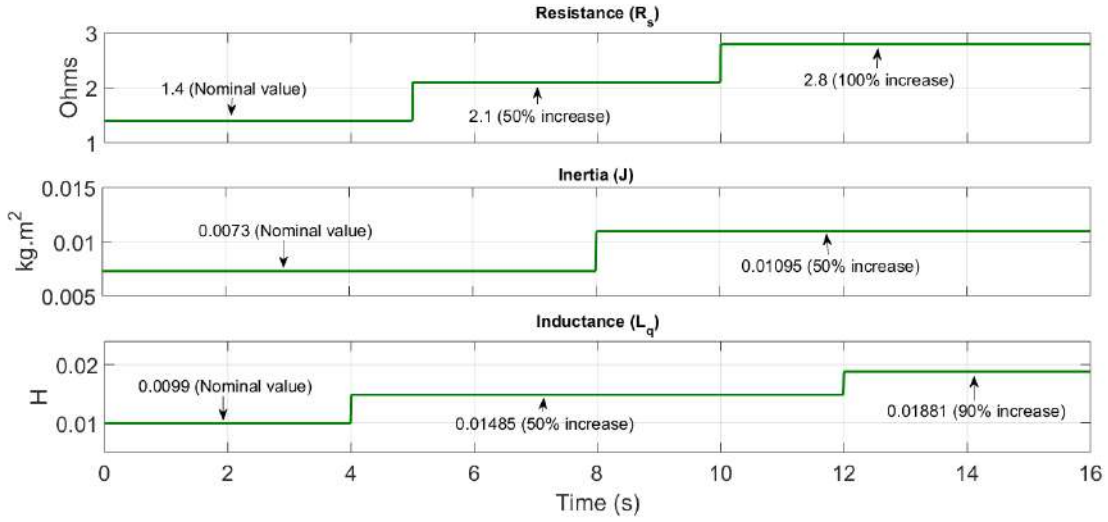

Figure 1.8 – Parameter variations in simulation tests

simulation, the performance and effectiveness of the proposed observer based on the extraction of the angular error e_θ during a time interval of 16 s will be shown by using the profiles of Figure 1.9, at high, low and zero speed, and under different load torque values.

1.5.1 Hardware description

The experimental setup is shown in Figure 1.10 which is composed by an IPMSM rated at 3 kW supplied by a three-phase voltages source inverter. The inverter is powered by 400 V DC voltage. The pulse width modulation (PWM) technique is generated by a dSPACE DS1103 with a switching frequency of 10 kHz. The digital board of dSPACE receives the stator currents and the dc link voltages data with a 10 kHz frequency, and the measured torque data with a 2 kHz frequency. The load torque is generated by a PMSM mechanically coupled with the shaft of the IPMSM, while angular position is measured by encoder. Moreover, a Kalman-filter applied to the measured position is used to calculate the rotor speed.

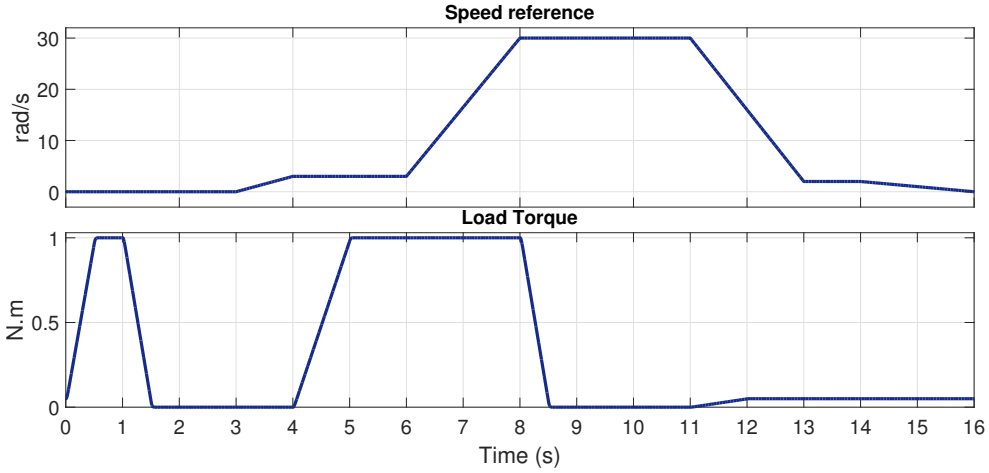

Figure 1.9 – Load torque and speed profiles considering a low-speed region with a very small load torque.

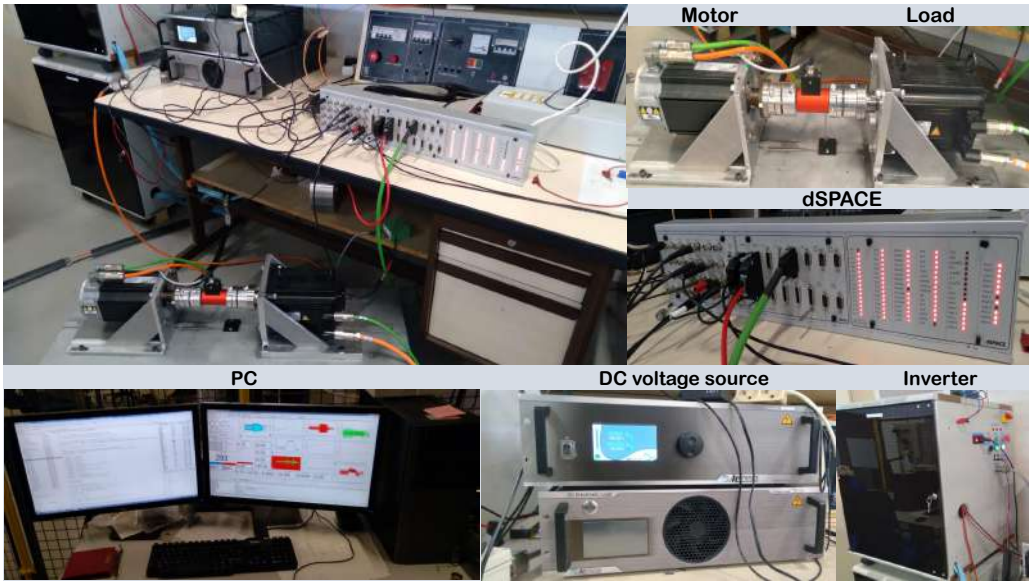

Figure 1.10 – Experimental setup

1.6 Conclusion

The basics of permanent magnets synchronous motor, including their main dynamical models, have been addressed in this chapter. It is well known that these dynamical model depends on parameters as stator resistance, inductance's and so on. Therefore, the use of dynamical models in the design of observer represents a problem as the parameters of the motor vary during the operation. For this reason, a parameter-free virtual system has

been introduced to avoid the parametric uncertainties. The virtual system will be used in the design of observer in the following chapter, taking into account the benchmark presented in this chapter.

Chapter 2

New strategy for the rotor position and speed estimation of Permanent Magnet Synchronous Motor

In this chapter a strategy to extract the angular position estimation error of the PMSM is addressed. After this, two adaptive observers based on sliding mode approach will be introduced. These observer use the information of the angular position estimation error extraction in order to estimate the angular position, speed and acceleration. Furthermore, the observer gains are reparameterized based on a single parameter to simplify the tuning procedure. Some test are addressed for each observer and a comparative study is carried out.

2.1 Extraction of angular position estimation error

A methodology to extract the angular position estimation error (1.43) of PMSM from a $\alpha\beta$ stationary reference frame, is addressed. Then, considering that the currents$-i_{\alpha\beta}$ are measurable and in order to extract e_{θ_e}, consider Park transformation, such that the currents i_d and i_q are expressed as

$$i_{dq} = \quad \mathbb{T}^T(\theta_e) \quad i_{\alpha\beta} \tag{2.1}$$

with

$$i_{dq} = \begin{bmatrix} i_d \\ i_q \end{bmatrix}, \quad \mathbb{T}^T(\theta_e) = \begin{bmatrix} cos(\theta_e) & sin(\theta_e) \\ -sin(\theta_e) & cos(\theta_e) \end{bmatrix}, \quad i_{\alpha\beta} = \begin{bmatrix} i_\alpha \\ i_\beta \end{bmatrix}, \tag{2.2}$$

where currents i_{dq} and angular position θ_e are not measurable. Therefore, considering

that there exists a control law for current-i_d and current-i_d tracks a reference current-i_d^*. Then, in order to extract e_θ, the following equation is introduced

$$\Lambda_{\theta_1} = \quad \mathbb{I}_{qn} - \mathbb{I}_{dn} + i_d^*\sqrt{2} \tag{2.3}$$

and the terms $\mathbb{I}_{dn}$ and $\mathbb{I}_{qn}$ are defined as follows,

$$\mathbb{I}_{dnqn} = \mathbb{M}(\hat{\theta}_e + \phi) \quad \mathbb{T}^{-T}(\theta) \quad i_{dq} \tag{2.4}$$

with $\mathbb{I}_{dnqn} = [\mathbb{I}_{dn} \quad \mathbb{I}_{qn}]^T$ and the transformation matrix $\mathbb{M}(\hat{\theta}_e + \phi)$ expressed as follows

$$\mathbb{M}(\hat{\theta}_e + \phi) = \begin{bmatrix} cos(\hat{\theta}_e + \phi) & sin(\hat{\theta}_e + \phi) \\ -sin(\hat{\theta}_e + \phi) & cos(\hat{\theta}_e + \phi) \end{bmatrix}, \tag{2.5}$$

defining $\hat{\theta}_e$ as the estimated angular position and ϕ is an offset angle that must be chosen appropriately to extract e_{θ_e}. In addition, notice that $(i_d^*, i_{\alpha\beta}, \phi)$ are known values and $\hat{\theta}$ will be computed by using the observer presented later, then

$$\Lambda_{\theta_1} = \Lambda_{\theta_1}(\hat{\theta}_e, i_{\alpha\beta}, i_d^*, \phi) \tag{2.6}$$

can be computed taking into account that

$$\mathbb{T}^{-T}(\theta_e) \quad i_{dq} \quad = \quad i_{\alpha\beta} \quad = \quad \begin{bmatrix} i_\alpha \\ i_\beta \end{bmatrix} \quad = \quad \begin{bmatrix} cos(\theta_e)i_d - sin(\theta_e)i_q \\ sin(\theta_e)i_d + cos(\theta_e)i_q \end{bmatrix} \tag{2.7}$$

Now, from transformation matrix $\mathbb{M}(\hat{\theta}_e + \phi)$, the currents $i_{\alpha\beta}$ can be transformed into alternate synchronous reference frame. Then, the terms $\mathbb{I}_{dn}$ and $\mathbb{I}_{qn}$ are defined as follows

$$\mathbb{I}_{dn} = cos(e_{\theta_e} - \phi)i_d - sin(e_{\theta_e} - \phi)i_q, \qquad \mathbb{I}_{qn} = sin(e_{\theta_e} - \phi)i_d + cos(e_{\theta_e} - \phi)i_q \tag{2.8}$$

where $\mathbb{I}_{dn}$ and $\mathbb{I}_{qn}$ are functions of e_{θ_e}. Nonetheless, extraction of e_{θ_e} in this structure is not possible. Therefore, in order to overcome this drawback, a selection for $\phi = \frac{\pi}{4}$ is made. In consequence, (2.3) is expressed in terms of e_{θ_e} as follows

$$\Lambda_{\theta_1} = \quad i_q\sqrt{2}\ sin(e_{\theta_e}) - i_d\sqrt{2}\ cos(e_{\theta_e}) + i_d^*\sqrt{2} \tag{2.9}$$

Considering that Λ_{θ_1} is calculated by using measurable currents $i_{\alpha\beta}$; and assuming i_d

tracks a desired reference i_d^*. Then, the above equation can be rewritten as follows

$$\Lambda_{\theta_1} = \quad i_q\sqrt{2}\ sin(e_{\theta_e}) + i_d^*\sqrt{2}\,[1 - cos(e_{\theta_e})] \tag{2.10}$$

and using a trigonometric identity, the following equation is obtained

$$\Lambda_{\theta_1} = \quad i_q\sqrt{2}\ sin(e_{\theta_e}) + i_d^*\sqrt{2}\left[2(sin(\frac{e_{\theta_e}}{2}))^2\right] \tag{2.11}$$

Therefore, for a small angular error e_{θ_e}, an approximation for Λ_{θ_1} is stated as

$$\Lambda_{\theta_1} \approx i_q e_{\theta_e}\sqrt{2} + \frac{i_d^*}{\sqrt{2}} e_{\theta_e}^2. \tag{2.12}$$

Moreover, consider that quadratic term is smaller than linear term. Then, Λ_{θ_1} is given by

$$\Lambda_{\theta_1} \approx \quad i_q e_{\theta_e}\sqrt{2} \tag{2.13}$$

Notice that (2.13) depends of the current i_q. It is worth mentioning that the changes in

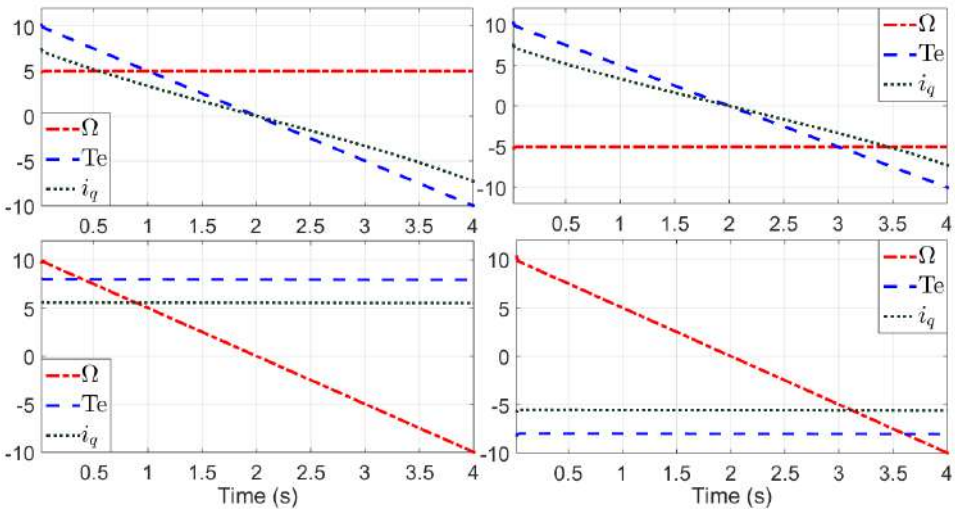

Figure 2.1 – Different scenarios to see the behavior of speed, electromagnetic torque and current-i_q.

the current i_q are directly proportional to the electromagnetic torque T_e [see [79]]. As can be seen in Figure 2.1, different profiles of speed and electromagnetic torque have been plotted and the behavior of the current i_q is shown. Then, from Figure 2.1, current i_q can be positive or negative depending on the electrical machine operation. Then, multiplying

$sign(i_q)$ in both side of the equation, it follows that

$$\begin{aligned} \Lambda_{\theta_1} sign(i_q) &\approx i_q sign(i_q)\sqrt{2}\ (e_{\theta_e}) \\ &\approx \sqrt{2}\ |i_q| e_{\theta_e} \end{aligned} \tag{2.14}$$

Taking into account that $i_{q_{max}} > |i_q|$. Finally, it follows that

$$\Lambda_\theta \approx \mu\, e_{\theta_e} \tag{2.15}$$

with $\Lambda_\theta = \Lambda_{\theta_1} sign(i_q)$, and $\mu = i_{q_{max}}\sqrt{2}$, where $i_{q_{max}}$ is the maximum value of i_q. Nevertheless, i_q is not available for measurement. Then, in (2.15), i_q will be replaced by the estimated current $\hat{i}_q$. In fact, $\hat{i}_q$ is obtained from the transformation of the measured currents i_α and i_β from the stator reference frame to synchronous reference frame as shown by these equations

$$\begin{bmatrix} \hat{i}_d \\ \hat{i}_q \end{bmatrix} = \mathbb{T}^T(\hat{\theta}_e) \begin{bmatrix} i_\alpha \\ i_\beta \end{bmatrix} \tag{2.16}$$

where $\mathbb{T}^T(\hat{\theta}_e) = \begin{bmatrix} cos(\hat{\theta}_e) & sin(\hat{\theta}_e) \\ -sin(\hat{\theta}_e) & cos(\hat{\theta}_e) \end{bmatrix}$ and since $\hat{\theta}_e$ will be calculated by the proposed observer, then,

$$\hat{i}_q = -sin(\hat{\theta}_e) i_\alpha + cos(\hat{\theta}_e) i_\beta \tag{2.17}$$

The initial rotor position information is needed for practical implementation to obtain $\hat{i}_q$. This problem is addressed in the literature by several research works (as it could be seen in [80]–[82]) and is supposed to be solved. In the experimental implementation, the rotor is moved very slightly by applying short voltage in order to detect the initial rotor position information. Once this information is obtained, the current $\hat{i}_q$ could be calculated using equation (2.17). Based on the calculated $\hat{i}_q$, the rotor position estimation error could be extracted by

$$e_{\theta_e} \approx \frac{\Lambda_\theta}{\mu} = \frac{\Lambda_{\theta_1} sign(\hat{i}_q)}{\mu} \tag{2.18}$$

where Λ_{θ_1} is computed from (2.3). In the sequel, (2.18) will be used in the observer for estimating the angular position, speed and acceleration.

2.2 Observer design based on a sliding modes approach: Proposal 1

In this section, an observer is designed by using the sliding mode approach. Consider the following class of nonlinear system given by

$$\begin{aligned} \dot{x}_1 &= x_2 \\ \dot{x}_2 &= x_3 \\ \dot{x}_3 &= \rho(t) \\ y &= x_1 \end{aligned} \tag{2.19}$$

where x_1, x_2 and x_3 are the states, $\rho(t)$ is an unknown and bounded term and $y \in \Re$ the output of the system.

Assumption 2.1. *The term $\rho(t)$ is bounded and unknown, i.e., $|\rho(t)| \leq \varrho_1$ for $\varrho_1 > 0$.*

Now, an observer based on sliding mode for the system (2.19) is expressed as follows

$$\begin{aligned} \dot{\hat{x}}_1 &= \hat{x}_2 + K_{1,1}|e_1|^{\frac{2}{3}} sign(e_1) \\ \dot{\hat{x}}_2 &= \hat{x}_3 + K_{2,1}|e_1|^{\frac{1}{3}} sign(e_1) \\ \dot{\hat{x}}_3 &= K_{3,1} sign(e_1) \\ \hat{y} &= \hat{x}_1 \end{aligned} \tag{2.20}$$

where $\hat{x}_1$, $\hat{x}_2$ and $\hat{x}_3$ are the estimated states and $\hat{y}$ is the estimated output. Moreover, the gains for the observer are reparameterized based on a single parameter L_o as follows

$$K_{1,1} = 3L_o^{\frac{5}{3}}, \qquad K_{2,1} = 2L_o^{\frac{10}{3}}, \qquad K_{3,1} = \left(\frac{4}{9}\right) L_o^5 \tag{2.21}$$

where L_o is an arbitrarily chosen gain large enough. However, if L_o is too large, it could cause an overestimation and increase the chattering amplitude, causing damage to the actuator. Currently, the design of an adaptive law for the gains is the best alternative to mitigate this problem.

2.2.1 Adaptive observer design

Now, an adaptive observer will be designed for the system (2.19). Then, the following observer

$$\begin{aligned}\dot{\hat{x}}_1 &= \hat{x}_2 + \tilde{K}_{1,1}|e_1|^{\frac{2}{3}}sign(e_1)\\ \dot{\hat{x}}_2 &= \hat{x}_3 + \tilde{K}_{2,1}|e_1|^{\frac{1}{3}}sign(e_1)\\ \dot{\hat{x}}_3 &= \tilde{K}_{3,1}sign(e_1)\\ \hat{y} &= \hat{x}_1\end{aligned} \tag{2.22}$$

is an AHOSMO-1 and its gains are defined as follows

$$\tilde{K}_{1,1} = 3L_o^{\frac{5}{3}}(t), \qquad \tilde{K}_{2,1} = 2L_o^{\frac{10}{3}}(t), \qquad \tilde{K}_{3,1} = \left(\frac{4}{9}\right)L_o^5(t) \tag{2.23}$$

where $L_o(t) > 0$ is an adaptive parameter that will be introduced later.

Remark 2.1: *The demonstration to calculate the proposed gains has been introduced in Appendix A (see A.1.1).*

Taking into account the observer (2.22), an analysis of convergence will be introduced and an adaptive law for $L_o(t)$ will be designed. Then, defining the following estimation errors

$$\begin{aligned}e_1 &= x_1 - \hat{x}_1\\ e_2 &= x_2 - \hat{x}_2\\ e_3 &= x_3 - \hat{x}_3\end{aligned} \tag{2.24}$$

the following dynamics can be calculated

$$\begin{aligned}\dot{e}_1 &= e_2 - 3L_o^{\frac{5}{3}}(t)|e_1|^{\frac{2}{3}}sign(e_1)\\ \dot{e}_2 &= e_3 - 2L_o^{\frac{10}{3}}(t)|e_1|^{\frac{1}{3}}sign(e_1)\\ \dot{e}_3 &= \rho(t) - \left(\frac{2}{3}\right)^2 L_o^5(t)sign(e_1)\end{aligned} \tag{2.25}$$

Now, taking into account the dynamics of the estimation errors, the following change of variable is established as follows

$$\zeta_1 = \frac{e_1}{L_o^2(t)}, \qquad \zeta_2 = \frac{e_2}{L_o^2(t)}, \qquad \zeta_3 = \frac{e_3}{L_o^2(t)} \tag{2.26}$$

and taking the first derivative in time, the dynamical system in terms of the new variables

is given by

$$\begin{aligned}
\dot{\zeta}_1 &= -3L_o(t)|\zeta_1|^{\frac{2}{3}}sign(\zeta_1) + \zeta_2 - 2\zeta_1\frac{\dot{L}_o(t)}{L_o(t)} \\
\dot{\zeta}_2 &= -2L_o^2(t)|\zeta_1|^{\frac{1}{3}}sign(\zeta_1) + \zeta_3 - 2\zeta_2\frac{\dot{L}_o(t)}{L_o(t)} \\
\dot{\zeta}_3 &= -\left(\frac{2}{3}\right)^2 L_o^3(t)sign(\zeta_1) + \frac{\rho(t)}{L_o^2(t)} - 2\zeta_3\frac{\dot{L}_o(t)}{L_o(t)}
\end{aligned} \tag{2.27}$$

On the other side, the following new change of variable is introduced

$$\xi_1 = |\zeta_1|^{\frac{2}{3}}sign(\zeta_1), \qquad \xi_2 = \frac{\zeta_2}{L_o(t)}, \qquad \xi_3 = \frac{3\zeta_3|\zeta_1|^{\frac{1}{3}}}{2L_o^2(t)} \tag{2.28}$$

and the dynamical system can be expressed by using the new variables as follows

$$\begin{aligned}
\dot{\xi}_1 &= \frac{2L_o(t)}{3|\zeta_1|^{\frac{1}{3}}}\left[-3\xi_1 + \xi_2\right] - \frac{4\dot{L}_o(t)}{3L_o(t)}\xi_1 \\
\dot{\xi}_2 &= \frac{2L_o(t)}{3|\zeta_1|^{\frac{1}{3}}}\left[-3\xi_1 + \xi_3\right] - \frac{3\dot{L}_o(t)}{L_o(t)}\xi_2 \\
\dot{\xi}_3 &= \frac{2L_o(t)}{3|\zeta_1|^{\frac{1}{3}}}\left[-\xi_1 + \left(\frac{3}{2}\right)^2\frac{|\zeta_1|^{\frac{2}{3}}\rho(t)}{L_o^5(t)} + \frac{\xi_3}{2|\zeta_1|^{\frac{2}{3}}}\left(-3\xi_1 + \xi_2\right)\right] - \frac{14\dot{L}_o(t)}{3L_o(t)}\xi_3
\end{aligned} \tag{2.29}$$

The resulting system (2.29) can be expressed in the following compact form

$$\dot{\xi} = \alpha_o\left[\left(A_o - P_o^{-1}C_o^TC_o\right)\xi + \Phi_o\right] - N_o\xi\frac{\dot{L}_o(t)}{L_o(t)} \tag{2.30}$$

where $\alpha_o = \dfrac{2L_o(t)}{3|\zeta_1|^{\frac{1}{3}}}$ and

$$\xi = \begin{bmatrix}\xi_1\\ \xi_2\\ \xi_3\end{bmatrix}, \quad A_o = \begin{bmatrix}0 & 1 & 0\\ 0 & 0 & 1\\ 0 & 0 & 0\end{bmatrix}, \quad C_o = \begin{bmatrix}1 & 0 & 0\end{bmatrix}, \quad P_o = \begin{bmatrix}1 & -1 & 1\\ -1 & 2 & -3\\ 1 & -3 & 6\end{bmatrix},$$

$$N_o = \begin{bmatrix}\frac{4}{3} & 0 & 0\\ 0 & 3 & 0\\ 0 & 0 & \frac{14}{3}\end{bmatrix}, \quad \Phi_o = \begin{bmatrix}0\\ 0\\ \left(\frac{3}{2}\right)^2\frac{|\zeta_1|^{\frac{2}{3}}\rho(t)}{L_o^5(t)} + \frac{\xi_3}{2|\zeta_1|^{\frac{2}{3}}}\left(-3\xi_1 + \xi_2\right)\end{bmatrix}.$$

Assumption 2.2. *The terms in vector Φ_o are locally Lipschitz with respect to ξ [83], i.e., $||\Phi_o|| \leq \hbar||\xi||$, for $\hbar > 0$.*

Moreover, P_o is a symmetric positive-definite matrix, whose solution is given by

$$P_o + A_o^T P_o + P_o A_o - C_o^T C_o = 0$$

Theorem 2.1. *Consider the dynamic system* (2.19) *and the Assumptions 2.1 and 2.2 are satisfied. Furthermore,*

$$\dot{L}_o(t) = \left[k_o^{\frac{1}{2}} \frac{|e_1|^{\frac{2}{3}}}{L_o^{\frac{1}{3}}(t)} - \gamma_o^{\frac{1}{2}} L_o^2(t) \right] \tag{2.31}$$

is an adaptive law-1 of $L_o(t)$, for $\gamma_o > 0$ and $k_o > 0$ chosen appropriately, where $k_o > \gamma_o > 0$. Then, the system (2.22) *is an Adaptive High Order Sliding Mode Observer (AHOSMO-1) for the dynamic system* (2.19) *such that estimation errors e_i, for $i = 1, 2, 3$; converge to zero in finite time.*

Proof

A Lyapunov candidate function is considered as follows

$$V_{(\xi, L_o(t))} = V_{(\xi)} + V_{(L_o(t))} \tag{2.32}$$

defining $V_{(\xi)} = \xi^T P_o \xi$ and $V_{(L_o(t))} = \dfrac{\gamma_o}{2} L_o(t)^2$. Then, considering the Lyapunov candidate function, it is possible to take its first derivative in time and replace the suitable expressions, it follows that

$$\begin{aligned} \dot{V}_{(\xi, L_o)} =& \alpha_o \xi^T \left[A_o^T P_o + P_o A_o \right] \xi - 2\alpha_o \xi^T C_o^T C_o \xi - \frac{\dot{L}_o(t)}{L_o(t)} \xi^T \left[P_o N_o + N_o P_o \right] \xi \\ &+ \gamma_o \dot{L}_o(t) L_o(t) + 2\alpha_o \xi^T P_o \Phi_o \end{aligned} \tag{2.33}$$

Taking into account that $A_o^T P_o + P_o A_o = -P_o + C_o^T C_o$. Then, equation (2.33) can be rewritten as follows

$$\dot{V}_{(\xi, L_o(t))} = -\alpha_o \xi^T P_o \xi - \alpha_o \xi^T C_o^T C_o \xi - \frac{\dot{L}_o(t)}{L_o(t)} \xi^T \left[P_o N_o + N_o P_o \right] \xi + \gamma_o \dot{L}_o(t) L_o(t) + 2\alpha_o \xi^T P_o \Phi_o \tag{2.34}$$

Now, taking into account that $P_o N_o + N_o P_o = R_o$, and defining R_o as a symmetric positive-definite matrix. Then, $\xi^T R_o \xi \geq \dfrac{\lambda_{min}(R_o)}{\lambda_{max}(P_o)} V_{(\xi)} = k_o V_{(\xi)}$, where $\lambda_{min}(R_o)$ and $\lambda_{max}(P_o)$

are the minimum and maximum singular values of R_o and P_o, respectively. Moreover, $-\alpha_o \xi^T C_o^T C_o \xi < 0$, for $L_o(t) > 0$. Then,

$$\dot{V}_{(\xi,L_o(t))} \leq -\alpha_o V_{(\xi)} - \frac{\dot{L}_o(t)}{L_o(t)} \left[k_o V_{(\xi)} - \gamma_o L_o^2(t) \right] + 2\alpha_o \xi^T P_o \Phi_o \tag{2.35}$$

Considering that

$$\left[k_o V_{(\xi)} - \gamma_o L_o^2(t) \right] = \left[k_o^{\frac{1}{2}} V_{(\xi)}^{\frac{1}{2}} + \gamma_o^{\frac{1}{2}} L_o(t) \right] \left[k_o^{\frac{1}{2}} V_{(\xi)}^{\frac{1}{2}} - \gamma_o^{\frac{1}{2}} L_o(t) \right]$$

and $f_{(V_{(\xi)},L_o(t))} = \left[k_o^{\frac{1}{2}} V_{(\xi)}^{\frac{1}{2}} + \gamma_o^{\frac{1}{2}} L_o(t) \right] > 0$. Then, equation (2.35) is written as

$$\dot{V}_{(\xi,L_o(t))} \leq -\alpha_o V_{(\xi)} - f_{(V_{(\xi)},L_o(t))} \frac{\dot{L}_o(t)}{L_o(t)} \left[k_o^{\frac{1}{2}} V_{(\xi)}^{\frac{1}{2}} - \gamma_o^{\frac{1}{2}} L_o(t) \right] + 2\alpha_o \xi^T P_o \Phi_o \tag{2.36}$$

On the other side, using the following inequalities

$$|\zeta_1|^{\frac{4}{3}} = |\xi_1|^2 \leq ||\xi||^2 \tag{2.37}$$

and

$$\lambda_{min}(P_o)||\xi||^2 \leq V_{(\xi)} \leq \lambda_{max}(P_o)||\xi||^2 \tag{2.38}$$

where $\lambda_{min}(P_o)$ and $\lambda_{max}(P_o)$ are the minimum and maximum singular values of P_o. Then, the following inequality is satisfied

$$|\zeta_1|^{\frac{2}{3}} \leq ||\xi|| \leq \left(\frac{V_{(\xi)}}{\lambda_{min}(P_o)} \right)^{\frac{1}{2}} \tag{2.39}$$

Therefore, from above inequality, it follows that

$$\dot{V}_{(\xi,L_o(t))} \leq -\alpha_o V_{(\xi)} - f_{(V_{(\xi)},L_o(t))} \frac{\dot{L}_o(t)}{L_o(t)} \left[k_o^{\frac{1}{2}} \frac{|e_1|^{\frac{2}{3}}}{L_o^{\frac{4}{3}}(t)} - \gamma_o^{\frac{1}{2}} L_o(t) \right] + 2\alpha_o \xi^T P_o \Phi_o \tag{2.40}$$

Choosing an adaptive law as follows $\dot{L}_o(t) = \left[k_o^{\frac{1}{2}} \frac{|e_1|^{\frac{2}{3}}}{L_o^{\frac{4}{3}}(t)} - \gamma_o^{\frac{1}{2}} L_o(t) \right] L_o(t)$. Then,

$$\dot{V}_{(\xi,L_o(t))} \leq -\alpha_o V_{(\xi)} - f_{(V_{(\xi)},L_o(t))} \left[k_o^{\frac{1}{2}} \frac{|e_1|^{\frac{2}{3}}}{L_o^{\frac{4}{3}}(t)} - \gamma_o^{\frac{1}{2}} L_o(t) \right]^2 + 2\alpha_o \xi^T P_o \Phi_o \tag{2.41}$$

Assuming that e_1 tend to zero faster than $L_o(t)$. Equation (2.41) is given by

$$\dot{V}_{(\xi,L_o(t))} \leq -\alpha_o V_{(\xi)} - f_{(V_{(\xi)},L_o(t))}\left[\gamma_o L_o^2(t)\right] + 2\alpha_o \xi^T P_o \Phi_o \tag{2.42}$$

From Assumption 2.2, taking the norm to the nonlinear term $2\alpha_o \xi^T P_o \Phi_o$ and the inequality (2.38), then, it follows that

$$\dot{V}_{(\xi,L_o(t))} \leq -\frac{2L_o(t)}{3|\zeta_1|^{\frac{1}{3}}}\left[1-\sigma_o\right] V_{(\xi)} - f_{(V_{(\xi)},L_o(t))}\left[\gamma_o L_o^2(t)\right] \tag{2.43}$$

where $\sigma_o = \dfrac{2||P_o||\hbar}{\lambda_{min}(P_o)}$. Furthermore, from $|\zeta_1|^{\frac{2}{3}} = |\xi_1| \leq |\xi_1|^2 \leq ||\xi||^2$, the following inequality is satisfied,

$$|\zeta_1|^{\frac{1}{3}} \leq ||\xi|| \leq \left(\frac{V_{(\xi)}}{\lambda_{min}(P_o)}\right)^{\frac{1}{2}} \tag{2.44}$$

Then,

$$\dot{V}_{(\xi,L_o(t))} \leq -L_o(t)\Gamma_o V_{(\xi)}^{\frac{1}{2}} - f_{(V_{(\xi)},L_o(t))}\left[\gamma_o L_o^2(t)\right] \tag{2.45}$$

where $\Gamma_o = \dfrac{2\left[1-\sigma_o\right]\lambda_{min}^{\frac{1}{2}}(P_o)}{3}$. Rewritten (2.45) as follows

$$\dot{V}_{(\xi,L_o(t))} \leq -L_o(t)\sqrt{2}\gamma_o^{\frac{1}{2}}\left[\frac{\Gamma_o}{\sqrt{2}\gamma_o^{\frac{1}{2}}} V_{(\xi)}^{\frac{1}{2}} + f_{(V_{(\xi)},L_o)}\frac{\gamma_o^{\frac{1}{2}}}{\sqrt{2}} L_o(t)\right] \tag{2.46}$$

and defining $\eta_0 = L_o(t)\sqrt{2}\gamma_o^{\frac{1}{2}}$ and $\varphi = min\left[\dfrac{\Gamma_o}{\sqrt{2}\gamma_o^{\frac{1}{2}}}, f_{(V_{(\xi)},L_o(t))}\right]$. It follows that

$$\dot{V}_{(\xi,L_o(t))} \leq -\eta\left[V_{(\xi)}^{\frac{1}{2}} + \frac{\gamma_o^{\frac{1}{2}}}{\sqrt{2}} L_o(t)\right] \tag{2.47}$$

where $\eta = \eta_0\varphi$. On the other hand, considering that Jensen´s inequality [84] is expressed as follows

$$\left[|a|^q + |b|^q\right]^{\frac{1}{q}} \leq |a| + |b| \tag{2.48}$$

and defining $a = V_{(\xi)}^{\frac{1}{2}}$, $b = V_{(L_o(t))}^{\frac{1}{2}}$ and $q = 2$. Then, the following inequality is satisfied

$$\left[|V_{(\xi)}^{\frac{1}{2}}|^2 + |V_{(L_o(t))}^{\frac{1}{2}}|^2\right]^{\frac{1}{2}} \leq |V_{(\xi)}^{\frac{1}{2}}| + |\frac{\gamma_o^{\frac{1}{2}}}{\sqrt{2}} L_o(t)| \tag{2.49}$$

and

$$V_{(\xi,L_o(t))}^{\frac{1}{2}} \leq V_{(\xi)}^{\frac{1}{2}} + \frac{\gamma_o^{\frac{1}{2}}}{\sqrt{2}} L_o(t). \tag{2.50}$$

Finally, the Lyapunov dynamic equation is satisfied as follows

$$\dot{V}_{(\xi,L_o(t))} \leq -\eta V_{(\xi,L_o(t))}^{\frac{1}{2}} \tag{2.51}$$

As mentioned before, $\dot{V}_{(\xi,L_o(t))}$ is a Lyapunov function, with $L_o(t)$ sufficiently large, satisfying $\eta > 0$. Then, $\dot{V}_{(\xi,L_o(t))}$ is negative definite and can guarantee the convergence of the observer in finite time. On the other side, taking into account the equation $\dot{v} = -\eta v^{\frac{1}{2}}$, whose solution is defined by $v(t) = (v(0)^{\frac{1}{2}} - \frac{1}{2}\eta t)^2$. Then, the comparison principle can be applied in order to estimate the convergence time T_1. Therefore, $V_{(\xi,L_o(t))} < v(t)$ when $V_{(\xi(0)),L_o(0))} < v(0)$, then ξ has a finite-time convergence in an estimated time defined by $T_1 = \dfrac{2V_{(\xi(0)),L_o(0))}^{\frac{1}{2}}}{\eta}$ for $L_o(t)$ sufficiently large. Thus, $V_{(\xi,L_o(t))}$ tends to zero in finite-time, which involves that the estimation errors e_i, for $i = 1, 2, 3$; tend to zero in finite time.

Remark 2.2. *As can be seen, the system* (2.30) *has a singularity when* $e_1 = 0$. *The singularity arise due to the change of variable* $\xi_1 = |\zeta_1|^{\frac{2}{3}} sign(\zeta_1)$, $\xi_2 = \dfrac{\zeta_2}{L_o(t)}$, $\xi_3 = \dfrac{3\zeta_3|\zeta_1|^{\frac{1}{3}}}{2L_o^2(t)}$; *converting system* (2.25) *into system* (2.30), *whose domain is defined as follows* $\mathcal{D} = \{(\xi_1, \xi_2, \xi_3) \in \Re^3 | \quad \xi_1 \neq 0\}$. *Nonetheless, considering convergence analysis, the singularity does not appear when the system is expressed in terms of the original coordinates (see for more details [85], [86]).*

2.2.2 Adaptive observer design for the IPMSM

Consider the adaptive law-1 in Theorem 2.1 and the virtual system (1.42), then, an adaptive observer based on the virtual system (1.42) is designed as follows

$$\begin{aligned} \dot{\hat{\theta}}_e &= \hat{\omega} + \tilde{K}_{1,1}|e_{\theta_e}|^{\frac{2}{3}} sign(e_{\theta_e}) \\ \dot{\hat{\omega}} &= \hat{\alpha} + \tilde{K}_{2,1}|e_{\theta_e}|^{\frac{1}{3}} sign(e_{\theta_e}) \\ \dot{\hat{\alpha}} &= \tilde{K}_{3,1} sign(e_{\theta_e}) \end{aligned} \tag{2.52}$$

where $\hat{\theta}_e$, $\hat{\omega}$ and $\hat{\alpha}$ are the estimation of electrical angular position, electrical speed and acceleration, respectively. However, θ_e is not measured directly, such that, the observer

(2.52) cannot be implemented. Therefore, considering the methodology to extract e_{θ_e} introduced in section 2.1, then, Λ_θ can be expressed in terms of the estimation error e_{θ_e} as $\Lambda_\theta = \mu e_{\theta_e}$, with $\mu > 0$. Thus, $e_{\theta_e} = \theta_e - \hat{\theta}_e$ can be replaced by $\theta_e - \hat{\theta}_e = \frac{\Lambda_\theta}{\mu}$ into the observer (2.52), i.e., the AHOSMO-1 for the IPMSM is given by

$$\begin{aligned} \dot{\hat{\theta}}_e &= \hat{\omega} + \tilde{K}_{1,1}|\frac{\Lambda_\theta}{\mu}|^{\frac{2}{3}} sign(\frac{\Lambda_\theta}{\mu}) \\ \dot{\hat{\omega}} &= \hat{\alpha} + \tilde{K}_{2,1}|\frac{\Lambda_\theta}{\mu}|^{\frac{1}{3}} sign(\frac{\Lambda_\theta}{\mu}) \\ \dot{\hat{\alpha}} &= \tilde{K}_{3,1} sign(\frac{\Lambda_\theta}{\mu}) \end{aligned} \tag{2.53}$$

Then, the observer (2.53) is used to estimate the angular position, speed and acceleration. As previously mentioned, $\hat{\theta} = \frac{\hat{\theta}_e}{p}$ is the estimated mechanical angular position and $\hat{\Omega} = \frac{\hat{\omega}}{p}$ is the mechanical speed. In Figure 2.2, a scheme of the proposed AHOSMO-1 (2.53) is introduced.

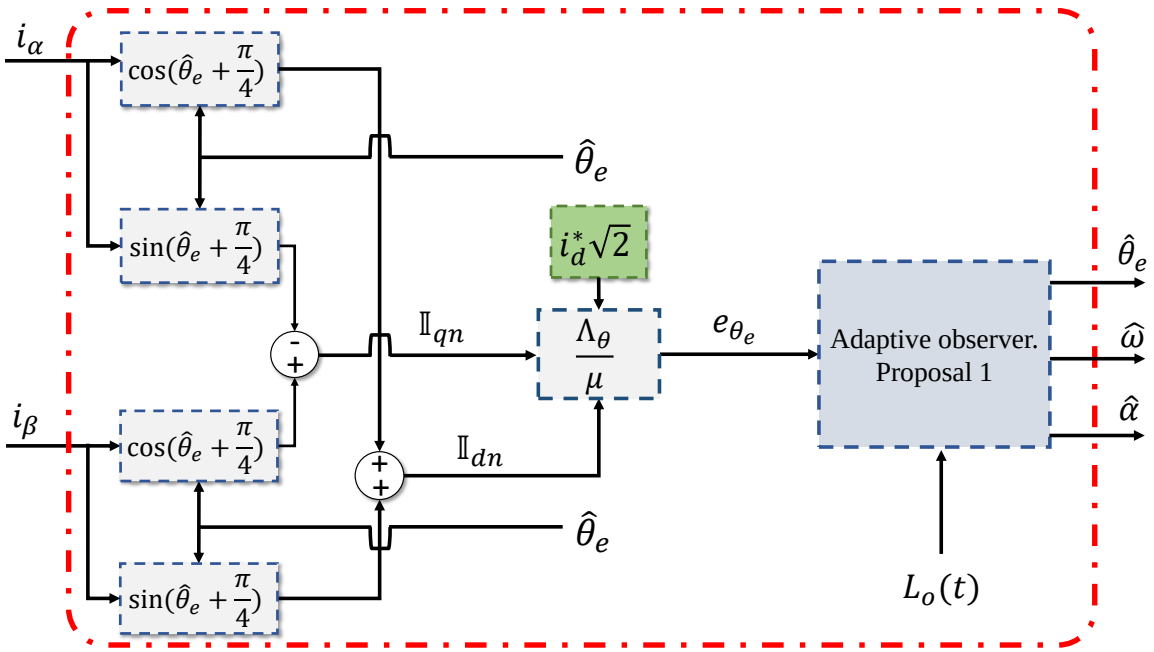

Figure 2.2 – Scheme of the proposed AHOSMO-1.

2.2.3 Simulation results

In this section, a simulation result is introduced to show the AHOSMO-1 performance in open-loop. Simulation test has been carried out in Matlab-Simulink environment, using a sampling time of 1×10^{-3} with a fixed-step *ode*4 solver. Moreover, the test has been made by considering the profiles and parametric uncertainties given by Figure 1.7 and Figure 1.8, respectively. The parameters of the adaptive observer are given in the Table 2.1. In Figure 2.3, the estimation of the angular position is given. It is possible to see that

Table 2.1 – Parameters for AHOSMO-1

Values		
$L_o(0)$	γ_0	k_o
1.5	0.003	120

observer has a good performance during the estimation.

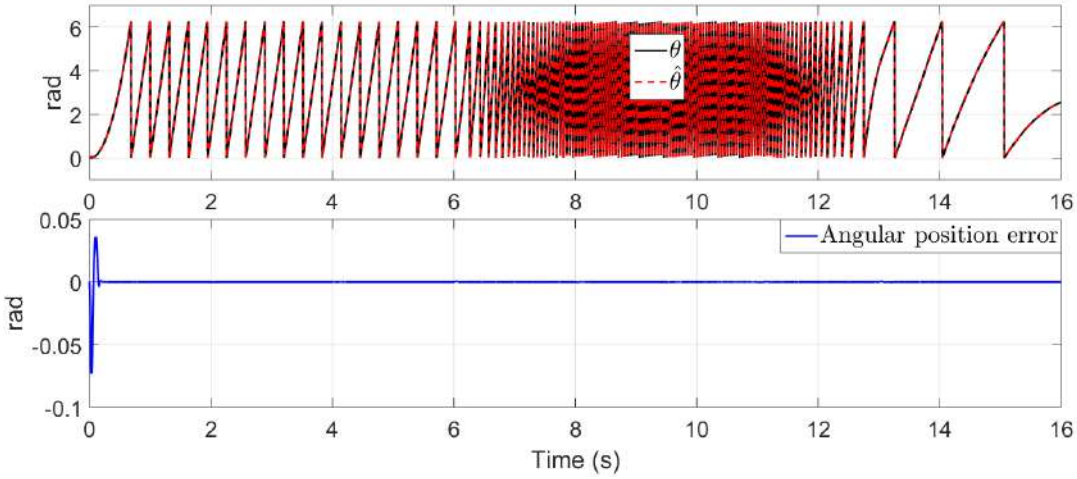

Figure 2.3 – AHOSMO-1. Rotor angular position estimation and its estimation error

In Figure 2.4 is introduced the speed estimation and its estimation error. The speed estimation error can show that observer is not affected by parametric uncertainties. Moreover, thanks to the estimation of the acceleration [see Figure 2.5-a)], a minimum error can be seen during speed profile change. This error is caused by the fast dynamic in the speed, for this reason, the acceleration estimation has been included to compensate those errors in fast transient modes, minimizing the estimation error.

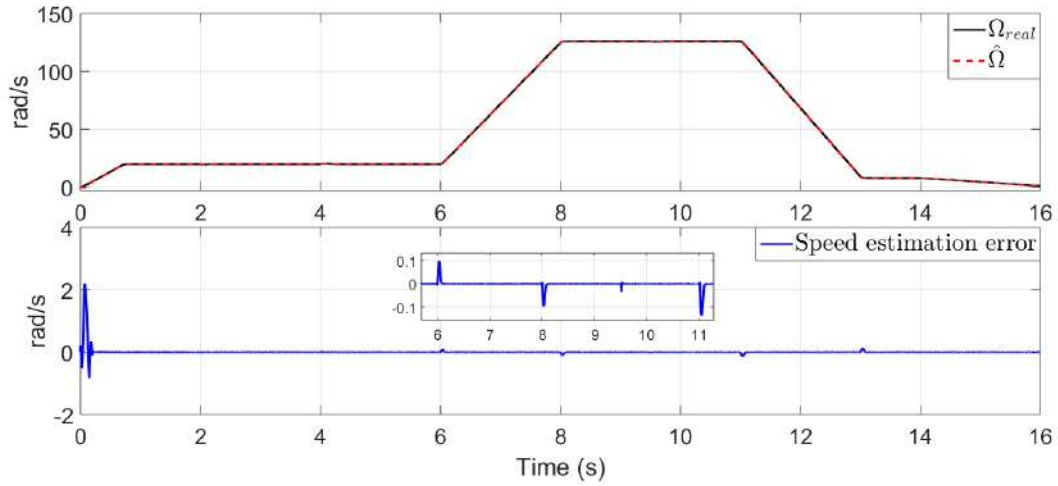

Figure 2.4 – AHOSMO-1. Rotor speed estimation and speed estimation error

On the other hand, in Figure 2.5-b), the behaviour of adaptive law for the observer is introduced, which takes values in order to achieve a good estimation of the observer avoiding overestimation of gain. Therefore, in this open-loop test for the first adaptive observer, good results have been obtained by simulation.

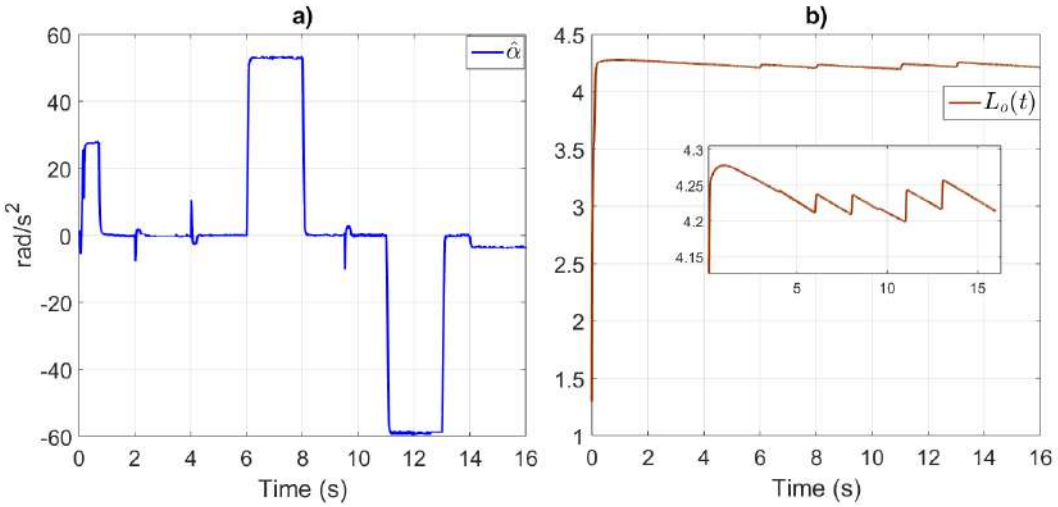

Figure 2.5 – AHOSMO-1. Estimation of acceleration (a) and behaviour of the adaptive law (b)

2.3 Observer design based on a sliding modes approach: Proposal 2

In this section, a second observer is designed for a class of nonlinear system given by (2.19). Then, an observer for the system (2.19) is expressed as follows

$$\begin{aligned}\dot{\hat{x}}_{1_2} &= \hat{x}_2 + K_{1,2}|e_{1_2}|^{\frac{2}{3}} sign(e_{1_2}) \\ \dot{\hat{x}}_{2_2} &= \hat{x}_3 + K_{2,2}|e_{1_2}|^{\frac{1}{3}} sign(e_{1_2}) \\ \dot{\hat{x}}_{3_2} &= K_{3,2} sign(e_{1_2}) \\ \hat{y} &= \hat{x}_{1_2}\end{aligned} \tag{2.54}$$

where $\hat{x}_{1_2}$, $\hat{x}_{2_2}$ and $\hat{x}_{3_2}$ represent the estimated states and $\hat{y}$ is the estimated output. Moreover, the gains for the observer are reparameterized in terms of L_{o_2} as follows

$$K_{1,2} = 3L_{o_2} \qquad K_{2,2} = 2L_{o_2}^2 \qquad K_{3,2} = \left(\frac{2}{3}\right)^2 L_{o_2}^3 \tag{2.55}$$

where $L_{o_2} > 0$ is a constant positive parameter large enough. However, if L_{o_2} is too large, it could cause an overestimation and increase the chattering amplitude, causing damage to the actuator. For this reason, in the next section, an adaptive law for the gains will be designed.

2.3.1 Adaptive observer design

Now, a second adaptive observer is proposed for the system (2.19). Consider the following system

$$\begin{aligned}\dot{\hat{x}}_{1_2} &= \hat{x}_2 + \tilde{K}_{1,2}|e_{1_2}|^{\frac{2}{3}} sign(e_{1_2}) \\ \dot{\hat{x}}_{2_2} &= \hat{x}_3 + \tilde{K}_{2,2}|e_{1_2}|^{\frac{1}{3}} sign(e_{1_2}) \\ \dot{\hat{x}}_{3_2} &= \tilde{K}_{3,2} sign(e_{1_2}) \\ \hat{y} &= \hat{x}_{1_2}\end{aligned} \tag{2.56}$$

which is an AHOSMO-2 and its reparameterized gains in terms of a single parameter are defined by

$$\tilde{K}_{1,2} = 3L_{o_2}(t) \qquad \tilde{K}_{2,2} = 2L_{o_2}^2(t) \qquad \tilde{K}_{3,2} = \left(\frac{2}{3}\right)^2 L_{o_2}^3(t) \tag{2.57}$$

where $L_{o_2}(t)$ is an adaptive parameter that will be introduced later.

Remark 2.3: *The demonstration to compute the proposed gains has been introduced in Appendix A (See A.1.2).*

Now, an analysis of convergence for the observer (2.56) and an adaptive law for the parameter $L_{o_2}(t)$ are introduced. Then, consider the following estimation errors

$$e_{1_2} = x_1 - \hat{x}_{1_2}, \qquad e_{2_2} = x_2 - \hat{x}_{2_2}, \qquad e_{3_2} = x_3 - \hat{x}_{3_2} \tag{2.58}$$

and their dynamics as follows

$$\begin{aligned} \dot{e}_{1_2} &= e_{2_2} - 3L_{o_2}(t)|e_{1_2}|^{\frac{2}{3}} sign(e_{1_2}) \\ \dot{e}_{2_2} &= e_{3_2} - 2L^2_{o_2}(t)|e_{1_2}|^{\frac{1}{3}} sign(e_{1_2}) \\ \dot{e}_{3_2} &= \rho(t) - \left(\frac{2}{3}\right)^2 L^3_{o_2}(t) sign(e_{1_2}) \end{aligned} \tag{2.59}$$

Now, a change of variable is introduced as follows

$$\xi_{1_2} = \frac{|e_{1_2}|^{\frac{2}{3}} sign(e_{1_2})}{L_{o_2}(t)} \qquad \xi_{2_2} = \frac{e_{2_2}}{L^2_{o_2}(t)} \qquad \xi_{3_2} = \frac{3e_{3_2}|e_{1_2}|^{\frac{1}{3}}}{2L^3_{o_2}(t)} \tag{2.60}$$

Then, it follows that the dynamical system can be expressed by using the new variables. Therefore, the following system can be obtained

$$\begin{aligned} \dot{\xi}_{1_2} &= \frac{2L_{o_2}(t)}{3|e_{1_2}|^{\frac{1}{3}}} \left[-3\xi_{1_2} + \xi_{2_2}\right] - \frac{\dot{L}_{o_2}(t)}{L_{o_2}(t)} \xi_{1_2} \\ \dot{\xi}_{2_2} &= \frac{2L_{o_2}(t)}{3|e_{1_2}|^{\frac{1}{3}}} \left[-3\xi_{1_2} + \xi_{3_2}\right] - \frac{2\dot{L}_{o_2}(t)}{L_{o_2}(t)} \xi_{2_2} \\ \dot{\xi}_{3_2} &= \frac{2L_{o_2}(t)}{3|e_{1_2}|^{\frac{1}{3}}} \left[-\xi_{1_2} + \left(\frac{3}{2}\right)^2 \frac{|e_{1_2}|^{\frac{2}{3}}\rho(t)}{L^4_{o_2}(t)} + \frac{L_{o_2}(t)\xi_{3_2}}{2|e_{1_2}|^{\frac{2}{3}}} \left[-3\xi_{1_2} + \xi_{2_2}\right]\right] - \frac{3\dot{L}_{o_2}(t)}{L_{o_2}(t)} \xi_{3_2} \end{aligned} \tag{2.61}$$

and can be simplified as follows

$$\dot{\xi}_{o_2} = \alpha_{o_2} \left[\left(A_o - P_o^{-1} C_o^T C_o\right) \xi_{o_2} + \Phi_{o_2}\right] - D_{o_2} \xi_{o_2} \frac{\dot{L}_{o_2}(t)}{L_{o_2}(t)} \tag{2.62}$$

defining $\alpha_{o_2} = \dfrac{2L_{o_2}(t)}{3|e_{1_2}|^{\frac{1}{3}}}$ and the following terms as follows

$$\xi_{o_2} = \begin{bmatrix} \xi_{1_2} \\ \xi_{2_2} \\ \xi_{3_2} \end{bmatrix}, \quad A_o = \begin{bmatrix} 0 & 1 & 0 \\ 0 & 0 & 1 \\ 0 & 0 & 0 \end{bmatrix}, \quad C_o = \begin{bmatrix} 1 & 0 & 0 \end{bmatrix}, \quad P_o = \begin{bmatrix} 1 & -1 & 1 \\ -1 & 2 & -3 \\ 1 & -3 & 6 \end{bmatrix}, \tag{2.63}$$

$$D_{o_2} = \begin{bmatrix} 1 & 0 & 0 \\ 0 & 2 & 0 \\ 0 & 0 & 3 \end{bmatrix}, \quad \Phi_{o_2} = \begin{bmatrix} 0 \\ 0 \\ \left(\frac{3}{2}\right)^2 \frac{|e_{1_2}|^{\frac{2}{3}}\rho(t)}{L_{o_2}^4(t)} + \frac{L_{o_2}(t)\xi_{3_2}}{2|e_{1_2}|^{\frac{2}{3}}}\left[-3\xi_{1_2} + \xi_{2_2}\right] \end{bmatrix}. \tag{2.64}$$

Assumption 2.3. *The term in the vector Φ_{o_2} is locally Lipschitz with respect to ξ_{o_2} [83], i.e., $||\Phi_{o_2}|| \leq \hbar_2||\xi_{o_2}||$, for $\hbar_2 > 0$.*

Moreover, P_o is a symmetric positive-definite matrix, whose solution is given by

$$P_o + A_o^T P_o + P_o A_o - C_o^T C_o = 0 \tag{2.65}$$

Theorem 2.2. *Consider the dynamic system* (2.19) *and the Assumptions 2.1 and 2.3 are satisfied. Furthermore,*

$$\dot{L}_{o_2}(t) = \left[k_{o_2}^{\frac{1}{2}}|e_{1_2}|^{\frac{2}{3}} - \gamma_{o_2}^{\frac{1}{2}} L_{o_2}^2(t)\right] \tag{2.66}$$

is an adaptive law-2 of $L_{o_2}(t)$, for $\gamma_{o_2} > 0$ and $k_{o_2} > 0$ chosen appropriately, where $k_{o_2} > \gamma_{o_2} > 0$. Then, the system (2.56) *is an Adaptive High-Order Sliding Mode Observer (AHOSMO-2) for the dynamic system* (2.19) *such that estimation errors e_{i_2}, for $i = 1, 2, 3$; converge to zero in finite time.*

Proof

A Lyapunov candidate function is considered as follows

$$V_{(\xi_{o_2}, L_{o_2}(t))} = V_{(\xi_{o_2})} + V_{(L_{o_2}(t))} \tag{2.67}$$

defining $V_{(\xi_{o_2})} = \xi_{o_2}^T P_o \xi_{o_2}$ and $V_{(L_{o_2}(t))} = \dfrac{\gamma_{o_2}}{2} L_{o_2}^2(t)$. Then, considering the Lyapunov candidate function, it is possible to take its first derivative in time and replace the suitable expressions, it follows that

$$\begin{aligned} \dot{V}_{(\xi_{o_2}, L_{o_2}(t))} =& \alpha_{o_2} \xi_{o_2}^T \left[A_o^T P_o + P_o A_o\right] \xi_{o_2} - 2\alpha_{o_2} \xi_{o_2}^T C_o^T C_o \xi_{o_2} \\ & - 2\frac{\dot{L}_{o_2}(t)}{L_{o_2}(t)} \xi_{o_2}^T P_o D_{o_2} \xi_{o_2} + \gamma_{o_2} \dot{L}_{o_2}(t) L_{o_2}(t) + 2\alpha_{o_2} \xi_{o_2}^T P_o \Phi_{o_2} \end{aligned} \tag{2.68}$$

Taking into account that $A_o^T P_o + P_o A_o = -P_o + C_o^T C_o$. Then, equation (2.68) can be rewritten as follows

$$\begin{aligned}\dot{V}_{(\xi_{o_2},L_{o_2}(t))} =& -\alpha_{o_2}\xi_{o_2}^T P_o \xi_{o_2} - \alpha_{o_2}\xi_{o_2}^T C_o^T C_o \xi_{o_2} - 2\frac{\dot{L}_{o_2}(t)}{L_{o_2}(t)}\xi_{o_2}^T P_o D_{o_2}\xi_{o_2} \\ &+ \gamma_{o_2}\dot{L}_{o_2}(t)L_{o_2}(t) + 2\alpha_{o_2}\xi_{o_2}^T P_o \Phi_{o_2}\end{aligned} \tag{2.69}$$

On the other hand, using the following inequalities

$$\frac{|e_{1_2}|^{\frac{4}{3}}}{L_{o_2}^2(t)} = |\xi_{1_2}|^2 \leq ||\xi_{o_2}||^2 \tag{2.70}$$

and

$$\lambda_{min}(P_o)||\xi_{o_2}||^2 \leq V_{(\xi_{o_2})} \leq \lambda_{max}(P_o)||\xi_{o_2}||^2 \tag{2.71}$$

where $\lambda_{min}(P_o)$ and $\lambda_{max}(P_o)$ are the minimum and maximum singular values of P_o. Moreover,

$$\lambda_{min}(P_o D_{o_2})||\xi_{o_2}||^2 \leq \xi_{o_2}^T P_o D_{o_2}\xi_{o_2} \leq \lambda_{max}(P_o D_{o_2})||\xi_{o_2}||^2 \tag{2.72}$$

where $\lambda_{min}(P_o D_{o_2})$ and $\lambda_{max}(P_o D_{o_2})$ are the minimum and maximum singular values of $P_o D_{o_2}$. Then,

$$\begin{aligned}\dot{V}_{(\xi_{o_2},L_{o_2}(t))} \leq& -\alpha_{o_2}\xi_{o_2}^T P_o \xi_{o_2} - \alpha_{o_2}\xi_{o_2}^T C_o^T C_o \xi_{o_2} - 2\lambda_{min}(P_o D_{o_2})||\xi_{o_2}||^2\frac{\dot{L}_{o_2}(t)}{L_{o_2}(t)} \\ &+ \gamma_{o_2}\dot{L}_{o_2}(t)L_{o_2}(t) + 2\alpha\xi_{o_2}^T P_o \Phi_{o_2}\end{aligned} \tag{2.73}$$

In this way,

$$\begin{aligned}\dot{V}_{(\xi_{o_2},L_{o_2}(t))} \leq& -\alpha_{o_2}\xi_{o_2}^T P_o \xi_{o_2} - \alpha_{o_2}\xi_{o_2}^T C_o^T C_o \xi_{o_2} - k_{o_2}||\xi_{o_2}||^2\frac{\dot{L}_{o_2}(t)}{L_{o_2}(t)} \\ &+ \gamma_{o_2}\dot{L}_{o_2}(t)L_{o_2}(t) + 2\alpha_{o_2}\xi_{o_2}^T P_o \Phi_{o_2}\end{aligned} \tag{2.74}$$

where $k_{o_2} = 2\lambda_{min}(P_o D_{o_2}) > 0$. The above equation can be established as follows

$$\begin{aligned}\dot{V}_{(\xi_{o_2},L_{o_2}(t))} \leq& -\alpha_{o_2}\xi_{o_2}^T P_o \xi_{o_2} - \alpha_{o_2}\xi_{o_2}^T C_o^T C_o \xi_{o_2} + 2\alpha_{o_2}\xi_{o_2}^T P_o \Phi_{o_2} \\ &- \frac{\dot{L}_{o_2}(t)}{L_{o_2}(t)}\left[k_{o_2}||\xi_{o_2}||^2 - \gamma_{o_2}L_{o_2}^2(t)\right]\end{aligned} \tag{2.75}$$

Now, the last term of the above equation can be expressed as follows

$$\frac{\dot{L}_{o_2}(t)}{L_{o_2}(t)}\left[k_{o_2}||\xi_{o_2}||^2-\gamma_{o_2}L_{o_2}^2(t)\right]=\frac{\dot{L}_{o_2}(t)}{L_{o_2}(t)}\left[k_{o_2}^{\frac{1}{2}}||\xi_{o_2}||+\gamma_{o_2}^{\frac{1}{2}}L_{o_2}(t)\right]\left[k_{o_2}^{\frac{1}{2}}||\xi_{o_2}||-\gamma_{o_2}^{\frac{1}{2}}L_{o_2}(t)\right] \tag{2.76}$$

and $f_{(\xi_{o_2},L_{o_2}(t))}=\left[k_{o_2}^{\frac{1}{2}}||\xi_{o_2}||+\gamma_{o_2}^{\frac{1}{2}}L_{o_2}(t)\right]>0$. Then,

$$\begin{aligned}\dot{V}_{(\xi_{o_2},L_{o_2}(t))}\leq&-\alpha_{o_2}\xi_{o_2}^TP_o\xi_{o_2}-\alpha_{o_2}\xi_{o_2}^TC_o^TC_o\xi_{o_2}+2\alpha_{o_2}\xi_{o_2}^TP_o\Phi_{o_2}\\&-f_{(\xi_{o_2},L_{o_2}(t))}\frac{\dot{L}_{o_2}(t)}{L_{o_2}(t)}\left[k_{o_2}^{\frac{1}{2}}||\xi_{o_2}||-\gamma_{o_2}^{\frac{1}{2}}L_{o_2}(t)\right]\end{aligned} \tag{2.77}$$

From inequalities (2.70) and (2.71), the following inequality is satisfied

$$\frac{|e_{1_2}|^{\frac{2}{3}}}{L_{o_2}(t)}\leq||\xi_{o_2}||\leq\left(\frac{V_{(\xi_{o_2})}}{\lambda_{min}(P_o)}\right)^{\frac{1}{2}} \tag{2.78}$$

Then, from (2.78), it follows that

$$\begin{aligned}\dot{V}_{(\xi_{o_2},L_{o_2}(t))}\leq&-\alpha_{o_2}V_{(\xi_{o_2})}-\alpha_{o_2}\xi_{o_2}^TC_o^TC_o\xi_{o_2}+2\alpha_{o_2}\xi_{o_2}^TP_o\Phi_{o_2}\\&-f_{(\xi_{o_2},L_{o_2}(t))}\frac{\dot{L}_{o_2}}{L_{o_2}(t)}\left[k_{o_2}^{\frac{1}{2}}\frac{|e_{1_2}|^{\frac{2}{3}}}{L_{o_2}(t)}-\gamma_{o_2}^{\frac{1}{2}}L_{o_2}(t)\right]\end{aligned} \tag{2.79}$$

Choosing an adaptive law as follows

$$\dot{L}_{o_2}(t)=\left[k_{o_2}^{\frac{1}{2}}\frac{|e_{1_2}|^{\frac{2}{3}}}{L_{o_2}(t)}-\gamma_{o_2}^{\frac{1}{2}}L_{o_2}(t)\right]L_{o_2}(t) \tag{2.80}$$

Then,

$$\dot{V}_{(\xi_{o_2},L_{o_2}(t))}\leq-\alpha_{o_2}V_{(\xi_{o_2})}-\alpha_{o_2}\xi_{o_2}^TC_o^TC_o\xi_{o_2}-f_{(\xi_{o_2},L_{o_2}(t))}\left[k^{\frac{1}{2}}\frac{|e_{1_2}|^{\frac{2}{3}}}{L_{o_2}(t)}-\gamma_{o_2}^{\frac{1}{2}}L_{o_2}(t)\right]^2+2\alpha_{o_2}\xi_{o_2}^TP_o\Phi_{o_2} \tag{2.81}$$

and assuming that e_{1_2} tend to zero faster than $L_{o_2}(t)$, and $-\alpha_{o_2}\xi_{o_2}^TC_o^TC_o\xi_{o_2}<0$, for $L_{o_2}(t)>0$. Equation (2.81) is given by

$$\dot{V}_{(\xi_{o_2},L_{o_2}(t))}\leq-\alpha_{o_2}V_{(\xi_{o_2})}-f_{(\xi_{o_2},L_{o_2}(t))}\left[\gamma_{o_2}L_{o_2}^2(t)\right]+2\alpha_{o_2}\xi_{o_2}^TP_o\Phi_{o_2} \tag{2.82}$$

Taking the norm to the nonlinear term $2\alpha_{o_2}\xi_{o_2}^TP_o\Phi_{o_2}$ and from Assumption 2.3, then (2.82)

is given by

$$\dot{V}_{(\xi_{o_2},L_{o_2}(t))} \leq -\alpha_{o_2} V_{(\xi_{o_2})} + 2\alpha_{o_2}||\xi_{o_2}||^2||P_o||\hbar_2 - f_{(\xi_{o_2},L_{o_2}(t))}\left[\gamma_{o_2} L_{o_2}^2(t)\right] \tag{2.83}$$

Now, from inequality (2.71). Then, it follows that

$$\dot{V}_{(\xi_{o_2},L_{o_2}(t))} \leq -\frac{2L_{o_2}(t)}{3|e_{1_2}|^{\frac{1}{3}}}\left[1-\sigma_{o_2}\right] V_{(\xi_{o_2})} - f_{(\xi_{o_2},L_{o_2}(t))}\left[\gamma_{o_2} L_{o_2}^2(t)\right] \tag{2.84}$$

where $\sigma_{o_2} = \dfrac{2||P_o||\hbar_2}{\lambda_{max}(P_{o_2})}$. Furthermore, from $\dfrac{|e_{1_2}|^{\frac{2}{3}}}{L_{o_2}(t)} = |\xi_{1_2}| \leq |\xi_{1_2}|^2 \leq ||\xi_{o_2}||^2$, the following inequality is satisfied

$$\frac{|e_{1_2}|^{\frac{1}{3}}}{L_{o_2}^{\frac{1}{2}}(t)} \leq ||\xi_{o_2}|| \leq \left(\frac{V_{(\xi_{o_2})}}{\lambda_{min}(P_o)}\right)^{\frac{1}{2}} \tag{2.85}$$

and considering that (2.84) can be written as follows

$$\dot{V}_{(\xi_{o_2},L_{o_2}(t))} \leq -\frac{2L_{o_2}(t)}{\frac{3|e_{1_2}|^{\frac{1}{3}} L_{o_2}^{\frac{1}{2}}(t)}{L_{o_2}^{\frac{1}{2}}(t)}}\left[1-\sigma_{o_2}\right] V_{(\xi_{o_2})} - f_{(\xi_{o_2},L_{o_2}(t))}\left[\gamma_{o_2} L_{o_2}^2(t)\right] \tag{2.86}$$

Then,

$$\dot{V}_{(\xi_{o_2},L_{o_2}(t))} \leq -L_{o_2}^{\frac{1}{2}}(t)\Gamma_{o_2} V_{(\xi_{o_2})}^{\frac{1}{2}} - f_{(\xi_{o_2},L_{o_2}(t))}\left[\gamma_{o_2} L_{o_2}^2(t)\right] \tag{2.87}$$

where $\Gamma_{o_2} = \dfrac{2\left[1-\sigma_{o_2}\right]\lambda_{min}^{\frac{1}{2}}(P_o)}{3}$. Rewritten (2.87) as follows

$$\dot{V}_{(\xi_{o_2},L_{o_2}(t))} \leq -L_{o_2}(t)\sqrt{2}\gamma_{o_2}^{\frac{1}{2}}\left[\frac{\Gamma_{o_2}}{\sqrt{2}\gamma_{o_2}^{\frac{1}{2}} L_{o_2}^{\frac{1}{2}}(t)} V_{(\xi_{o_2})}^{\frac{1}{2}} + f_{(\xi_{o_2},L_{o_2}(t))}\frac{\gamma_{o_2}^{\frac{1}{2}}}{\sqrt{2}} L_{o_2}(t)\right] \tag{2.88}$$

and defining $\eta_{0_2} = L_{o_2}(t)\sqrt{2}\gamma_{o_2}^{\frac{1}{2}}$ and $\varphi_{o_2} = min\left(\dfrac{\Gamma_{o_2}}{\sqrt{2}\gamma_{o_2}^{\frac{1}{2}} L_{o_2}^{\frac{1}{2}}(t)}, f_{(\xi_{o_2},L_{o_2}(t))}\right)$. We can write the following equation

$$\dot{V}_{(\xi_{o_2},L_{o_2}(t))} \leq -\tilde{\eta}\left[V_{(\xi_{o_2})}^{\frac{1}{2}} + \frac{\gamma_{o_2}^{\frac{1}{2}}}{\sqrt{2}} L_{o_2}(t)\right] \tag{2.89}$$

where $\tilde{\eta} = \eta_{0_2}\varphi_{o_2}$. On the other hand, considering that Jensen´s inequality [84] is expressed

as follows

$$[|a_{o_2}|^q + |b_{o_2}|^q]^{\frac{1}{q}} \leq |a_{o_2}| + |b_{o_2}| \tag{2.90}$$

and defining $a_{o_2} = V_{(\xi_{o_2})}^{\frac{1}{2}}$, $b_{o_2} = V_{(L_{o_2}(t))}^{\frac{1}{2}}$ and $q = 2$. Then, the following inequality is satisfied

$$\left[|V_{(\xi_{o_2})}^{\frac{1}{2}}|^2 + |V_{(L_{o_2}(t))}^{\frac{1}{2}}|^2\right]^{\frac{1}{2}} \leq |V_{(\xi_{o_2})}^{\frac{1}{2}}| + |\frac{\gamma_{o_2}^{\frac{1}{2}}}{\sqrt{2}} L_{o_2}(t)| \tag{2.91}$$

such that

$$V_{(\xi_{o_2}, L_{o_2}(t))}^{\frac{1}{2}} \leq V_{(\xi_{o_2})}^{\frac{1}{2}} + \frac{\gamma_{o_2}^{\frac{1}{2}}}{\sqrt{2}} L_{o_2}(t) \tag{2.92}$$

Finally, the Lyapunov dynamic equation is satisfied as follows

$$\dot{V}_{(\xi_{o_2}, L_{o_2}(t))} \leq -\tilde{\eta} V_{(\xi_{o_2}, L_{o_2}(t))}^{\frac{1}{2}} \tag{2.93}$$

As mentioned before, $\dot{V}_{(\xi_{o_2}, L_{o_2}(t))}$ is a Lyapunov function, with $L_{o_2}(t)$ sufficiently large, satisfying $\tilde{\eta} > 0$. Then, $\dot{V}_{(\xi_{o_2}, L_{o_2}(t))}$ is negative definite and can guarantee the convergence of the observer in finite time. On the other side, taking into account the equation $\dot{v} = -\tilde{\eta} v^{\frac{1}{2}}$, whose solution is defined by $v(t) = (v(0)^{\frac{1}{2}} - \frac{1}{2}\tilde{\eta} t)^2$. Then, the comparison principle can be applied in order to estimate the convergence time T_{1_2}. Therefore, $V_{(\xi_{o_2}, L_{o_2})} < v(t)$ when $V_{(\xi_{o_2}(0)), L_{o_2}(0))} < v(0)$, then ξ_{o_2} has a finite-time convergence in an estimated time defined by

$$T_{1_2} = \frac{2V_{(\xi_{o_2}(0)), L_{o_2}(0))}^{\frac{1}{2}}}{\tilde{\eta}}$$

for $L_{o_2}(t)$ sufficiently large. Thus, $V_{(\xi_{o_2}, L_{o_2}(t))}$ tends to zero in finite-time, which involves that the estimation errors e_{i_2}, for $i = 1, 2, 3$; tend to zero in finite time.

Remark 2.4. *As we can see, the system* (2.62) *has a singularity when* $e_1 = 0$. *The singularity arise due to the change of variable*

$$\xi_{1_2} = \frac{|e_{1_2}|^{\frac{2}{3}} sign(e_{1_2})}{L_{o_2}(t)}, \qquad \xi_{2_2} = \frac{e_{2_2}}{L_{o_2}^2(t)}, \qquad \xi_{3_2} = \frac{3e_{3_2}|e_{1_2}|^{\frac{1}{3}}}{2L_{o_2}^3(t)}$$

converting system (2.59) *into system* (2.62), *whose domain is defined as follows*

$$\mathcal{D}_{\in} = \left\{(\xi_{1_2}, \xi_{2_2}, \xi_{3_2}) \in \Re^3 | \quad \xi_{1_2} \neq 0\right\}.$$

Nonetheless, considering convergence analysis, the singularity does not appear when the

system is expressed in terms of the original coordinates (see for more details [85], [86]).

2.3.2 Adaptive observer design for the IPMSM

Consider the adaptive law-2 in Theorem 2.2 and the virtual system (1.42), then, an AHOSMO-2 for the virtual system (1.42) is designed as follows

$$\begin{aligned}\dot{\hat{\theta}}_e &= \hat{\omega} + \tilde{K}_{1,2}|e_{\theta_e}|^{\frac{2}{3}} sign(e_{\theta_e}) \\ \dot{\hat{\omega}} &= \hat{\alpha} + \tilde{K}_{2,2}|e_{\theta_e}|^{\frac{1}{3}} sign(e_{\theta_e}) \\ \dot{\hat{\alpha}} &= \tilde{K}_{3,2} sign(e_{\theta_e})\end{aligned} \tag{2.94}$$

where $\hat{\theta}_e$, $\hat{\omega}$ and $\hat{\alpha}$ are the estimation of electrical angular position, electrical speed and acceleration, respectively. However, θ_e is not measured directly, such that, the observer (2.94) cannot be implemented. Therefore, considering the methodology to extract e_{θ_e} introduced in section 2.1, then, Λ_θ can be expressed in terms of the estimation error e_{θ_e} as $\Lambda_\theta = \mu e_{\theta_e}$, with $\mu > 0$. Thus, $e_{\theta_e} = \theta_e - \hat{\theta}_e$ can be replaced by $\theta_e - \hat{\theta}_e = \dfrac{\Lambda_\theta}{\mu}$ into the observer (2.94), i.e., the AHOSMO-2 for the IPMSM is given by

$$\begin{aligned}\dot{\hat{\theta}}_e &= \hat{\omega} + \tilde{K}_{1,2}|\frac{\Lambda_\theta}{\mu}|^{\frac{2}{3}} sign(\frac{\Lambda_\theta}{\mu}) \\ \dot{\hat{\omega}} &= \hat{\alpha} + \tilde{K}_{2,2}|\frac{\Lambda_\theta}{\mu}|^{\frac{1}{3}} sign(\frac{\Lambda_\theta}{\mu}) \\ \dot{\hat{\alpha}} &= \tilde{K}_{3,2} sign(\frac{\Lambda_\theta}{\mu})\end{aligned} \tag{2.95}$$

Then, the observer (2.95) is used to estimate the angular position, speed and acceleration. In Figure 2.6, a scheme of the proposed adaptive observer-2 is introduced. As previously mentioned, $\hat{\theta} = \dfrac{\hat{\theta}_e}{p}$ is the estimated mechanical angular position and $\hat{\Omega} = \dfrac{\hat{\omega}}{p}$ is the estimated mechanical speed.

2.3.3 Simulation results

Considering the second adaptive observer introduced in this section. Simulation results in open-loop are going to introduced to estimate angular position, speed and acceleration. As previously mentioned, simulation test has been carried out in Matlab-Simulink environment, using a sampling time of 1×10^{-3} with a fixed-step *ode*4 solver. The profiles

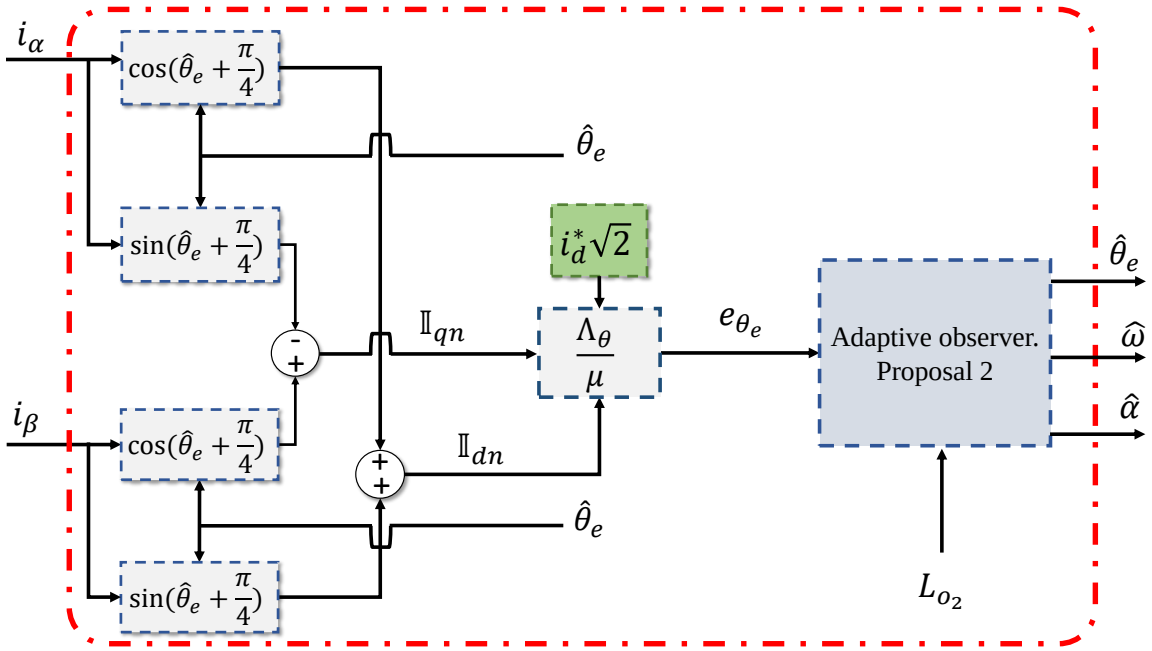

Figure 2.6 – Scheme of the proposed AHOSMO-2.

in Figure 1.7 and the parameter variations in Figure 1.8 have been used. Moreover, the parameters of the adaptive observer are given in Table 2.2.

Table 2.2 – Parameters for the AHOSMO-2

Values		
$L_{o_2}(0)$	γ_{o_2}	k_{o_2}
8	0.0001	80

In Figure 2.7, angular position estimation and its estimation error are illustrated, showing good effectiveness during the estimation despite parametric uncertainties. In Figure 2.8, speed estimation and its speed estimation error can show that the strategy based on the virtual system without parameters has a good performance. Moreover, it is compensated with the estimation of the acceleration (see Figure. 2.9-a) to avoid large estimation errors in the speed and angular position. In addition, in Figure. 2.9-b, the adaptive parameter $L_o(t)$ is introduced, showing the profile it takes to achieve the correct estimation of the estimates.

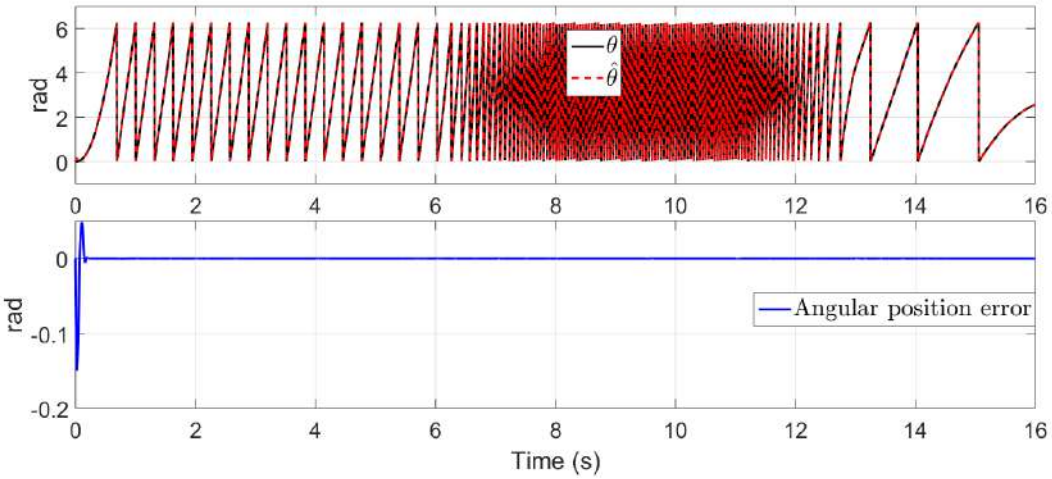

Figure 2.7 – AHOSMO-2. Rotor angular position estimation and its angular error

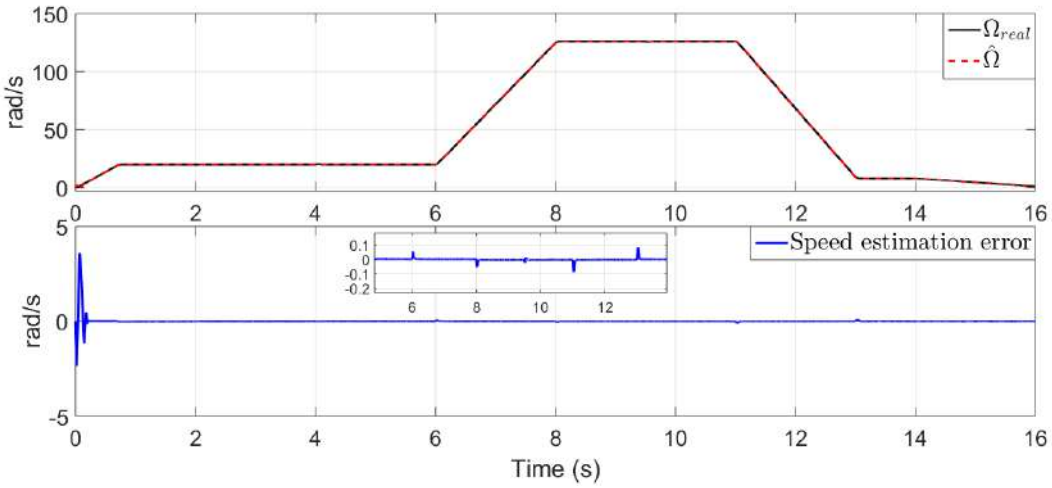

Figure 2.8 – AHOSMO-2. Rotor speed estimation and speed estimation error

2.4 Comparative study

In this section, from simulations, a comparative study is approached. A comparison among an observer based on back-electromotive force, an observer based on mechanical system by using first-order sliding modes and an observer based on high frequency signal injection is carried out by simulation test under parameter variations (see Figure 1.8). First, an observer based on back-electromotive force is introduced in Figure 2.10 for estimating angular position and speed. In this class of observers, the use of low pass filter

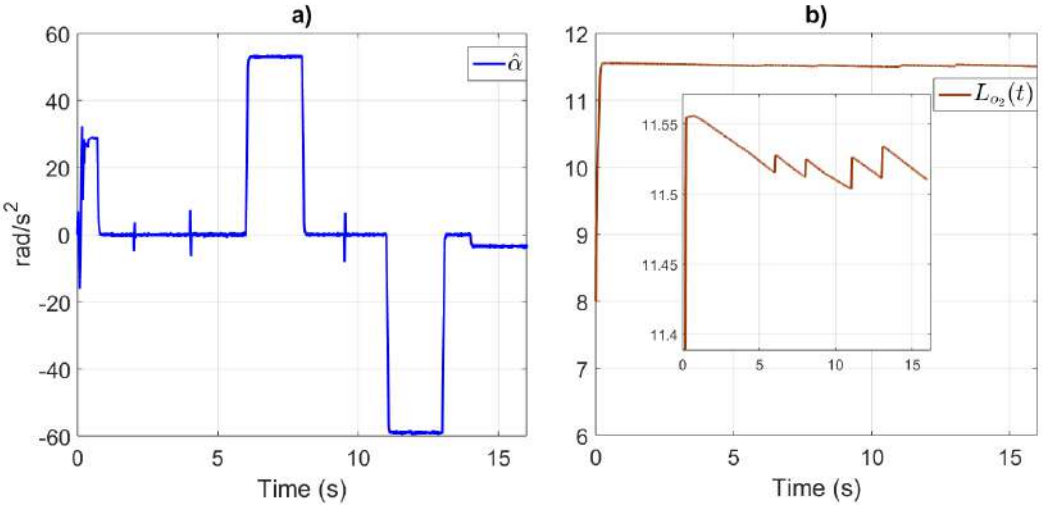

Figure 2.9 – AHOSMO-2. Estimation of the acceleration (a) and behaviour of the adaptive law (b)

generates a phase-delay in the estimation of the angular position, and the parameter variations causes an error increment. After that, an observer based on mechanical system by using first-order sliding modes is shown in Figure 2.11, estimating speed, angular position and load torque. The chattering effect can be seen in the angular error and the speed estimation error. Moreover, the effect of parameter variations causes an error increase in the estimation of the load torque. Another strategy often used in sensorless methods is the observer based on high frequency signal injection, which considers an extraction of angular error from high frequency signal injection. In Figure 2.12, this strategy is introduced in order to estimate angular position and speed. Then, from the errors in speed and angular position, it is possible to see the performance of this strategy under the variation of parameters. A disadvantage of this strategy is the sensitivity to variations in inductance.

A performance index, Integral Absolute Error (IAE), is computed in order to show numerically the performance of each observer for the angular position estimation error and the speed estimation error as can be illustrated in Figure 2.14 and Figure 2.13, respectively.

The proposed observers (AHOSMO-1, AHOSMO-2) based on virtual system achieve a better performance compared with the other strategies. The improvement can be shown from the performance index, validating the effectiveness of the proposed observers. Therefore, it is possible to say that extraction of the angular error e_{θ_e} introduced in section 2.1 has been achieved successfully.

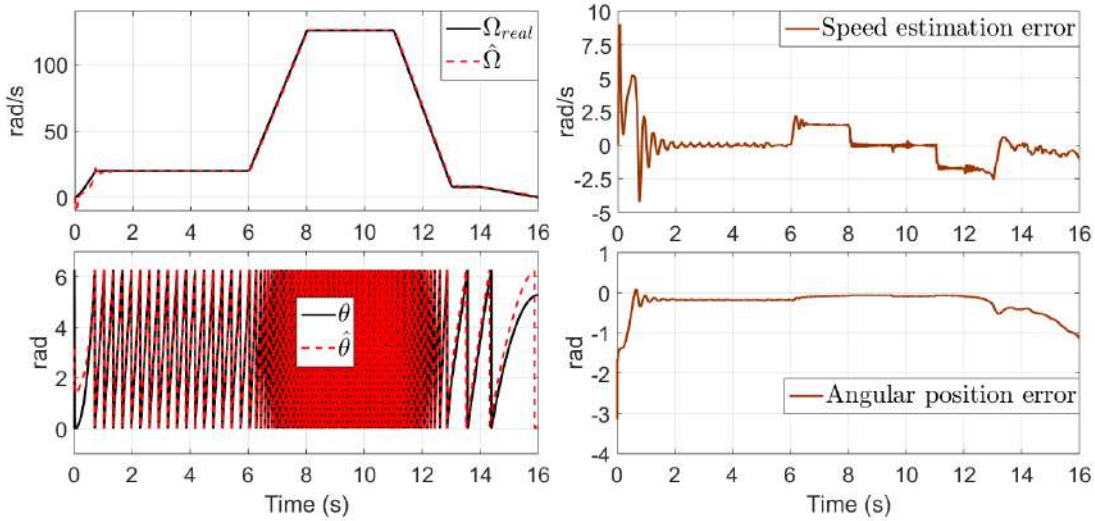

Figure 2.10 – Simulation test: Observer based on back-electromotive force

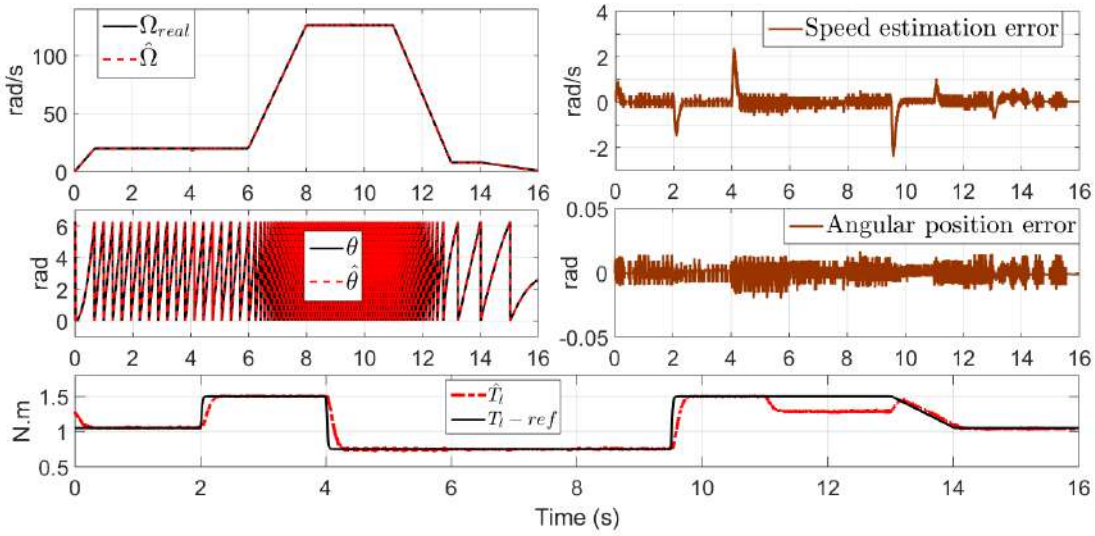

Figure 2.11 – Simulation test: Observer based on mechanical system by using first-order sliding modes

In addition, a simulation test to show the convergence of the observer has been carried out, as can be seen in Figure 2.15. The initial conditions for the estimated speed and estimated angular position are $\hat{\Omega}(0) = 20$ rad/s and $\hat{\theta}(0) = 5.5$ rad, respectively. We can see as the convergence is ensured such that convergence of the observer is achieved in finite time.

On the other hand, this work proposes adaptive observers for the observer. Therefore,

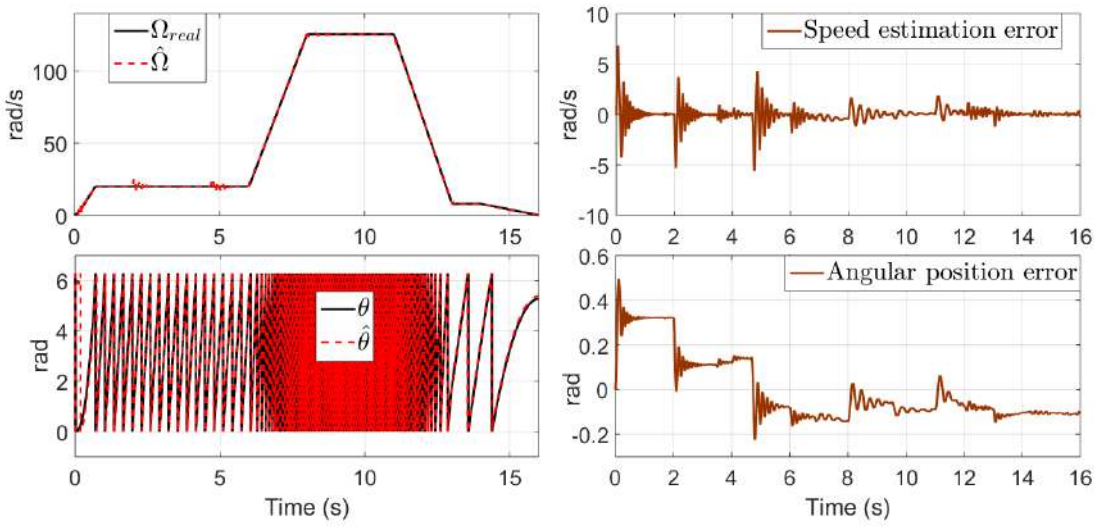

Figure 2.12 – Simulation test: Observer based on high frequency signal injection

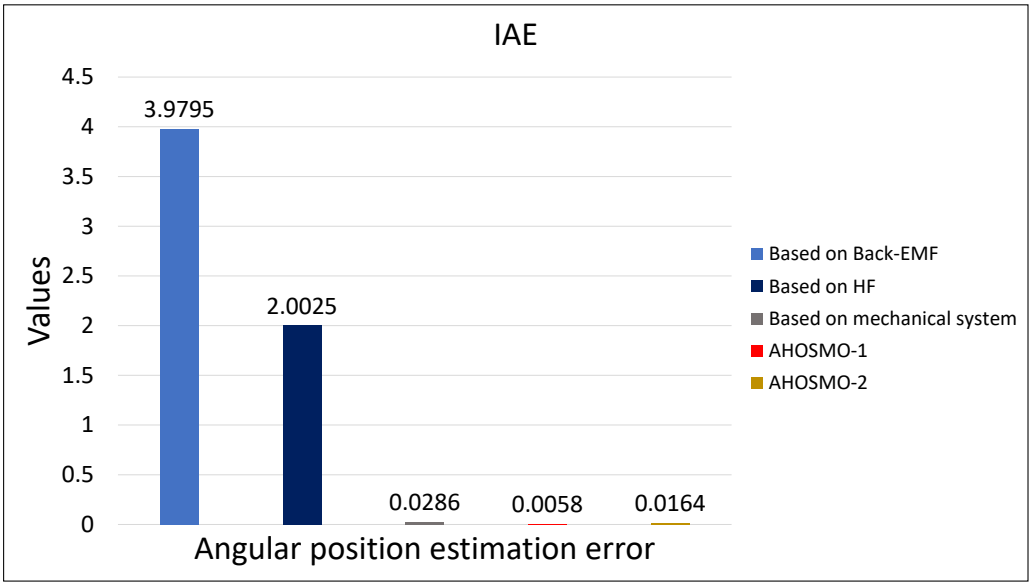

Figure 2.13 – Performance index for the angular position estimation error

two simulation tests have been carried out to show the advantages of using adaptive gain instead of constant gains. These demo tests have been applied in AHOSMO-1 taking into account that gains $K_{1,1}$, $K_{2,1}$ and $K_{3,1}$ are a function of the parameter L_o. Then, in Figure 2.16, a test is introduced by considering constant gains, i.e., L_o is constant. During this test, the gain L_o has taken 3 values; 4, 6 and 8, respectively. It is possible to see that estimation of speed, angular position and acceleration has a good performance

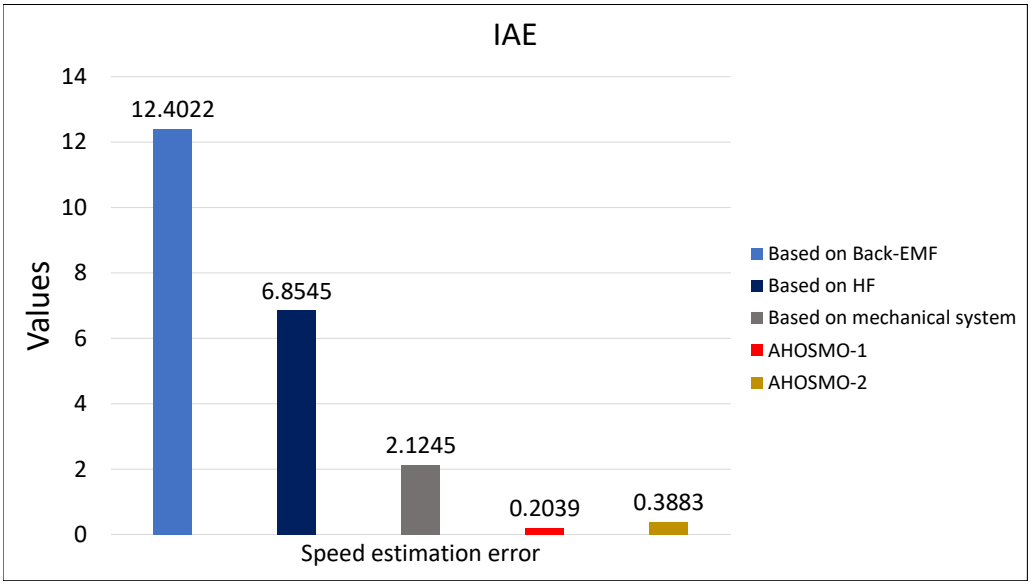

Figure 2.14 – Performance index for speed estimation error

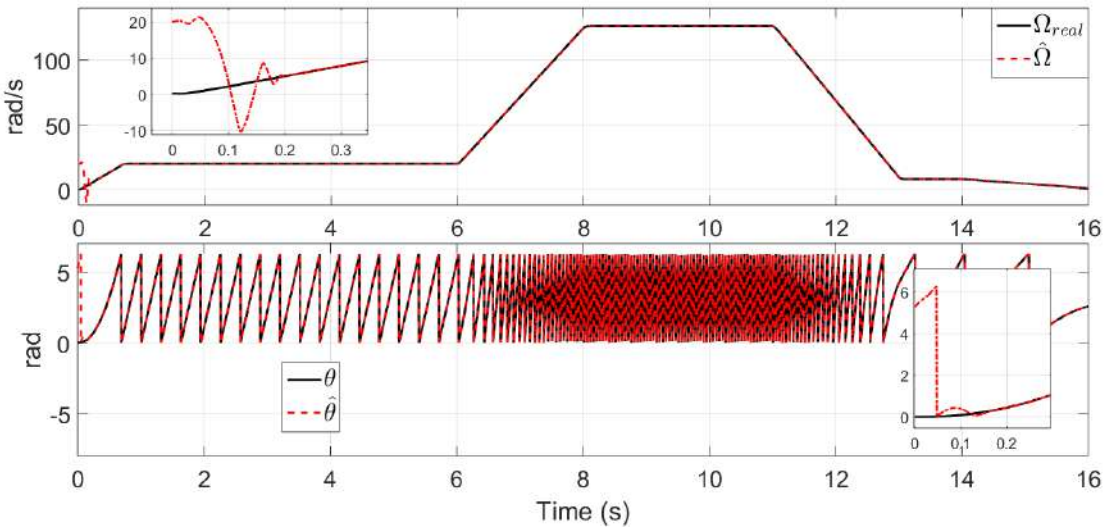

Figure 2.15 – Simulation test: Initial condition for the speed (Top) and initial condition for the angular position (Bottom)

when $L_o = 4$, avoiding the increase of chattering. However, at 5 seconds when $L_o = 6$, it is possible to see the increase of chattering in the estimation errors and estimated acceleration. Similarly occurs when $L_o = 8$ at 10 seconds. It is due to a gain overestimation, causing chattering in the estimations. Then, in order to avoid this issue, the use of adaptive gain have been an alternative, as shown in Figure 2.17, where is possible to illustrate how

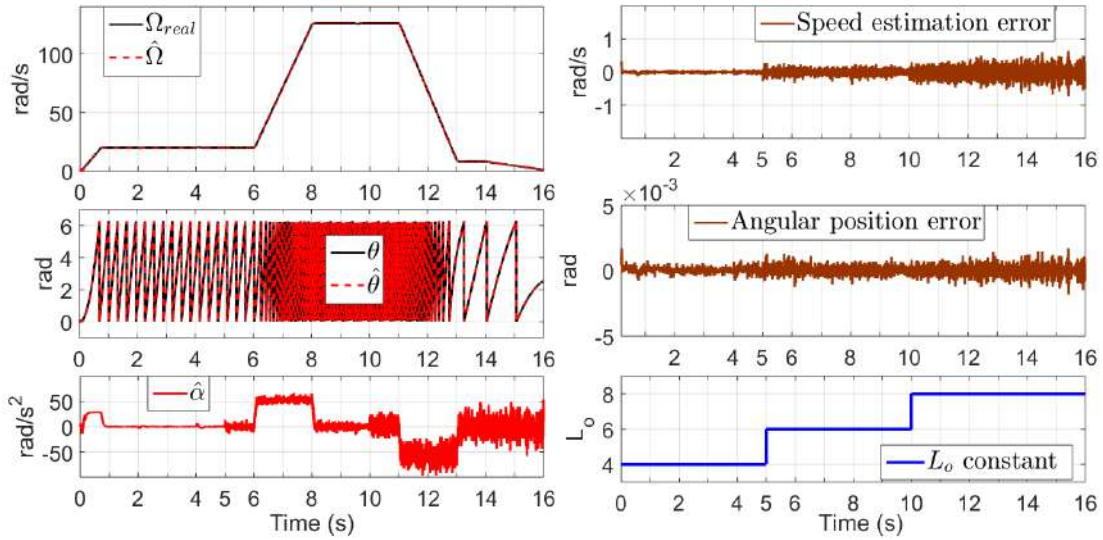

Figure 2.16 – AHOSMO-1. State estimation using different constant gains

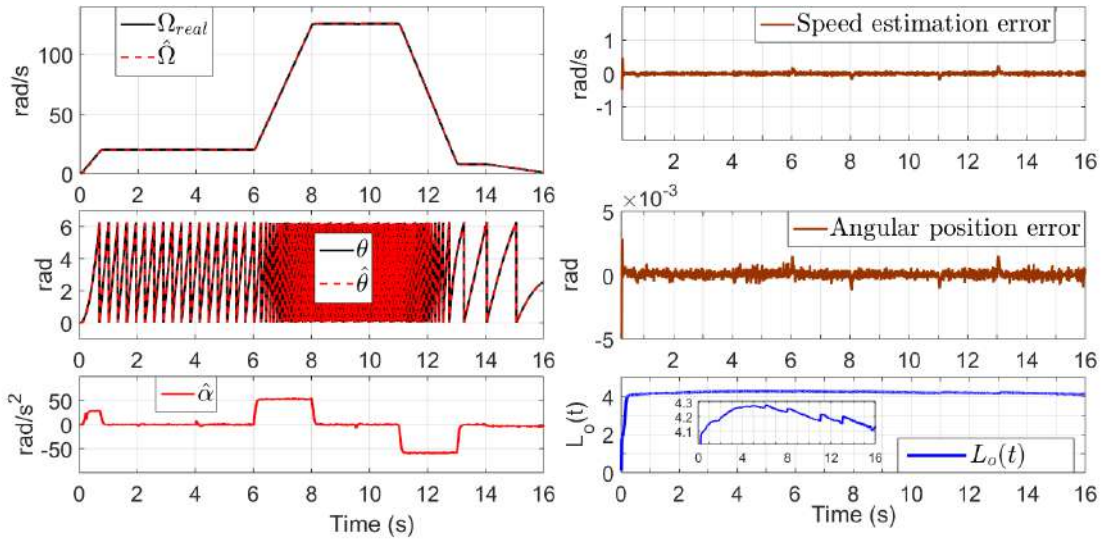

Figure 2.17 – AHOSMO-1. State estimation using adaptive gains

the gain $L_o(t)$ is adapted and finds the best value, avoiding an overestimation of gain, reducing chattering in the estimate and achieving a good estimation. Therefore, it has been shown that an adaptive gain can improve the result obtained by constant gains.

In addition, the proposed adaptive laws, for the parameters $L_o(t)$ and $L_{o_2}(t)$ of the observers AHOSMO-1 and AHOSMO-2, have been numerically evaluated at 5 seconds, as can be show in Table 2.3. The final value of each gain at 5 seconds can show that both adaptive laws have a similar behavior with respect to the energy used. However, the

adaptive for $L_{o_2}(t)$ has slightly higher values, such that it could be concluded that the adaptive law $L_o(t)$ is more conservative.

Table 2.3 – Value for the gains of both adaptive observers at 5 seconds

AHOSMO-1			
$L_o(5)$	$\tilde{K}_{1,1}$	$\tilde{K}_{2,1}$	$\tilde{K}_{3,1}$
4.14	32.07	228.5	542.9
AHOSMO-2			
$L_{o_2}(5)$	$\tilde{K}_{1,2}$	$\tilde{K}_{2,2}$	$\tilde{K}_{3,2}$
11.53	34.58	265.8	680.9

2.5 Proposed observer analysis

The performance of the proposed observer based on the extraction of e_{θ_e} is evaluated in a simulation and experimental test considering the profiles of Figure 1.9. A low-speed and zero region is taken into account due to that in this region most of the observers present observability problems. It is well known that IPMSM is not observable when the angular speed is equal to zero. However, in the proposed strategy, the angular position estimation error e_{θ_e} extracted depends on the dynamics of the current$-i_q$ directly. Therefore, the observability is ensured for a current$-i_q$ different to zero, i.e., $i_q \neq 0$, such that this condition is satisfied when the load torque or the speed are different to zero. In this way, the load torque profile considered in the validation has values equals to zero and different to zero with small values.

A simulation test is introduced in Figure 2.18 and an experimental test is introduced in Figure 2.19. Then, from Figure 2.18 and Figure 2.19, it is shown that at the beginning, the speed is 0 rad/s with a load torque going from 0.05 $N.m$ to 1 $N.m$. Then, the observer converges to real angular position and speed. After that, from 1.5 s to 4s the load torque is 0 $N.m$ and the speed is still 0 rad/s until 3 s. Therefore, from 1.5 s, the observer diverges, since, there exist a loss of observability when both speed and load torque are zero, since at that moment the electric machine is standstill and there is not a persistent current$-i_q$ in Λ_θ. However, from 3 s the speed increase until 2.5 rad/s, such that, the current$-i_q$ is different to 0, then the observer tends towards real speed and angular position. Therefore, from 3.5 s is possible to see the convergence in the angular position. Then, the speed stays

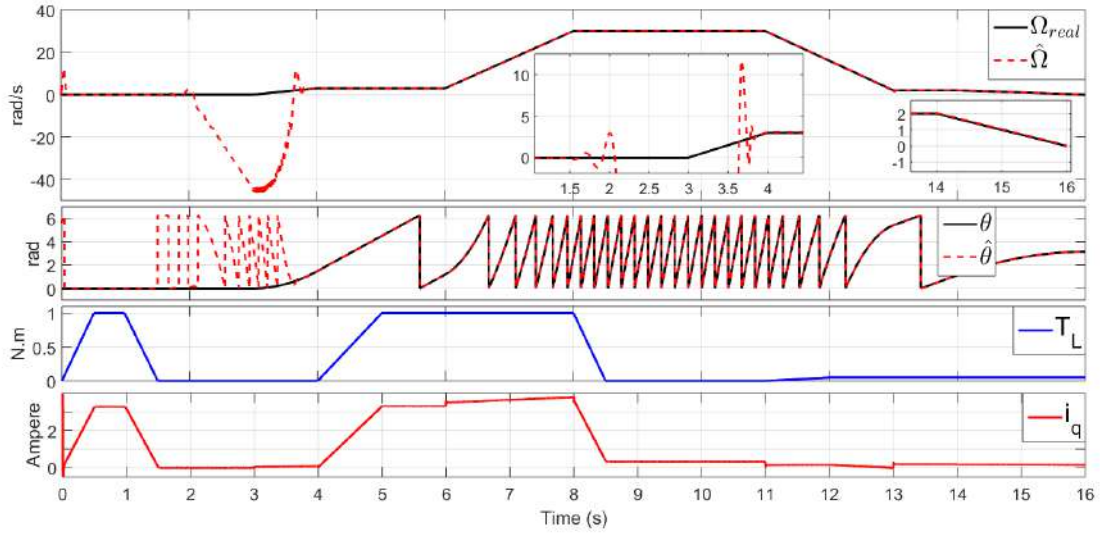

Figure 2.18 – Simulation test: Convergence of proposed adaptive observer and behaviour of current i_q, applying different profiles of small load Torque and low-speed.

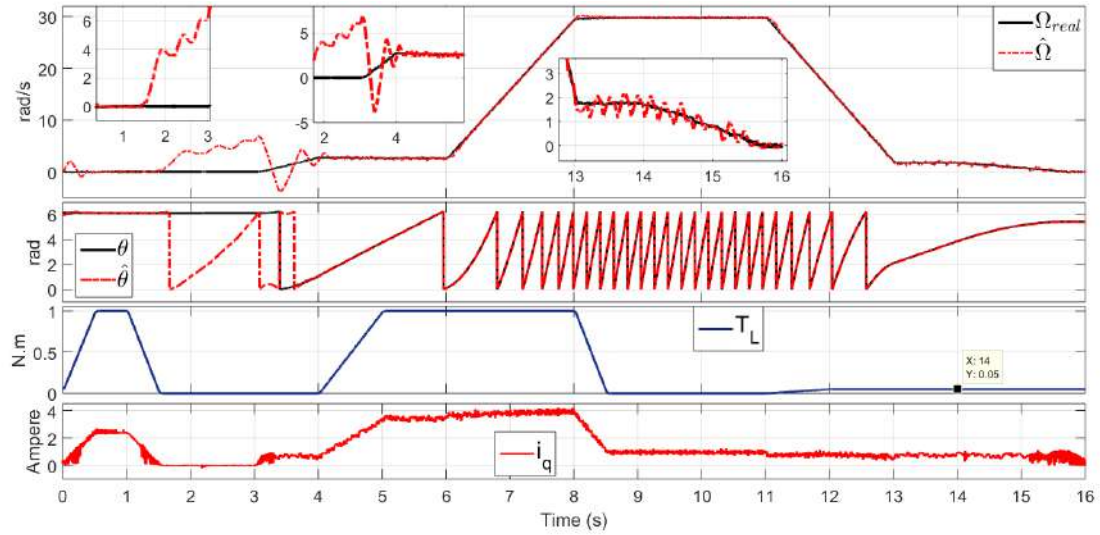

Figure 2.19 – Experimental test: Convergence of proposed adaptive observer and behaviour of current i_q, applying different profiles of small load Torque and low-speed.

at low speed (2.5 rad/s) for 2 s with a load torque different to 0 $N.m$, such that, a good estimation is achieved for the observer. After that, the speed increases until 30 rad/s and stays there for 3 s, and the load torque tends to 0 $N.m$ and stays there from 8.5 s to 11 s, such that, the observer achieves a very accurate estimate. Finally, the speed decreases until 2 rad/s and from 13 s until 16 s, the speed continues to decrease until it reaches 0

rad/s with an small load torque of 0.05 $N.m$. From this test it can be concluded that the observability depends on i_q directly, which must be different from zero ($i_q \neq 0$) to ensure the observability.

2.6 Conclusion

The extraction of the angular position estimation error has been the main challenge in this work in order to apply a sensorless technique. In this chapter, an new alternative for the extraction of the angular error e_θ in PMSM was presented. Considering that measurable currents $i_{\alpha\beta}$ can be taken from the abc triphasic components of the machine, this information has been considered and represented by using the Park transformation. Moreover, taking into account some ideas of the saliency method-based, one equation was defined without considering the high frequency signal injection characteristic. Then, after some calculations, one approximation of the angular error was obtained. It is worth mentioned that the extraction of the angular position error does not require the use of additional elements like filters and high frequency signal injection.

A sensorless scheme requires information of the angular position and speed. Then, the extracted angular error has been a key piece to design two adaptable observers based on a virtual system without machine parameters to estimate angular position and speed of the IPMSM. These adaptive observer have been designed by considering reparameterized gains, i.e., all gains are in terms of a single parameter to reduce the tuning time and facilitate the design of adaptive laws for the observers. Simulation tests were introduced as well as a comparative study. The effectiveness and performance of the adaptive observers based on the extraction of the angular error has been illustrated.

Chapter 3

Controller design for the Interior Permanent Magnet Synchronous motor

In this chapter, two adaptive controllers are designed. The gains of these controllers are based on a single parameter to reduce the tuning time. The controllers will be applied to track a reference of direct-axis current and speed. Some tests for the adaptive controllers are addressed and a comparative study is introduced.

3.1 Control design based on Super-Twisting approach: Proposal-1

Consider the class of nonlinear system given by

$$\begin{aligned} \dot{\chi}_1 &= \chi_2 \\ \dot{\chi}_2 &= f(\chi) + g(\chi)u + \delta(t) \\ y &= C\chi \end{aligned} \tag{3.1}$$

where $\chi = [\chi_1 \quad \chi_2]^T$ is a state vector, for $\chi \in \Re^2$; $u \in \Re$ is the input, $f(\chi)$ and $g(\chi)$ are nonlinear terms, $y \in \Re$ is the output of the system, $\delta(t)$ is a time-varying external disturbance and $C = [1 \quad 0]$.

Assumption 3.1. *The nonlinear terms $f(\chi)$ and $g(\chi)$ are globally Lipschitz with respect to χ [87].*

Now, a sliding surface S is defined as follows

$$S = \vartheta_{11} e_{1_\chi} + e_{2_\chi} \tag{3.2}$$

where $e_{1_\chi} = \chi_1 - \chi_{ref}$ is a tracking error, $e_{2_\chi} = \dot{\chi}_1 - \dot{\chi}_{ref}$ and $\vartheta_{11} > 0$; whose dynamic is given by

$$\dot{S} = \vartheta_{11} e_{2_\chi} + f(\chi) + g(\chi)u + \delta(t) - \ddot{\chi}_{ref} \tag{3.3}$$

A control input is chosen as follows

$$u = \frac{1}{g(\chi)} \left[-\vartheta_{11} e_{2_\chi} - f(\chi) + \ddot{\chi}_{ref} + \mathcal{V}_{st} \right], \tag{3.4}$$

with

$$\mathcal{V}_{st} = -K_{c1} |S|^{\frac{1}{2}} sign(s) - \int K_{c2} sign(S) dt \tag{3.5}$$

where $K_{c1} = 2L_c^2$ and $K_{c2} = \dfrac{L_c^4}{2}$ are reparameterized based on a single parameter L_c, such that L_c is a constant positive parameter large enough. Then, equation (3.4) is a super twisting control for the system (3.1). However, tuning with constant gains sometimes causes gain overestimation. Therefore, in the next section, an adaptive control will be presented to avoid this problem.

3.1.1 Adaptive super-twisting control design

Consider the following control

$$u = \frac{1}{g(\chi)} \left[-\vartheta_{11} e_{2_\chi} - f(\chi) + \ddot{\chi}_{ref} + \mathcal{V}_{st} \right], \tag{3.6}$$

with

$$\mathcal{V}_{st} = -\tilde{K}_{c1} |S|^{\frac{1}{2}} sign(s) - \int_0^t \tilde{K}_{c2} sign(S) d\tau \tag{3.7}$$

which is an Adaptive Super-Twisting Control (ASTWC-1) for the system (3.1) and their reparameterized gains, in terms of a single parameter, are defined by

$$\tilde{K}_{c1} = 2L_c^2(t) \qquad \tilde{K}_{c2} = \frac{L_c^4(t)}{2} \tag{3.8}$$

where $L_c(t)$ is an adaptive parameter that will be introduced later.

Remark 3.1. *A demonstration to compute the proposed gains has been introduced in Appendix A (See A.2.1).*

A stability analysis and the adaptive law design for the parameter $L_c(t)$ will be introduced in the sequel.

Consider that the dynamic of the sliding surface (3.3) in closed-loop with the control (3.6) is given by

$$\dot{S} = -\tilde{K}_{c1}|S|^{\frac{1}{2}}sign(S) - \int_0^t \tilde{K}_{c2}sign(S)d\tau + \delta(t) \tag{3.9}$$

where (3.9) can be expressed as follows

$$\begin{cases} \dot{S} = -\tilde{K}_{c1}|S|^{1/2}sign(S) + \nu + \delta(t) \\ \dot{\nu} = -\tilde{K}_{c2}sign(S) \end{cases} \tag{3.10}$$

then, sliding variable S and its time derivative $\dot{S}$ converge to 0 in finite time.

Assumption 3.2. *$\delta(t)$ and its time derivative $\dot{\delta}(t)$ are bounded for unknown positive constants, i.e., $|\delta(t)| < \delta_M$, $|\dot{\delta}(t)| \leq \Delta_M$; with $\delta_M, \Delta_M > 0$, $\forall t \geq 0$ [88].*

Now, introducing the following change of variable: $\Upsilon_1 = S$ and $\Upsilon_2 = \nu + \delta(t)$. System (3.10) is expressed as

$$\Sigma_{STW} : \begin{cases} \dot{\Upsilon}_1 = -\tilde{K}_{c1}|\Upsilon_1|^{1/2}sign(\Upsilon_1) + \Upsilon_2, \\ \dot{\Upsilon}_2 = -\tilde{K}_{c2}sign(\Upsilon_1) + d(t) \end{cases} \tag{3.11}$$

with $d(t) = \dot{\delta}(t)$. Consider the following change of coordinates

$$z_1 = \frac{\Upsilon_1}{L_c^2(t)} \qquad z_2 = \frac{\Upsilon_2}{L_c^2(t)} \tag{3.12}$$

and its first derivative in time as follows

$$\begin{aligned} \dot{z}_1 &= -2L_c(t)|z_1|^{\frac{1}{2}}sign(z_1) + z_2 - \frac{2z_1\dot{L}_c(t)}{L_c(t)} \\ \dot{z}_2 &= -\frac{L_c^2(t)}{2}sign(z_1) + \frac{d(t)}{L_c^2(t)} - \frac{2z_2\dot{L}_c(t)}{L_c(t)} \end{aligned} \tag{3.13}$$

After that, a new change of variable is given by

$$\pounds_1 = |z_1|^{\frac{1}{2}}sign(z_1) \qquad \pounds_2 = \frac{z_2}{L_c(t)} \tag{3.14}$$

then the dynamics, in terms of these new variables, are given by

$$\begin{aligned}\dot{\pounds}_1 &= \frac{L_c(t)}{2|z_1|^{\frac{1}{2}}}\left[-2\pounds_1 + \pounds_2\right] - \pounds_1\frac{\dot{L}_c(t)}{L_c(t)} \\ \dot{\pounds}_2 &= \frac{L_c(t)}{2|z_1|^{\frac{1}{2}}}\left[-\pounds_1 + \frac{2|z_1|^{\frac{1}{2}}d(t)}{L_c^4(t)}\right] - 3\pounds_2\frac{\dot{L}_c(t)}{L_c(t)}\end{aligned} \tag{3.15}$$

To make some calculations easier, system (3.15) can be expressed in compact form as follows

$$\dot{\pounds} = \alpha_c\left[\left(A_c - P_c^{-1}C_c^TC_c\right)\pounds + \Phi_c\right] - N_c\pounds\frac{\dot{L}_c(t)}{L_c(t)} \tag{3.16}$$

with $\alpha_c = \dfrac{L_c(t)}{2|z_1|^{\frac{1}{2}}}$, and

$$\pounds = \begin{bmatrix}\pounds_1 & \pounds_2\end{bmatrix}^T, \qquad C_c = \begin{bmatrix}1 & 0\end{bmatrix},$$

$$A_c = \begin{bmatrix}0 & 1\\ 0 & 0\end{bmatrix}, \qquad N_c = \begin{bmatrix}1 & 0\\ 0 & 3\end{bmatrix}, \qquad \Phi_c = \begin{bmatrix}0\\ \dfrac{2|z_1|^{\frac{1}{2}}}{L_c^4(t)}\left(d(t)\right)\end{bmatrix} \qquad P_c = \begin{bmatrix}1 & -1\\ -1 & 2\end{bmatrix},$$

where P_c is a symmetric positive-definite matrix, solution of the following equation

$$P_c + A_c^TP_c + P_cA_c - C_c^TC_c = 0 \tag{3.17}$$

Assumption 3.3. *The terms in Φ_c are uniformly bounded with respect to u and locally Lipschitz with respect to $\pounds$, i.e., $||\Phi_c|| \leq \wp||\pounds||$, for $\wp > 0$.*

Theorem 3.1. *Consider the system* (3.11) *and the Assumption 3.1, 3.2 and 3.3 are fulfilled. Furthermore,*

$$\dot{L}_c(t) = k_c^{\frac{1}{2}}|S|^{\frac{1}{2}} - \gamma_c^{\frac{1}{2}}L_c^2(t) \tag{3.18}$$

is an adaptive law-1 for $L_c(t)$, with $k_c > 0$ and $\gamma_c > 0$ chosen appropriately, where $k_c > \gamma_c > 0$. Then, the trajectories of Σ_{STW} converge towards a vicinity of the origin in finite time.

Proof

Consider a Lyapunov candidate function as follows

$$V_{(\pounds,L_c(t))} = V_{(\pounds)} + V_{(L_c(t))} \tag{3.19}$$

with $V_{(\pounds)} = \pounds^TP_c\pounds$ and $V_{(L_c(t))} = \dfrac{\gamma_c}{2}L_c^2(t)$, for $\gamma_c > 0$. Then, taking its first derivative in

time and replacing the suitable expressions, it follows that

$$\begin{aligned}\dot{V}_{(\pounds,L_c(t))} =&\alpha_c \pounds^T \left[A_c^T P_c + P_c A_c\right] \pounds - 2\alpha_c \pounds^T C^T C \pounds - \frac{\dot{L}_c(t)}{L_c(t)} \pounds^T \left[P_c N_c + N_c P_c\right] \pounds \\ &+ \gamma_c \dot{L}_c(t) L_c(t) + 2\alpha_c \pounds^T P_c \Phi_c\end{aligned} \tag{3.20}$$

From $A_c^T P_c + P_c A_c = -P_c + C_c^T C_c$, it follows that above equation can be expressed as follows

$$\begin{aligned}\dot{V}_{(\pounds,L_c(t))} =& -\alpha_c \pounds^T P_c \pounds - \alpha_c \pounds^T C_c^T C_c \pounds - \frac{\dot{L}_c(t)}{L_c(t)} \pounds^T \left[P_c N_c + N_c P_c\right] \pounds \\ &+ \gamma_c \dot{L}_c(t) L_c(t) + 2\alpha_c \pounds^T P_c \Phi_c\end{aligned} \tag{3.21}$$

Now, considering that $P_c N_c + N_c P_c = R_c$ and defining R_c as a symmetric positive-definite matrix. Then, $\pounds^T R_c \pounds \geq \dfrac{\lambda_{min}(R_c)}{\lambda_{max}(P_c)} V_{(\pounds)} = k_c V_{(\pounds)}$, where $\lambda_{min}(R_c)$ and $\lambda_{max}(P_c)$ are minimum and maximum singular values of R_c and P_c, respectively; moreover, considering that $-\alpha_c \pounds^T C_c^T C_c \pounds < 0$; for $L_c(t) > 0$. Then,

$$\dot{V}_{(\pounds,L_c(t))} \leq -\alpha_c V_{(\pounds)} - \frac{\dot{L}_c(t)}{L_c(t)} \left[k_c V_{(\pounds)} - \gamma_c L_c^2(t)\right] + 2\alpha_c \pounds^T P_c \Phi_c \tag{3.22}$$

Now, from (3.22), the term

$$\left[k_c V_{(\pounds)} - \gamma_c L_c^2(t)\right] = \left[k_c^{\frac{1}{2}} V_{(\pounds)}^{\frac{1}{2}} + \gamma_c^{\frac{1}{2}} L_c(t)\right] \left[k_c^{\frac{1}{2}} V_{(\pounds)}^{\frac{1}{2}} - \gamma_c^{\frac{1}{2}} L_c(t)\right]$$

and defining $f_{(V_{(\pounds)},L_c(t))} = \left[k_c^{\frac{1}{2}} V_{(\pounds)}^{\frac{1}{2}} + \gamma_c^{\frac{1}{2}} L_c(t)\right] > 0$. It follows that

$$\dot{V}_{(\pounds,L_c(t))} \leq -\alpha_c V_{(\pounds)} - f_{(V_{(\pounds)},L_c(t))} \frac{\dot{L}_c(t)}{L_c(t)} \left[k_c^{\frac{1}{2}} V_{(\pounds)}^{\frac{1}{2}} - \gamma_c^{\frac{1}{2}} L_c(t)\right] + 2\alpha_c \pounds^T P_c \Phi_c \tag{3.23}$$

Consider that the following inequalities are satisfied,

$$|z_1| = |\pounds_1|^2 \leq ||\pounds||^2 \tag{3.24}$$

and

$$\lambda_{min}(P_c)||\pounds||^2 \leq V_{(\xi)} \leq \lambda_{max}(P_c)||\pounds||^2 \tag{3.25}$$

where $\lambda_{min}(P_c)$ and $\lambda_{max}(P_c)$ are the minimum and maximum singular values of P_c. Then,

it follows that the following inequality hold,

$$|z_1|^{\frac{1}{2}} \leq ||\pounds|| \leq \left(\frac{V_{(\pounds)}}{\lambda_{min}(P_c)}\right)^{\frac{1}{2}} \tag{3.26}$$

for $z_1 = \dfrac{\Upsilon_1}{L_c^2(t)} = \dfrac{S}{L_c^2(t)}$. Now, taking into account the above inequality, equation (3.23) can be expressed as

$$\dot{V}_{(\pounds,L_c(t))} \leq -\alpha_c V_{(\pounds)} - f_{(V_{(\pounds)},L_c(t))}\frac{\dot{L}_c}{L_c(t)}\left[k_c^{\frac{1}{2}}\left(\frac{|S|}{L_c^2(t)}\right)^{\frac{1}{2}} - \gamma_c^{\frac{1}{2}}L_c(t)\right] + 2\alpha_c \pounds^T P_c \Phi_c \tag{3.27}$$

Therefore, an adaptive law can be chosen as follows,

$$\dot{L}_c(t) = \left[k_c^{\frac{1}{2}}\left(\frac{|S|}{L_c^2(t)}\right)^{\frac{1}{2}} - \gamma_c^{\frac{1}{2}}L_c(t)\right]L_c(t) \tag{3.28}$$

Then, it follows that

$$\dot{V}_{(\pounds,L_c(t))} \leq -\alpha_c V_{(\pounds)} - f_{(V_{(\pounds)},L_c(t))}\left[k_c^{\frac{1}{2}}\left(\frac{|S|}{L_c^2(t)}\right)^{\frac{1}{2}} - \gamma_c^{\frac{1}{2}}L_c(t)\right]^2 + 2\alpha_c \pounds^T P_c \Phi_c \tag{3.29}$$

Assuming that S tends to zero faster than $L_c(t)$. Then, (3.29) is given by

$$\dot{V}_{(\pounds,L_c(t))} \leq -\alpha_c V_{(\pounds)} - f_{(V_{(\pounds)},L_c(t))}\gamma_c L_c^2(t) + 2\alpha_c \pounds^T P_c \Phi_c \tag{3.30}$$

Moreover, from Assumption 3.3 and taking into account the norm for the term $2\alpha_c \pounds^T P_c \Phi_c$, it follows that

$$\dot{V}_{(\pounds,L_c(t))} \leq -\alpha_c V_{(\pounds)} + 2\alpha_c \wp ||\pounds||^2 ||P_c|| - f_{(V_{(\pounds)},L_c(t))}\gamma_c L_c^2(t) \tag{3.31}$$

and considering the inequality (3.25), it is obtained the following

$$\dot{V}_{(\pounds,L_c(t))} \leq -\frac{L_c(t)}{2|z_1|^{\frac{1}{2}}}[1-\sigma_c]V_{(\pounds)} - f_{(V_{(\pounds)},L_c(t))}\gamma_c L_c^2(t) \tag{3.32}$$

with $\sigma_c = \dfrac{2\wp||P_c||}{\lambda_{min}(P_c)}$. Moreover, taking into account (3.26), the above equation can be

expressed as follows

$$\dot{V}_{(\pounds,L_c(t))} \leq -L_c(t)\Gamma_c V_{(\pounds)}^{\frac{1}{2}} - f_{(V_{(\pounds)},L_c(t))}\gamma_c L_c^2(t) \tag{3.33}$$

with $\Gamma_c = \dfrac{[1-\sigma_c]\lambda_{min}^{\frac{1}{2}}(P_c)}{2}$. Now, equation (3.33) will be factored as follows

$$\dot{V}_{(\pounds,L_c(t))} \leq -L_c(t)\sqrt{2}\gamma_c^{\frac{1}{2}}\left[\frac{\Gamma_c}{\sqrt{2}\gamma_c^{\frac{1}{2}}}V_{(\pounds)}^{\frac{1}{2}} + f_{(V_{(\pounds)},L_c(t))}\frac{\gamma_c^{\frac{1}{2}}}{\sqrt{2}}L_c(t)\right] \tag{3.34}$$

Thus, selecting $\eta_1 = \left[L_c(t)\sqrt{2}\gamma_c^{\frac{1}{2}}\right]$ and $\varphi_c = min\left[\dfrac{\Gamma_c}{\sqrt{2}\gamma_c^{\frac{1}{2}}}, f_{(V_{(\pounds)},L_c(t))}\right]$, it is possible to express the following equation

$$\dot{V}_{(\pounds,L_c(t))} \leq -\eta_2\left[V_{(\pounds)}^{\frac{1}{2}} + \frac{\gamma_c^{\frac{1}{2}}}{\sqrt{2}}L_c(t)\right] \tag{3.35}$$

with $\eta_2 = \eta_1\varphi_c$. Then, from Jensen´s inequality [84],

$$[|a_c|^m + |b_c|^m]^{\frac{1}{m}} \leq |a_c| + |b_c|, \tag{3.36}$$

defining $a_c = V_{(\pounds)}^{\frac{1}{2}}$, $b_c = V_{(L_c)}^{\frac{1}{2}}$ and $m = 2$. Thus, the following inequality can be established

$$\left[|V_{(\pounds)}^{\frac{1}{2}}|^2 + |V_{(L_c(t))}^{\frac{1}{2}}|^2\right]^{\frac{1}{2}} \leq |V_{(\pounds)}^{\frac{1}{2}}| + \frac{\gamma_c^{\frac{1}{2}}}{\sqrt{2}}|L_c(t)| \tag{3.37}$$

In this way

$$V_{(\pounds,L_c(t))}^{\frac{1}{2}} \leq |V_{(\pounds)}^{\frac{1}{2}}| + \frac{\gamma_c^{\frac{1}{2}}}{\sqrt{2}}|L_c(t)| \tag{3.38}$$

Therefore, the dynamic of Lyapunov function can be expressed as

$$\dot{V}_{(\pounds,L_c(t))} \leq -\eta_2 V_{(\pounds,L_c(t))}^{\frac{1}{2}}. \tag{3.39}$$

Then, from the Lyapunov function, $\dot{V}_{(\pounds,L_c(t))}$ is negative definite and ensures convergence in finite-time, for $L_c(t)$ sufficiently large, satisfying $\eta_2 > 0$. Moreover, the comparison principle is taken into account to estimate the convergence time. Thus, considering the equation $\dot{v} = -\eta_2 v^{\frac{1}{2}}$ and its solution defined as $v(t) = (v(0)^{\frac{1}{2}} - \frac{1}{2}\eta_2 t)^2$. Then,

$V_{(\pounds,L_c(t))} < v(t)$ when $V_{(\pounds(0),L_c(0))} < v(0)$, such that, $\pounds$ has a convergence in finite-time in an estimated time given by $T_2 = \frac{2V^{\frac{1}{2}}_{(\pounds(0),L_c(0))}}{\eta_2}$. Therefore, $\pounds$ tends to zero as well as S tends to zero in finite-time.

3.1.2 Control design for IPMSM

The design of controllers for the speed and the direct-axis current are presented by considering the adaptive law-1 given by Theorem 3.1.

Control loop for speed$-\Omega$

Consider a sliding surface given by

$$S_\Omega = \vartheta_{12} e_{1_\Omega} + e_{2_\Omega} \tag{3.40}$$

where $e_{1_\Omega} = \Omega - \Omega^*$ is speed tracking error, $e_{2_\Omega} = \dot{\Omega} - \dot{\Omega}^*$ and $\vartheta_{12} > 0$. Therefore, the dynamic of the sliding surface S_Ω is given by

$$\dot{S}_\Omega = \vartheta_{12} e_{2_\Omega} + a_1 b_1 + a_2 b_2 + a_3 b_2 - b_3 - \ddot{\Omega}^* + v_q c_1 \tag{3.41}$$

where $a_1 = \frac{p(L_d - L_q) i_q}{J}$, $a_2 = \frac{p(L_d - L_q) i_d}{J}$, $a_3 = \frac{p\psi_r}{J}$, $b_1 = \frac{v_d}{L_d} - \frac{R_s i_d}{L_d} + \frac{L_q p \Omega i_q}{L_d}$, $b_2 = -\frac{R_s i_q}{L_q} - \frac{L_d p \Omega i_d}{L_q} - \frac{\psi_r p \Omega}{L_q}$, $b_3 = \frac{f_v}{J}\left[\frac{p(L_d - L_q) i_d i_q}{J} + \frac{p\psi_r i_q}{J} - \frac{f_v \Omega}{J}\right]$ and $c_1 = \frac{p(L_d - L_q) i_d}{J L_q} + \frac{p\psi_r}{J L_q}$. Then, the control input v_q is given by

$$v_q = \frac{1}{c_1}\left[-\vartheta_{12} e_{2_\Omega} - a_1 b_1 - a_2 b_2 - a_3 b_2 + b_3 + \ddot{\Omega}^* + \mathcal{V}_{st-\Omega}\right] \tag{3.42}$$

with

$$\mathcal{V}_{st-\Omega} = -\tilde{K}_{c1_\Omega} |S_\Omega|^{\frac{1}{2}} sign(S_\Omega) - \int_0^t \tilde{K}_{c2_\Omega} sign(S_\Omega) d\tau \tag{3.43}$$

where $\tilde{K}_{c1_\Omega} = 2L^2_{c_\Omega}(t)$, $\tilde{K}_{c2_\Omega} = \frac{L^4_{c_\Omega}(t)}{2}$ and according to Theorem 3.1, $L_{c_\Omega}(t)$ is an adaptive parameter given by

$$\dot{L}_{c_\Omega}(t) = k^{\frac{1}{2}}_{c_\Omega} |S_\Omega|^{\frac{1}{2}} - \gamma^{\frac{1}{2}}_{c_\Omega} L^2_{c_\Omega}(t) \tag{3.44}$$

with $k_{c_\Omega} > \gamma_{c_\Omega} > 0$. Therefore, 3.42 is an ASTWC-1 for the speed of the IPMSM.

Control loop for current$-i_d$

A sliding surface is given by

$$S_{i_d} = \vartheta_{13} e_{i_d} + \int_0^t e_{i_d} d\tau \tag{3.45}$$

where $e_{i_d} = i_d - i_d^*$ is a current tracking error and $\vartheta_{13} > 0$. Moreover, the dynamic of the sliding surface S_{i_d} is given by

$$\dot{S}_{i_d} = -\frac{\vartheta_{13} R_s i_d}{L_d} + \frac{\vartheta_{13} p \Omega L_q i_q}{L_d} + \frac{\vartheta_{13} v_d}{L_d} - \vartheta_{13} \dot{i}_d^* + e_{i_d} \tag{3.46}$$

Then, the control input v_d can be chosen as follows

$$v_d = \frac{L_d}{\vartheta_{13}} \left(\frac{\vartheta_{13} R_s i_d}{L_d} - \frac{\vartheta_{13} p \Omega L_q i_q}{L_d} + \vartheta_{13} \dot{i}_d^* - e_{i_d} + \mathcal{V}_{st-i_d} \right) \tag{3.47}$$

with

$$\mathcal{V}_{st-i_d} = -\tilde{K}_{c1_{i_d}} |S_{i_d}|^{\frac{1}{2}} sign(S_{i_d}) - \int_0^t \tilde{K}_{c2_{i_d}} sign(S_{i_d}) d\tau \tag{3.48}$$

where $\tilde{K}_{c1_{i_d}} = 2L_{c_{i_d}}^2(t)$ and $\tilde{K}_{c2_{i_d}} = \dfrac{L_{c_{i_d}}^4(t)}{2}$ and according to Theorem 3.1, $L_{c_{i_d}}(t)$ is an adaptive parameter given by

$$\dot{L}_{c_{i_d}}(t) = k_{c_{i_d}}^{\frac{1}{2}} |S_{i_d}|^{\frac{1}{2}} - \gamma_{c_{i_d}}^{\frac{1}{2}} L_{c_{i_d}}^2(t) \tag{3.49}$$

with $k_{c_{i_d}} > \gamma_{c_{i_d}} > 0$. Therefore, 3.47 is an ASTWC-1 for the current$-i_d$ of the IPMSM.

3.1.3 Simulation result

Consider the adaptive law-1 established by Theorem 3.1 and the system (1.36)-(1.37) in closed-loop with the controllers given by (3.42) and (3.47). Then, simulation result are introduced in this section in order to show the performance of the system under the action of adaptive controllers. The parameters of the adaptive control are given in Table 3.1.

Table 3.1 – Parameters for the ASTWCs-1

Values							
$L_{c_\Omega}(0)$	ϑ_{12}	γ_{c_Ω}	k_{c_Ω}	$L_{c_{i_d}}(0)$	ϑ_{13}	$\gamma_{c_{i_d}}$	$k_{c_{i_d}}$
20	400	0.05	90	20	200	0.1	1

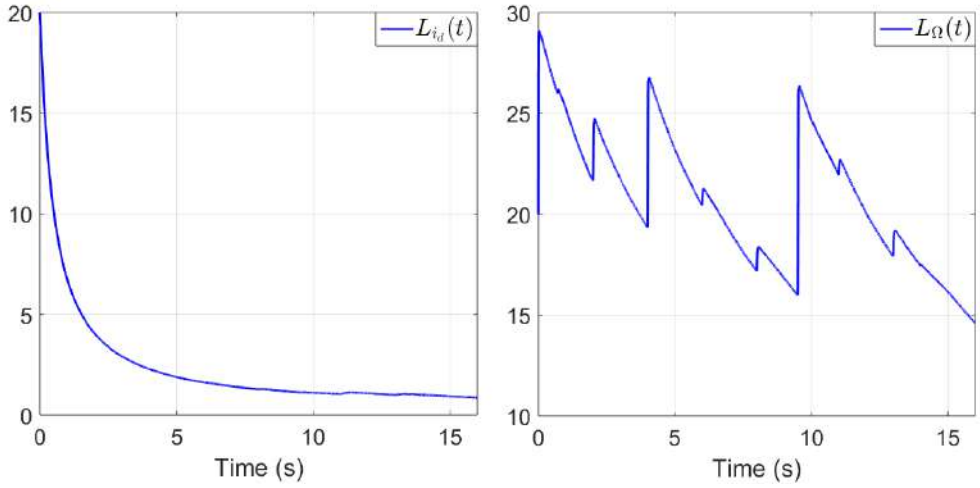

Figure 3.1 – ASTWC-1. Behaviour of adaptive law for the speed and current-i_d controllers

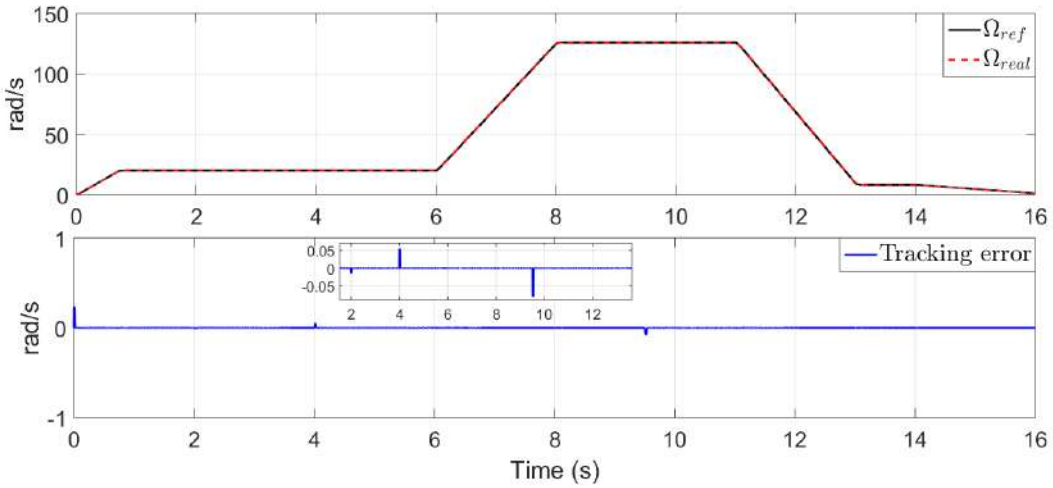

Figure 3.2 – ASTWC-1. Speed tracking and speed tracking error

The profile given by the Figure 1.7 and the parameter variation given by Figure 1.8 are considered in this test. In the first instance, it is possible to see the behavior of the adaptive gains in Figure 3.1, $L_{i_d}(t)$ and $L_\Omega(t)$, respectively. Then, considering this adaptive laws,

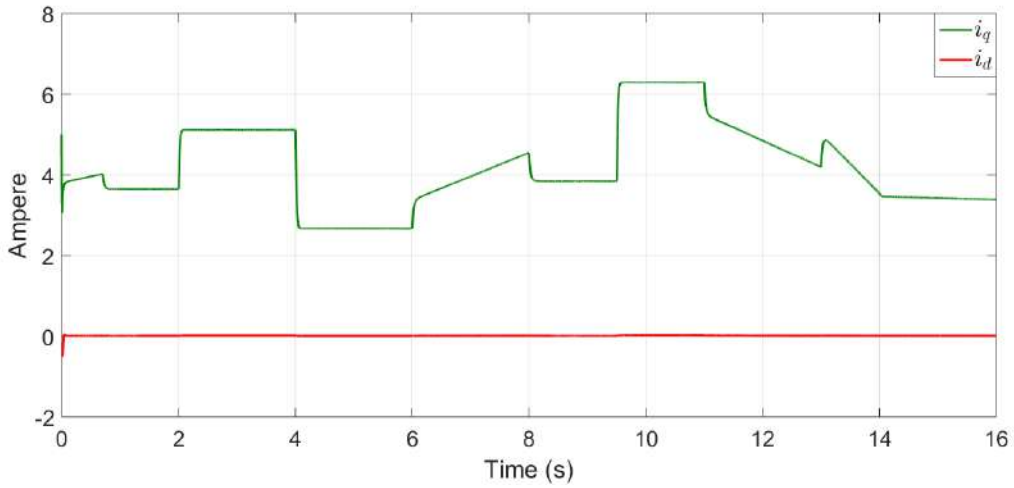

Figure 3.3 – ASTWC-1. Behaviour of the currents i_{dq}

the speed (see Figure 3.2) has been controlled. The tracking error can show a minimum error under the action of the load torque and parameters variations. In fact, in Figure 3.1, it is possible to see the reaction of the adaptive parameter in the controller when the load torque change its value, so that the adaptive gains adjust their values in order to reject system disturbances. Moreover, in Figure 3.3, the currents i_{dq} are introduced. The current$-i_d$ tracks a reference current equal to zero and the current$-i_q$ takes different values according to the speed and load torque. A good performance of ASTWCs-1 can be seen in this simulation test.

In Chapter 4, the ASTWCs-1 of the IPMSM will be interconnected with the AHOSMO-1 presented in Chapter 2. From this, the sensorless scheme for the IPMSM will be introduced.

3.2 Control design based on Super-Twisting approach: Proposal-2

In this section, a second adaptive control is designed for the system given by (3.1).

Consider that at [89], an adaptive super- twisting control was proposed with reparameterized gains, taking into account the following structure:

A sliding surface S_2 was defined by

$$S_2 = \vartheta_{21} e_{1_\chi} + e_{2_\chi} \tag{3.50}$$

where $e_{1_\chi} = \chi_1 - \chi_{ref}$ is a tracking error, $e_{2_\chi} = \dot{\chi}_1 - \dot{\chi}_{ref}$ and $\vartheta_{21} > 0$; whose dynamic is given by

$$\dot{S}_2 = \vartheta_{21} e_{2_\chi} + f(\chi) + g(\chi)u + \delta(t) - \ddot{\chi}_{ref} \tag{3.51}$$

Then, a control input was chosen as follows

$$u = \frac{1}{g(\chi)} \left(-\vartheta_{21} e_{2_\chi} - f(\chi) + \ddot{\chi}_{ref} - K_{G1} |S_2|^{\frac{1}{2}} sign(S_2) - \int_0^t K_{G2} sign(S_2) d\tau \right), \tag{3.52}$$

where $K_{G1} = 2L_G(t)$ and $K_{G2} = \dfrac{L_G^2(t)}{2}$ have been reparameterized based on a single parameter $L_G(t) > 0$. Then, for the above controller, the following adaptive law was proposed

$$\dot{L}_G(t) = \frac{-\dfrac{k_G}{\sqrt{2}} |L_G(t) - L_{G_{ref}}| + \dfrac{L_G(t)}{2} |S_2|^{\frac{1}{2}}}{(L_G(t) - L_{G_{ref}}) + \dfrac{2}{L_G(t)^2} \left(|S_2|^{\frac{1}{2}} + \dfrac{1}{L_G(t)} \int_0^t L_G^2(\tau) sign(S_2) d\tau \right) \left(- \int_0^t \dfrac{L_G^2(\tau)}{2} sign(S_2) d\tau \right)} \tag{3.53}$$

for $L_{G_{ref}}, k_G > 0$. In this section, an adaptive law will be designed by using the same reparameterized gains. However, the proposed adaptive law in this work has been simplified. Next, an adaptive law will be designed.

3.2.1 Adaptive super-twisting control design

Based on [89], in this section the design of one adaptive super-twisting control is introduced in order to simplify the adaptive law given by (3.53). Then, the following equation

$$u = \frac{1}{g(\chi)} \left(-\vartheta_{21} e_{2_\chi} - f(\chi) + \ddot{\chi}_{ref} + \mathcal{V}_{st} \right), \tag{3.54}$$

with

$$\mathcal{V}_{st} = -\tilde{K}_{c3} |S_2|^{\frac{1}{2}} sign(S_2) - \int_0^t \tilde{K}_{c4} sign(S_2) d\tau \tag{3.55}$$

is an Adaptive Super-Twisting Control (ASTWC-2) for the system (3.1) and the reparameterized gains, in terms of a single parameter, are given by

$$\tilde{K}_{c3} = 2L_{c_2}(t) \qquad \tilde{K}_{c4} = \frac{L_{c_2}^2(t)}{2} \tag{3.56}$$

where $L_{c_2}(t) > 0$ is an adaptive parameter.

Remark 3.2. *A demonstration to calculate the proposed gains has been introduced in the Appendix A (See A.2.2).*

An stability analysis and an adaptive law for the parameter $L_{c_2}(t)$ will be presented in the sequel. Consider that the dynamic of the sliding surface (3.51) in closed-loop with the control (3.54) is given by

$$\dot{S}_2 = -\tilde{K}_{c3}|S_2|^{\frac{1}{2}} sign(S_2) - \int_0^t \tilde{K}_{c4} sign(S_2) d\tau + \delta(t) \tag{3.57}$$

where the super-twisting (STW) control (3.57) can be expressed as follows

$$\begin{cases} \dot{S}_2 = -\tilde{K}_{c3}|S_2|^{\frac{1}{2}} sign(S_2) + \nu_2 + \delta(t) \\ \dot{\nu}_2 = -\tilde{K}_{c4} sign(S_2) \end{cases} \tag{3.58}$$

Assumption 3.4. *The disturbance $\delta(t)$ and its time derivative $\dot{\delta}(t)$ are bounded for unknown positive constants δ_M, Δ_M, respectively, i.e., $|\delta(t)| < \delta_M$, $|\dot{\delta}(t)| \leq \Delta_M$; $\forall t \geq 0$ [88].*

Now, introducing the following change of variable $z_{1_2} = S_2$ and $z_{2_2} = \nu_2 + \delta(t)$. Then, system (3.58) is rewritten as

$$\Sigma_{STW_2} : \begin{cases} \dot{z}_{1_2} = -2L_{c_2}(t)|z_{1_2}|^{\frac{1}{2}} sign(z_{1_2}) + z_{2_2} \\ \dot{z}_{2_2} = -\dfrac{L_{c_2}^2(t)}{2} sign(z_{1_2}) + d(t) \end{cases} \tag{3.59}$$

with $d(t) = \dot{\delta}(t)$. Consider the following change of variable

$$\pounds_{1_2} = \frac{|z_{1_2}|^{\frac{1}{2}} sign(z_{1_2})}{L_{c_2}(t)} \qquad \pounds_{2_2} = \frac{z_{2_2}}{L_{c_2}^2(t)} \tag{3.60}$$

then the dynamics, in terms of these new variables, are given by

$$\begin{aligned}\dot{\pounds}_{1_2} &= \frac{L_{c_2}(t)}{2|z_{1_2}|^{\frac{1}{2}}}\left[-2\pounds_{1_2}+\pounds_{2_2}\right]-\pounds_{1_2}\frac{\dot{L}_{c_2}(t)}{L_{c_2}(t)}\\ \dot{\pounds}_{2_2} &= \frac{L_{c_2}(t)}{2|z_{1_2}|^{\frac{1}{2}}}\left[-\pounds_{1_2}+\frac{2|z_{1_2}|^{\frac{1}{2}}d(t)}{L^3_{c_2}(t)}\right]-2\pounds_{2_2}\frac{\dot{L}_{c_2}(t)}{L_{c_2}(t)}\end{aligned} \tag{3.61}$$

To make some calculations easier, system (3.61) can be expressed in compact form as follows

$$\dot{\pounds}_{c_2} = \alpha_{c_2}\left[\left(A_c - P_c^{-1}C_c^TC_c\right)\pounds_{c_2}+\Phi_{c_2}\right]-D_{c_2}\pounds_{c_2}\frac{\dot{L}_{c_2}(t)}{L_{c_2}(t)} \tag{3.62}$$

with $\alpha_{c_2} = \dfrac{L_{c_2}(t)}{2|z_{1_2}|^{\frac{1}{2}}}$ and $\pounds_{c_2} = \begin{bmatrix}\pounds_{1_2} & \pounds_{2_2}\end{bmatrix}^T$, $C_c = \begin{bmatrix}1 & 0\end{bmatrix}^T$

$$A_c = \begin{bmatrix}0 & 1\\ 0 & 0\end{bmatrix} \qquad P_c = \begin{bmatrix}1 & -1\\ -1 & 2\end{bmatrix} \qquad D_{c_2} = \begin{bmatrix}1 & 0\\ 0 & 2\end{bmatrix} \qquad \Phi_{c_2} = \begin{bmatrix}0\\ \dfrac{2|z_{1_2}|^{\frac{1}{2}}}{L^3_{c_2}(t)}\left[d(t)\right]\end{bmatrix} \tag{3.63}$$

Furthermore, P_c is a symmetric positive-definite matrix, solution of the following algebraic Lyapunov equation

$$P_c + A_c^TP_c + P_cA_c - C_c^TC_c = 0 \tag{3.64}$$

Assumption 3.5. *The terms in the vector Φ_{c_2} are uniformly bounded with respect to u and locally Lipschitz with respect to $\pounds_{c_2}$, i.e., $||\Phi_{c_2}|| \leq \wp_2||\pounds_{c_2}||$, for $\wp_2 > 0$.*

Theorem 3.2. *Consider the system* (3.59) *and the Assumption 3.1, 3.4 and 3.5 are fulfilled. Furthermore,*

$$\dot{L}_{c_2}(t) = k_{c_2}^{\frac{1}{2}}|S_2|^{\frac{1}{2}} - \gamma_{c_2}^{\frac{1}{2}}L^2_{c_2}(t) \tag{3.65}$$

is an adaptive law-2 for $L_{c_2}(t)$, with $k_{c_2} > 0$ and $\gamma_{c_2} > 0$ chosen appropriately, where $k_{c_2} > \gamma_{c_2} > 0$. Then, the trajectories of Σ_{STW_2} converge towards a vicinity of the origin in finite time.

Proof

A Lyapunov candidate function is introduced as follows

$$V_{(\pounds_{c_2},L_{c_2}(t))} = V_{(\pounds_{c_2})} + V_{(L_{c_2}(t))} \tag{3.66}$$

with $V_{(\pounds_{c_2})} = \pounds_{c_2}^TP_c\pounds_{c_2}$ and $V_{(L_{c_2}(t))} = \dfrac{\gamma_{c_2}}{2}L^2_{c_2}(t)$, for $\gamma_{c_2} > 0$. Then, taking first time derivative of (3.66) and replacing the suitable expressions, it follows that

$$\begin{aligned}\dot{V}_{(\pounds_{c_2},L_{c_2}(t))} =&\alpha_{c_2}\pounds_{c_2}^T\left[A_{c_2}^TP_c+P_cA_{c_2}\right]\pounds_{c_2}-2\alpha_{c_2}\pounds_{c_2}^TC_c^TC_c\pounds_{c_2}\\&-2\frac{\dot{L}_{c_2}(t)}{L_{c_2}(t)}\pounds_{c_2}^TP_cD_{c_2}\pounds_{c_2}+\gamma_{c_2}\dot{L}_{c_2}(t)L_{c_2}(t)+2\alpha_{c_2}\pounds_{c_2}^TP_c\Phi_{c_2}\end{aligned}\tag{3.67}$$

From $A_c^TP_c+P_cA_c=-P_c+C_c^TC_c$, it follows that equation (3.67) can be rewritten as follows

$$\begin{aligned}\dot{V}_{(\pounds_{c_2},L_{c_2}(t))} =&-\alpha_{c_2}\pounds_{c_2}^TP_c\pounds_{c_2}-\alpha_{c_2}\pounds_{c_2}^TC_c^TC_c\pounds_{c_2}-2\frac{\dot{L}_{c_2}(t)}{L_{c_2}(t)}\pounds_{c_2}^TP_cD_{c_2}\pounds_{c_2}\\&+\gamma_{c_2}\dot{L}_{c_2}(t)L_{c_2}(t)+2\alpha_{c_2}\pounds_{c_2}^TP_c\Phi_{c_2}\end{aligned}\tag{3.68}$$

Now, consider that the following inequalities are satisfied

$$\frac{|z_{1_2}|}{L_{c_2}^2(t)}=|\pounds_{1_2}|^2\leq||\pounds_{c_2}||^2\tag{3.69}$$

and

$$\lambda_{min}(P_c)||\pounds_{c_2}||^2\leq V_{(\pounds_{c_2})}\leq\lambda_{max}(P_c)||\pounds_{c_2}||^2\tag{3.70}$$

where $\lambda_{min}(P_c)$ and $\lambda_{max}(P_c)$ are the minimum and maximum singular values of P_c. Moreover,

$$\lambda_{min}(P_cD_{c_2})||\pounds_{c_2}||^2\leq\pounds_{c_2}^TP_cD_{c_2}\pounds_{c_2}\leq\lambda_{max}(P_cD_{c_2})||\pounds_{c_2}||^2\tag{3.71}$$

where $\lambda_{min}(P_cD_{c_2})$ and $\lambda_{max}(P_cD_{c_2})$ are the minimum and maximum singular values of $P_cD_{c_2}$. Then,

$$\begin{aligned}\dot{V}_{(\pounds_{c_2},L_{c_2}(t))}\leq&-\alpha_{c_2}\pounds_{c_2}^TP_c\pounds_{c_2}-\alpha_{c_2}\pounds_{c_2}^TC_c^TC_c\pounds_{c_2}-2\lambda_{min}(P_cD_{c_2})||\pounds_{c_2}||^2\frac{\dot{L}_{c_2}(t)}{L_{c_2}(t)}\\&+\gamma_{c_2}\dot{L}_{c_2}(t)L_{c_2}(t)+2\alpha_{c_2}\pounds_{c_2}^TP_c\Phi_{c_2}\end{aligned}\tag{3.72}$$

such that,

$$\dot{V}_{(\pounds_{c_2},L_{c_2}(t))}\leq-\alpha_{c_2}V_{(\pounds_{c_2})}-\alpha_{c_2}\pounds_{c_2}^TC_c^TC_c\pounds_{c_2}-\frac{\dot{L}_{c_2}(t)}{L_{c_2}(t)}\left[k_{c_2}||\pounds_{c_2}||^2-\gamma_{c_2}L_{c_2}^2(t)\right]+2\alpha_{c_2}\pounds_{c_2}^TP_c\Phi_{c_2}\tag{3.73}$$

where $k_{c_2}=2\lambda_{min}(P_cD_{c_2})>0$. Now, from (3.73), the term

$$\left[k_{c_2}||\pounds_{c_2}||^2 - \gamma_{c_2}L_{c_2}^2(t)\right] = \left[k_{c_2}^{\frac{1}{2}}||\pounds_{c_2}|| + \gamma_{c_2}^{\frac{1}{2}}L_{c_2}(t)\right]\left[k_{c_2}^{\frac{1}{2}}||\pounds_{c_2}|| - \gamma_{c_2}^{\frac{1}{2}}L_{c_2}(t)\right]$$

Moreover, since $f_{(\pounds_{c_2},L_{c_2}(t))} = \left[k_{c_2}^{\frac{1}{2}}||\pounds_{c_2}|| + \gamma_{c_2}^{\frac{1}{2}}L_{c_2}(t)\right] > 0$. Then, equation (3.73) can be expressed as follows

$$\begin{aligned}\dot{V}_{(\pounds_{c_2},L_{c_2}(t))} \leq & -\alpha_{c_2}V_{(\pounds_{c_2})} - \alpha_{c_2}\pounds_{c_2}^T C_c^T C_c \pounds_{c_2} + 2\alpha_{c_2}\pounds_{c_2}^T P_c \Phi_{c_2} \\ & - f_{(\pounds_{c_2},L_{c_2}(t))}\frac{\dot{L}_{c_2}(t)}{L_{c_2}(t)}\left[k_{c_2}^{\frac{1}{2}}||\pounds_{c_2}|| - \gamma_{c_2}^{\frac{1}{2}}L_{c_2}(t)\right]\end{aligned} \tag{3.74}$$

Now, considering the inequalities (3.69) and (3.70), it follows that the following inequalities hold

$$|\pounds_{1_2}| \leq ||\pounds_{c_2}|| \leq \left(\frac{V_{(\pounds_{c_2})}}{\lambda_{min}(P_c)}\right)^{\frac{1}{2}} \tag{3.75}$$

for $|\pounds_{1_2}| = \dfrac{|z_{1_2}|^{\frac{1}{2}}}{L_{c_2}(t)} = \dfrac{|S_2|^{\frac{1}{2}}}{L_{c_2}(t)}$. Therefore, taking into account the inequality given by (3.75), equation (3.74) can be expressed as

$$\begin{aligned}\dot{V}_{(\pounds_{c_2},L_{c_2}(t))} \leq & -\alpha_{c_2}V_{(\pounds_{c_2})} - \alpha_{c_2}\pounds_{c_2}^T C_c^T C_c \pounds_{c_2} + 2\alpha_{c_2}\pounds_{c_2}^T P_c \Phi_{c_2} \\ & - f_{(\pounds_{c_2},L_{c_2}(t))}\frac{\dot{L}_{c_2}(t)}{L_{c_2}(t)}\left[k_{c_2}^{\frac{1}{2}}\left(\frac{|S_2|^{\frac{1}{2}}}{L_{c_2}(t)}\right) - \gamma_{c_2}^{\frac{1}{2}}L_{c_2}(t)\right]\end{aligned} \tag{3.76}$$

Then, choosing an adaptive law as follows

$$\dot{L}_{c_2}(t) = \left[k_{c_2}^{\frac{1}{2}}\left(\frac{|S_2|^{\frac{1}{2}}}{L_{c_2}(t)}\right) - \gamma_{c_2}^{\frac{1}{2}}L_{c_2}(t)\right]L_{c_2}(t) \tag{3.77}$$

the following expression is obtained

$$\begin{aligned}\dot{V}_{(\pounds_{c_2},L_{c_2}(t))} \leq & -\alpha_{c_2}V_{(\pounds_{c_2})} - \alpha_{c_2}\pounds_{c_2}^T C_c^T C_c \pounds_{c_2} + 2\alpha_{c_2}\pounds_{c_2}^T P_c \Phi_{c_2} \\ & - f_{(\pounds_{c_2},L_{c_2}(t))}\left[k_{c_2}^{\frac{1}{2}}\left(\frac{|S_2|^{\frac{1}{2}}}{L_{c_2}(t)}\right) - \gamma_{c_2}^{\frac{1}{2}}L_{c_2}(t)\right]^2\end{aligned} \tag{3.78}$$

Assuming that S_2 tends to zero faster than $L_{c_2}(t)$ and $-\alpha_{c_2}\pounds_{c_2}^T C_c^T C_c \pounds_{c_2} < 0$; for $L_{c_2}(t) > 0$. Then, (3.78) is given by

$$\dot{V}_{(\pounds_{c_2},L_{c_2}(t))} \leq -\alpha_{c_2}V_{(\pounds_{c_2})} - f_{(\pounds_{c_2},L_{c_2}(t))}\gamma_{c_2}L_{c_2}^2(t) + 2\alpha_{c_2}\pounds_{c_2}^T P_c \Phi_{c_2} \tag{3.79}$$

Moreover, taking into account the norm for the term $2\alpha_{c_2}\pounds_{c_2}^T P_c \Phi_{c_2}$ and Assumption 3.5, it follows that

$$\dot{V}_{(\pounds_{c_2}, L_{c_2}(t))} \leq -\alpha_{c_2} V_{(\pounds_{c_2})} + 2\alpha_{c_2}\wp_2 ||\pounds_{c_2}||^2 ||P_c|| - f_{(\pounds_{c_2}, L_{c_2}(t))}\gamma_{c_2} L_{c_2}^2(t) \tag{3.80}$$

Now, consider the inequality (3.70), then,

$$\dot{V}_{(\pounds_{c_2}, L_{c_2}(t))} \leq -\frac{L_{c_2}(t)}{2|z_{1_2}|^{\frac{1}{2}}}[1-\sigma_{c_2}]V_{(\pounds_{c_2})} - f_{(\pounds_{c_2}, L_{c_2}(t))}\gamma_{c_2} L_{c_2}^2(t) \tag{3.81}$$

with $\sigma_{c_2} = \dfrac{2\wp_2 ||P_c||}{\lambda_{max}(P_c)}$. The above equation can be written as

$$\dot{V}_{(\pounds_{c_2}, L_{c_2}(t))} \leq -\frac{L_{c_2}(t)}{\frac{2|z_{1_2}|^{\frac{1}{2}} L_{c_2}(t)}{L_{c_2}(t)}}[1-\sigma_{c_2}]V_{(\pounds_{c_2})} - f_{(\pounds_{c_2}, L_{c_2}(t))}\gamma_{c_2} L_{c_2}^2(t) \tag{3.82}$$

Therefore, from (3.75), the above equation can be expressed as follows

$$\dot{V}_{(\pounds_{c_2}, L_{c_2}(t))} \leq -\Gamma_{c_2} V_{(\pounds_{c_2})}^{\frac{1}{2}} - f_{(\pounds_{c_2}, L_{c_2}(t))}\gamma_{c_2} L_{c_2}^2(t) \tag{3.83}$$

with $\Gamma_{c_2} = \dfrac{[1-\sigma_{c_2}]\lambda_{min}^{\frac{1}{2}}(P_c)}{2}$. Now, equation (3.83) will be factorized

$$\dot{V}_{(\pounds_{c_2}, L_{c_2}(t))} \leq -L_{c_2}(t)\sqrt{2}\gamma_{c_2}^{\frac{1}{2}}\left[\frac{\Gamma_{c_2}}{L_{c_2}(t)\sqrt{2}\gamma_{c_2}^{\frac{1}{2}}} V_{(\pounds_{c_2})}^{\frac{1}{2}} + f_{(\pounds_{c_2}, L_{c_2}(t))}\frac{\gamma_{c_2}^{\frac{1}{2}}}{\sqrt{2}} L_{c_2}(t)\right] \tag{3.84}$$

Thus, selecting $\eta_{1_2} = \left[L_{c_2}(t)\sqrt{2}\gamma_{c_2}^{\frac{1}{2}}\right]$ and $\varphi_{c_2} = min\left(\dfrac{\Gamma_{c_2}}{L_{c_2}(t)\sqrt{2}\gamma_{c_2}^{\frac{1}{2}}}, f_{(\pounds_{c_2}, L_{c_2}(t))}\right)$, it is possible to express the following equation

$$\dot{V}_{(\pounds_{c_2}, L_{c_2}(t))} \leq -\eta_{2_2}\left[V_{(\pounds_{c_2})}^{\frac{1}{2}} + \frac{\gamma_{c_2}^{\frac{1}{2}}}{\sqrt{2}} L_{c_2}(t)\right] \tag{3.85}$$

with $\eta_{2_2} = \eta_{1_2}\varphi_{c_2}$.

On the other side, Jensen´s inequality [84] is given by

$$[|a_{c_2}|^m + |b_{c_2}|^m]^{\frac{1}{m}} \leq |a_{c_2}| + |b_{c_2}| \tag{3.86}$$

defining $a_{c_2} = V_{(\pounds_{c_2})}^{\frac{1}{2}}$, $b_{c_2} = V_{(L_{c_2}(t))}^{\frac{1}{2}}$ and $m = 2$. Thus, the following inequality can be established

$$\left[|V_{(\pounds_{c_2})}^{\frac{1}{2}}|^2 + |V_{(L_{c_2}(t))}^{\frac{1}{2}}|^2\right]^{\frac{1}{2}} \leq |V_{(\pounds_{c_2})}^{\frac{1}{2}}| + \frac{\gamma_{c_2}^{\frac{1}{2}}}{\sqrt{2}}|L_{c_2}(t)| \tag{3.87}$$

and

$$V_{(\pounds_{c_2}, L_{c_2}(t))}^{\frac{1}{2}} \leq |V_{(\pounds_{c_2})}^{\frac{1}{2}}| + \frac{\gamma_{c_2}^{\frac{1}{2}}}{\sqrt{2}}|L_{c_2}(t)| \tag{3.88}$$

Finally, the dynamic of Lyapunov function can be expressed as follows

$$\dot{V}_{(\pounds_{c_2}, L_{c_2}(t))} \leq -\eta_{2_2} V_{(\pounds_{c_2}, L_{c_2}(t))}^{\frac{1}{2}} \tag{3.89}$$

Then, from the Lyapunov function, $\dot{V}_{(\pounds_{c_2}, L_{c_2}(t))}$ is negative definite and ensures convergence in finite-time, for $L_{c_2}(t)$ sufficiently large, satisfying $\eta_{2_2} > 0$. Moreover, the comparison principle is taken into account to estimate the convergence time. Thus, considering the equation $\dot{v} = -\eta_{2_2} v^{\frac{1}{2}}$ and its solution defined as $v(t) = (v(0)^{\frac{1}{2}} - \frac{1}{2}\eta_{2_2} t)^2$. Then, $V_{(\pounds_{c_2}, L_{c_2}(t))} < v(t)$ when $V_{(\pounds_{c_2}(0), L_{c_2}(0))} < v(0)$, such that, $\pounds_{c_2}$ has a convergence in finite-time in an estimated time given by $T_{2_2} = \dfrac{2V_{(\pounds_{c_2}(0), L_{c_2}(0))}^{\frac{1}{2}}}{\eta_{2_2}}$. Therefore, $\pounds$ tends to zero as well as S_2 tends to zero in finite-time.

3.2.2 Control design for IPMSM

In this section, the design of controllers for the speed and the direct-axis current are presented by considering the adaptive law-2 given by Theorem 3.2.

Control loop for Ω

Consider a sliding surface given by

$$S_{\Omega_2} = \vartheta_{22} e_{1_\Omega} + e_{2_\Omega} \tag{3.90}$$

where $e_{1_\Omega} = \Omega - \Omega^*$ is speed tracking error, $e_{2_\Omega} = \dot{\Omega} - \dot{\Omega}^*$ and $\vartheta_{22} > 0$. Therefore, the dynamic of the sliding surface S_Ω is given by

$$\dot{S}_{\Omega_2} = \vartheta_{22} e_{2_\Omega} + a_1 b_1 + a_2 b_2 + a_3 b_2 - b_3 - \ddot{\Omega}^* + v_q c_1 \tag{3.91}$$

where $a_1 = \dfrac{p(L_d - L_q)i_q}{J}$, $a_2 = \dfrac{p(L_d - L_q)i_d}{J}$, $a_3 = \dfrac{p\psi_r}{J}$, $b_1 = \dfrac{v_d}{L_d} - \dfrac{R_s i_d}{L_d} + \dfrac{L_q p\Omega i_q}{L_d}$, $b_2 = -\dfrac{R_s i_q}{L_q} - \dfrac{L_d p\Omega i_d}{L_q} - \dfrac{\psi_r p\Omega}{L_q}$, $b_3 = \dfrac{f_v}{J}\left(\dfrac{p(L_d - L_q)i_d i_q}{J} + \dfrac{p\psi_r i_q}{J} - \dfrac{f_v\Omega}{J} - \dfrac{T_l}{J}\right)$ and $c_1 = \dfrac{p(L_d - L_q)i_d}{JL_q} + \dfrac{p\psi_r}{JL_q}$.
Then, the control input v_q is given by

$$v_q = \frac{1}{c_1}\left(-\vartheta_{22}e_{2_\Omega} - a_1 b_1 - a_2 b_2 - a_3 b_2 + b_3 + \ddot{\Omega}^* + \mathcal{V}_{st-\Omega_2}\right) \tag{3.92}$$

with

$$\mathcal{V}_{st-\Omega_2} = -\tilde{K}_{c3_\Omega}|S_{\Omega_2}|^{\frac{1}{2}} sign(S_{\Omega_2}) - \int_0^t \tilde{K}_{c4_\Omega} sign(S_{\Omega_2}) d\tau \tag{3.93}$$

where $\tilde{K}_{c3_\Omega} = 2L_{c_{\Omega_2}}(t)$, $\tilde{K}_{c4_\Omega} = \dfrac{L^2_{c_{\Omega_2}}(t)}{2}$ and according to Theorem 3.2, $L_{c_{\Omega_2}}(t)$ is an adaptive parameter given by

$$\dot{L}_{c_{\Omega_2}}(t) = k^{\frac{1}{2}}_{c_{\Omega_2}}|S_\Omega|^{\frac{1}{2}} - \gamma^{\frac{1}{2}}_{c_{\Omega_2}} L^2_{c_{\Omega_2}}(t) \tag{3.94}$$

with $k_{c_{\Omega_2}} > \gamma_{c_{\Omega_2}} > 0$. Therefore, 3.92 is an ASTWC-2 for the speed of the IPMSM.

Control loop for i_d

Now, a sliding surface is introduced

$$S_{i_{d_2}} = \vartheta_{23} e_{i_d} + \int_0^t e_{i_d} d\tau \tag{3.95}$$

where $e_{i_d} = i_d - i_d^*$ is a current tracking error and $\vartheta_{23} > 0$. Moreover, the dynamic of the sliding surface S_{i_d} is given by

$$\dot{S}_{i_{d_2}} = -\frac{\vartheta_{23} R_s i_d}{L_d} + \frac{\vartheta_{23} p\Omega L_q i_q}{L_d} + \frac{\vartheta_{23} v_d}{L_d} - \vartheta_{23}\dot{i}_d^* + e_{i_d} \tag{3.96}$$

Then, the control input v_d can be chosen as follows

$$v_d = \frac{L_d}{\vartheta_{23}}\left(\frac{\vartheta_{23} R_s i_d}{L_d} - \frac{\vartheta_{23} p\Omega L_q i_q}{L_d} + \vartheta_{23}\dot{i}_d^* - e_{i_d} + \mathcal{V}_{st-i_{d_2}}\right) \tag{3.97}$$

with

$$\mathcal{V}_{st-i_{d_2}} = -\tilde{K}_{c3_{i_d}}|S_{i_{d_2}}|^{\frac{1}{2}} sign(S_{i_{d_2}}) - \int_0^t \tilde{K}_{c4_{i_d}} sign(S_{i_{d_2}}) d\tau \tag{3.98}$$

where $\tilde{K}_{c3_{i_d}} = 2L_{c_{i_{d_2}}}(t)$, $\tilde{K}_{c4_{i_d}} = \dfrac{L^2_{c_{i_{d_2}}}(t)}{2}$ and according to Theorem 3.2, $L_{c_{i_{d_2}}}(t)$ is an adaptive parameter given by

$$\dot{L}_{c_{i_{d_2}}}(t) = k^{\frac{1}{2}}_{c_{i_{d_2}}} |S_{i_{d_2}}|^{\frac{1}{2}} - \gamma^{\frac{1}{2}}_{c_{i_{d_2}}} L^2_{c_{i_{d_2}}}(t) \tag{3.99}$$

with $k_{c_{i_{d_2}}} > \gamma_{c_{i_{d_2}}} > 0$. Therefore, 3.97 is an ASTWC-2 for the current$-i_d$ of the IPMSM.

3.2.3 Simulation results

Consider the adaptive law established by Theorem 3.2 and the system (1.36)-(1.37) in closed-loop with the controllers given by (3.92) and (3.97). Then, similarly to the previous adaptive law introduced in section 3.1.1, simulation result are illustrated in this section in order to show the performance of the system in closed-loop under the action of adaptive controllers. The parameters of the adaptive controllers (ASTWCs-2) are given in Table 3.2.

Table 3.2 – Parameters for ASTWCs-2

Values							
$L_{c_{\Omega_2}}(0)$	ϑ_{22}	$\gamma_{c_{\Omega_2}}$	$k_{c_{\Omega_2}}$	$L_{c_{i_{d_2}}}(0)$	ϑ_{23}	$\gamma_{c_{i_{d_2}}}$	$k_{c_{i_{d_2}}}$
100	400	0.001	300	500	200	0.06	100

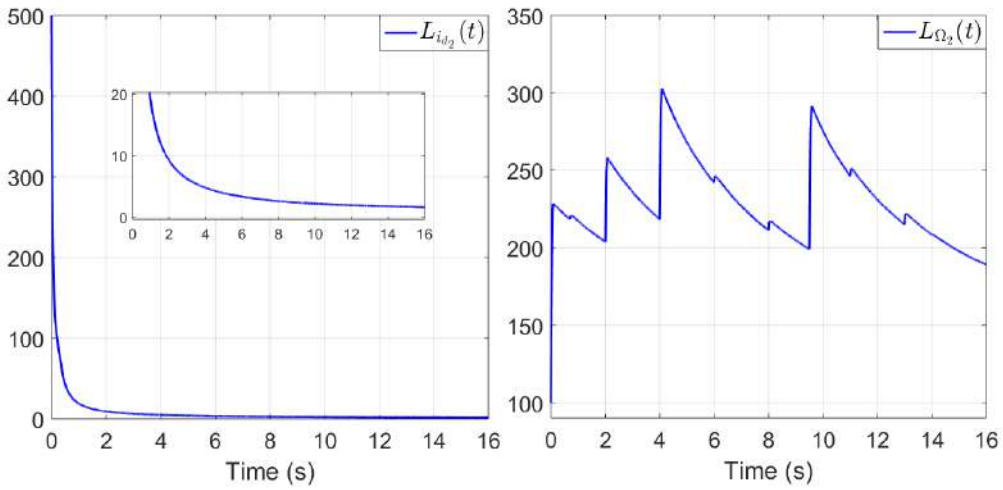

Figure 3.4 – ASTWC-2. Behaviour of adaptive law for the speed and current-i_d controllers

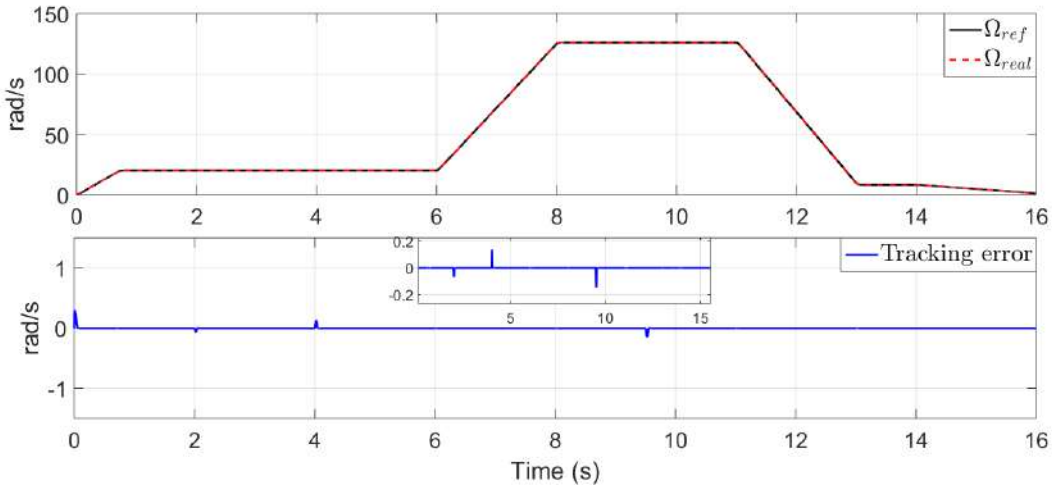

Figure 3.5 – ASTWC-2. Speed tracking and speed tracking error

In Figure 3.4, the adaptive gains for the controllers (3.92) and (3.97) are shown, respectively. Moreover, considering the adaptive gain for the speed controller, in Figure 3.5 is illustrated the speed tracking and its tracking error. Then, according to the adaptive parameter $L_{\Omega_2}(t)$, the tracking error is minimized when there are changes in the load torque, such that, it possible to see the value increase in adaptive gain in order to reduce the error. On the other hand, the currents$-i_{dq}$ are introduced in Figure 3.6. The behaviour of the adaptive parameter $L_{i_{d_2}}(t)$ for the current$-i_d$ control can be seen in Figure 3.4, obtaining a good performance for a current$-i_d$ reference equal to zero. Therefore, we can say that the controllers based on adaptive gains have had a satisfactory result in the presence of disturbances and parametric uncertainties. In addition, an evaluation for the proposed adaptive laws is given. The adaptive parameters $L_{c_\Omega}(t), L_{c_{i_d}}(t)$, whose solution is given by Theorem 3.1, are evaluated at a specific time (5s). Similarly, the adaptive parameters $L_{c_{\Omega_2}}(t), L_{c_{i_{d_2}}}(t)$, whose solution is given by Theorem 3.2, are evaluated at a specific time (5s), as can be seen in Table 3.3. The final value in each gain can show that the adaptive parameter $(L_{c\Omega_2})$ is more conservative for the speed controller. However, for the current controller, both strategies have achieved to adjust the gains with similar values. Therefore, it is possible to say that the adaptive law given by Theorem 3.1 provides more energy in the presence of disturbances (Load torque).

In Chapter 4, the ASTWCs-2 of the IPMSM will be interconnected with the AHOSMO-2 presented in Chapter 2. From this, the sensorless scheme for the IPMSM will be introduced.

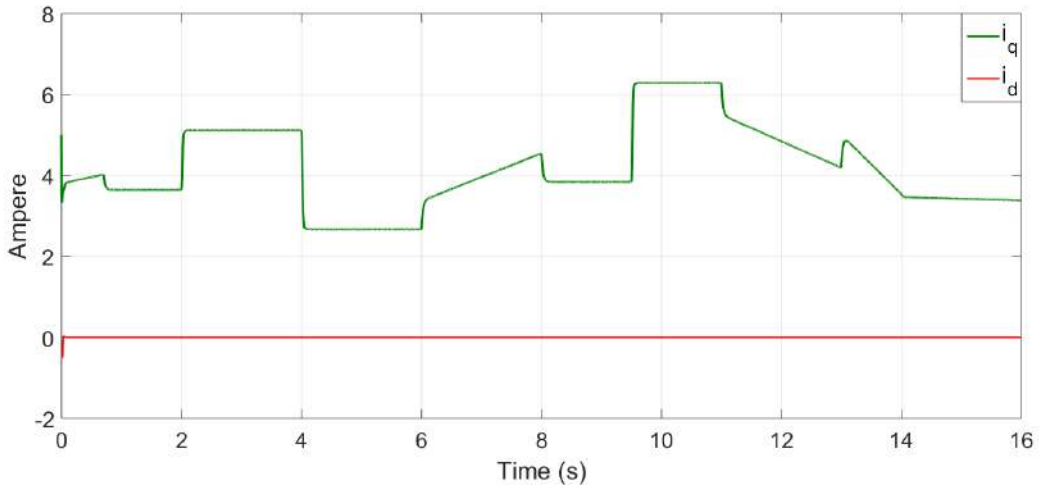

Figure 3.6 – ASTWC-2. Behaviour of the currents$-i_{dq}$

Table 3.3 – Value for the gains of both adaptive controllers at 5 seconds

ASTWCs-1					
$L_{c_\Omega}(5)$	$\tilde{K}_{c1_\Omega}$	$\tilde{K}_{c2_\Omega}$	$L_{c_{i_d}}(5)$	$\tilde{K}_{c1_{i_d}}$	$\tilde{K}_{c2_{i_d}}$
24.9	1248	1.9 e^5	2.07	8.57	9.19
ASTWCs-2					
$L_{c_{\Omega_2}}(5)$	$\tilde{K}_{c3_\Omega}$	$\tilde{K}_{c4_\Omega}$	$L_{c_{i_{d_2}}}(5)$	$\tilde{K}_{c3_{i_d}}$	$\tilde{K}_{c4_{i_d}}$
285.4	570.7	$4.07e^4$	4.3	8.61	9.27

3.3 Comparative study

In this section, two comparative studies are addressed. First, considering constant gains, the proposed controllers based on reparameterized gains are compared with two similar strategies of the literature. After that, the proposed adaptive controllers are compared with three adaptive strategies of the literature. The performance of each strategy will be shown by considering simulation tests.

3.3.1 Comparative study with constant gains

In this work have been proposed two strategies with parameterized gains in order to tune the gains in an easier way, i.e., the gains are based on a single parameter. Then, a comparative study will be carried out by considering only constant gains, i.e., the proposed

adaptive laws are not considered. Therefore, considering that $(* = \Omega, i_d)$, the gains for the proposal 1 are given by $K_{c1*} = 2L_{c*}^2, K_{c2*} = \dfrac{L_{c*}^4}{2}$ where L_{c*} is positive constant. Similarly, the gains for the proposal 2 are given by $K_{c3*} = 2L_{c*_2}, K_{c4*} = \dfrac{L_{c*_2}^2}{2}$ where L_{c*_2} is positive constant. Then, considering the proposed strategies in this work, two similar strategies have been taken from the literature to compare the performance of each of them.

Levant [90] *Super-twisting strategy was proposed in [39]. However, in [39], the super-twisting control has two gains, which results complex to tune, causing overestimation of gains. For this reason, in [90] was proposed an alternative to tune the gains as follows*

$$\begin{aligned} \sigma_L &= -k_{1_L}|s|^{1/2}sign(s) + \nu_L \\ \dot{\nu}_L &= -k_{2_L}sign(s) \end{aligned} \tag{3.100}$$

where s is the sliding surface, $k_{1_L} = 1.5L_L^{1/2}$ and $k_{2_L} = 1.1L_L$ where L_L is the parameter to be tuned.

Moreno [85] *A second alternative to tune the gains of the super twisting was proposed in [85]. In this strategy the super twisting is given by*

$$\begin{aligned} \sigma_M &= -k_{1_M}|s|^{1/2}sign(s) + \nu_M \\ \dot{\nu}_M &= -k_{2_M}sign(s) \end{aligned} \tag{3.101}$$

and its gains are defined by

$$k_{1_M} = \mu_M\sqrt{\frac{2\gamma_M}{(1-\beta_M)\alpha_M}}\sqrt{L_M} \qquad k_{2_M} = \frac{(\beta_M+1)}{(1-\beta_M)}L_M$$

where μ_M, α_M, β_M and γ_M are positive constants, such that $0 < \beta_M < 1$ and $\gamma_M > 1$, satisfying the following inequality

$$\mu_M - \frac{2}{\gamma_M}\alpha_M > \alpha_M^2 - \beta_M(1+\mu_M)\alpha_M + \frac{1}{4}(1+\mu_M)^2 \tag{3.102}$$

Now, the comparative study will be introduced by considering the best values of each strategy in order to make a fair comparison.

In this way, the parameter value L_{c*} in the proposal-1 is given by $L_{c*} = 16$ and the parameter value L_{c*_2} in the proposal-2 is given by $L_{c*_2} = 254$.

Now, considering the strategy (3.100) and applying the strategy in the speed and

current controller, a value of $L_L = 30000$ is chosen.

On the other hand, in (3.101), the chosen values are the following: $\mu_M = 3.5$, $\alpha_M = 2.8$, $\beta_M = 0.8$, $\gamma_M = 12$ and $L_M = 600$. Similar values are applied in the speed and current controller.

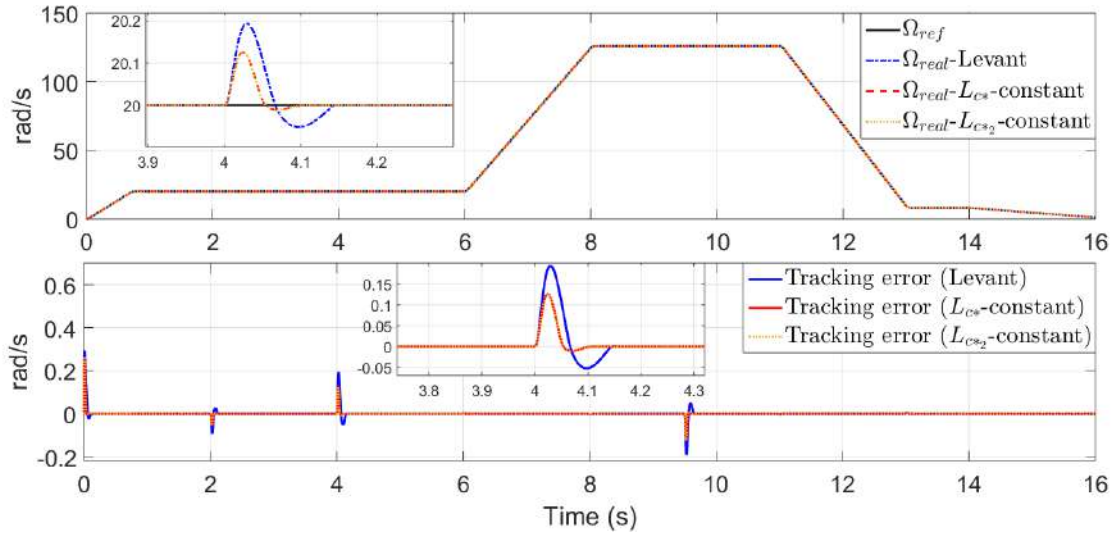

Figure 3.7 – Speed tracking. Comparative study among Levant strategy and proposed strategies

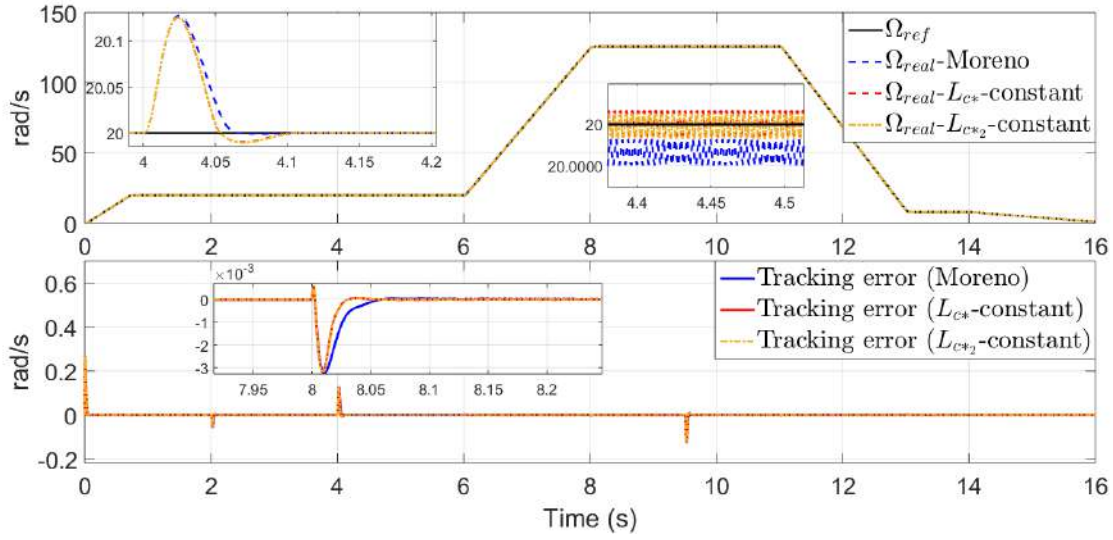

Figure 3.8 – Speed tracking. Comparative study among Moreno strategy and proposed strategies

Then, taking into account the information for each strategy, a comparison for the speed

tracking is illustrated. In Figure 3.7, the proposed strategies are compared with (3.100) and in Figure 3.8, the proposed strategies are compared with (3.101). Then, it is possible show that the adjust of gains of (3.100) is not enough to attenuate the disturbance, it can be seen at 4 s (see Figure 3.7). In Figure 3.8 is possible to illustrate a similar behaviour among the strategies. On the other side, the currents i_{dq} are illustrated in Figure 3.9

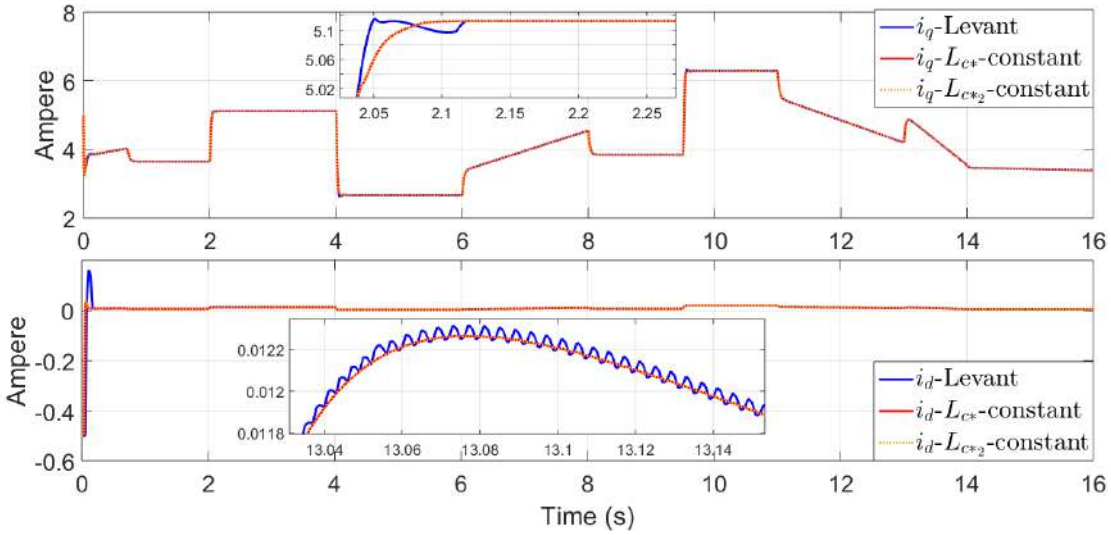

Figure 3.9 – Currents−i_{dq}. Comparative study among Levant strategy and proposed strategies

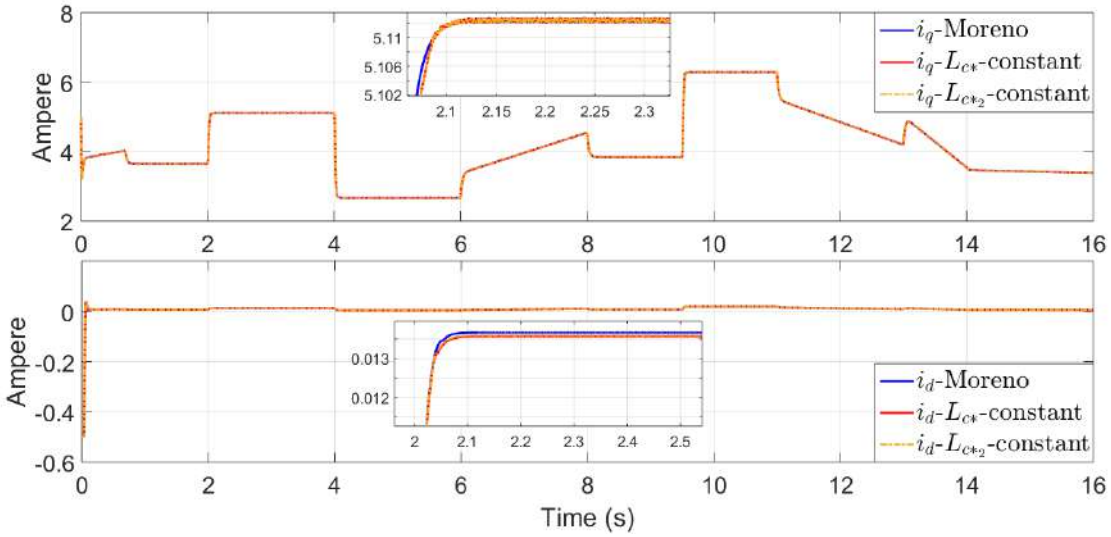

Figure 3.10 – Currents−i_{dq}. Comparative study among Moreno strategy and proposed strategies

and Figure 3.10. According to comparison, strategy (3.100) presents more chattering in the current$-i_d$, while the strategy (3.101) has a similar behaviour with the proposed strategies.

Similarly, in Figure 3.11 and Figure 3.12, the voltages$-dq$ are introduced. A behaviour with more chattering in the signal can be seen for the strategy (3.100)(See Figure 3.11). On the other side, considering the strategy (3.101), in Figure 3.12 can be seen a similar performance of the voltages with proposed strategies. In addition, a performance index

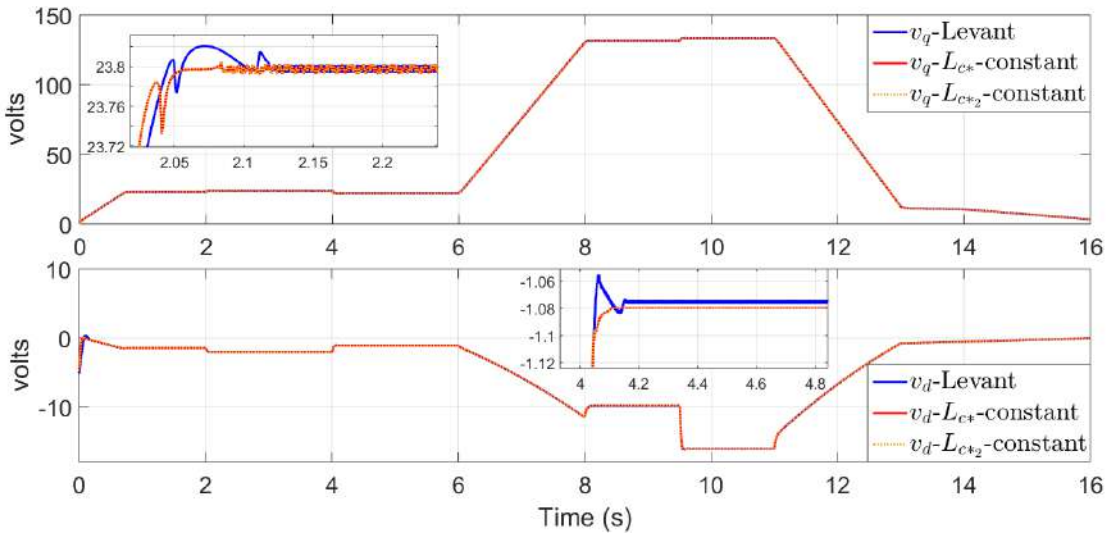

Figure 3.11 – Voltages$-v_{dq}$. Comparative study among Levant strategy and proposed strategies

(Integral Absolute Value-IAE) is considered. In Figure 3.13 is possible to show that the strategy (3.101) and the proposed strategies have a similar performance, except (3.100). Finally, we can conclude that in (3.100), the value for L_L need to be very large, which turns out to be somewhat complex to find a more precise value. Moreover, the main disadvantage in (3.101) is that it is necessary to find and adjust different parameters for satisfying the inequality and after that, gain adjustment can be done. However, the proposed strategies in this work only need to adjust one parameter satisfying the tracking with a good performance, which has allowed to design the proposed adaptive laws for the controller in the sections 3.1.1 and 3.2.1.

It is worth mentioning that the choice of constant gains could generate an overestimation of the gains and cause chattering in the signals. A simulation test is shown in Figure 3.14, where the proposed strategy given in the section 3.1.1 (Proposal 1) has been

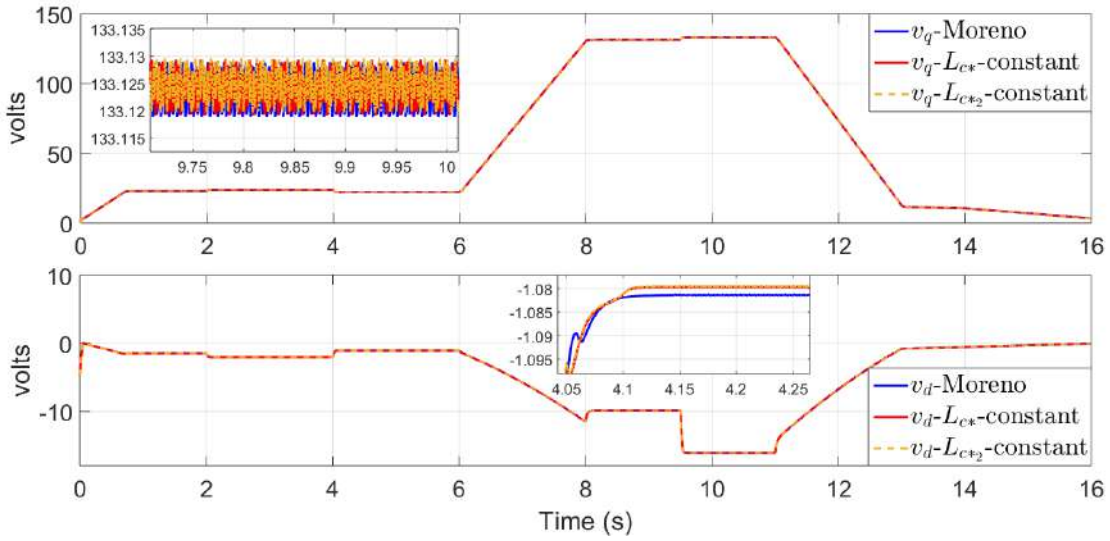

Figure 3.12 – Voltages−v_{dq}. Comparative study among Moreno strategy and proposed strategies

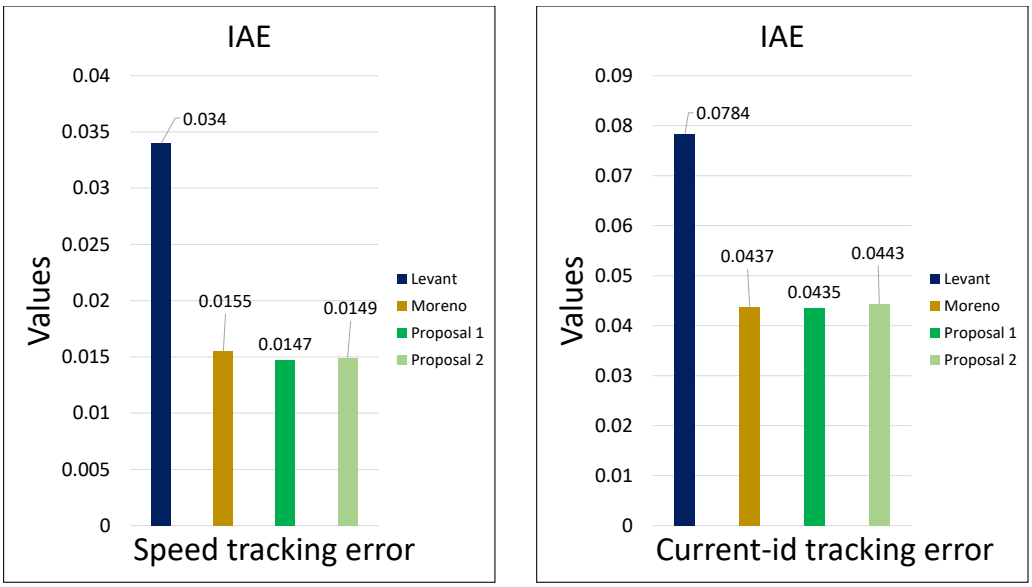

Figure 3.13 – Performance index: Comparative study using constant gains

considered using constant gains. The parameter value L_{c*} can be seen with different values, 10 at the beginning, 40 at 4.5 seconds and 70 at 10 seconds, respectively. At the beginning, the gain is small and the tracking is achieved with less precision, after that, at 4.5 seconds, the gains is increased achieving a correct estimation. However, at 10 seconds, it is possible to illustrate the chattering effect for a value of $L_{c*} = 70$. Similarly, this can

be illustrate for the voltages and currents.

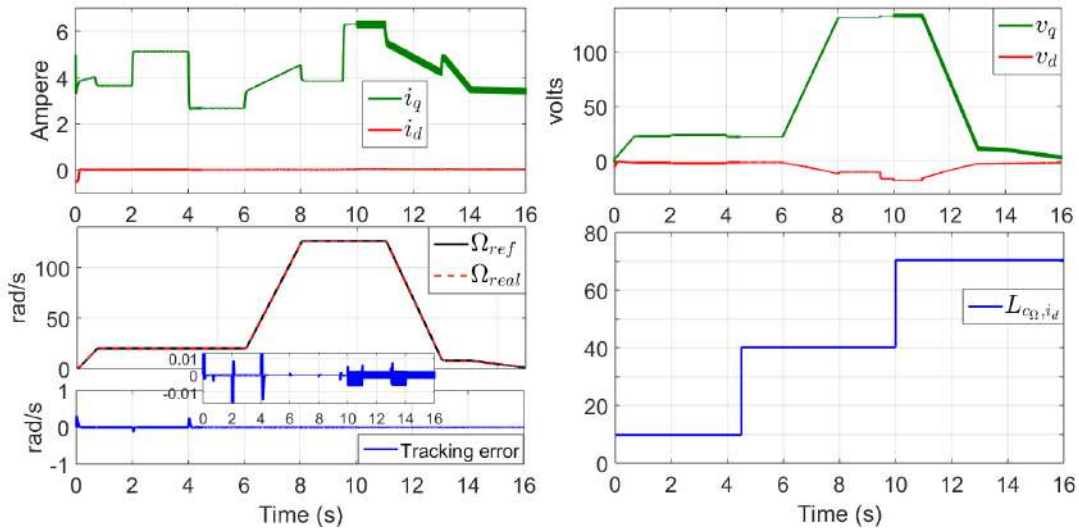

Figure 3.14 – Proposal 1. Performance using different constant gain values

For this reason, the design of adaptive laws is necessary to avoid this issue. In Figure 3.15, the action of the adaptive parameters, L_{c_Ω} and $L_{c_{i_d}}$, are shown such that the gains are adjusted according to the need of the controller to achieve the minimum error, avoiding overestimation of gains and chattering in the signals.

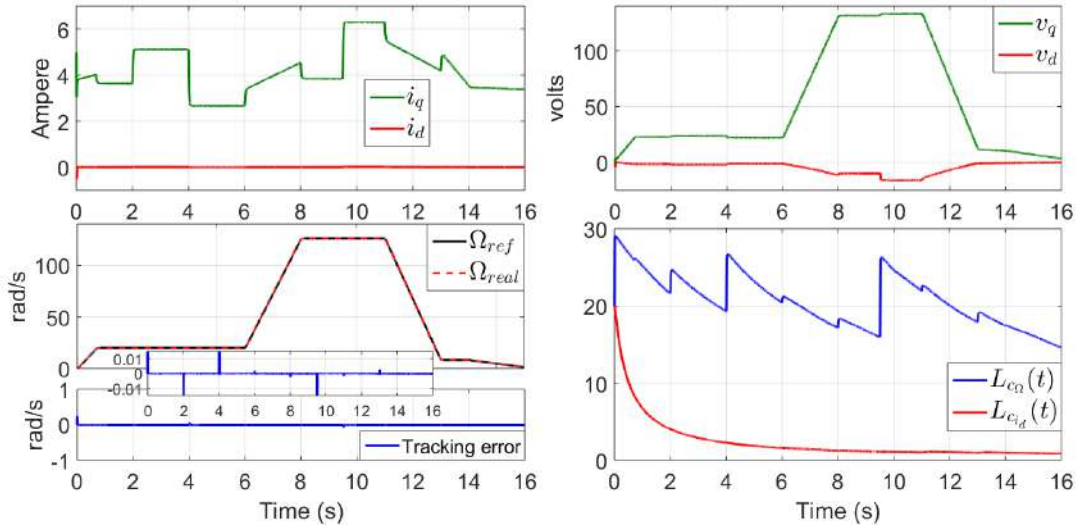

Figure 3.15 – Proposal 1 (ASTWC-1). Performance using adaptive gains

3.3.2 Comparative study with adaptive strategies

The adaptive laws introduced in Theorem 3.1 and Theorem 3.2 are compared with three proposed strategies in the literature.

The term $\mathcal{V}_{st-*}$ for $* = \Omega, i_d$ will be defined for each controller.

Firstly, an Adaptive Sliding mode Control (ASMC) has been introduced in [91], with the control input $\mathcal{V}_{st-*}$ given by

$$\mathcal{V}_{st-*} = -K_*(t)sign(S_*) \tag{3.103}$$

where $K_*(t)$ is an adaptive law defined by

$$\dot{K}_*(t) \begin{cases} \bar{K}_*|S_*|sign(|S_*| - \epsilon_*) & if \quad K_* > \mu_* \\ \mu_* & if \quad K_* \leq \mu_* \end{cases} \tag{3.104}$$

where $K_*(0) > 0$, $\bar{K}_* > 0$, $\mu_* > 0$ and $\epsilon_* = 2K_*(t)T_e$ with T_e is the sampling time.

Secondly, an Adaptive Super twisting (ASTW) was introduced in [92], where the control input $\mathcal{V}_{st-*}$ is given by

$$\mathcal{V}_{st-*} = -\alpha_*(t)|S_*|^{\frac{1}{2}}sign(S_*) - \int_0^t \frac{\beta_*(t)}{2}sign(S_*)d\tau \tag{3.105}$$

with $\alpha_*(t)$ and $\beta_*(t)$ defined by

$$\dot{\alpha}_*(t) = \begin{cases} \varpi\sqrt{\frac{\gamma_*}{2}}sign(|S_*| - \mu_*) & if \quad \alpha_* > 0 \\ 0 & if \quad \alpha_* = 0 \end{cases} \tag{3.106}$$

$$\beta_*(t) = 2\epsilon_*\alpha_*$$

where ϖ, γ_*, μ_* and ϵ_* are positive constants.

The third adaptive law was introduced in [89] and a simplified adaptive super twisting (SAST) was proposed, with the control input $\mathcal{V}_{st-*}$ given by

$$\mathcal{V}_{st-*} = -K_{G1*}|S_*|^{\frac{1}{2}}sign(S_*) - \int_0^t K_{G2*}sign(S_*)dt \tag{3.107}$$

where $K_{G1*} = 2L_{G*}(t)$ and $K_{G2*} = \dfrac{L_{G*}(t)^2}{2}$ and $L_{G*}(t) > 0$ is an adaptive parameter,

solution of

$$\dot{L}_{G*}(t) = \frac{-\frac{k_{G*}}{\sqrt{2}}|L_{G*}(t) - L_{ref}| + \frac{L_{G*}(t)}{2}|S_*|^{\frac{1}{2}}}{\left(L_{G*}(t) - L_{ref}\right) + \frac{2}{L_{G*}(t)^2}(|S_*|^{\frac{1}{2}} + \frac{1}{L_{G*}(t)}\int L_{G*}^2(\tau)sign(S_*)d\tau\right)\left(-\int \frac{L_{G*}^2(\tau)}{2}sign(S_*)d\tau\right)} \tag{3.108}$$

for $L_{ref} > 0$ and $k_{G*} > 0$.

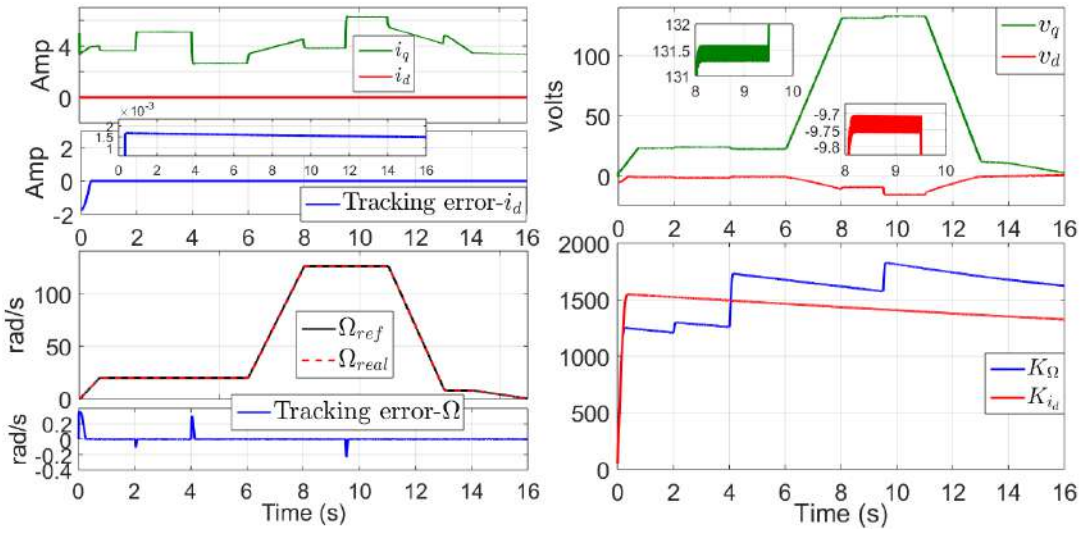

Figure 3.16 – Control performance using ASMC strategy

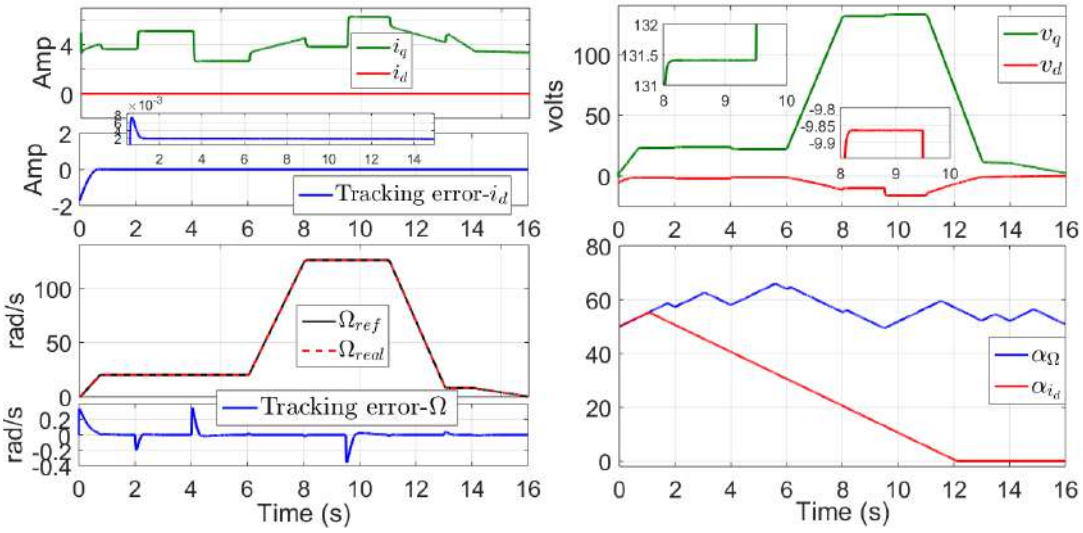

Figure 3.17 – Control performance using ASTW strategy

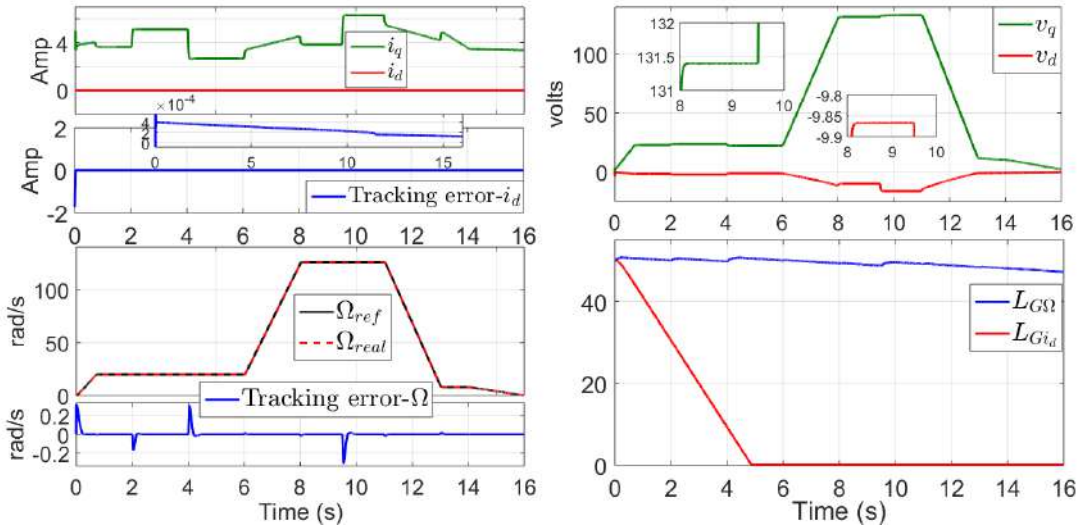

Figure 3.18 – Control performance using SAST strategy

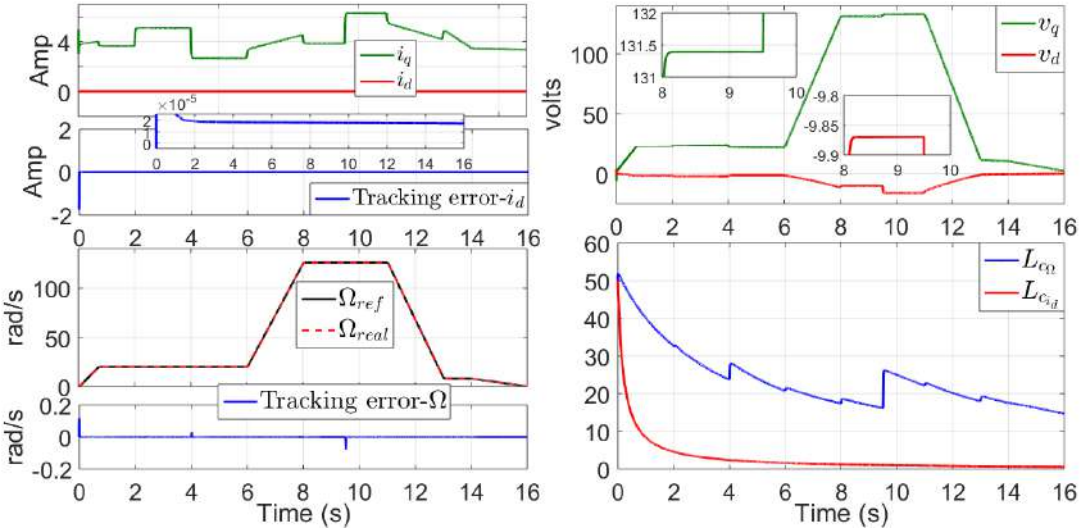

Figure 3.19 – Control performance using proposed ASTWC-1 strategy

The ASMC, ASTW and SAST are compared with the proposal 1 (ASTWC-1) given by Theorem 3.1 and the proposal 2 (ASTWC-2) given by Theorem 3.2 under the same conditions in order to evaluate the performance of each adaptive control in terms of tracking error and tuning process (number of parameters).

Simulation test has been carried out in Matlab-Simulink environment, using a sampling time of 1×10^{-3} with a fixed-step *ode*4 solver. The profile for the speed and the disturbance (Load Torque) are given by Figure 1.7 and the parameters used in the adaptive strategies

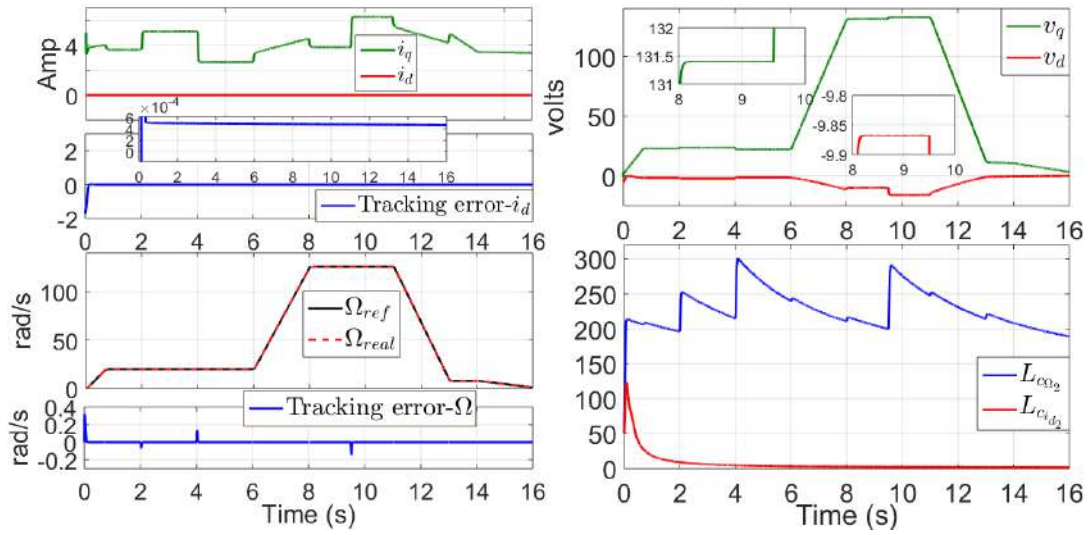

Figure 3.20 – Control performance using proposed ASTWC-2 strategy

have been chosen in order to get the best results.
ASMC: $\bar{K}_{i_d} = 20$, $\mu_{i_d} = 0.5$, $\bar{K}_{\Omega} = 20$, $\mu_{\Omega} = 0.5$ $T_e = 1 \times 10^{-3}$.
ASTW: $\bar{\omega}_{i_d} = 5$, $\gamma_{i_d} = 2$, $\mu_{i_d} = 0.1$, $\epsilon_{i_d} = 2$, $\bar{\omega}_{\Omega} = 5$, $\gamma_{\Omega} = 2$, $\mu_{\Omega} = 0.1$, $\epsilon_{\Omega} = 2$.
SAST: $k_{Gi_d} = 15$, $k_{G\Omega} = 10$, $L_{ref} = 0.1$.
ASTWC-1: $k_{c_{i_d}} = 1$, $\gamma_{c_{i_d}} = 0.1$, $k_{c_{\Omega}} = 90$, $\gamma_{c_{\Omega}} = 0.05$.
ASTWC-2: $k_{c_{i_{d_2}}} = 100$, $\gamma_{c_{i_{d_2}}} = 0.06$, $k_{c_{\Omega_2}} = 200$, $\gamma_{c_{\Omega_2}} = 0.001$.
In Figure 3.16, the Adaptive Sliding Mode Controller (ASMC) is addressed. An increase in the chattering can be seen in the voltages. It has been improved in the Adaptive Super Twisting (ASTW)(See Figure 3.17). However, to get good results, it is necessary to adjust different parameters in the adaptive law. Then, in order to reduce the number of parameters for tuning the adaptive controller, a Simplified Adaptive Super Twisting (SAST) is illustrated in Figure 3.18 achieving good results in the tracking errors. However, the structure of the adaptive law is complex. Therefore, considering a reparameterization of gains, similarly to SAST, in this work an effort has been made to simplify adaptive law, achieving better results, as shown in Figure 3.19 and Figure 3.20, ASTWC-1 and ASTWC-2, respectively. The tracking errors has been greatly decreased as well as the time of convergence. Moreover, the adaptive laws only need two parameters to be adjusted, similarly as the SAST. Nevertheless, the structure is less complex.

In order to compare the strategies, a performance index, Integral Absolute Error (IAE), is considered. From Figure 3.21, it can be concluded that the two proposed strategies

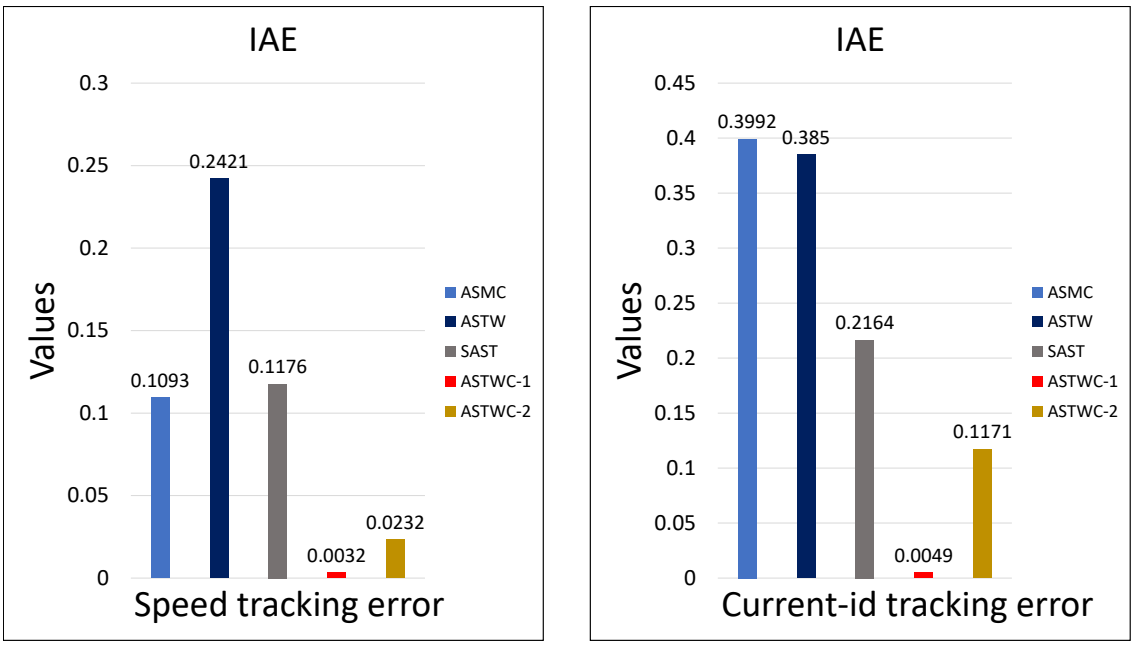

Figure 3.21 – Performance index: Comparative study using adaptive gains

(ASTWC-1, ASTWC-2) can guarantee a high level of accuracy in the tracking error. Moreover, from the Figures. 3.16-3.20, a reduced level of chattering can be illustrated in all strategies, except for ASMC.

3.4 Conclusion

In this chapter, two adaptive controllers based on super-twisting approach have been introduced. The gains of the controllers have been reparameterized in terms of a single parameter to reduce the tuning time. From reparameterized gains, an adaptive law was designed for each controller in order to avoid overestimation of gains and the classical chattering. Simulation tests have been carried out in closed-loop. Some tests were performed to justify the use of adaptive laws. Moreover, considering constant and adaptive gains, a comparative study was carried out taking into account some important results from the literature, to show the performance of each of them with respect to the proposed strategies, so that the proposed strategies can show an easier adjustment with good performance, effectiveness and a less complex structure.

Chapter 4

Sensorless control of the Interior Permanent Magnet Synchronous Motor

In this Chapter, two sensorless control scheme for the IPMSM are introduced, i.e., the proposed observers are interconnected with the proposed controllers in closed-loop. First, the stability analysis for the first scheme is addressed, interconnecting in closed-loop the adaptive observer given in the section 2.2.1 (AHOSMO-1) with the adaptive control given in the section 3.1.1(ASTWC-1). Simulation and experimental results are introduced for this strategy. After that, the adaptive observer given in the section 2.3.1 (AHOSMO-2) is interconnected in closed-loop with the adaptive control given in the section 3.2.1 (ASTWC-2). An stability analysis is introduced and simulation and experimental results are illustrated for this strategy.

4.1 Closed-loop analysis: Scheme 1

Consider the proposed control in section 3.1.1 (ASTWC-1) using the estimates provided by the proposed observer in section 2.2.1 (AHOSMO-1). Then, the stability analysis of the system in closed-loop with the control-observer scheme is established as follows

Theorem 4.1. *Consider the dynamical model of the IPMSM* (1.36)-(1.37) *in closed-loop with the controllers* (3.42) *and* (3.47) *using the estimates provided by the observer* (2.53)*. Then, tracking errors* e_{1_Ω} *and* $e_{1_{i_d}}$*; and estimation error* e_{θ_e} *converge to zero in finite time.*

Proof: Since the control input $v_q(\hat{x})$ depends on estimates $\hat{\Omega}$, $\hat{i}_d$ and $\hat{i}_q$; and taking into account the sliding surface given by (3.41), then the dynamic of the sliding surface is given by

$$\dot{S}_\Omega = \vartheta_{12} e_{2_\Omega} + a_1 b_1 + a_2 b_2 + a_3 b_2 - b_3 - \ddot{\Omega}^* + c_1 v_q(\hat{x}). \tag{4.1}$$

Now, adding and subtracting the term $c_1 v_q(x)$ in the sliding surface, it follows that

$$\dot{S}_\Omega = \vartheta_{12} e_{2_\Omega} + a_1 b_1 + a_2 b_2 + a_3 b_2 - b_3 - \ddot{\Omega}^* + c_1 v_q(x) + c_1[v_q(\hat{x}) - v_q(x)] \tag{4.2}$$

Notice that the term $c_1[v_q(\hat{x}) - v_q(x)]$ is Lipschitz, i. e., there exists a positive constant μ_{11} such that $||c_1[v_q(\hat{x}) - v_q(x)]|| \leq \mu_{11}||\hat{x} - x||$. Then, applying the control input $v_q(x)$ in (4.2), the dynamic of the sliding surface is given by

$$\dot{S}_\Omega = -2L^2_{c_\Omega}(t)|S_\Omega|^{\frac{1}{2}} sign(S_\Omega) - \int_0^t \frac{L^4_{c_\Omega}(t)}{2} sign(S_\Omega) d\tau + c_1[v_q(\hat{x}) - v_q(x)] + \delta_\Omega(t) \tag{4.3}$$

The dynamic of S_Ω can be expressed as follows

$$\begin{cases} \dot{S}_\Omega = -2L^2_{c_\Omega}(t)|S_\Omega|^{1/2} sign(S_\Omega) + \nu_\Omega + \delta_\Omega(t) + c_1[v_q(\hat{x}) - v_q(x)] \\ \dot{\nu}_\Omega = -\dfrac{L^4_{c_\Omega}(t)}{2} sign(S_\Omega) \end{cases} \tag{4.4}$$

Now, defining the following change of coordinates $\Upsilon_{1_\Omega} = S_\Omega$ and $\Upsilon_{2_\Omega} = \nu_\Omega + \delta_\Omega(t)$. It follows that

$$\begin{aligned} \dot{\Upsilon}_{1_\Omega} &= -2L^2_{c_\Omega}(t)|\Upsilon_{1_\Omega}|^{1/2} sign(\Upsilon_{1_\Omega}) + \Upsilon_{2_\Omega} + c_1[v_q(\hat{x}) - v_q(x)] \\ \dot{\Upsilon}_{2_\Omega} &= -\frac{L^4_{c_\Omega}(t)}{2} sign(\Upsilon_{1_\Omega}) + d_\Omega(t) \end{aligned} \tag{4.5}$$

with $d_\Omega(t) = \dot{\delta}_\Omega(t)$. To analyze the stability of the system (4.5), consider the following change of coordinates as follows

$$z_{1_\Omega} = \frac{\Upsilon_{1_\Omega}}{L^2_{c_\Omega}(t)} \qquad z_{2_\Omega} = \frac{\Upsilon_{2_\Omega}}{L^2_{c_\Omega}(t)}. \tag{4.6}$$

whose dynamics are given by

$$\begin{aligned} \dot{z}_{1_\Omega} &= -2L_{c_\Omega}(t)|z_{1_\Omega}|^{\frac{1}{2}} sign(z_{1_\Omega}) + z_{2_\Omega} + \frac{c_1[v_q(\hat{x}) - v_q(x)]}{L^2_{c_\Omega}(t)} - \frac{2z_{1_\Omega}\dot{L}_{c_\Omega}(t)}{L_{c_\Omega}(t)} \\ \dot{z}_{2_\Omega} &= -\frac{L^2_{c_\Omega}(t)}{2} sign(z_{1_\Omega}) + \frac{d_\Omega(t)}{L^2_{c_\Omega}(t)} - \frac{2z_{2_\Omega}\dot{L}_{c_\Omega}(t)}{L_{c_\Omega}(t)} \end{aligned} \tag{4.7}$$

After that, in order to represent system in a simple form, a new change of variable is

introduced as follows

$$\pounds_{1_\Omega} = |z_{1_\Omega}|^{\frac{1}{2}} sign(z_{1_\Omega}) \qquad \pounds_{2_\Omega} = \frac{z_{2_\Omega}}{L_{c_\Omega}(t)} \tag{4.8}$$

then, the dynamical behavior, in the new coordinates, is given by

$$\begin{aligned}
\dot{\pounds}_{1_\Omega} &= \frac{L_{c_\Omega}(t)}{2|z_{1_\Omega}|^{\frac{1}{2}}}\left[-2\pounds_{1_\Omega} + \pounds_{2_\Omega} + \frac{c_1[v_q(\hat{x}) - v_q(x)]}{L^3_{c_\Omega}(t)}\right] - \pounds_{1_\Omega}\frac{\dot{L}_{c_\Omega}(t)}{L_{c_\Omega}(t)} \\
\dot{\pounds}_{2_\Omega} &= \frac{L_{c_\Omega}(t)}{2|z_{1_\Omega}|^{\frac{1}{2}}}\left[-\pounds_{1_\Omega} + \frac{2|z_{1_\Omega}|^{\frac{1}{2}} d_\Omega(t)}{L^4_{c_\Omega}(t)}\right] - 3\pounds_{2_\Omega}\frac{\dot{L}_{c_\Omega}(t)}{L_{c_\Omega}(t)}
\end{aligned} \tag{4.9}$$

which can be represented in a compact form as follows

$$\dot{\pounds}_\Omega = \alpha_\Omega\left[\left(A_\Omega - P_\Omega^{-1}C_\Omega^T C_\Omega\right)\pounds_\Omega + \Phi_\Omega\right] - N_\Omega \pounds_\Omega \frac{\dot{L}_{c_\Omega}(t)}{L_{c_\Omega}(t)} \tag{4.10}$$

with $\alpha_\Omega = \dfrac{L_{c_\Omega}(t)}{2|z_{1_\Omega}|^{\frac{1}{2}}}$, $\pounds_\Omega = \begin{bmatrix}\pounds_{1_\Omega} & \pounds_{2_\Omega}\end{bmatrix}^T$, $C_\Omega = \begin{bmatrix}1 & 0\end{bmatrix}$,

$$A_\Omega = \begin{bmatrix}0 & 1\\ 0 & 0\end{bmatrix}, \quad P_\Omega = \begin{bmatrix}1 & -1\\ -1 & 2\end{bmatrix}, \quad N_\Omega = \begin{bmatrix}1 & 0\\ 0 & 3\end{bmatrix}, \quad \Phi_\Omega = \begin{bmatrix}\dfrac{c_1[v_q(\hat{x}) - v_q(x)]}{L^3_{c_\Omega}(t)} \\ \dfrac{2|z_{1_\Omega}|^{\frac{1}{2}}}{L^4_{c_\Omega}(t)}\left[d_\Omega(t)\right]\end{bmatrix},$$

where, from Assumption 3.3, the nonlinear term Φ_Ω satisfies the following inequality, $||\Phi_\Omega|| \leq \varsigma_{11}||\pounds_\Omega||$ for $\varsigma_{11} > 0$.

Following the same steps of the previous analysis, consider the control input v_d, expressed in terms of the estimates as follows

$$\begin{aligned}
v_d(\hat{x}) = &\frac{L_d}{\vartheta_{13}}\left(\frac{\vartheta_{13}R_s\hat{i}_d}{L_d} - \frac{\vartheta_{13}p\hat{\Omega}L_q\hat{i}_q}{L_d} + \vartheta_{13}\dot{i}^*_d - e_{i_d}\right. \\
&\left. -2L^2_{c_{i_d}}(t)|S_{i_d}|^{\frac{1}{2}}sign(S_{i_d}) - \int_0^t \frac{L^4_{c_{i_d}}(t)}{2}sign(S_{i_d})d\tau\right)
\end{aligned} \tag{4.11}$$

Then, from sliding surface (3.46) and the control input (4.11) depending on the estimated states, the dynamic of the sliding surface is given by

$$\dot{S}_{i_d} = -\frac{\vartheta_{13} R_s i_d}{L_d} + \frac{\vartheta_{13} p\Omega L_q i_q}{L_d} + \frac{\vartheta_{13}}{L_d} v_d(\hat{x}) - \vartheta_{13}\dot{i}_d^* + e_{i_d} \tag{4.12}$$

Adding and subtracting the term $\frac{\vartheta_{13}}{L_d} v_d(x)$ in (4.12), it follows that

$$\dot{S}_{i_d} = -\frac{\vartheta_{13} R_s i_d}{L_d} + \frac{\vartheta_{13} p\Omega L_q i_q}{L_d} + \frac{\vartheta_{13}}{L_d} v_d(x) - \vartheta_{13}\dot{i}_d^* + e_{i_d} + \frac{\vartheta_{13}}{L_d}[v_d(\hat{x}) - v_d(x)] \tag{4.13}$$

where the term $\frac{\vartheta_{13}}{L_d}[v_d(\hat{x}) - v_d(x)]$ is Lipschitz, i.e., there exist a positive constant μ_{12} such that $||\frac{\vartheta_{13}}{L_d}[v_d(\hat{x}) - v_d(x)]|| \leq \mu_{12}||\hat{x} - x||$. Moreover, applying the control input $v_d(x)$ in the above system, the dynamic of the sliding surface is given by

$$\dot{S_{i_d}} = -2L^2_{c_{i_d}}(t)|S_{i_d}|^{\frac{1}{2}} sign(S_{i_d}) - \int_0^t \frac{L^4_{c_{i_d}}(t)}{2} sign(S_{i_d}) d\tau + \frac{\vartheta_2}{L_d}[v_d(\hat{x}) - v_d(x)] + \delta_{i_d}(t) \tag{4.14}$$

which can be represented as follows

$$\begin{cases} \dot{S_{i_d}} = -2L^2_{c_{i_d}}(t)|S_{i_d}|^{1/2} sign(S_{i_d}) + \nu_{i_d} + \delta_{i_d}(t) + \frac{\vartheta_2}{L_d}[v_d(\hat{x}) - v_d(x)] \\ \dot{\nu}_{i_d} = -\dfrac{L^4_{c_{i_d}}(t)}{2} sign(S_{i_d}) \end{cases} \tag{4.15}$$

Now, defining $\Upsilon_{1_{i_d}} = S_{i_d}$ and $\Upsilon_{2_{i_d}} = \nu_{i_d} + \delta_{i_d}(t)$. The system $\dot{S}_{i_d}$ can be expressed as follows

$$\begin{aligned} \dot{\Upsilon}_{1_{i_d}} &= -2L^2_{c_{i_d}}(t)|\Upsilon_{1_{i_d}}|^{1/2} sign(\Upsilon_{1_{i_d}}) + \Upsilon_{2_{i_d}} + \frac{\vartheta_2}{L_d}[v_d(\hat{x}) - v_d(x)] \\ \dot{\Upsilon}_{2_{i_d}} &= -\frac{L^4_{c_{i_d}}(t)}{2} sign(\Upsilon_{1_{i_d}}) + d_{i_d}(t) \end{aligned} \tag{4.16}$$

with $d_{i_d}(t) = \dot{\delta}_{i_d}(t)$. Then, from (4.16), consider the following change of coordinates, $z_{1_{i_d}} = \dfrac{\Upsilon_{1_{i_d}}}{L^2_{c_{i_d}}(t)}$ and $z_{2_{i_d}} = \dfrac{\Upsilon_{2_{i_d}}}{L^2_{c_{i_d}}(t)}$, whose dynamics are given by

$$\begin{aligned} \dot{z}_{1_{i_d}} &= -2L_{c_{i_d}}(t)|z_{1_{i_d}}|^{\frac{1}{2}} sign(z_{1_{i_d}}) + z_{2_{i_d}} + \frac{\frac{\vartheta_{13}}{L_d}[v_d(\hat{x}) - v_d(x)]}{L^2_{c_{i_d}}(t)} - \frac{2z_{1_{i_d}}\dot{L}_{c_{i_d}}}{L_{c_{i_d}}(t)} \\ \dot{z}_{2_{i_d}} &= -\frac{L^2_{c_{i_d}}(t)}{2} sign(z_{1_{i_d}}) + \frac{d_{i_d}(t)}{L^2_{c_{i_d}}(t)} - \frac{2z_{2_{i_d}}\dot{L}_{c_{i_d}}(t)}{L_{c_{i_d}}(t)} \end{aligned} \tag{4.17}$$

After that, a new change of variable is introduced as

$$\pounds_{1_{i_d}} = |z_{1_{i_d}}|^{\frac{1}{2}} sign(z_{1_{i_d}}) \qquad \pounds_{2_{i_d}} = \frac{z_{2_{i_d}}}{L_{c_{i_d}}(t)} \tag{4.18}$$

whose dynamics are given by

$$\begin{aligned} \dot{\pounds}_{1_{i_d}} &= \frac{L_{c_{i_d}}(t)}{2|z_{1_{i_d}}|^{\frac{1}{2}}} \left[-2\pounds_{1_{i_d}} + \pounds_{2_{i_d}} + \frac{\frac{\vartheta_{13}}{L_d}[v_d(\hat{x}) - v_d(x)]}{L^3_{c_{i_d}}(t)} \right] - \pounds_{1_{i_d}} \frac{\dot{L}_{c_{i_d}}(t)}{L_{c_{i_d}}(t)} \\ \dot{\pounds}_{2_{i_d}} &= \frac{L_{c_{i_d}}(t)}{2|z_{1_{i_d}}|^{\frac{1}{2}}} \left[-\pounds_{1_{i_d}} + \frac{2|z_{1_{i_d}}|^{\frac{1}{2}} d_{i_d}(t)}{L^4_{c_{i_d}}(t)} \right] - 3\pounds_{2_{i_d}} \frac{\dot{L}_{c_{i_d}}(t)}{L_{c_{i_d}}(t)} \end{aligned} \tag{4.19}$$

Then, system (4.19) can be rewritten in a compact form as follows

$$\dot{\pounds}_{i_d} = \alpha_{i_d} \left[\left(A_{i_d} - P^{-1}_{i_d} C^T_{i_d} C_{i_d} \right) \pounds_{i_d} + \Phi_{i_d} \right] - N_{i_d} \pounds_{i_d} \frac{\dot{L}_{c_{i_d}}(t)}{L_{c_{i_d}}(t)} \tag{4.20}$$

with $\alpha_{i_d} = \dfrac{L_{c_{i_d}}(t)}{2|z_{1_{i_d}}|^{\frac{1}{2}}}$, $\pounds_{i_d} = \begin{bmatrix} \pounds_{1_{i_d}} & \pounds_{2_{i_d}} \end{bmatrix}^T$, $C_{i_d} = \begin{bmatrix} 1 & 0 \end{bmatrix}$,

$$A_{i_d} = \begin{bmatrix} 0 & 1 \\ 0 & 0 \end{bmatrix}, \quad P_{i_d} = \begin{bmatrix} 1 & -1 \\ -1 & 2 \end{bmatrix}, \quad N_{i_d} = \begin{bmatrix} 1 & 0 \\ 0 & 3 \end{bmatrix}, \quad \Phi_{i_d} = \begin{bmatrix} \dfrac{\frac{\vartheta_{13}}{L_d}[v_d(\hat{x}) - v_d(x)]}{L^3_{c_{i_d}}(t)} \\ \dfrac{2|z_{1_{i_d}}|^{\frac{1}{2}}}{L^4_{c_{i_d}}(t)} [d_{i_d}(t)] \end{bmatrix}.$$

From Assumption 3.3, the term Φ_{i_d} is Lipschitz, i.e. there exists $\varsigma_{12} > 0$, such that $||\Phi_{i_d}|| \leq \varsigma_{12} ||\pounds_{i_d}||$.

Then, considering the adaptive observer-1 given in section 2.2.1 and the adaptive control-1 given in section 3.1.1 the dynamics in closed-loop, controller-observer, are established as follows

$$\begin{cases} \dot{\xi} = & \alpha_o \left[\left(A_o - P_o^{-1} C_o^T C_o \right) \xi + \Phi_o \right] - N_o \xi \dfrac{\dot{L}_o(t)}{L_o(t)} \\ \dot{\pounds}_\Omega = & \alpha_\Omega \left[\left(A_\Omega - P_\Omega^{-1} C_\Omega^T C_\Omega \right) \pounds_\Omega + \Phi_\Omega \right] - N_\Omega \pounds_\Omega \dfrac{\dot{L}_{c_\Omega}(t)}{L_{c_\Omega}(t)} \\ \dot{\pounds}_{i_d} = & \alpha_{i_d} \left[\left(A_{i_d} - P^{-1}_{i_d} C^T_{i_d} C_{i_d} \right) \pounds_{i_d} + \Phi_{i_d} \right] - N_{i_d} \pounds_{i_d} \dfrac{\dot{L}_{c_{i_d}}(t)}{L_{c_{i_d}}(t)} \end{cases} \tag{4.21}$$

If $\forall t > T_1$, such that ξ tend to zero, then, e_i tend to zero. Therefore, from Theorem 2.1, the observer converges in finite time to zero, it follows that the terms $c_1[v_q(\hat{x}) - v_q(x)]$ and $\frac{\vartheta_{13}}{L_d}[v_d(\hat{x}) - v_d(x)]$ contained in Φ_Ω and Φ_{i_d}, respectively; tend to zero in finite time. Therefore, the system given by (3.16) is obtained. Finally, from the same procedure given in the proof of the Theorem 3.1, the stability of the closed-loop system is proved.

4.2 Simulation and experimental results: Scheme 1

In this section, simulation and experimental results have been evaluated in order to show the performance of the proposed strategy. The adaptive observer introduced in section 2.2.1 and the adaptive control introduced in section 3.1.1 have been interconnected to illustrate the performance of the control in closed-loop under the action of the observer estimates, i.e., controller+observer (ASTWC-1 + AHOSMO-1). A scheme of the proposed sensorless control-1 is shown in Figure 4.1.

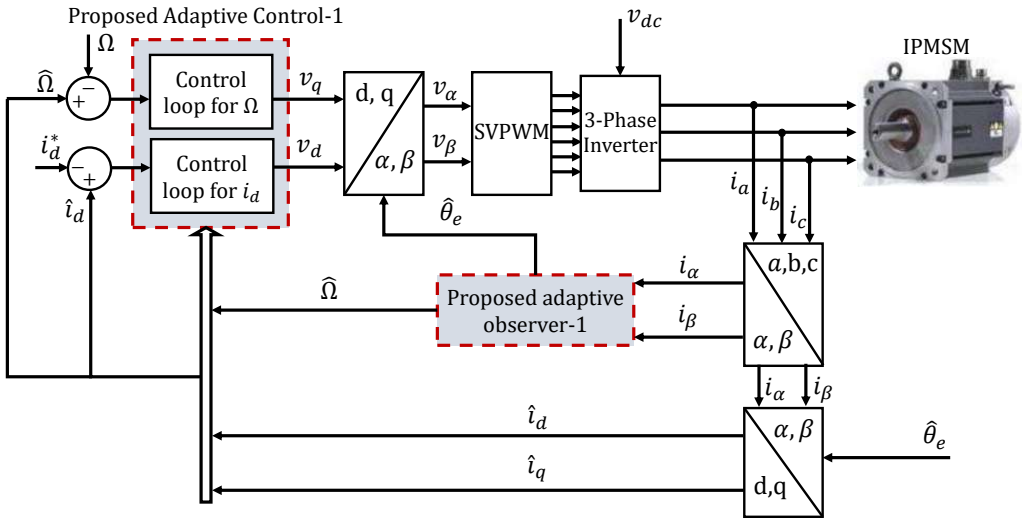

Figure 4.1 – Proposed sensorless control: Scheme-1.

4.2.1 Simulation tests

Simulation test has been carried out in Matlab-Simulink environment, using a sampling time of 1×10^{-3} with a fixed-step *ode*4 solver and white noise was added in the

measurable currents$-i_{\alpha\beta}$ with a power noise of 1×10^{-7} in order to illustrate a realistic situation. The parameter variation given in Figure 1.8 and the profile given in Figure 1.7 are considered. Therefore, from simulations, the behaviour of adaptive law L_o for the

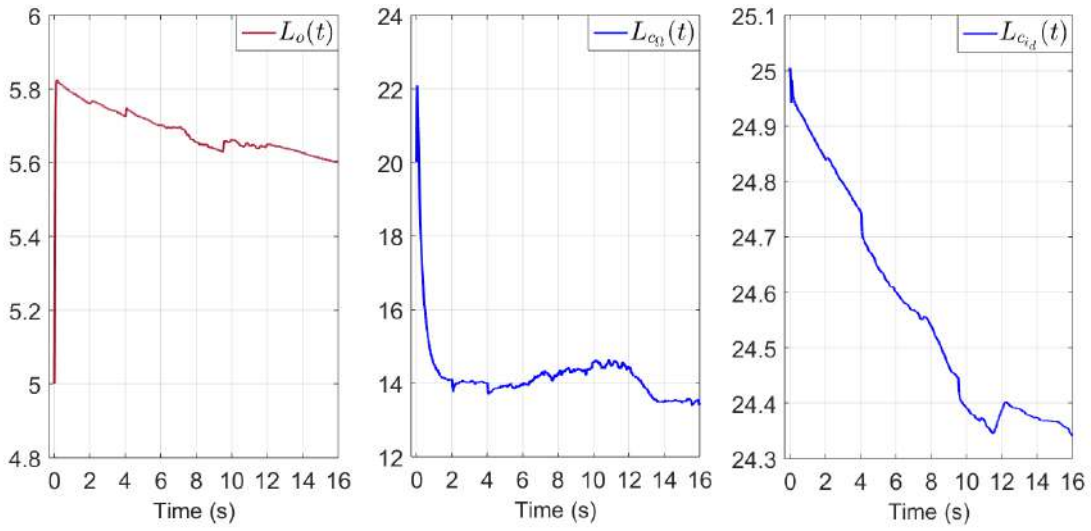

Figure 4.2 – Simulation test: Behaviour of the adaptive gains, observer and control

observer; and the adaptive laws L_{c_Ω} and $L_{c_{i_d}}$ for the speed and current$-i_d$ controllers, respectively, are shown in Figure 4.2. The adaptive laws have been implemented by considering the parameters of the Table 4.1. Then, in Figure 4.3, the speed estimation and

Table 4.1 – Parameters for the sensorless control-1 in simulation test.

AHOSMO-1		ASTWC-1					
γ_0	k_o	ϑ_{12}	γ_{c_Ω}	k_{c_Ω}	ϑ_{13}	$\gamma_{c_{i_d}}$	$k_{c_{i_d}}$
0.01	90	400	0.1	3	200	0.002	0.8

its estimation error are plotted. Small overshoots can be seen under the load torque variations. However, the performance of the adaptive observer is good under these variations. On the other hand, the estimated angular position compared with the real angular position is plotted in Figure 4.4. It easy to see that angular position error converges to zero ensuring observability for a wide speed range, i.e., high, medium and close to zero. In Figure 4.5, the estimation of acceleration is plotted and an estimation with noise can be seen due to the application of the additive noise in the currents$-i_{\alpha\beta}$. Now, taking into account the estimates of the observer, the controllers of speed and current$-i_d$ are applied

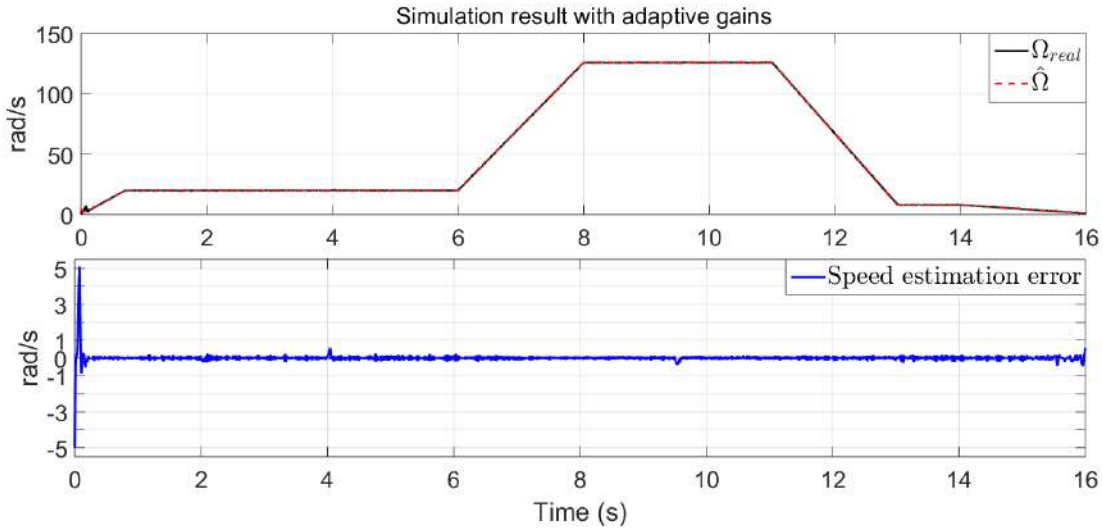

Figure 4.3 – Simulation test: Speed estimation and estimation error

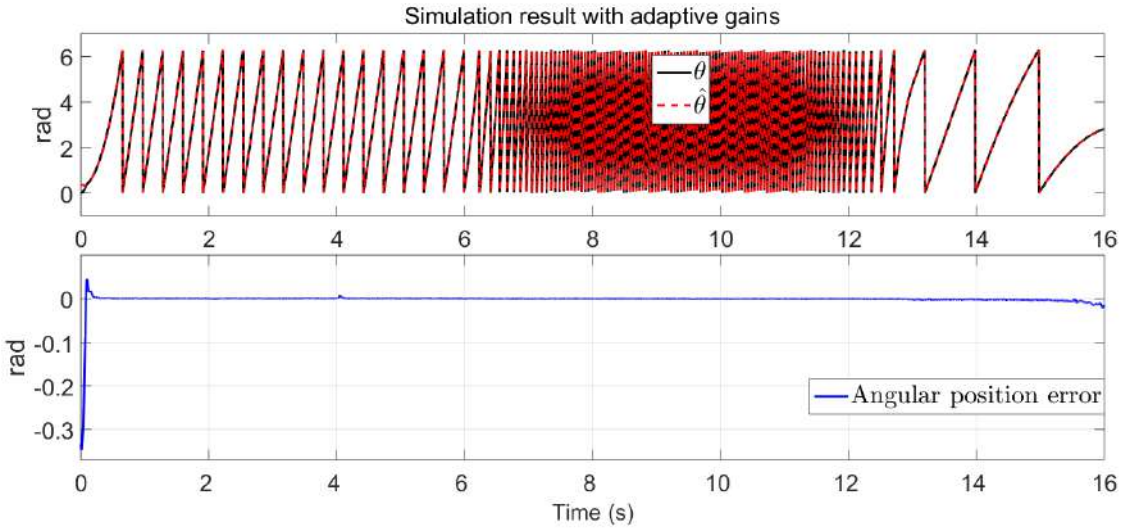

Figure 4.4 – Simulation test: Angular position estimation and angular position error

in closed-loop in order to control the IPMSM. Therefore, IPMSM has been controlled and rotor speed tracking is plotted in Figure 4.6 showing a tracking with good performance. Similarly, in Figure 4.7, the current-i_d tracks the desired reference $i_d^* = 0$ and the current i_q takes different values according to the speed and load torque profiles. Then, from these figures, the effectiveness of the proposed scheme based on sliding mode is shown by simulations under parameter variations. Finally, from simulations can be shown that the angular position estimation error e_{θ_e} has been extracted successfully showing good

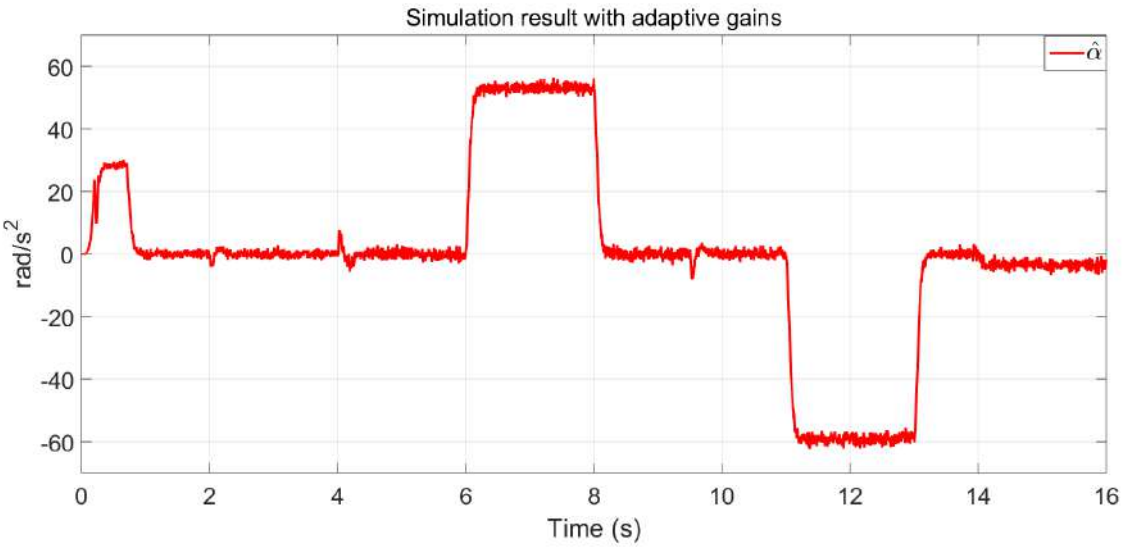

Figure 4.5 – Simulation test: Estimation of acceleration

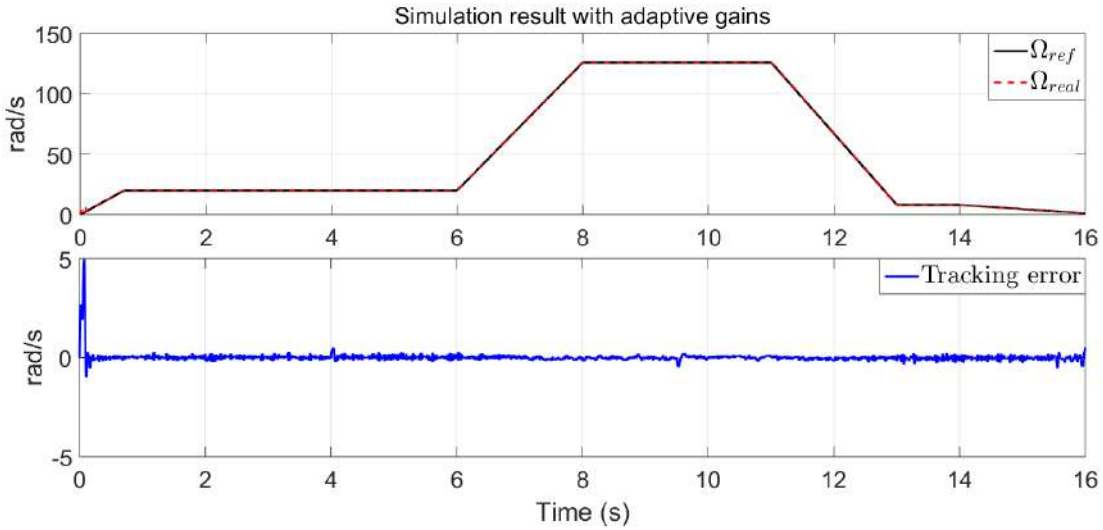

Figure 4.6 – Simulation test: Speed tracking and tracking error

performance in closed loop.

4.2.2 Experimental test

The proposed strategy is implemented taking into account the profiles defined in Figure 1.7. Moreover, as previously mentioned, during the experiments an encoder is used to measure the real angular position. Then, considering measured position, a Kalman-filter

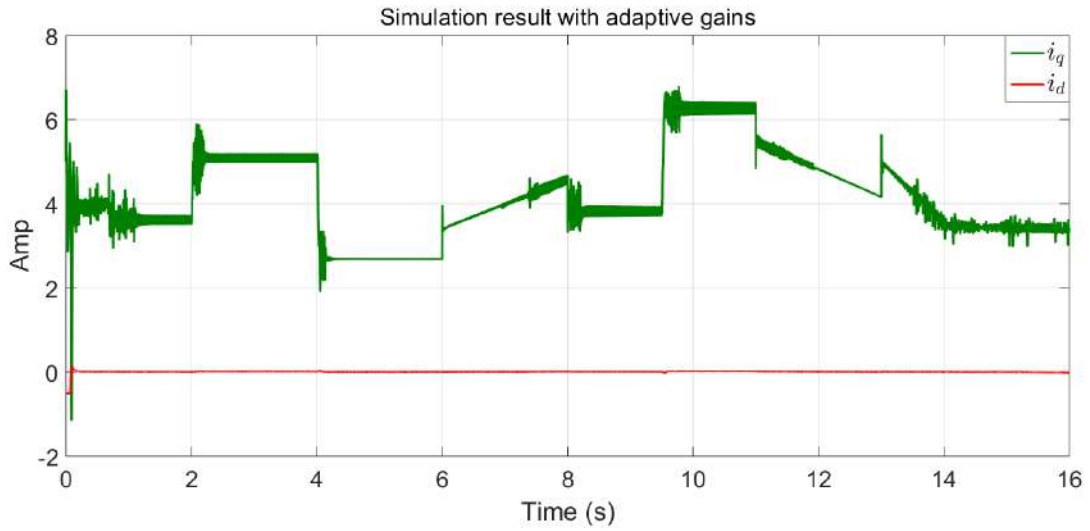

Figure 4.7 – Simulation test: Behaviour of the currents$-i_{dq}$

is applied in order to calculate the rotor speed. Therefore, from this information, it is possible to know if the proposed observer does a correct estimation and the controller a correct reference tracking.

Now, considering the proposed adaptive observer, the speed, angular position and acceleration are going to be estimated to control the speed and current$-i_d$ of IPMSM using adaptive controllers. A comparison is carried out with the same proposed strategy using constant gains in order to see the improvement with the implementation of adaptive gains. It is worth mentioning that during the experiments with constant gains, the constant gains have been chosen in order to avoid damaging the hardware. Experimental validation has been carried out considering the following parameters: for the case with constant gains, the observer is implemented with $L_o = 4.5$; $\vartheta_{12} = 180$ and $L_{c_\Omega} = 35$ in the speed controller; and $\vartheta_{13} = 20$ and $L_{c_{i_d}} = 20$ in the current$-i_d$ controller. On the other hand, the adaptive observer and adaptive control parameters are given in Table 4.2. The behaviour of the

Table 4.2 – Parameters for the sensorless control-1 in experimental test.

AHOSMO-1		ASTWC-1					
γ_0	k_o	ϑ_{12}	γ_{c_Ω}	k_{c_Ω}	ϑ_{13}	$\gamma_{c_{i_d}}$	$k_{c_{i_d}}$
0.07	35	180	0.0003	0.1	20	0.0009	0.2

adaptive laws for the observer and controllers are illustrated in Figure 4.8.

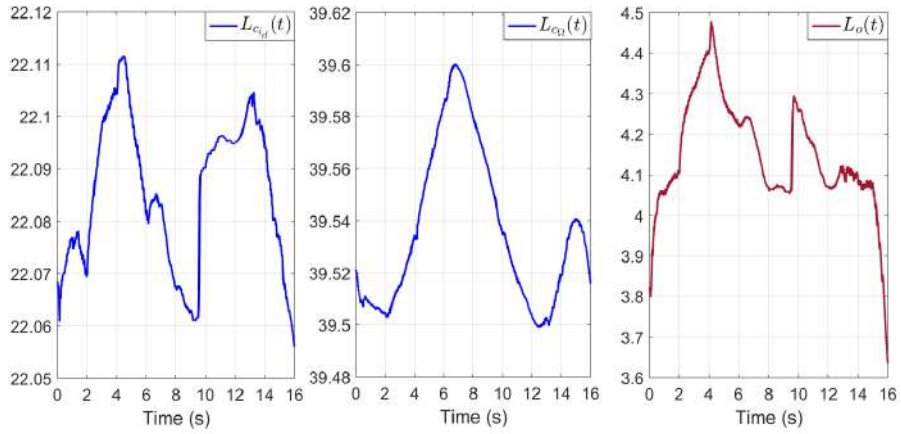

Figure 4.8 – Experimental test. Adaptive laws: Control ($L_{c_{i_d}}(t)$, $L_{c_\Omega}(t)$) and observer ($L_o(t)$).

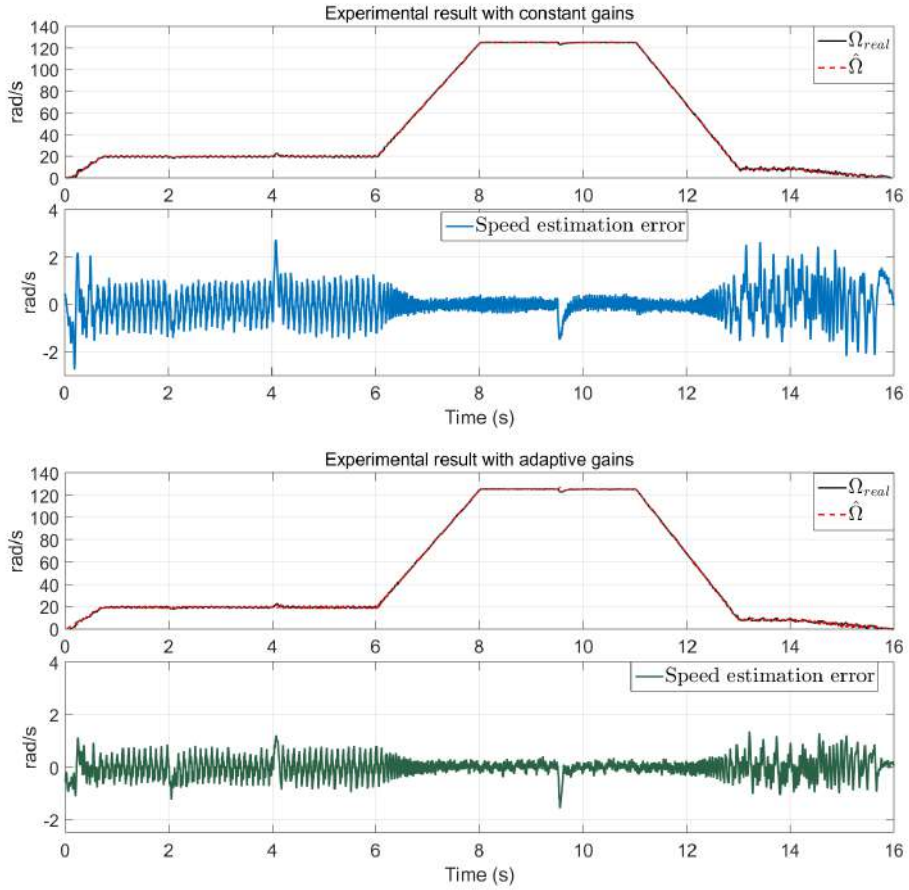

Figure 4.9 – Experimental test: Speed estimation and estimation error.

Then, the speed and the angular position have been estimated using constant gain and

adaptive gain as can be shown in Figure 4.9 and Figure 4.10, respectively. At first glance, it is not possible to see the improvement in detail through speed estimation error and angular error. However, in Figure 4.11, in order to show numerically the improvement,

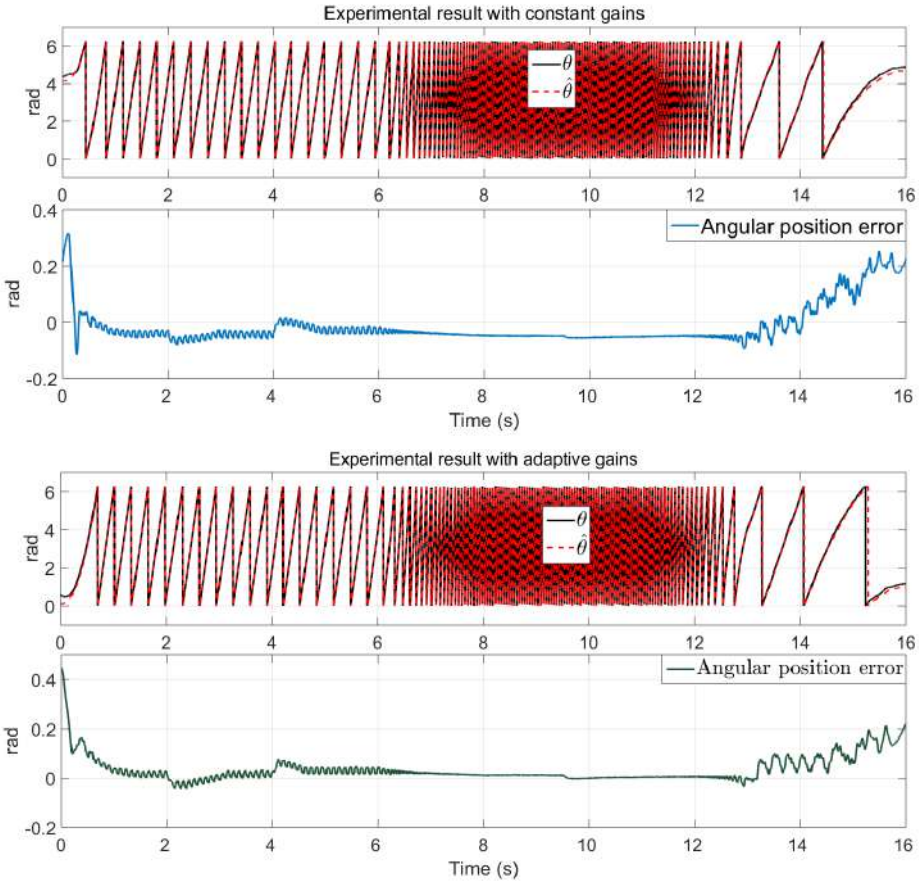

Figure 4.10 – Experimental test: Angular position estimation and estimation error.

a performance index is computed: Integral Absolute Error (IAE). Therefore, it possible to see that proposed adaptive observer improves the estimation adjusting the gains in order to obtain a minimum error. On the other side, the estimation of the acceleration is shown in Figure 4.12 using constant gains and adaptive gains. Then, the estimation with adaptive gains has an improvement avoiding overestimation with large gains and reducing the chattering. Now, the estimates of the observer have been used in the controllers to control the machine in closed-loop. In Figure 4.13, the speed tracking and its tracking error are shown. A comparative study using constant gains and adaptive gains is given. It is clear that an improvement can be seen numerically in Figure 4.11 using the adaptive gains in the scheme. On the other hand, the currents$-i_{dq}$ are plotted in Figure 4.14. Then,

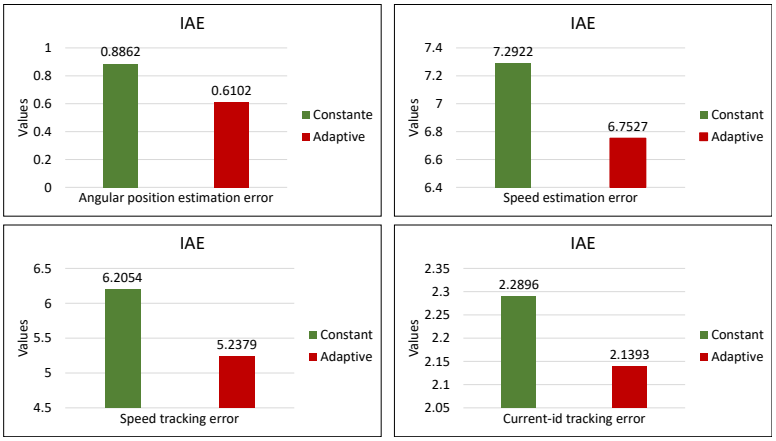

Figure 4.11 – Performance index for the estimation and tracking of states during experiments

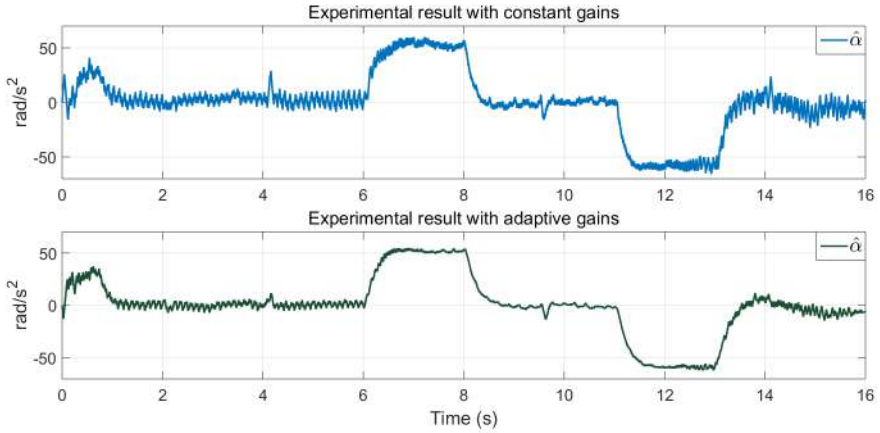

Figure 4.12 – Experimental test: Estimation of the acceleration.

the closed-loop in IPMSM is achieved successfully.

Therefore, as can be seen the proposed strategy only requires the current $-i_{\alpha\beta}$ signals for extracting the angular position estimation error e_{θ_e}, directly, without any additional information or elements, then, e_{θ_e} can be used in the observer based on the virtual system to estimate angular position, speed and acceleration, such that the proposed strategy has been validated experimentally, with good effectiveness at low, medium and high speed in closed loop. Moreover, as can be seen in simulation, the tracking errors and estimation errors show the effect of adding white noise. It is clear that the chattering has been attenuated. However, the effects of white noise are present in the signals. On the other hand, during the experimental test, these errors are more important compared to those obtained

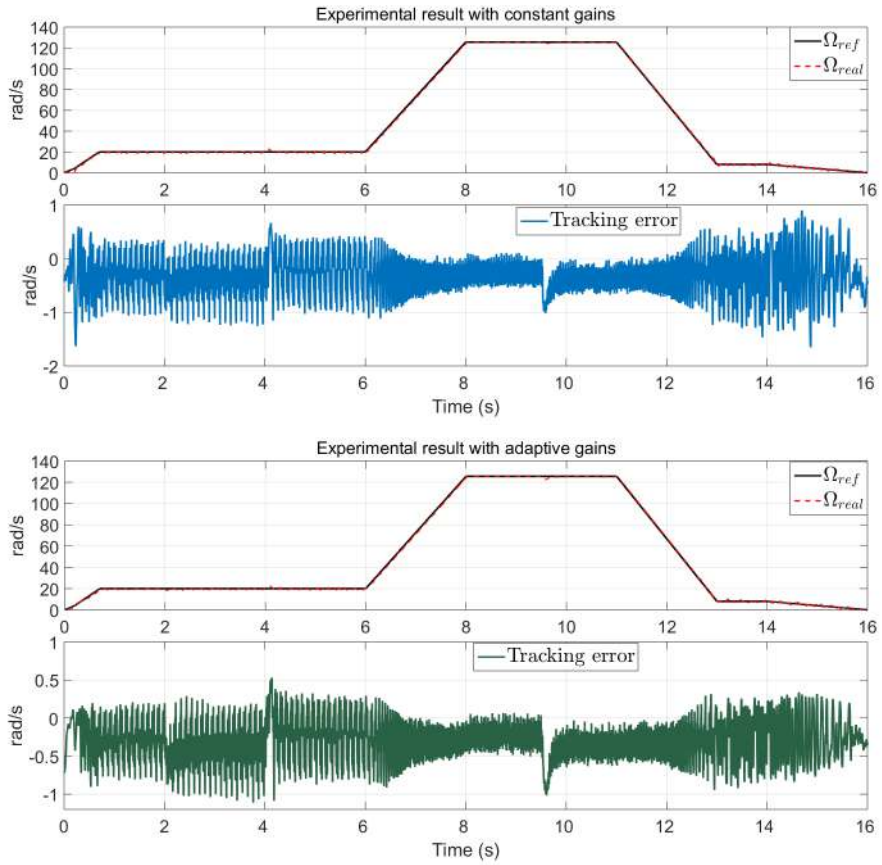

Figure 4.13 – Experimental test: Speed tracking and tracking error

in the simulation. It is well-known that in the experiments the effect caused by external disturbances (inverter effect) and the noise appears in the measured signals. However, the proposed strategy works well and attenuate the effects of chattering, uncertain parameters and unmodeled dynamics.

4.3 Closed-loop analysis: Scheme 2

Consider the proposed control given in the section 3.2.1 (ASTWC-2) using the estimates provided by the proposed observer given in section 2.3.1 (AHOSMO-2). Then, the stability analysis of the system in closed-loop, control-observer scheme, is established as follows

Theorem 4.2. *Consider the dynamical model of the IPMSM* (1.36)-(1.37) *in closed-loop with the controllers* (3.92)-(3.97) *using the estimates provided by the observer* (2.95).

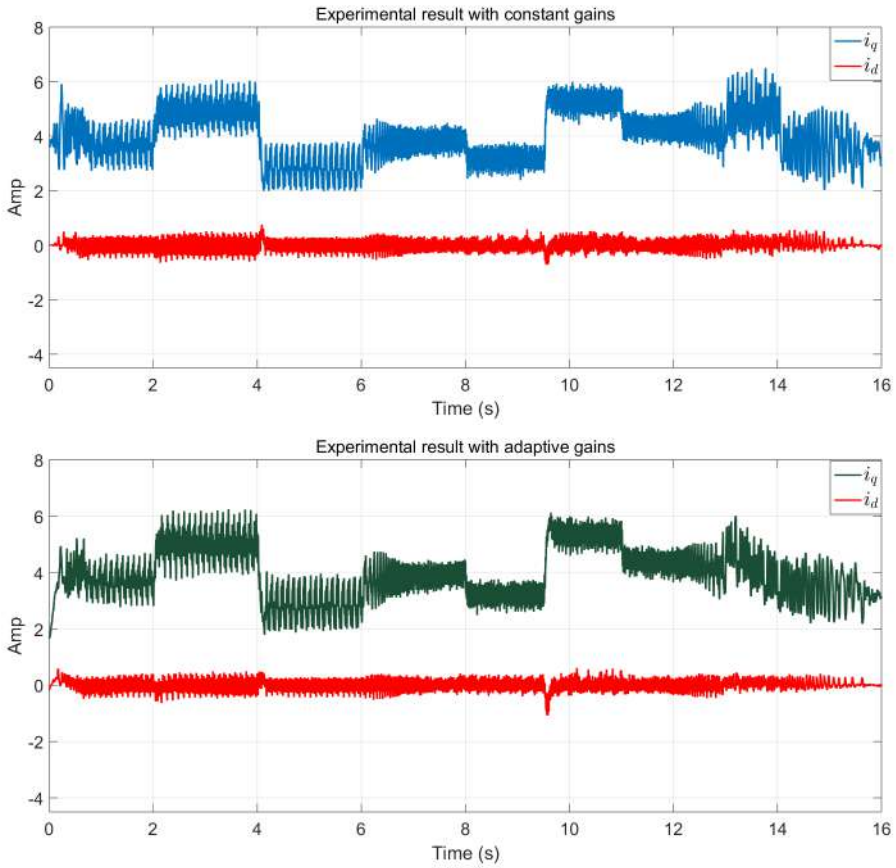

Figure 4.14 – Experimental test: Profiles of the currents$-i_{dq}$

Then, tracking errors e_{1_ω} and $e_{1_{i_d}}$; and estimation error e_{θ_e} converge to zero in finite time.

Proof: Since the control input $v_q(\hat{x})$ depends on estimates $\hat{\Omega}$, $\hat{i}_d$ and $\hat{i}_q$; and taking into account the sliding surface given by (3.91), then the dynamic of the sliding surface is given as follows

$$\dot{S}_{\Omega_2} = \vartheta_{22} e_{2_\Omega} + a_1 b_1 + a_2 b_2 + a_3 b_2 - b_3 - \ddot{\Omega}^* + c_1 v_q(\hat{x}) \tag{4.22}$$

Now, adding and subtracting the term $c_1 v_q(x)$ in the sliding surface, it follows that

$$\dot{S}_{\Omega_2} = \vartheta_{22} e_{2_\Omega} + a_1 b_1 + a_2 b_2 + a_3 b_2 - b_3 - \ddot{\Omega}^* + c_1 v_q(x) + c_1[v_q(\hat{x}) - v_q(x)] \tag{4.23}$$

Notice that the term $c_1[v_q(\hat{x}) - v_q(x)]$ is Lipschitz, i. e., there exists a positive constant μ_{21} such that $||c_1[v_q(\hat{x}) - v_q(x)]|| \leq \mu_{21}||\hat{x} - x||$.
Applying the control input $v_q(x)$ in the above system, the dynamic of the sliding surface

is given by

$$\dot{S_{\Omega_2}} = -2L_{c_{\Omega_2}}(t)|S_{\Omega_2}|^{\frac{1}{2}}sign(S_{\Omega_2}) - \int_0^t \frac{L_{c_{\Omega_2}}^2(t)}{2}sign(S_{\Omega_2})d\tau + c_1[v_q(\hat{x}) - v_q(x)] + \delta_\Omega(t) \quad (4.24)$$

Then, the dynamic of S_{Ω_2} can be expressed as follows

$$\begin{cases} \dot{S}_{\Omega_2} = -2L_{c_{\Omega_2}}(t)|S_{\Omega_2}|^{\frac{1}{2}}sign(S_{\Omega_2}) + \nu_{\Omega_2} + \delta_{\Omega_2}(t) + c_1[v_q(\hat{x}) - v_q(x)] \\ \dot{\nu}_{\Omega_2} = -\dfrac{L_{c_{\Omega_2}}^2(t)}{2}sign(S_{\Omega_2}) \end{cases} \quad (4.25)$$

Now, defining the following change of coordinates $z_{1_{\Omega_2}} = S_{\Omega_2}$ and $z_{2_{\Omega_2}} = \nu_{\Omega_2} + \delta_\Omega(t)$. The system (4.25) is given by

$$\begin{aligned} \dot{z}_{1_{\Omega_2}} &= -2L_{c_{\Omega_2}}(t)|z_{1_{\Omega_2}}|^{\frac{1}{2}}sign(z_{1_{\Omega_2}}) + z_{2_{\Omega_2}} + c_1[v_q(\hat{x}) - v_q(x)] \\ \dot{z}_{2_{\Omega_2}} &= -\frac{L_{c_{\Omega_2}}^2(t)}{2}sign(z_{1_{\Omega_2}}) + d_\Omega(t) \end{aligned} \quad (4.26)$$

with $d_\Omega(t) = \dot{\delta}_\Omega(t)$. Now, a change of variable is introduced

$$\pounds_{1_{\Omega_2}} = \frac{|z_{1_{\Omega_2}}|^{\frac{1}{2}}sign(z_{1_{\Omega_2}})}{L_{c_{\Omega_2}}(t)} \qquad \pounds_{2_{\Omega_2}} = \frac{z_{2_{\Omega_2}}}{L_{c_{\Omega_2}}^2(t)} \quad (4.27)$$

then, the dynamical behavior of system (4.27), in the new coordinates, is given by

$$\begin{aligned} \dot{\pounds}_{1_{\Omega_2}} &= \frac{L_{c_{\Omega_2}}(t)}{2|z_{1_{\Omega_2}}|^{\frac{1}{2}}}\left[-2\pounds_{1_{\Omega_2}} + \pounds_{2_{\Omega_2}} + \frac{c_1[v_q(\hat{x}) - v_q(x)]}{L_{c_{\Omega_2}}^2(t)}\right] - \pounds_{1_{\Omega_2}}\frac{\dot{L}_{c_{\Omega_2}}(t)}{L_{c_{\Omega_2}}(t)} \\ \dot{\pounds}_{2_{\Omega_2}} &= \frac{L_{c_{\Omega_2}}(t)}{2|z_{1_{\Omega_2}}|^{\frac{1}{2}}}\left[-\pounds_{1_{\Omega_2}} + \frac{2|z_{1_{\Omega_2}}|^{\frac{1}{2}}d_\Omega(t)}{L_{c_{\Omega_2}}^3(t)}\right] - 2\pounds_{2_{\Omega_2}}\frac{\dot{L}_{c_{\Omega_2}}(t)}{L_{c_{\Omega_2}}(t)} \end{aligned} \quad (4.28)$$

which can be represented in a compact form as follows

$$\dot{\pounds}_{\Omega_2} = \alpha_{\Omega_2}\left[\left(A_{\Omega_2} - P_{\Omega_2}^{-1}C_{\Omega_2}^T C_{\Omega_2}\right)\pounds_{\Omega_2} + \Phi_{\Omega_2}\right] - D_{\Omega_2}\pounds_{\Omega_2}\frac{\dot{L}_{c_{\Omega_2}}(t)}{L_{c_{\Omega_2}}(t)} \quad (4.29)$$

with $\alpha_{\Omega_2} = \dfrac{L_{c_{\Omega_2}}(t)}{2|z_{1_{\Omega_2}}|^{\frac{1}{2}}}$ and

$$\pounds_{\Omega_2} = \begin{bmatrix} \pounds_{1_{\Omega_2}} \\ \pounds_{2_{\Omega_2}} \end{bmatrix} \qquad A_{\Omega_2} = \begin{bmatrix} 0 & 1 \\ 0 & 0 \end{bmatrix} \qquad C_{\Omega_2} = \begin{bmatrix} 1 & 0 \end{bmatrix} \tag{4.30}$$

$$P_{\Omega_2} = \begin{bmatrix} 1 & -1 \\ -1 & 2 \end{bmatrix} \qquad D_{\Omega_2} = \begin{bmatrix} 1 & 0 \\ 0 & 2 \end{bmatrix} \qquad \Phi_{\Omega_2} = \begin{bmatrix} \dfrac{c_1[v_q(\hat{x}) - v_q(x)]}{L^2_{c_{\Omega_2}}(t)} \\ \dfrac{2|z_{1_{\Omega_2}}|^{\frac{1}{2}}}{L^3_{c_{\Omega_2}}(t)}\,[d_\Omega(t)] \end{bmatrix} \tag{4.31}$$

From Assumption 3.5, the nonlinear term Φ_{Ω_2} satisfies the following inequality, $||\Phi_{\Omega_2}|| \leq \varsigma_{21}||\pounds_{\Omega_2}||$ for $\varsigma_{21} > 0$.

Following the same steps of the previous analysis, consider the control input v_d, expressed in terms of the estimates as follows

$$\begin{aligned} v_d(\hat{x}) = & \frac{L_d}{\vartheta_{23}} \left(\frac{\vartheta_{23} R_s \hat{i}_d}{L_d} - \frac{\vartheta_{23} p \hat{\Omega} L_q \hat{i}_q}{L_d} + \vartheta_{23} \dot{i}_d^* - e_{i_d} \right. \\ & \left. -2L_{c_{i_{d_2}}}(t)|S_{i_{d_2}}|^{\frac{1}{2}} sign(S_{i_{d_2}}) - \int_0^t \frac{L^2_{c_{i_{d_2}}}(t)}{2} sign(S_{i_{d_2}}) d\tau \right) \end{aligned} \tag{4.32}$$

Then, from sliding surface (3.96) and the control input (4.32) depending on the estimated states, the dynamic of the sliding surface is given by

$$\dot{S}_{i_{d_2}} = -\frac{\vartheta_{23} R_s i_d}{L_d} + \frac{\vartheta_{23} p \Omega L_q i_q}{L_d} + \frac{\vartheta_{23}}{L_d} v_d(\hat{x}) - \vartheta_{23} \dot{i}_d^* + e_{i_d} \tag{4.33}$$

Adding and subtracting the term $\dfrac{\vartheta_{23}}{L_d} v_d(x)$ in (4.33), it follows that

$$\dot{S}_{i_{d_2}} = -\frac{\vartheta_{23} R_s i_d}{L_d} + \frac{\vartheta_{23} p \Omega L_q i_q}{L_d} + \frac{\vartheta_{23}}{L_d} v_d(x) - \vartheta_{23} \dot{i}_d^* + e_{i_d} + \frac{\vartheta_{23}}{L_d}[v_d(\hat{x}) - v_d(x)] \tag{4.34}$$

where the term $\dfrac{\vartheta_{23}}{L_d}[v_d(\hat{x}) - v_d(x)]$ is Lipschitz, i.e., there exist a positive constant μ_{22} such that $||\dfrac{\vartheta_{23}}{L_d}[v_d(\hat{x}) - v_d(x)]|| \leq \mu_{22}||\hat{x} - x||$.

Moreover, applying the control input $v_d(x)$ in the above system, the dynamic of the sliding

surface is given by

$$\dot{S_{i_{d_2}}} = -2L_{c_{i_{d_2}}}(t)|S_{i_{d_2}}|^{\frac{1}{2}}sign(S_{i_{d_2}}) - \int_0^t \frac{L^2_{c_{i_{d_2}}}(t)}{2}sign(S_{i_{d_2}})d\tau + \frac{\vartheta_{23}}{L_d}[v_d(\hat{x}) - v_d(x)] + \delta_{i_d}(t) \tag{4.35}$$

which can be represented as follows

$$\begin{cases} \dot{S}_{i_{d_2}} = -2L_{c_{i_{d_2}}}(t)|S_{i_{d_2}}|^{\frac{1}{2}}sign(S_{i_{d_2}}) + \nu_{i_{d_2}} + \delta_{i_d}(t) + \dfrac{\vartheta_{23}}{L_d}[v_d(\hat{x}) - v_d(x)] \\ \dot{\nu}_{i_{d_2}} = -\dfrac{L^2_{c_{i_{d_2}}}(t)}{2}sign(S_{i_{d_2}}) \end{cases} \tag{4.36}$$

Now, defining $z_{1_{i_{d_2}}} = S_{i_{d_2}}$ and $z_{2_{i_{d_2}}} = \nu_{i_{d_2}} + \delta_{i_d}(t)$. The system $\dot{S}_{i_{d_2}}$ can be expressed as follows

$$\begin{aligned} \dot{z}_{1_{i_{d_2}}} &= -2L_{c_{i_{d_2}}}(t)|z_{1_{i_{d_2}}}|^{\frac{1}{2}}sign(z_{1_{i_{d_2}}}) + z_{2_{i_{d_2}}} + \frac{\vartheta_{23}}{L_d}[v_d(\hat{x}) - v_d(x)] \\ \dot{z}_{2_{i_{d_2}}} &= -\frac{L^2_{c_{i_{d_2}}}(t)}{2}sign(z_{1_{i_{d_2}}}) + d_{i_d}(t) \end{aligned} \tag{4.37}$$

with $d_{i_d}(t) = \dot{\delta}_{i_d}(t)$ Now, a new change of variable is introduced

$$\pounds_{1_{i_{d_2}}} = \frac{|z_{1_{i_{d_2}}}|^{\frac{1}{2}}sign(z_{1_{i_{d_2}}})}{L_{c_{i_{d_2}}}(t)} \qquad \pounds_{2_{i_{d_2}}} = \frac{z_{2_{i_{d_2}}}}{L^2_{c_{i_{d_2}}}(t)} \tag{4.38}$$

whose dynamics are given by

$$\begin{aligned} \dot{\pounds}_{1_{i_{d_2}}} &= \frac{L_{c_{i_{d_2}}}(t)}{2|z_{1_{i_{d_2}}}|^{\frac{1}{2}}}\left[-2\pounds_{1_{i_{d_2}}} + \pounds_{2_{i_{d_2}}} + \frac{\frac{\vartheta_{23}}{L_d}[v_d(\hat{x}) - v_d(x)]}{L^2_{c_{i_{d_2}}}(t)}\right] - \pounds_{1_{i_{d_2}}}\frac{\dot{L}_{c_{i_{d_2}}}(t)}{L_{c_{i_{d_2}}}(t)} \\ \dot{\pounds}_{2_{i_{d_2}}} &= \frac{L_{c_{i_{d_2}}}(t)}{2|z_{1_{i_{d_2}}}|^{\frac{1}{2}}}\left[-\pounds_{1_{i_{d_2}}} + \frac{2|z_{1_{i_{d_2}}}|^{\frac{1}{2}}d_{i_d}(t)}{L^3_{c_{i_{d_2}}}(t)}\right] - 2\pounds_{2_{i_{d_2}}}\frac{\dot{L}_{c_{i_{d_2}}}(t)}{L_{c_{i_{d_2}}}(t)} \end{aligned} \tag{4.39}$$

Then, system (4.39) can be rewritten in a compact form as follows

$$\dot{\pounds}_{i_{d_2}} = \alpha_{i_{d_2}}\left[\left(A_{i_{d_2}} - P^{-1}_{i_{d_2}}C^T_{i_{d_2}}C_{i_{d_2}}\right)\pounds_{i_{d_2}} + \Phi_{i_{d_2}}\right] - D_{i_{d_2}}\pounds_{i_{d_2}}\frac{\dot{L}_{c_{i_{d_2}}}(t)}{L_{c_{i_{d_2}}}(t)} \tag{4.40}$$

with $\alpha_{i_{d_2}} = \dfrac{L_{c_{i_{d_2}}}(t)}{2|z_{1_{i_{d_2}}}|^{\frac{1}{2}}}$ and

$$\pounds_{i_{d_2}} = \begin{bmatrix} \pounds_{1_{i_{d_2}}} \\ \pounds_{2_{i_{d_2}}} \end{bmatrix} \qquad A_{i_{d_2}} = \begin{bmatrix} 0 & 1 \\ 0 & 0 \end{bmatrix} \qquad C_{i_{d_2}} = \begin{bmatrix} 1 & 0 \end{bmatrix} \tag{4.41}$$

$$P_{i_{d_2}} = \begin{bmatrix} 1 & -1 \\ -1 & 2 \end{bmatrix} \qquad D_{i_{d_2}} = \begin{bmatrix} 1 & 0 \\ 0 & 2 \end{bmatrix} \qquad \Phi_{i_{d_2}} = \begin{bmatrix} \dfrac{\frac{\vartheta_{23}}{L_d}[v_d(\hat{x}) - v_d(x)]}{L^2_{c_{i_{d_2}}}(t)} \\ \dfrac{2|z_{1_{i_{d_2}}}|^{\frac{1}{2}}}{L^3_{c_{i_{d_2}}}(t)}[d_{i_d}(t)] \end{bmatrix} \tag{4.42}$$

From Assumption 3.5, the term $\Phi_{i_{d_2}}$ is Lipschitz, i.e. there exists $\varsigma_{22} > 0$, such that $||\Phi_{i_{d_2}}|| \leq \varsigma_{22}||\pounds_{i_{d_2}}||$.

Then, considering the adaptive observer given in section 2.3.1 and the adaptive control given in section 3.2.1, the dynamics in closed-loop, controller-observer, are establishes as follows

$$\begin{cases} \dot{\xi}_{o_2} = & \alpha_{o_2}\left[\left(A_{o_2} - P^{-1}_{o_2}C^T_{o_2}C_{o_2}\right)\xi_{o_2} + \Phi_{o_2}\right] - D_{o_2}\xi_{o_2}\dfrac{\dot{L}_{o_2}(t)}{L_{o_2}(t)} \\ \dot{\pounds}_{\Omega_2} = & \alpha_{\Omega_2}\left[\left(A_{\Omega_2} - P^{-1}_{\Omega_2}C^T_{\Omega_2}C_{\Omega_2}\right)\pounds_{\Omega_2} + \Phi_{\Omega_2}\right] - D_{\Omega_2}\pounds_{\Omega_2}\dfrac{\dot{L}_{c_{\Omega_2}}(t)}{L_{c_{\Omega_2}}(t)} \\ \dot{\pounds}_{i_{d_2}} = & \alpha_{i_d}\left[\left(A_{i_{d_2}} - P^{-1}_{i_{d_2}}C^T_{i_{d_2}}C_{i_{d_2}}\right)\pounds_{i_{d_2}} + \Phi_{i_{d_2}}\right] - D_{i_{d_2}}\pounds_{i_{d_2}}\dfrac{\dot{L}_{c_{i_{d_2}}}(t)}{L_{c_{i_{d_2}}}(t)} \end{cases} \tag{4.43}$$

If $\forall t > T_{1_2}$, such that ξ_{o_2} tend to zero, then, e_{i_2} tend to zero. Therefore, from Theorem 2.2, the observer converges in finite time to zero, it follows that the terms $c_1[v_q(\hat{x}) - v_q(x)]$ and $\dfrac{\vartheta_{23}}{L_d}[v_d(\hat{x}) - v_d(x)]$ contained in Φ_{Ω_2} and $\Phi_{i_{d_2}}$, respectively; tend to zero in finite time. Therefore, the system given by (3.62) is obtained. Finally, from the same procedure given in the proof of the Theorem 3.2, the stability of the closed-loop system is proved.

4.4 Simulation and experimental results: Scheme 2

In this section, simulation and experimental results have been evaluated in order to show the performance of the proposed strategy. The adaptive observer introduced in section 2.3.1 (AHOSMO-2) and the adaptive control introduced in section 3.2.1 (ASTWC-2)

have been interconnected to illustrate the performance of the control in closed-loop under the action of the observer estimates, i.e., controller+observer (ASTWC-2 + AHOSMO-2). A scheme of the proposed sensorless control strategy-2 is shown in Figure 4.15.

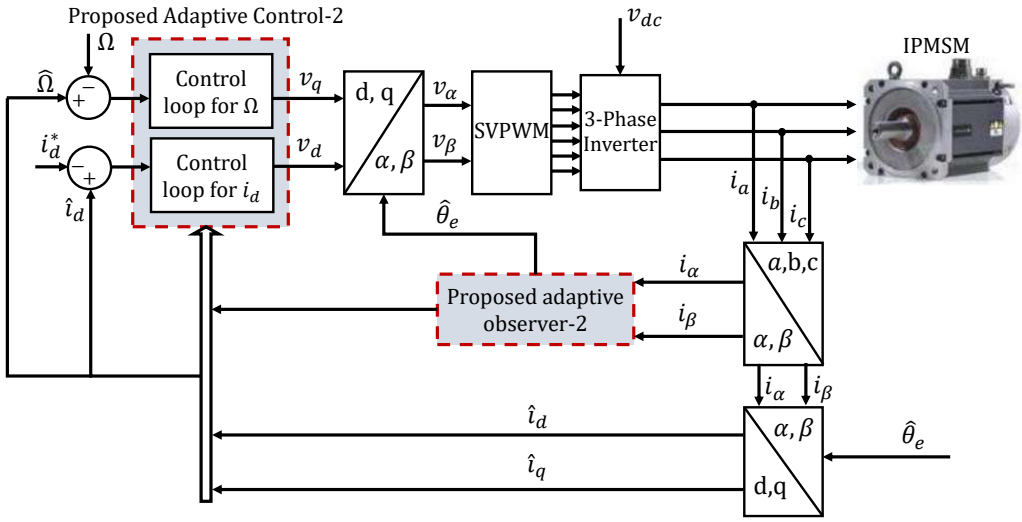

Figure 4.15 – Proposed sensorless control: Scheme-2.

4.4.1 Simulation test

Simulation test is carried out in Matlab-Simulink environment, using a sampling time of 1×10^{-3} with a fixed-step *ode*4 solver. Moreover, white noise was added in the measurable currents$-i_{\alpha\beta}$ with a power noise of 1×10^{-7} in order to illustrate a realistic situation. Moreover, the adaptive laws have been implemented by considering the parameters of the Table 4.3. The behaviour of adaptive law $L_{o_2}(t)$ for the observer; and the adaptive laws

Table 4.3 – Parameters for the sensorless control-2 in simulation test

AHOSMO-2		ASTWCs-2					
γ_{o_2}	k_{o_2}	ϑ_{22}	$\gamma_{c_{\Omega_2}}$	$k_{c_{\Omega_2}}$	ϑ_{23}	$\gamma_{c_{i_{d_2}}}$	$k_{c_{i_{d_2}}}$
0.016	200	400	0.008	120	200	0.0011	120

$L_{c_{\Omega_2}}(t)$ and $L_{c_{i_{d_2}}}(t)$ for speed and current$-i_d$ controllers are shown in the Figure 4.16, respectively.

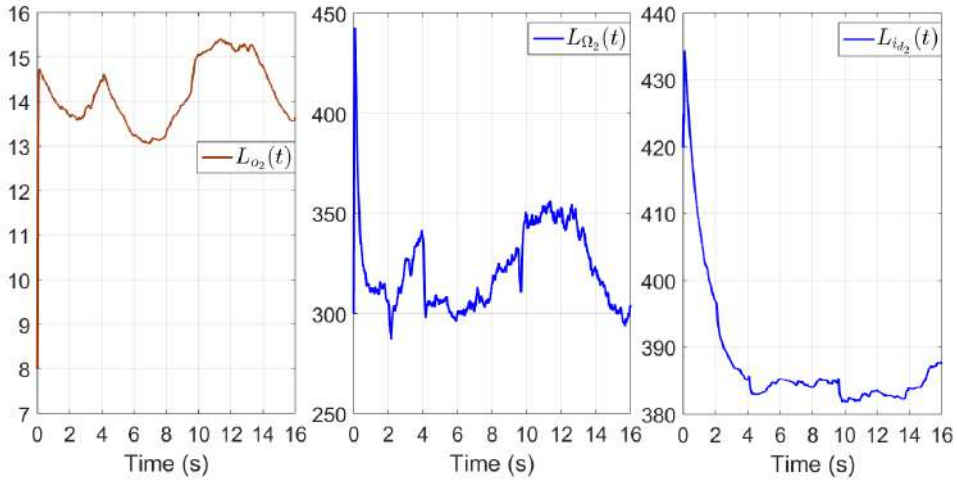

Figure 4.16 – Simulation test: Behaviour of adaptive gains for the observer ($L_{o_2}(t)$) and controllers ($L_{\Omega_2}(t), L_{i_{d_2}}(t)$)

Considering the adaptive laws, in Figure 4.17, the speed estimation and its estimation error are introduced, showing a minimum error. In Figure 4.18, the angular position

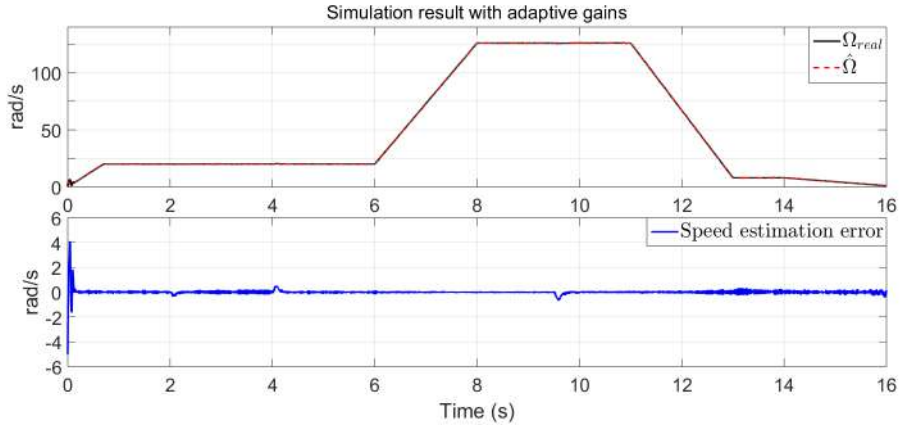

Figure 4.17 – Simulation test: Speed estimation and estimation error

estimation and its angular position estimation error are plotted. As can be seen, the estimation is ensured over a wide speed range in presence of parametric uncertainties (see Figure 1.8). Moreover, in Figure 4.19, acceleration has been estimated in order to compensate the fast dynamics in the system and reduce the estimation error in the speed and angular position.

Information from observer estimates has been interconnected with the controllers in closed-loop, as can be seen in the scheme 4.15. Then, in Figure 4.20, speed tracking and

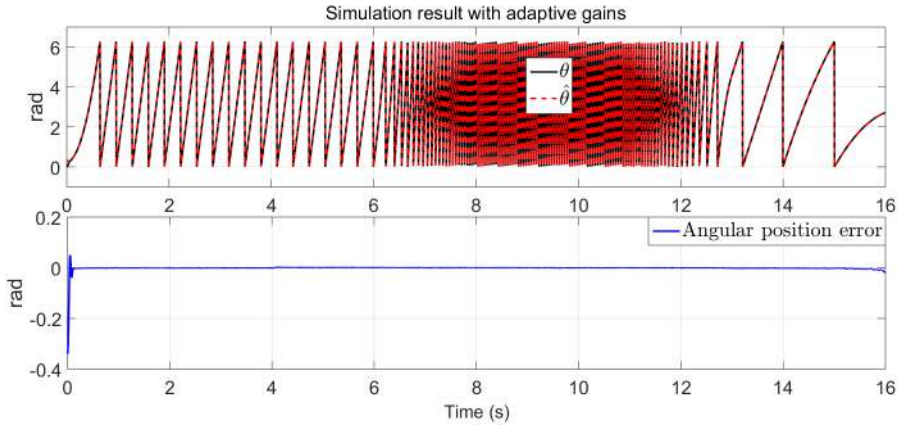

Figure 4.18 – Simulation test: Angular position estimation and angular position error

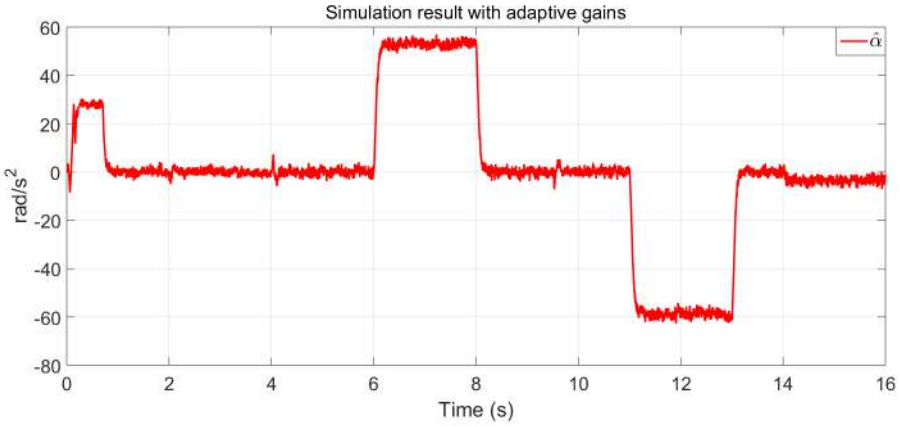

Figure 4.19 – Simulation test: Estimation of acceleration

its tracking error are illustrated with a good performance.

Moreover, the currents$-i_{dq}$ are plotted in Figure 4.21. Therefore, from the illustrations, it is possible to see that the behaviour of the adaptive laws with the system in closed loop (controller+observer) have a good performance. Moreover, the extraction of e_{θ_e} introduced in section 2.1 has been achieved successfully.

4.4.2 Experimental test

One experimental test is addressed to see in real time the performance of the strategy. The proposed strategy is implemented taking into account the profiles defined in Figure 1.7. Moreover, as previously mentioned, a sensor (encoder) has been used to measure the real angular position in the experiments. From this information, a Kalman-filter is applied

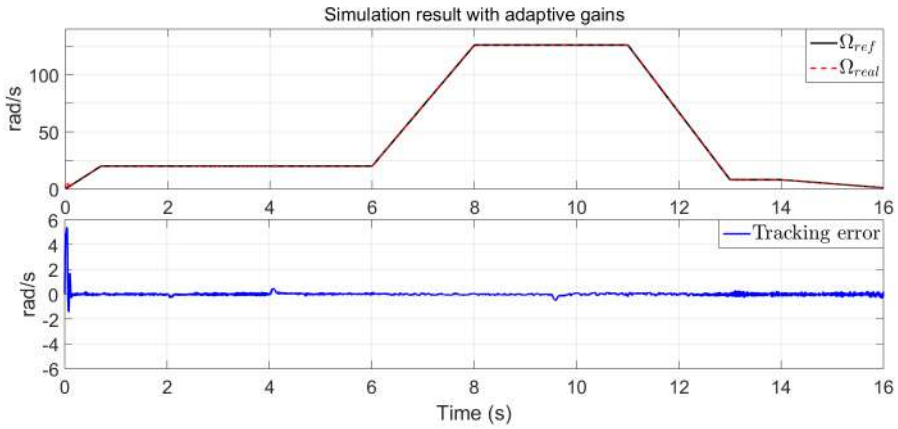

Figure 4.20 – Simulation test: Speed tracking and tracking error

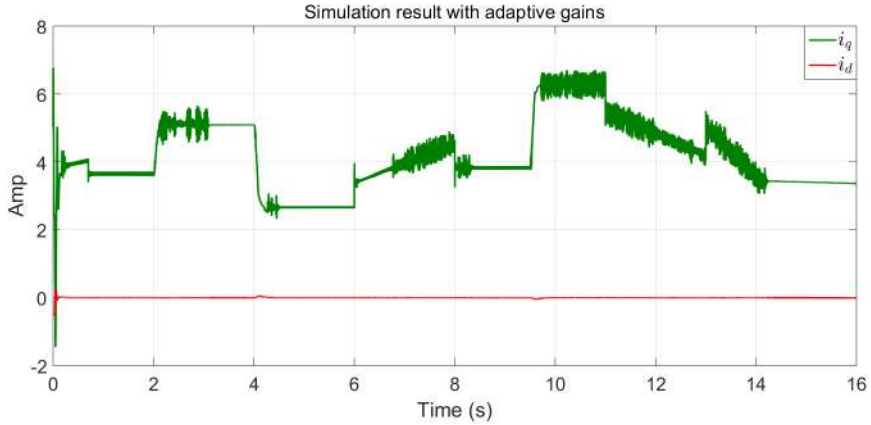

Figure 4.21 – Simulation test: Behaviour of the currents$-i_{dq}$

to calculate the rotor speed. Therefore, it is possible to know if the proposed observer does a correct estimation of the speed and angular position. Similarly, it possible to know if the controller does a correct reference tracking. The adaptive laws have been implemented by considering the parameters given in Table 4.4 and are shown in Figure 4.22.

Table 4.4 – Parameters for the sensorless control-2 in experimental test

AHOSMO-2		ASTWCs-2					
γ_{0_2}	k_{o_2}	ϑ_{22}	$\gamma_{c_{\Omega_2}}$	$k_{c_{\Omega_2}}$	ϑ_{23}	$\gamma_{c_{i_{d_2}}}$	$k_{c_{i_{d_2}}}$
0.001	3	180	0.0001	35	20	0.0005	30

Then, in Figure 4.23, it possible to see the convergence of the estimated speed towards

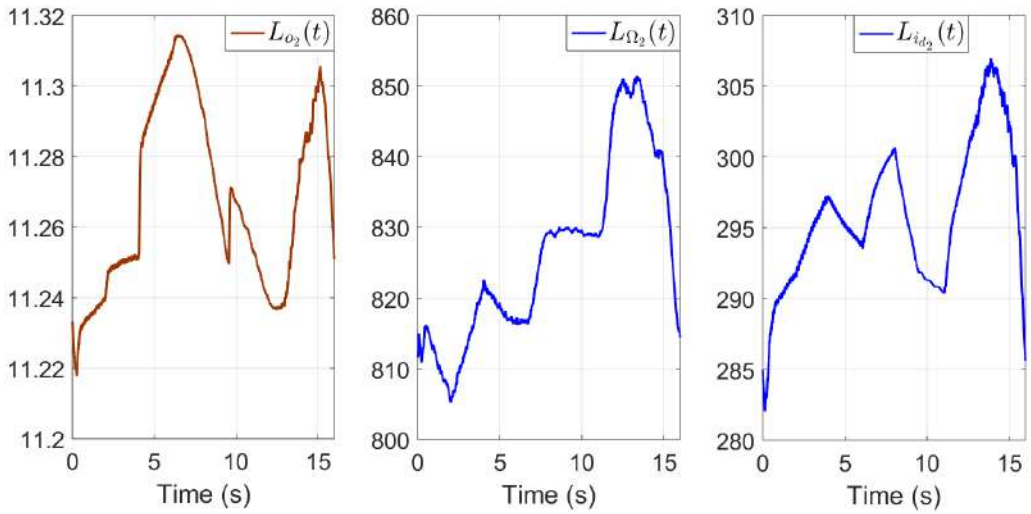

Figure 4.22 – Experimental test: Behaviour of adaptive gains for the observer and controllers

the real speed with good performance. In Figure 4.24, the estimation of the angular

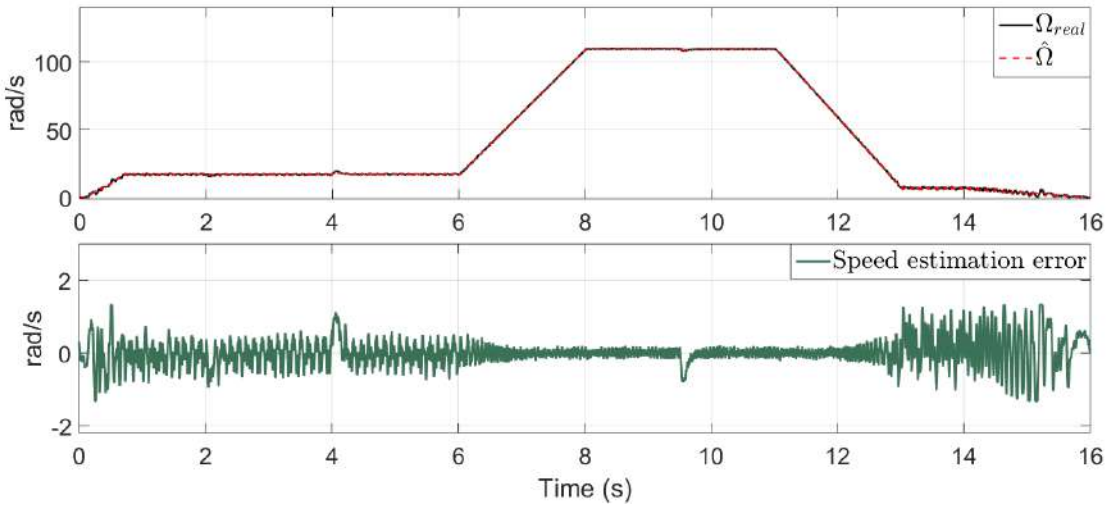

Figure 4.23 – Experimental test: Speed estimation and estimation error

position and its angular error are plotted and a small error is obtained. It is possible to see a good performance over wide speed range, i.e., high, medium and low speed. However, the error increases when the speed is very close to zero. On the other hand, in Figure 4.25, the acceleration has been estimated in order to compensate the estimation error of angular position and speed.

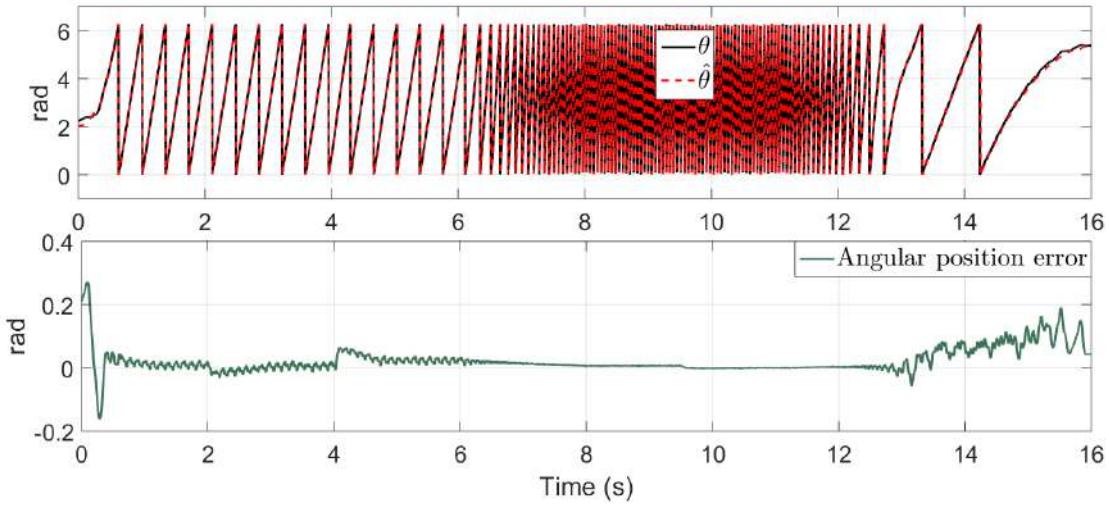

Figure 4.24 – Experimental test: Angular position estimation and angular position estimation error

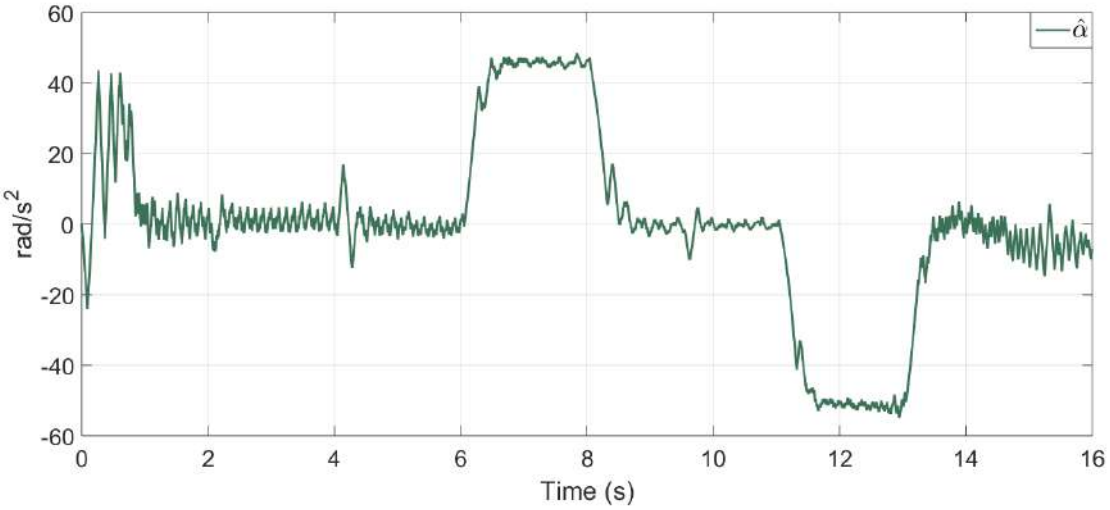

Figure 4.25 – Experimental test: Estimation of acceleration

The estimates of the observer are interconnected in the controllers to control the speed and the current of the IPMSM. In Figure 4.26, the tracking of the speed and the tracking error are showed. The tracking error shows that the performance of the proposed strategy is good and the tracking is ensured with good accuracy even close to zero.

Moreover, the tracking of the current i_d and the behaviour of the current i_q are showed in Figure 4.27. The current i_d tracks a reference equal to 0, and the current i_q has a

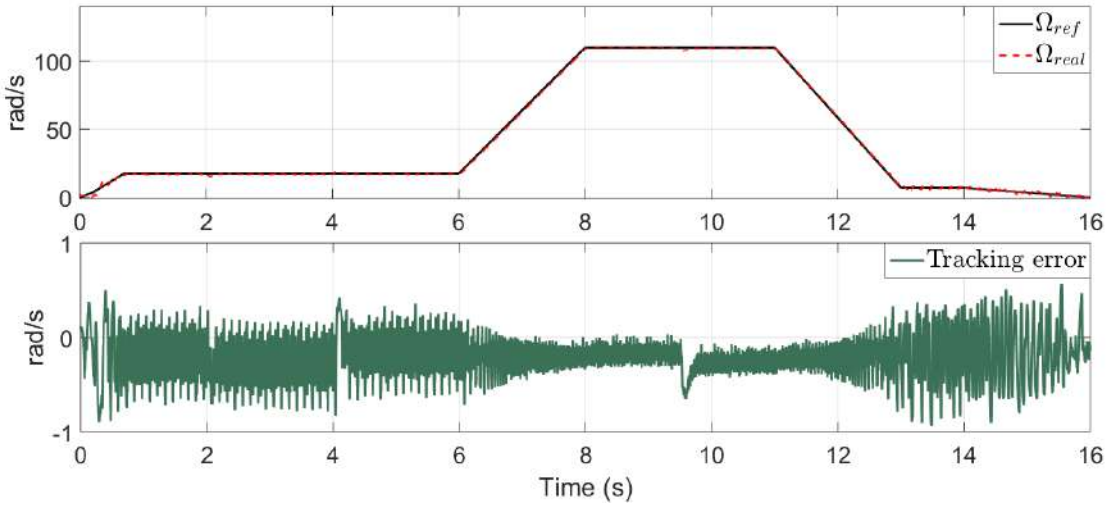

Figure 4.26 – Experimental test: Speed tracking and tracking error

behaviour according to the load torque and the speed.

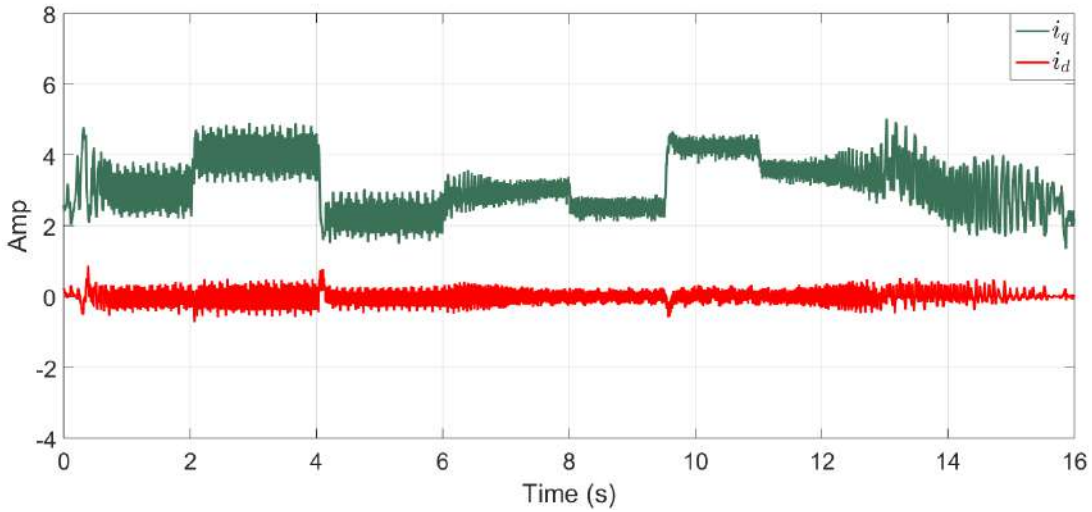

Figure 4.27 – Experimental test: Behaviour of the currents$-i_{dq}$

As can be seen the proposed strategy only requires the angular position estimation error e_{θ_e} to estimate angular position, speed and acceleration using an observer based on a parameter free virtual system. From this information, the sensorless scheme is possible. The proposed strategy has been validated experimentally, with good effectiveness at low, medium and high speed in closed loop.

On the other hand, it is possible to see in simulation that the tracking errors and estimation errors show the effect of adding white noise. It is clear that the chattering has been attenuated. However, the effects of white noise are present in the signals. On the other hand, during the experimental test, these errors are more important compared to those obtained in the simulation. It is well-known that in the experiments the effect caused by external disturbances (inverter effect) and the noise appears in the measured signals. However, the proposed strategy works well and attenuate the effects of chattering, uncertain parameters and unmodeled dynamics.

4.5 Conclusion

In this chapter, experimental and simulation tests were introduced to show the performance of the proposed sensorless control. The experimental tests have been carried out in Laboratoire des Sciences du Numérique de Nantes (LS2N) of the Ecole Centrale De Nantes, France. The extraction of the angular position estimation error has been successfully achieved from the measurable currents $i_{\alpha\beta}$ and the observers have been implemented obtaining good results. Then, angular position, speed and acceleration have been estimated. These estimates have been interconnected with the controller in closed-loop to control the electrical machine. In this way, the sensorless control applied in the experimental setup has shown a good performance under a wide speed range, even very close to zero.

An stability analysis under the action of the observer estimates has been introduced. This analysis is simpler due to that the separation principle holds.

CONCLUSION

In this work a new alternative for sensorless control of the IPMSM was proposed. The main contributions of this work were the following:

— A strategy to extract the angular error e_{θ_e} was proposed, and based on a virtual system without parameters of the IPMSM, two Adaptive High-Order Sliding Mode Observers (AHOSMOs) have been designed to estimate angular position, speed and acceleration over a wide speed range, and overcome the issues caused by parametric uncertainties. The angular position estimation error is independent of all machine parameters and high frequency signal injection characteristics. Therefore, this improved the feasibility of design, which reduces the cost of the implementation.

— Two Adaptive Super-Twisting Controllers (ASTWCs) were designed to track a desired speed reference and a desired d-axis current reference. These controllers were interconnected with the AHOSMOs achieving a sensorless control strategy.

— The gains for both, control and observer, were reparameterized in terms of a single parameter to reduce the tuning time. The main advantage of this strategy is that adaptive laws are easy to implement, which avoids overestimation of gains that increases chattering, reduces time to adjust gains, and reduces damage to the system.

— The closed-loop stability analysis under the action of the observer has been improved because the separation principle holds.

This work has been presented as follows:

In the first place, a state of the art of electrical machines and their main characteristics, as well as their applications, where control is required, was presented. After this, the two main classifications of sensorless control methods were presented, as well as their advantages and disadvantages. Then, the organization of the thesis was addressed. In addition, a list of publications in indexed journals and conferences has been presented.

In chapter one, a summary of the different types of PMSM was presented, as well as

a brief introduction to the IPMSM. Considering that the dynamic model of the IPMSM is necessary for the design of control strategies, the modeling of the IPMSM was carried out. In addition, the problem statement of this work is presented in order to justify why the thesis project is carried out as well as the objectives to follow. On the other hand, in order to test the performance of the different proposals of this thesis, the benchmark used in simulation and experimental tests is provided, as well as the description of the hardware of the experimental setup.

In chapter two, a new method to extract the angular position estimation error e_{θ_e} in PMSM was introduced. The information of e_{θ_e} was extracted by considering the currents $i_{\alpha\beta}$ without machine model information. The extraction of e_{θ_e} has been used to design observers based on a virtual system without machine parameters in order to overcome the issues caused by parametric uncertainties. Then, two adaptive observers have been designed. Both adaptive observers have been proposed with reparameterized gains, i.e., the gains depend on a single parameter. Based on this reparametrization, an adaptive law was designed for each observer. The designed observers have been applied considering the extraction of the angular error to estimate the angular position, speed and acceleration. Simulation results and a comparative study were introduced.

In chapter three, two adaptive controls based on super twisting were proposed. Both adaptive controllers have the reparameterized gains in terms of a single parameter such as the proposed adaptive observers in chapter two. This has allowed designing an adaptive law for each control in order to improve its performance, avoiding large gains and saving tuning time. Simulation results were presented to show the performance of this strategies. Moreover, considering some results of the literature, a comparative study was introduced.

In chapter four, two scheme of sensorless control were introduced. The interconnection among the proposed observers and controllers is carried out to show the performance of the system under the action of observer estimates. Then, two sensorless controllers were applied to the IPMSM. Simulation and experimental results have been illustrated showing a good performance and effectiveness for a wide speed range, showing that the extraction of e_{θ_e} has been made successfully. Therefore, thanks to the virtual system without parameters of the IPMSM, greater precision has been achieved in the estimates. It is worth mentioning that thanks to the robustness of the sliding modes, good results have been obtained in the tracking of references despite uncertainties and disturbance.

In this work, a new alternative to sensorless control has been introduced. Therefore, based on the presented alternative, it is possible to show that to extract the angular error

of the electrical motor, it is not always necessary to use dynamic equations of the motor, allowing to design observers without the use of a dynamic model of the machine.

Some perspectives are given below:

For the design of observers in the sensorless control of electrical motor, it is necessary to know the initial condition of the motor rotor, which is an open problem that requires further study to improve the performance of the proposed schemes. In addition, when the electrical machine is stopped and it is desired to know the angular position for the control application, it is necessary to inject high frequency signals to excite the system, which generates noise in the signals and the need to use filters. For this reason, it is necessary to investigate more about the elimination of filters and high frequency injection to avoid phase shifts in the obtained signal as well as acoustic noise, so that the speed control at zero speed can be less complex.

Appendix A

Reparameterized gains

A.1 Reparameterized gains for the proposed observers

Consider the following algebraic Lyapunov equation in order to compute the observer gains

$$P_o + A_o^T P_o + P_o A_o - C_o^T C_o = 0 \tag{A.1}$$

where P_o is a symmetric positive-definite matrix,

$$A_o = \begin{bmatrix} 0 & 1 & 0 \\ 0 & 0 & 1 \\ 0 & 0 & 0 \end{bmatrix}, \quad C_o = \begin{bmatrix} 1 & 0 & 0 \end{bmatrix}, \tag{A.2}$$

then the solution of P_o for (A.1) is given by

$$P_o = \begin{bmatrix} 1 & -1 & 1 \\ -1 & 2 & -3 \\ 1 & -3 & 6 \end{bmatrix} \tag{A.3}$$

Now, consider the following LTI system

$$\begin{aligned} \dot{\mathbf{x}} &= A_o \mathbf{x} \\ \mathbf{y} &= C_o \mathbf{x} \end{aligned} \tag{A.4}$$

where $\mathbf{x} \in \Re^3$ is a state vector and $\mathbf{y} \in \Re$ the output. Then, an observer for the system (A.4) is given by

$$\begin{aligned} \dot{\hat{\mathbf{x}}} &= A_o \hat{\mathbf{x}} + K_o(\mathbf{y} - \hat{\mathbf{y}}) \\ \hat{\mathbf{y}} &= C_o \hat{\mathbf{x}} \end{aligned} \tag{A.5}$$

where K_o is the gain. Then, the estimation error is given by $e = \mathbf{x} - \hat{\mathbf{x}}$ and its dynamics can be expressed by

$$\dot{e} = (A_o - K_o C_o)e \tag{A.6}$$

Then, the gain K_o has the following values

$$K_o = \begin{bmatrix} K_{o1} \\ K_{o2} \\ K_{o3} \end{bmatrix} = P_o^{-1} C_o^T = \begin{bmatrix} 3 \\ 3 \\ 1 \end{bmatrix} \tag{A.7}$$

A.1.1 Adaptive observer: Proposal 1

In this section, the gains of the proposed observer will be determined and computed in terms of a single parameter.
Consider the following class of nonlinear system given by

$$\begin{aligned} \dot{x}_1 &= x_2 \\ \dot{x}_2 &= x_3 \\ \dot{x}_3 &= \rho(t) \\ y &= x_1 \end{aligned} \tag{A.8}$$

where x_1, x_2 and x_3 are the states, $\rho(t)$ is bounded function whose bound is unknown, and $y \in \Re$ the output of the system.
Now, a sliding mode observers for the system (A.8) is given by

$$\begin{aligned} \dot{\hat{x}}_1 &= \hat{x}_2 + \tilde{K}_{1,1}|e_1|^{\frac{2}{3}} sign(e_1) \\ \dot{\hat{x}}_2 &= \hat{x}_3 + \tilde{K}_{2,1}|e_1|^{\frac{1}{3}} sign(e_1) \\ \dot{\hat{x}}_3 &= \tilde{K}_{3,1} sign(e_1) \\ \hat{y} &= \hat{x}_1 \end{aligned} \tag{A.9}$$

where $\hat{x}_1$, $\hat{x}_2$, and $\hat{x}_3$ are the estimated states, $\hat{y}$ is the estimated output and $\tilde{K}_{1,1}$, $\tilde{K}_{2,1}$ and $\tilde{K}_{3,1}$ are the gains.
Now, an analysis of convergence for the observer will be introduced. Then, defining the following estimation errors $e_i = x_i - \hat{x}_i$, for $i = 1, 2, 3$; the dynamics are given by

$$
\begin{aligned}
\dot{e}_1 &= e_2 - \tilde{K}_{1,1}|e_1|^{\frac{2}{3}} sign(e_1) \\
\dot{e}_2 &= e_3 - \tilde{K}_{2,1}|e_1|^{\frac{1}{3}} sign(e_1) \\
\dot{e}_3 &= \rho(t) - \tilde{K}_{3,1} sign(e_1)
\end{aligned}
\tag{A.10}
$$

and taking into account the dynamics of the estimation errors, the following change of variable is established as follows

$$
\zeta_1 = \frac{e_1}{L_o^2(t)}, \qquad \zeta_2 = \frac{e_2}{L_o^2(t)}, \qquad \zeta_3 = \frac{e_3}{L_o^2(t)} \tag{A.11}
$$

where $L_o(t) > 0$ is the single adaptive parameter. The dynamical system in terms of the new variables is given by

$$
\begin{aligned}
\dot{\zeta}_1 &= -\frac{\tilde{K}_{1,1}}{L_o^{\frac{2}{3}}(t)}|\zeta_1|^{\frac{2}{3}} sign(\zeta_1) + \zeta_2 - 2\zeta_1 \frac{\dot{L}_o(t)}{L_o(t)} \\
\dot{\zeta}_2 &= -\frac{\tilde{K}_{2,1}}{L_o^{\frac{4}{3}}(t)}|\zeta_1|^{\frac{1}{3}} sign(\zeta_1) + \zeta_3 - 2\zeta_2 \frac{\dot{L}_o(t)}{L_o(t)} \\
\dot{\zeta}_3 &= -\frac{\tilde{K}_{3,1}}{L_o^2(t)} sign(\zeta_1) + \frac{\rho(t)}{L_o^2(t)} - 2\zeta_3 \frac{\dot{L}_o(t)}{L_o(t)}
\end{aligned}
\tag{A.12}
$$

Moreover, in order to simplify the state space representation, the following new change of variable is introduced

$$
\xi_1 = |\zeta_1|^{\frac{2}{3}} sign(\zeta_1), \qquad \xi_2 = \frac{\zeta_2}{L_o(t)}, \qquad \xi_3 = \frac{3\zeta_3 |\zeta_1|^{\frac{1}{3}}}{2L_o^2(t)} \tag{A.13}
$$

and the dynamical system can be expressed by using the new variables as follows

$$
\begin{aligned}
\dot{\xi}_1 &= \frac{2L_o(t)}{3|\zeta_1|^{\frac{1}{3}}} \left[-\frac{\tilde{K}_{1,1}}{L_o^{\frac{5}{3}}(t)} \xi_1 + \xi_2 \right] - \frac{4\dot{L}_o(t)}{3L_o(t)} \xi_1 \\
\dot{\xi}_2 &= \frac{2L_o(t)}{3|\zeta_1|^{\frac{1}{3}}} \left[-\frac{3\tilde{K}_{2,1}}{2L_o^{\frac{10}{3}}(t)} \xi_1 + \xi_3 \right] - \frac{3\dot{L}_o(t)}{L_o(t)} \xi_2 \\
\dot{\xi}_3 &= \frac{2L_o(t)}{3|\zeta_1|^{\frac{1}{3}}} \left[-(\frac{3}{2})^2 \frac{\tilde{K}_{3,1}}{L_o^5(t)} \xi_1 + \left(\frac{3}{2}\right)^2 \frac{|\zeta_1|^{\frac{2}{3}} \rho(t)}{L_o^5(t)} + \frac{\xi_3}{2|\zeta_1|^{\frac{2}{3}}} \left(-3\xi_1 + \xi_2\right) \right] - \frac{14\dot{L}_o(t)}{3L_o(t)} \xi_3
\end{aligned}
\tag{A.14}
$$

The resulting system (A.14) can be expressed in the following compact form

$$\dot{\xi} = \alpha_o \left[\left(A_o - \tilde{G}_o C_o \right) \xi + \Phi_o \right] - N_o \xi \frac{\dot{L}_o(t)}{L_o(t)} \tag{A.15}$$

where $\alpha_o = \dfrac{2L_o(t)}{3|\zeta_1|^{\frac{1}{3}}}$, $\xi = \begin{bmatrix} \xi_1 & \xi_2 & \xi_3 \end{bmatrix}^T$ and

$$\tilde{G}_o = \begin{bmatrix} \dfrac{\tilde{K}_{1,1}}{L_o^{\frac{5}{3}}(t)} \\ \dfrac{3\tilde{K}_{2,1}}{2L_o^{\frac{10}{3}}(t)} \\ (\dfrac{3}{2})^2 \dfrac{\tilde{K}_{3,1}}{L_o^5(t)} \end{bmatrix}, N_o = \begin{bmatrix} \frac{4}{3} & 0 & 0 \\ 0 & 3 & 0 \\ 0 & 0 & \frac{14}{3} \end{bmatrix}, \Phi_o = \begin{bmatrix} 0 \\ 0 \\ \left(\frac{3}{2}\right)^2 \frac{|\zeta_1|^{\frac{2}{3}} \rho(t)}{L_o^5(t)} + \frac{\xi_3}{2|\zeta_1|^{\frac{2}{3}}} \left(-\frac{\tilde{K}_{1,1}}{L_o^{\frac{5}{3}}(t)} \xi_1 + \xi_2 \right) \end{bmatrix}. \tag{A.16}$$

Then, from (A.6), it is obtained that $\tilde{G}_o = P_o^{-1} C_o^T$. Then, setting $\tilde{G}_o$ equal to (A.7), it follows that

$$\begin{bmatrix} \dfrac{\tilde{K}_{1,1}}{L_o^{\frac{5}{3}}(t)} \\ \dfrac{3\tilde{K}_{2,1}}{2L_o^{\frac{10}{3}}(t)} \\ (\dfrac{3}{2})^2 \dfrac{\tilde{K}_{3,1}}{L_o^5(t)} \end{bmatrix} = \begin{bmatrix} 3 \\ 3 \\ 1 \end{bmatrix} \tag{A.17}$$

Therefore, the gains for the observer are computed and reparameterized in terms of $L_o(t)$ as follows

$$\tilde{K}_{1,1} = 3L_o^{\frac{5}{3}}(t) \qquad \tilde{K}_{2,1} = 2L_o^{\frac{10}{3}}(t) \qquad \tilde{K}_{3,1} = \left(\frac{4}{9}\right) L_o^5(t) \tag{A.18}$$

such that, the compact system (A.15) can be rewritten as

$$\dot{\xi} = \alpha_o \left[\left(A_o - P_o^{-1} C_o^T C_o \right) \xi + \Phi_o \right] - N_o \xi \frac{\dot{L}_o(t)}{L_o(t)} \tag{A.19}$$

A.1.2 Adaptive observer: Proposal 2

In this section, a second observer is designed for a class of nonlinear system given by (A.8). The gains of the proposed observer will be determined and computed in terms of a single parameter.

Consider the following sliding mode observer for the system (A.8),

$$\begin{aligned}\dot{\hat{x}}_{1_2} &= \hat{x}_2 + \tilde{K}_{1,2}|e_{1_2}|^{\frac{2}{3}} sign(e_{1_2}) \\ \dot{\hat{x}}_{2_2} &= \hat{x}_3 + \tilde{K}_{2,2}|e_{1_2}|^{\frac{1}{3}} sign(e_{1_2}) \\ \dot{\hat{x}}_{3_2} &= \tilde{K}_{3,2} sign(e_{1_2}) \\ \hat{y} &= \hat{x}_{1_2}\end{aligned} \tag{A.20}$$

where $\hat{x}_{1_2}$, $\hat{x}_{2_2}$ and $\hat{x}_{3_2}$ are the estimated states, $\hat{y}$ is the output of the system and $\tilde{K}_{1,2}$, $\tilde{K}_{2,2}$ and $\tilde{K}_{3,2}$ are the gains of the observer. Now, an analysis of convergence for the observer will be introduced. Then, defining the following estimation errors.
Consider the following estimation errors $e_{i_2} = x_1 - \hat{x}_{i_2}$, for $i = 1, 2, 3$; and their dynamics as follows

$$\begin{aligned}\dot{e}_{1_2} &= e_{2_2} - \tilde{K}_{1,2}|e_{1_2}|^{\frac{2}{3}} sign(e_{1_2}) \\ \dot{e}_{2_2} &= e_{3_2} - \tilde{K}_{2,2}|e_{1_2}|^{\frac{1}{3}} sign(e_{1_2}) \\ \dot{e}_{3_2} &= \rho(t) - \tilde{K}_{3,2} sign(e_{1_2})\end{aligned} \tag{A.21}$$

Taking into account the dynamics of the estimation errors, the following change of variable is established as follows

$$\xi_{1_2} = \frac{|e_{1_2}|^{\frac{2}{3}} sign(e_{1_2})}{L_{o_2}(t)} \qquad \xi_{2_2} = \frac{e_{2_2}}{L_{o_2}^2(t)} \qquad \xi_{3_2} = \frac{3e_{3_2}|e_{1_2}|^{\frac{1}{3}}}{2L_{o_2}^3(t)} \tag{A.22}$$

where $L_{o_2}(t)$ is the single adaptive parameter. The dynamical system in terms of the new variables is given by

$$\begin{aligned}\dot{\xi}_{1_2} &= \frac{2L_{o_2}(t)}{3|e_{1_2}|^{\frac{1}{3}}}\left[-\frac{\tilde{K}_{1,2}}{L_{o_2}(t)}\xi_{1_2} + \xi_{2_2}\right] - \frac{\dot{L}_{o_2}(t)}{L_{o_2}(t)}\xi_{1_2} \\ \dot{\xi}_{2_2} &= \frac{2L_{o_2}(t)}{3|e_{1_2}|^{\frac{1}{3}}}\left[-\frac{3\tilde{K}_{2,2}}{2L_{o_2}^2(t)}\xi_{1_2} + \xi_{3_2}\right] - \frac{2\dot{L}_{o_2}(t)}{L_{o_2}(t)}\xi_{2_2} \\ \dot{\xi}_{3_2} &= \frac{2L_{o_2}(t)}{3|e_{1_2}|^{\frac{1}{3}}}\left[-\left(\frac{3}{2}\right)^2\frac{\tilde{K}_{3,2}}{L_{o_2}^3(t)}\xi_{1_2} + \left(\frac{3}{2}\right)^2\frac{|e_{1_2}|^{\frac{2}{3}}\rho(t)}{L_{o_2}^4(t)} + \frac{\xi_{3_2}}{2|e_{1_2}|^{\frac{2}{3}}}\left[-\tilde{K}_{1,2}\xi_{1_2} + L_{o_2}(t)\xi_{2_2}\right]\right] \\ &\quad - \frac{3\dot{L}_{o_2}(t)}{L_{o_2}(t)}\xi_{3_2}\end{aligned} \tag{A.23}$$

and can be written in a compact form as follows

$$\dot{\xi}_{o_2} = \alpha_{o_2}\left[\left(A_o - \tilde{G}_{o_2}C_o\right)\xi_{o_2} + \Phi_{o_2}\right] - D_{o_2}\xi_{o_2}\frac{\dot{L}_{o_2}(t)}{L_{o_2}(t)} \tag{A.24}$$

where $\alpha_{o_2} = \dfrac{2L_{o_2}(t)}{3|e_{1_2}|^{\frac{1}{3}}}$, $\xi_{o_2} = \begin{bmatrix}\xi_{1_2} & \xi_{2_2} & \xi_{3_2}\end{bmatrix}^T$ and

$$\tilde{G}_{o_2} = \begin{bmatrix} \dfrac{\tilde{K}_{1,2}}{L_{o_2}(t)} \\ \dfrac{3\tilde{K}_{2,2}}{2L_{o_2}^2(t)} \\ \left(\dfrac{3}{2}\right)^2 \dfrac{\tilde{K}_{3,2}}{L_{o_2}^3(t)} \end{bmatrix}, D_{o_2} = \begin{bmatrix}1 & 0 & 0\\ 0 & 2 & 0\\ 0 & 0 & 3\end{bmatrix}, \Phi_{o_2} = \begin{bmatrix} 0 \\ 0 \\ \left(\dfrac{3}{2}\right)^2 \dfrac{|e_{1_2}|^{\frac{2}{3}}\rho(t)}{L_{o_2}^4(t)} + \dfrac{\xi_{3_2}}{2|e_{1_2}|^{\frac{2}{3}}}\left[-\tilde{K}_{1,2}\xi_{1_2} + L_{o_2}(t)\xi_{2_2}\right] \end{bmatrix}. \tag{A.25}$$

Then, from (A.6), it is obtained that $\tilde{G}_{o_2} = P_o^{-1}C_o^T$. Then, setting $\tilde{G}_{o_2}$ equal to (A.7), it follows that

$$\begin{bmatrix} \dfrac{\tilde{K}_{1,2}}{L_{o_2}(t)} \\ \dfrac{3\tilde{K}_{2,2}}{2L_{o_2}^2(t)} \\ (\dfrac{3}{2})^2 \dfrac{\tilde{K}_{3,2}}{L_{o_2}^3(t)} \end{bmatrix} = \begin{bmatrix}3\\3\\1\end{bmatrix} \tag{A.26}$$

Therefore, the gains for the observer (A.20) are computed and reparameterized in terms of $L_{o_2}(t)$ as follows

$$\tilde{K}_{1,2} = 3L_{o_2}(t) \qquad \tilde{K}_{2,2} = 2L_{o_2}^2(t) \qquad \tilde{K}_{3,2} = \left(\frac{2}{3}\right)^2 L_{o_2}^3(t) \tag{A.27}$$

such that, the compact system (A.24) can be rewritten as

$$\dot{\xi}_{o_2} = \alpha_{o_2}\left[\left(A_o - P_o^{-1}C_o^TC_o\right)\xi_{o_2} + \Phi_{o_2}\right] - D_{o_2}\xi_{o_2}\frac{\dot{L}_{o_2}(t)}{L_{o_2}(t)} \tag{A.28}$$

A.2 Reparameterized gains for the proposed controllers

Consider the following algebraic Lyapunov equation in order to compute the control gains

$$P_c + A_c^TP_c + P_cA_c - C_c^TC_c = 0 \tag{A.29}$$

where P_c is a symmetric positive-definite matrix,

$$A_c = \begin{bmatrix} 0 & 1 \\ 0 & 0 \end{bmatrix}, \quad C_c = \begin{bmatrix} 1 & 0 \end{bmatrix}. \tag{A.30}$$

Then the solution of P_c for A.29 is given by

$$P_c = \begin{bmatrix} 1 & -1 \\ -1 & 2 \end{bmatrix}. \tag{A.31}$$

Similarly, as the previous section A.1, consider the following LTI system

$$\begin{aligned} \dot{\mathbf{x}}_c &= A_c \mathbf{x}_c \\ \mathbf{y}_c &= C_c \mathbf{x}_c \end{aligned} \tag{A.32}$$

where $\mathbf{x}_c \in \Re^2$ is a state vector and $\mathbf{y}_c \in \Re$ the output. Then, an observer for the system (A.32) is given by

$$\begin{aligned} \dot{\hat{\mathbf{x}}}_c &= A_c \hat{\mathbf{x}}_c + K_c(\mathbf{y}_c - \hat{\mathbf{y}}_c) \\ \hat{\mathbf{y}}_c &= C_c \hat{\mathbf{x}}_c \end{aligned} \tag{A.33}$$

where K_c are the gains. Then, the estimation error is given by $e_c = \mathbf{x}_c - \hat{\mathbf{x}}_c$ and its dynamics can be expressed by

$$\dot{e}_c = (A_c - K_c C_c) e_c = (A_c - P_c^{-1} C_c^T C_c) e_c \tag{A.34}$$

Then, the gain K_c has the following values

$$K_c = \begin{bmatrix} K_{c1} \\ K_{c2} \end{bmatrix} = P_c^{-1} C_c^T = \begin{bmatrix} 2 \\ 1 \end{bmatrix} \tag{A.35}$$

A.2.1 Adaptive control: Proposal 1

In this section, the gains of the proposed controller (3.6) will be determined and computed in terms of a single parameter.

Consider the following system

$$\Sigma_{STW} : \begin{cases} \dot{\Upsilon}_1 = -\tilde{K}_{c1} |\Upsilon_1|^{1/2} sign(\Upsilon_1) + \Upsilon_2, \\ \dot{\Upsilon}_2 = -\tilde{K}_{c2} sign(\Upsilon_1) + d(t) \end{cases} \tag{A.36}$$

with $d(t) = \dot{\delta}(t)$. Now, consider the following change of coordinates

$$z_1 = \frac{\Upsilon_1}{L_c^2(t)} \qquad z_2 = \frac{\Upsilon_2}{L_c^2(t)} \tag{A.37}$$

where $L_c(t)$ is the single adaptive parameter. The dynamical system in terms of the new variables is given by

$$\begin{aligned} \dot{z}_1 &= -\frac{\tilde{K}_{c1}}{L_c(t)}|z_1|^{\frac{1}{2}} sign(z_1) + z_2 - \frac{2z_1\dot{L}_c(t)}{L_c(t)} \\ \dot{z}_2 &= -\frac{\tilde{K}_{c2}}{L_c^2(t)} sign(z_1) + \frac{d(t)}{L_c^2(t)} - \frac{2z_2\dot{L}_c(t)}{L_c(t)} \end{aligned} \tag{A.38}$$

Moreover, in order to simplify the state space representation, the following new change of variable is introduced

$$\pounds_1 = |z_1|^{\frac{1}{2}} sign(z_1) \qquad \pounds_2 = \frac{z_2}{L_c(t)} \tag{A.39}$$

and the dynamical system can be expressed by using the new variables as follows

$$\begin{aligned} \dot{\pounds}_1 &= \frac{L_c(t)}{2|z_1|^{\frac{1}{2}}}\left[-\frac{\tilde{K}_{c1}}{L_c^2(t)}\pounds_1 + \pounds_2\right] - \pounds_1\frac{\dot{L}_c(t)}{L_c(t)} \\ \dot{\pounds}_2 &= \frac{L_c(t)}{2|z_1|^{\frac{1}{2}}}\left[-\frac{2\tilde{K}_{c2}}{L_c^4(t)}\pounds_1 + \frac{2|z_1|^{\frac{1}{2}}d(t)}{L_c^4(t)}\right] - 3\pounds_2\frac{\dot{L}_c(t)}{L_c(t)} \end{aligned} \tag{A.40}$$

System (A.40) can be expressed in compact form as follows

$$\dot{\pounds} = \alpha_c\left[\left(A_c - \tilde{G}_c C_c\right)\pounds + \Phi_c\right] - N_c\pounds\frac{\dot{L}_c(t)}{L_c(t)} \tag{A.41}$$

with $\alpha_c = \dfrac{L_c(t)}{2|z_1|^{\frac{1}{2}}}$, $\pounds = \begin{bmatrix}\pounds_1 & \pounds_2\end{bmatrix}^T$ and

$$\tilde{G}_c = \begin{bmatrix}\dfrac{\tilde{K}_{c1}}{L_c^2(t)} \\ \dfrac{2\tilde{K}_{c2}}{L_c^4(t)}\end{bmatrix}, \quad N_c = \begin{bmatrix}1 & 0 \\ 0 & 3\end{bmatrix}, \quad \Phi_c = \begin{bmatrix}0 \\ \dfrac{2|z_1|^{\frac{1}{2}}}{L_c^4(t)}\left(d(t)\right)\end{bmatrix}. \tag{A.42}$$

Then, from (A.34), it is obtained that $\tilde{G}_c = P_c^{-1}C_c^T$. Then, setting $\tilde{G}_c$ equal to (A.35), it

follows that

$$\begin{bmatrix} \dfrac{\tilde{K}_{c1}}{L_c^2(t)} \\ \dfrac{2\tilde{K}_{c2}}{L_c^4(t)} \end{bmatrix} = \begin{bmatrix} 2 \\ 1 \end{bmatrix} \tag{A.43}$$

Therefore, the gains for the controller (3.6) are computed and reparameterized in terms of $L_c(t)$ as follows

$$\tilde{K}_{c1} = 2L_c^2(t) \qquad \tilde{K}_{c2} = \frac{L_c^4(t)}{2} \tag{A.44}$$

Finally, the compact system (A.41) can be expressed as follows

$$\dot{\pounds} = \alpha_c \left[\left(A_c - P_c^{-1} C_c^T C_c \right) \pounds + \Phi_c \right] - N_c \pounds \frac{\dot{L}_c(t)}{L_c(t)} \tag{A.45}$$

A.2.2 Adaptive control: Proposal 2

In this section, the gains of the proposed controller (3.54) will be determined and computed in terms of a single parameter.

Consider the following system as follows

$$\Sigma_{STW_2} : \begin{cases} \dot{z}_{1_2} = -\tilde{K}_{c3} |z_{1_2}|^{\frac{1}{2}} sign(z_{1_2}) + z_{2_2} \\ \dot{z}_{2_2} = -\tilde{K}_{c4} sign(z_{1_2}) + d(t) \end{cases} \tag{A.46}$$

with $d(t) = \dot{\delta}(t)$. Now, introducing the following change of variable

$$\pounds_{1_2} = \frac{|z_{1_2}|^{\frac{1}{2}} sign(z_{1_2})}{L_{c_2}(t)} \qquad \pounds_{2_2} = \frac{z_{2_2}}{L_{c_2}^2(t)} \tag{A.47}$$

where $L_{c_2}(t)$ is the single adaptive parameter. Then the dynamics of the system, in terms of these new variables, are given by

$$\begin{aligned} \dot{\pounds}_{1_2} &= \frac{L_{c_2}(t)}{2|z_{1_2}|^{\frac{1}{2}}} \left[-\frac{\tilde{K}_{c3}}{L_{c_2}(t)} \pounds_{1_2} + \pounds_{2_2} \right] - \pounds_{1_2} \frac{\dot{L}_{c_2}(t)}{L_{c_2}(t)} \\ \dot{\pounds}_{2_2} &= \frac{L_{c_2}(t)}{2|z_{1_2}|^{\frac{1}{2}}} \left[-\frac{2\tilde{K}_{c4}}{L_{c_2}^2(t)} \pounds_{1_2} + \frac{2|z_{1_2}|^{\frac{1}{2}} d(t)}{L_{c_2}^3(t)} \right] - 2\pounds_{2_2} \frac{\dot{L}_{c_2}(t)}{L_{c_2}(t)} \end{aligned} \tag{A.48}$$

System (A.48) can be expressed in compact form as follows

$$\dot{\pounds}_{c_2} = \alpha_{c_2}\left[\left(A_c - \tilde{G}_{c2}C_c\right)\pounds_{c_2} + \Phi_{c_2}\right] - D_{c_2}\pounds_{c_2}\frac{\dot{L}_{c_2}(t)}{L_{c_2}(t)} \tag{A.49}$$

with $\alpha_{c_2} = \dfrac{L_{c_2}(t)}{2|z_{1_2}|^{\frac{1}{2}}}$, $\pounds_{c_2} = \begin{bmatrix}\pounds_{1_2} & \pounds_{2_2}\end{bmatrix}^T$

$$\tilde{G}_{c2} = \begin{bmatrix}\dfrac{\tilde{K}_{c3}}{L_{c_2}(t)} \\ \dfrac{2\tilde{K}_{c4}}{L_{c_2}^2(t)}\end{bmatrix} \qquad D_{c_2} = \begin{bmatrix}1 & 0 \\ 0 & 2\end{bmatrix} \qquad \Phi_{c_2} = \begin{bmatrix}0 \\ \dfrac{2|z_{1_2}|^{\frac{1}{2}}}{L_{c_2}^3(t)}\left[d(t)\right]\end{bmatrix} \tag{A.50}$$

Then, from (A.34), it is obtained that $\tilde{G}_{c2} = P_c^{-1}C_c^T$. Then, setting $\tilde{G}_{c2}$ equal to (A.35), it follows that

$$\begin{bmatrix}\dfrac{\tilde{K}_{c3}}{L_{c_2}(t)} \\ \dfrac{2\tilde{K}_{c4}}{L_{c_2}^2(t)}\end{bmatrix} = \begin{bmatrix}2 \\ 1\end{bmatrix} \tag{A.51}$$

Therefore, the gains for the controller (3.54) are computed and reparameterized in terms of $L_{c_2}(t)$ as follows

$$\tilde{K}_{c3} = 2L_{c_2}(t) \qquad \tilde{K}_{c4} = \frac{L_{c_2}^2(t)}{2} \tag{A.52}$$

Finally, the system (A.49) can be expressed as follows

$$\dot{\pounds}_{c_2} = \alpha_{c_2}\left[\left(A_c - P_c^{-1}C_c^TC_c\right)\pounds_{c_2} + \Phi_{c_2}\right] - D_{c_2}\pounds_{c_2}\frac{\dot{L}_{c_2}(t)}{L_{c_2}(t)} \tag{A.53}$$

BIBLIOGRAPHY

[1] M. J. Melfi, S. Evon, and R. McElveen, « Induction versus permanent magnet motors », *IEEE Industry Applications Magazine*, vol. 15, no. 6, pp. 28–35, 2009.

[2] R. Menon, A. H. Kadam, N. A. Azeez, and S. S. Williamson, « A comprehensive survey on permanent magnet synchronous motor drive systems for electric transportation applications », in *IECON 2016-42nd Annual Conference of the IEEE Industrial Electronics Society*, IEEE, 2016, pp. 6627–6632.

[3] P. Kakosimos, E. Tsampouris, A. Kladas, and C. Gerada, « Aerospace actuator design: a comparative analysis of permanent magnet and induction motor configurations », in *2012 XXth International Conference on Electrical Machines*, IEEE, 2012, pp. 2538–2544.

[4] J. Puranen *et al.*, « Induction motor versus permanent magnet synchronous motor in motion control applications: a comparative study », 2006.

[5] T. Noguchi, « Trends of permanent-magnet synchronous machine drives », *IEEJ Transactions on Electrical and Electronic Engineering*, vol. 2, no. 2, pp. 125–142, 2007.

[6] T. Kabashima, Y. Arinaga, K. Uemura, I. Murokita, and M. Ohto, « A novel magnetic rotary encoder for servo motors », *IEEJ Transactions on Industry Applications*, vol. 126, no. 9, pp. 1202–1207, 2006.

[7] M. M. I. Chy and M. N. Uddin, « Development and implementation of a new adaptive intelligent speed controller for ipmsm drive », *IEEE Transactions on Industry Applications*, vol. 45, no. 3, pp. 1106–1115, 2009.

[8] M. N. Uddin and M. A. Rahman, « High-speed control of ipmsm drives using improved fuzzy logic algorithms », *IEEE transactions on industrial electronics*, vol. 54, no. 1, pp. 190–199, 2007.

[9] L. Sheng, G. Xiaojie, and Z. Lanyong, « Robust adaptive backstepping sliding mode control for six-phase permanent magnet synchronous motor using recurrent wavelet fuzzy neural network », *IEEE Access*, vol. 5, pp. 14 502–14 515, 2017.

[10] A. Ghafarri-Kashani, M. Yazdanpanah, and J. Faiz, « Robust speed control of pmsm using mixed nonlinear h∞/smc techniques », *IFAC Proceedings Volumes*, vol. 41, no. 2, pp. 8413–8418, 2008.

[11] G. Wang, M. Valla, and J. Solsona, « Position sensorless permanent magnet synchronous machine drives—a review », *IEEE Transactions on Industrial Electronics*, vol. 67, no. 7, pp. 5830–5842, 2019.

[12] S.-K. Sul and S. Kim, « Sensorless control of ipmsm: past, present, and future », *IEEJ Journal of Industry Applications*, vol. 1, no. 1, pp. 15–23, 2012.

[13] S.-K. Sul, Y.-C. Kwon, and Y. Lee, « Sensorless control of ipmsm for last 10 years and next 5 years », *CES Transactions on Electrical Machines and Systems*, vol. 1, no. 2, pp. 91–99, 2017.

[14] D. Liang, J. Li, and R. Qu, « Sensorless control of permanent magnet synchronous machine based on second-order sliding-mode observer with online resistance estimation », *IEEE Transactions on Industry Applications*, vol. 53, no. 4, pp. 3672–3682, 2017.

[15] K.-W. Lee and J.-I. Ha, « Evaluation of back-emf estimators for sensorless control of permanent magnet synchronous motors », *Journal of Power Electronics*, vol. 12, no. 4, pp. 604–614, 2012.

[16] F. Genduso, R. Miceli, C. Rando, and G. R. Galluzzo, « Back emf sensorless-control algorithm for high-dynamic performance pmsm », *IEEE Transactions on Industrial Electronics*, vol. 57, no. 6, pp. 2092–2100, 2009.

[17] J. Liu and Z. Zhu, « Improved sensorless control of permanent-magnet synchronous machine based on third-harmonic back emf », *IEEE Transactions on Industry Applications*, vol. 50, no. 3, pp. 1861–1870, 2013.

[18] M. Naidu and B. K. Bose, « Rotor position estimation scheme of a permanent magnet synchronous machine for high performance variable speed drive », in *Conference Record of the 1992 IEEE Industry Applications Society Annual Meeting*, IEEE, 1992, pp. 48–53.

[19] C. Lascu and G.-D. Andreescu, « Pll position and speed observer with integrated current observer for sensorless pmsm drives », *IEEE Transactions on Industrial Electronics*, vol. 67, no. 7, pp. 5990–5999, 2020.

[20] P. Bernard and L. Praly, « Estimation of position and resistance of a sensorless pmsm: a nonlinear luenberger approach for a nonobservable system », *IEEE Transactions on Automatic Control*, vol. 66, no. 2, pp. 481–496, 2020.

[21] P. Niedermayr, L. Alberti, S. Bolognani, and R. Abl, « Implementation and experimental validation of ultra-high speed pmsm sensor-less control by means of extended kalman filter », *IEEE Journal of Emerging and Selected Topics in Power Electronics*, 2020.

[22] H. Al-Ghossini, F. Locment, M. Sechilariu, L. Gagneur, and C. Forgez, « Adaptive-tuning of extended kalman filter used for small scale wind generator control », *Renewable Energy*, vol. 85, pp. 1237–1245, 2016.

[23] A. Bist and S. V. Jadhav, « Sensorless control based on sliding mode observer for pmsm drive », in *2020 IEEE PEDES*, IEEE, 2020, pp. 1–6.

[24] K. V. Tejan, R. M. Pindoriya, and B. S. Rajpurohit, « Rotor position sensorless technique using high-speed sliding mode observer for pmsm drive », in *Conf. Rec. Ind. Appl. Soc. IEEE-IAS Annu. Meet.*, IEEE, 2021, pp. 1–8.

[25] F. Sellschopp and M. Arjona, « Dc decay test for estimating d-axis synchronous machine parameters: a two-transfer-function approach », *IEE Proceedings-Electric Power Applications*, vol. 153, no. 1, pp. 123–128, 2006.

[26] P. Turner, A. Reece, and D. Macdonald, « The dc decay test for determining synchronous machine parameters: measurement and simulation », *IEEE Transactions on Energy Conversion*, vol. 4, no. 4, pp. 616–623, 1989.

[27] Y. Gao, R. Qu, and Y. Liu, « An improved ac standstill method for inductance measurement of interior permanent magnet synchronous motors », in *2013 International Conference on Electrical Machines and Systems (ICEMS)*, IEEE, 2013, pp. 927–931.

[28] T. Sun, S.-O. Kwon, J.-J. Lee, and J.-P. Hong, « An improved ac standstill method for testing inductances of interior pm synchronous motor considering cross-magnetizing effect », in *2009 IEEE Energy Conversion Congress and Exposition*, IEEE, 2009, pp. 2415–2422.

[29] S. J. Underwood and I. Husain, « Online parameter estimation and adaptive control of permanent-magnet synchronous machines », *IEEE Transactions on Industrial Electronics*, vol. 57, no. 7, pp. 2435–2443, 2009.

[30] Y. Shi, K. Sun, L. Huang, and Y. Li, « Online identification of permanent magnet flux based on extended kalman filter for ipmsm drive with position sensorless control », *IEEE Transactions on Industrial Electronics*, vol. 59, no. 11, pp. 4169–4178, 2011.

[31] M. A. Hamida, J. De Leon, A. Glumineau, and R. Boisliveau, « An adaptive interconnected observer for sensorless control of pm synchronous motors with online parameter identification », *IEEE Transactions on Industrial Electronics*, vol. 60, no. 2, pp. 739–748, 2012.

[32] C. Wu, Y. Zhao, and M. Sun, « Enhancing low-speed sensorless control of pmsm using phase voltage measurements and online multiple parameter identification », *IEEE Transactions on Power Electronics*, vol. 35, no. 10, pp. 10 700–10 710, 2020.

[33] M. S. Rafaq, F. Mwasilu, J. Kim, H. H. Choi, and J.-W. Jung, « Online parameter identification for model-based sensorless control of interior permanent magnet synchronous machine », *IEEE Transactions on Power Electronics*, vol. 32, no. 6, pp. 4631–4643, 2016.

[34] V. Utkin, « Variable structure systems with sliding modes », *IEEE Transactions on Automatic control*, vol. 22, no. 2, pp. 212–222, 1977.

[35] S. K. Spurgeon, « Sliding mode observers: a survey », *International Journal of Systems Science*, vol. 39, no. 8, pp. 751–764, 2008.

[36] Y.-S. Jung and M.-G. Kim, « Sliding mode observer for sensorless control of ipmsm drives », *Journal of Power Electronics*, vol. 9, no. 1, pp. 117–123, 2009.

[37] O. Saadaoui, A. Khlaief, M. Abassi, A. Chaari, and M. Boussak, « A sliding-mode observer for high-performance sensorless control of pmsm with initial rotor position detection », *International Journal of Control*, vol. 90, no. 2, pp. 377–392, 2017.

[38] N. Ren, L. Fan, and Z. Zhang, « Sensorless pmsm control with sliding mode observer based on sigmoid function », *J. Electr. Eng. Technol.*, vol. 16, no. 2, pp. 933–939, 2021.

[39] A. Levant, « Sliding order and sliding accuracy in sliding mode control », *International journal of control*, vol. 58, no. 6, pp. 1247–1263, 1993.

[40] A. Ferreira de Loza, L. Fridman, L. Aguilar, and R. Iriarte, « High-order sliding-mode observer–based input-output linearization », *Int. J. Robust Nonlinear Control*, vol. 29, no. 10, pp. 3183–3199, 2019.

[41] B. Wang, Y. Shao, Y. Yu, Q. Dong, Z. Yun, and D. Xu, « High-order terminal sliding-mode observer for chattering suppression and finite-time convergence in sensorless spmsm drives », *IEEE Trans. Power Electron.*, vol. 36, no. 10, pp. 11 910–11 920, 2021.

[42] T. Zhang, Z. Xu, J. Li, H. Zhang, and C. Gerada, « A third-order super-twisting extended state observer for dynamic performance enhancement of sensorless ipmsm drives », *IEEE Transactions on Industrial Electronics*, vol. 67, no. 7, pp. 5948–5958, 2019.

[43] D. Liang, J. Li, R. Qu, and W. Kong, « Adaptive second-order sliding-mode observer for pmsm sensorless control considering vsi nonlinearity », *IEEE Transactions on Power Electronics*, vol. 33, no. 10, pp. 8994–9004, 2017.

[44] C. L. Baratieri and H. Pinheiro, « New variable gain super-twisting sliding mode observer for sensorless vector control of nonsinusoidal back-emf pmsm », *Control Engineering Practice*, vol. 52, pp. 59–69, 2016.

[45] S. Wu, J. Zhang, and B. Chai, « Adaptive super-twisting sliding mode observer based robust backstepping sensorless speed control for ipmsm », *ISA transactions*, vol. 92, pp. 155–165, 2019.

[46] Y. Zhan, J. Guan, and Y. Zhao, « An adaptive second-order sliding-mode observer for permanent magnet synchronous motor with an improved phase-locked loop structure considering speed reverse », *Transactions of the Institute of Measurement and Control*, vol. 42, no. 5, pp. 1008–1021, 2020.

[47] P. L. Jansen and R. D. Lorenz, « Transducerless position and velocity estimation in induction and salient ac machines », *IEEE transactions on industry applications*, vol. 31, no. 2, pp. 240–247, 1995.

[48] X. Zhao, C. Wang, W. Duan, and J. Jiang, « Research on sensorless control system of low speed and high power pmsm based on improved high frequency signal injection », *Energy Reports*, vol. 7, pp. 499–504, 2021.

[49] S. Wang, K. Yang, and K. Chen, « An improved position-sensorless control method at low speed for pmsm based on high-frequency signal injection into a rotating reference frame », *IEEE Access*, vol. 7, pp. 86 510–86 521, 2019.

[50] A. Messali, M. Ghanes, M. A. Hamida, and M. Koteich, « A resilient adaptive sliding mode observer for sensorless ac salient pole machine drives based on an improved hf injection method », *Control Engineering Practice*, vol. 93, p. 104 163, 2019.

[51] Y. Zhang, Z. Yin, J. Liu, R. Zhang, and X. Sun, « Ipmsm sensorless control using high-frequency voltage injection method with random switching frequency for audible noise improvement », *IEEE Transactions on Industrial Electronics*, vol. 67, no. 7, pp. 6019–6030, 2019.

[52] S.-I. Kim, J.-H. Im, E.-Y. Song, and R.-Y. Kim, « A new rotor position estimation method of ipmsm using all-pass filter on high-frequency rotating voltage signal injection », *IEEE Transactions on Industrial Electronics*, vol. 63, no. 10, pp. 6499–6509, 2016.

[53] B. Shuang, Z. Zhu, and X. Wu, « Improved cross-coupling effect compensation method for sensorless control of ipmsm with high frequency voltage injection », *IEEE Transactions on Energy Conversion*, vol. 37, no. 1, pp. 347–358, 2021.

[54] Y. Tauchi and H. Kubota, « Audible noise reduction method in ipmsm position sensorless control based on high-frequency current injection », *IEEJ Journal of Industry Applications*, vol. 4, no. 3, pp. 180–186, 2015.

[55] G. Wang, D. Xiao, N. Zhao, X. Zhang, W. Wang, and D. Xu, « Low-frequency pulse voltage injection scheme-based sensorless control of ipmsm drives for audible noise reduction », *IEEE Transactions on Industrial Electronics*, vol. 64, no. 11, pp. 8415–8426, 2017.

[56] Z. Yang, K. Wang, and X. Sun, « Novel random square-wave voltage injection method based on markov chain for ipmsm sensorless control », *IEEE Transactions on Power Electronics*, 2022.

[57] G. Wang, L. Yang, B. Yuan, B. Wang, G. Zhang, and D. Xu, « Pseudo-random high-frequency square-wave voltage injection based sensorless control of ipmsm drives for audible noise reduction », *IEEE Transactions on Industrial Electronics*, vol. 63, no. 12, pp. 7423–7433, 2016.

[58] Z. Lin, X. Li, Z. Wang, T. Shi, and C. Xia, « Minimization of additional high-frequency torque ripple for square-wave voltage injection ipmsm sensorless drives », *IEEE Transactions on Power Electronics*, vol. 35, no. 12, pp. 13 345–13 355, 2020.

[59] X. Wu, Y. Feng, X. Liu, *et al.*, « Initial rotor position detection for sensorless interior pmsm with square-wave voltage injection », *IEEE Transactions on Magnetics*, vol. 53, no. 11, pp. 1–4, 2017.

[60] C.-E. Hwang, Y. Lee, and S.-K. Sul, « Analysis on position estimation error in position-sensorless operation of ipmsm using pulsating square wave signal injection », *IEEE Transactions on Industry Applications*, vol. 55, no. 1, pp. 458–470, 2018.

[61] R. Ni, D. Xu, F. Blaabjerg, K. Lu, G. Wang, and G. Zhang, « Square-wave voltage injection algorithm for pmsm position sensorless control with high robustness to voltage errors », *IEEE Transactions on Power Electronics*, vol. 32, no. 7, pp. 5425–5437, 2016.

[62] D. Surroop, « Commande sans capteur de moteurs électriques par injection de signal », 2022.

[63] S. Wu and J. Zhang, « A terminal sliding mode observer based robust backstepping sensorless speed control for interior permanent magnet synchronous motor », *International Journal of Control, Automation and Systems*, vol. 16, no. 6, pp. 2743–2753, 2018.

[64] R. Cai, R. Zheng, M. Liu, and M. Li, « Robust control of pmsm using geometric model reduction and μ-synthesis », *IEEE Transactions on Industrial Electronics*, vol. 65, no. 1, pp. 498–509, 2017.

[65] F. M. Zaihidee, S. Mekhilef, and M. Mubin, « Application of fractional order sliding mode control for speed control of permanent magnet synchronous motor », *IEEE Access*, vol. 7, pp. 101 765–101 774, 2019.

[66] X. Zhang, L. Sun, K. Zhao, and L. Sun, « Nonlinear speed control for pmsm system using sliding-mode control and disturbance compensation techniques », *IEEE transactions on power electronics*, vol. 28, no. 3, pp. 1358–1365, 2012.

[67] C. Xia, X. Wang, S. Li, and X. Chen, « Improved integral sliding mode control methods for speed control of pmsm system », *International Journal of Innovative Computing, Information and Control*, vol. 7, no. 4, pp. 1971–1982, 2011.

[68] A. K. Junejo, W. Xu, C. Mu, M. M. Ismail, and Y. Liu, « Adaptive speed control of pmsm drive system based a new sliding-mode reaching law », *IEEE Transactions on Power Electronics*, vol. 35, no. 11, pp. 12 110–12 121, 2020.

[69] Z. Li, F. Wang, D. Ke, J. Li, and W. Zhang, « Robust continuous model predictive speed and current control for pmsm with adaptive integral sliding-mode approach », *IEEE Transactions on Power Electronics*, vol. 36, no. 12, pp. 14 398–14 408, 2021.

[70] X. Liu and H. Yu, « Continuous adaptive integral-type sliding mode control based on disturbance observer for pmsm drives », *Nonlinear dynamics*, vol. 104, no. 2, pp. 1429–1441, 2021.

[71] D. A. Haghighi and S. Mobayen, « Design of an adaptive super-twisting decoupled terminal sliding mode control scheme for a class of fourth-order systems », *ISA transactions*, vol. 75, pp. 216–225, 2018.

[72] V. I. Utkin and A. S. Poznyak, « Adaptive sliding mode control with application to super-twist algorithm: equivalent control method », *Automatica*, vol. 49, no. 1, pp. 39–47, 2013.

[73] Y. Shtessel, M. Taleb, and F. Plestan, « A novel adaptive-gain supertwisting sliding mode controller: methodology and application », *Automatica*, vol. 48, no. 5, pp. 759–769, 2012.

[74] C. Edwards and Y. Shtessel, « Adaptive dual-layer super-twisting control and observation », *International Journal of Control*, vol. 89, no. 9, pp. 1759–1766, 2016.

[75] S. Singh and A. Tiwari, « Various techniques of sensorless speed control of pmsm: a review », in *2017 Second International Conference on Electrical, Computer and Communication Technologies (ICECCT)*, IEEE, 2017, pp. 1–6.

[76] M. A. Hamida, J. De Leon, and A. Glumineau, « High-order sliding mode observers and integral backstepping sensorless control of ipms motor », *International Journal of Control*, vol. 87, no. 10, pp. 2176–2193, 2014.

[77] G. Wang, H. Zhan, G. Zhang, X. Gui, and D. Xu, « Adaptive compensation method of position estimation harmonic error for emf-based observer in sensorless ipmsm drives », *IEEE Transactions on Power Electronics*, vol. 29, no. 6, pp. 3055–3064, 2013.

[78] S. Ichikawa, Z. Chen, M. Tomita, S. Doki, and S. Okuma, « Sensorless control of an interior permanent magnet synchronous motor on the rotating coordinate using an extended electromotive force », in *IECON'01. 27th Annual Conference of the IEEE Industrial Electronics Society (Cat. No. 37243)*, IEEE, vol. 3, 2001, pp. 1667–1672.

[79] S. Zheng, X. Tang, B. Song, S. Lu, and B. Ye, « Stable adaptive pi control for permanent magnet synchronous motor drive based on improved jitl technique », *Isa Transactions*, vol. 52, no. 4, pp. 539–549, 2013.

[80] M. C. Harke, D. Raca, and R. Lorenz, « Implementation issues for fast initial position and magnet polarity identification of pm synchronous machines with near zero saliency », in *2005 European Conference on Power Electronics and Applications*, IEEE, 2005, 10–pp.

[81] H. Kim, K.-K. Huh, R. D. Lorenz, and T. M. Jahns, « A novel method for initial rotor position estimation for ipm synchronous machine drives », *IEEE Transactions on Industry Applications*, vol. 40, no. 5, pp. 1369–1378, 2004.

[82] M. C. Harke, D. Raca, and R. D. Lorenz, « Fast and smooth initial position and magnet polarity estimation of salient and near zero saliency pm synchronous machines », in *IEEE International Conference on Electric Machines and Drives, 2005.*, IEEE, 2005, pp. 1037–1044.

[83] F. Deutsch, W. Li, and S.-H. Park, « Characterizations of continuous and lipschitz continuous metric selections in normed linear spaces », *Journal of Approximation Theory*, vol. 58, no. 3, pp. 297–314, 1989.

[84] J. L. W. V. Jensen, « Sur les fonctions convexes et les inégalités entre les valeurs moyennes », *Acta mathematica*, vol. 30, no. 1, pp. 175–193, 1906.

[85] J. A. Moreno and M. Osorio, « Strict lyapunov functions for the super-twisting algorithm », *IEEE transactions on automatic control*, vol. 57, no. 4, pp. 1035–1040, 2012.

[86] H. Liu and H. K. Khalil, « Output feedback stabilization using super-twisting control and high-gain observer », *International Journal of Robust and Nonlinear Control*, vol. 29, no. 3, pp. 601–617, 2019.

[87] G. Bornard and H. Hammouri, « A high gain observer for a class of uniformly observable systems », in *[1991] Proceedings of the 30th IEEE Conference on Decision and Control*, IEEE, 1991, pp. 1494–1496.

[88] Y. B. Shtessel, J. A. Moreno, F. Plestan, L. M. Fridman, and A. S. Poznyak, « Super-twisting adaptive sliding mode control: a lyapunov design », in *49th IEEE conference on decision and control (CDC)*, IEEE, 2010, pp. 5109–5113.

[89] S. V. Gutierrez, J. De León-Morales, F. Plestan, and O. Salas-Peña, « A simplified version of adaptive super-twisting control », *International Journal of Robust and Nonlinear Control*, vol. 29, no. 16, pp. 5704–5719, 2019.

[90] A. Levant, « Principles of 2-sliding mode design », *automatica*, vol. 43, no. 4, pp. 576–586, 2007.

[91] F. Plestan, Y. Shtessel, V. Bregeault, and A. Poznyak, « New methodologies for adaptive sliding mode control », *International journal of control*, vol. 83, no. 9, pp. 1907–1919, 2010.

[92] Y. Shtessel, F. Plestan, and M. Taleb, « Lyapunov design of adaptive super-twisting controller applied to a pneumatic actuator », *IFAC Proceedings Volumes*, vol. 44, no. 1, pp. 3051–3056, 2011.

Titre : Stratégies de commande des machines synchrones à aimants permanents sans capteurs mécaniques par modes glissants

Mots clés : MSAP, Contrôle sans capteur, Observateurs adaptatifs, Contrôleurs adaptatifs, Mode glissant

Résumé : Cette thèse propose deux commandes adaptatives sans capteur basées sur l'approche en mode glissant pour les moteurs synchrones à aimants permanents internes (MSAP). Les stratégies proposées sont composées d'un observateur adaptatif en mode glissant d'ordre élevé (OAMGOE) en boucle fermée avec un contrôle adaptatif basé sur la super torsion, où les gains de contrôle et d'observateur de la stratégie proposée sont paramétrés en termes d'un seul paramètre. Ensuite, le principal avantage de cette stratégie est que les lois adaptables sont faciles à mettre en œuvre, évitant les surestimations des gains qui augmentent le broutage, réduisant le temps de réglage des gains et réduisant les dommages des actionneurs. En outre, une stratégie d'extraction d'erreur d'estimation de position angulaire est proposée. Ensuite, sur la base de ces informations et en utilisant un système virtuel sans paramètre, OAMGOE est conçu pour estimer la position angulaire et la vitesse dans une large plage de vitesse, où les variables estimées fournies par cet observateur sont obtenues avec une plus grande précision, malgré les variations des paramètres, atteignant une plus grande robustesse. Ces états estimés sont utilisés dans la commande robuste proposée pour suivre une référence de vitesse souhaitée et une référence de courant d'axe d souhaitée. Une analyse de stabilité du système en boucle fermée est présentée, en utilisant une approche de Lyapunov. De plus, la stratégie proposée est validée tout au long du montage expérimental et de simulation afin de montrer son efficacité.

Title : Control strategies for permanent magnet synchronous machines without mechanical sensors by sliding modes

Keywords : IPMSM, Sensorless control, Adaptive observers, Adaptive controllers, Sliding mode

Abstract : This thesis proposes two adaptive sensorless controls based on sliding mode approach for interior permanent magnet synchronous motor (IPMSM). The proposed strategies are composed of an Adaptive High-Order Sliding Mode Observer (AHOSMO) in closed-loop with an Adaptive Super-Twisting Control (ASTWC), where the control and observer gains of the proposed strategy are reparameterized in terms of a single parameter. Then, the main advantage of this strategy is the adaptable laws are easy to implement, avoiding overestimates of gains that increases of chattering, reducing the time to tune the gains, and reducing the damage of the actuators. Furthermore, a strategy for angular position estimation error extraction is proposed. Then, from this information and using a parameter-free virtual system, AHOSMO is designed for estimating the angular position and speed in a wide speed range, where the estimated variables provided by this observer are obtained with greater precision, despite the variations of the parameters, achieving greater robustness. These estimated states are used in the proposed robust control to track a desired reference of speed and direct-axis current. A stability analysis of the closed-loop system is presented, using a Lyapunov approach. In addition, the proposed strategy is validated throughout experimental and simulation set-up in order to show its effectiveness.